Results in Earth Sciences 3 (2025) 100088

Contents lists available at ScienceDirect

Results in Earth Sciences

journal homepage: www.sciencedirect.com/journal/results-in-earth-sciences

Global review on shale: Focus on hydrocarbon geoscience & carbon sequestration

Ankita Paul [a], Soumyajit Mukherjee [b,*], Mery Biswas [c]

[a] Department of Earth Sciences and Remote Sensing, JIS University, 81, Nilgunj Road, Agarpara, Kolkata, West Bengal 700 109, India
[b] Department of Earth Sciences, Indian Institute of Technology Bombay, Mumbai, Maharashtra 400 076, India
[c] Department of Geography, Presidency University, 86, 1, College St, Kolkata, West Bengal 700 073, India

ARTICLE INFO

Keywords:
Petroleum geology
Tectonics sedimentology
Hydrocarbon exploration
Carbon sequestration

ABSTRACT

Shale gas is a potential unconventional resource meeting the challenges of the energy crisis. Among the 195 countries of the world, 52 countries contain 108 established shale basins and 156 shale formations for commercial shale oil and gas exploration. For commercial development, the following factors are important- *(i)* thickness of the shale formation and their depths, (ii) (low) permeability of the cap-rock / seal, and *(iii)* geochemical and hydraulic properties of potential organic-rich source rocks. The carbon sequestration potential is unique to each hydrocarbon potential shale formation and basin. Shale formation designated as tight rocks act as storage/reservoirs for carbon sequestration as it captures CO_2 permanently and does not permit it to move upward across the seal. This reduces atmospheric emission level and has potential to check global warming. However, CO_2 capture in shale has not been in global focus for researchers. The study of the prospective shale oil and gas formations worldwide reveals that hydrocarbons are found within 3280–16,500 ft (999.74–5029.2 m) depth. Their average total organic carbon (TOC) and thermal maturity range from 1 % to 10 % and 0.6–3.8 %, respectively, for original type I and II kerogens. The geologic CO_2 sequestration process in potential and active shale basins are discussed with respect of several tectonic events, and past climatic changes such as glacial and interglacial periods and sea-level variation. The Russian Bazhenov Formation is the world's most prosperous hydrocarbon reservoir while the black organic-rich shale in the Vaca Muerta Formation (Neuquen basin, Argentina) ranks second.

Unconventional hydrocarbon reservoirs, viz., coals and shales, have received considerable research interest in the past decade or so, due to their strategic significance as they have emerged as a vast and cleaner energy option, and providing the dual benefit of sequestrating atmospheric CO_2 emissions due to theor storage properties. - Hazra et al. (2024)

1. Introduction

The world's sedimentary rock mass comprises of 50–65 % of shale. A shale with > 0.5 wt% of original organic matter content is called as *organic-rich shale* (Surimin and Ko 2022 and references therein). Though not all organic-rich shales in the world constitute hydrocarbon reservoirs nor are organic rich, such shales are nevertheless significant sediment hydrocarbon resource as they include > 90 % of the global oil and gas reserves (Sorkhabi, 2009; Soua, 2015).

Shale is a fine-grained clastic sedimentary source rock (Rani et al., 2020), *"of unspecified chemical composition"* (Allaby, 2013; for other definitions see reviewes in Bates and Jackson, 1980, O'Brien and Slatt, 1990, Zimmerele, 1995) and can occur with diverse colours (Weller, 1960). However, as per Schon (2011), shale on average contains 59 % clay minerals, whohc is dominantly illite. Shale consists of framework silicates, clay minerals, carbonates, sulphates and organic matters with or without fossils (Potter et al., 1980; Boggs, 2016; Dasgupta, 2017) *(Repository file 1, Section 1)*. Shale is also known as the *"resource play"* since it is the source as well as the reservoir rock (Sahai, 2022). The rock has been considered as the source rock for both conventional and non-conventional reservoirs. Presently shale is considered as a source rock for conventional petroleum system and both source/reservoir rock for the unconventional system (Sahai, 2022, Suriamin and Ko, 2022). Shale's colour has been used to prepare "shale colour map" and has been

* Corresponding author.
E-mail addresses: soumyajitm@gmail.com, smukherjee@iitb.ac.in (S. Mukherjee).

https://doi.org/10.1016/j.rines.2025.100088
Received 23 August 2024; Received in revised form 18 March 2025; Accepted 15 April 2025
Available online 30 April 2025

linked with different environments of deposition (Conybeare, 1979).

Black shale is a dark coloured organic-rich mudrock with ≥ 1 % organic carbon. The grain sizes are dominantly silt and clay (Swanson, 1961; Tourtelot, 1979). The variation in its chemical and mineral constituents and proportion during burial diagenesis alters the color of the rock. Shales can also be red, brown, green and yellow (Morse and Mackenzie, 1990). Black shales are fine-grained organic-rich strata formed in suboxic to anoxic, and euxinic conditions (oxygen-deficient bottom waters) (Soua, 2015). Shale with an organic carbon content of 5–8 % can easily be identified due to their intense black color (Paproth, 1986; Duba et al., 1988). Black shales containing 5 % organic matter have a low resistivity than a shale with no organic matter (Duba, 1988). They are laminated, enriched with pyrite, contains type II marine organic matter with 1–20 % total organic carbon (TOC) and 350–850 mg Hc g^{-1} HI (Soua, 2015). The North African Lower Palaeozoic black shales are the most productive source rocks of the world (Armstrong et al., 2009).

The deposition of shale and formation of an organic-rich reservoir are functions of the geologic CO_2 sorption, biochemical cycle, climate and environmental changes (Beckmann et al., 2005a; Page et al., 2007; Armstrong et al., 2009; Sharma et al., 2021). For example, adsorption capacity of CO_2 is proportional to the TOC (Nutall et al., 2009; Zhou et al., 2018). Shale reservoirs can sequester organic matters buried for millions of years, resulting in natural carbon sequestration. Shale strata have the potential to naturally absorb and store carbon dioxide (CO2) for a very long period. The sequestration of carbon in siliciclastic reservoirs in the underwater saline and terrestrial aquifers governs the hydrocarbon potential reservoirs (Aagaard et al., 2011; Shaw et al., 2022). Though molecular diffusion of CO_2 is slow, cap/impermeable rock sealing efficiency of geologic CO_2 storage reservoirs is important in hydrocarbon reservoir (Busch et al., 2008). According to Yue et al. (2022), less permeable rocks hold maximum volume of CO_2 in the reservoirs. As per Sun et al. (2020), post-rift basins, extensional passive margins and compressional foreland basins are the prime geologic reservoir settings for carbon capture/storage. The time required for carbon sequestration process depends on mineral dissolution and precipitation in the rock system (Xu et al., 2005).

Mineral constituents, depositional periods, type of organic materials and environments are important factors for shale samples to act as source rocks. For example, in terms of mineral constituents, the oil shale sample number 17 (Bradely, 1931) from the Eocene lacustrine Green River Formation of the United States consists of dolomite (31.6 % by weight), calcite (6.8 %), siderite (0.2 %), analcite (17.1 %), quartz (12.1 %), sanidine and orthoclase (7.2 %), pyrite (1.6 %), collophanite (0.4 %), apophyllite (1.0 %), octaherdite (0.1 %), organic matter minus combined water (21.6 %) and excess K_2O (0.3 %). This sample has an estimated 38 gallons of shale oil. In China, the matrix of the oil shale contains kaolinite and mica-based clay whereas the oil shales in Russia, Green River in America and Estonia consist of carbonates (Qian et al., 2011; Toro et al., 2015; Kang et al., 2020). As noted by Asef et al. (2013), the classification of shale is mainly based on factors like silt content, the presence and type of lamination, mineralogy, chemical composition and color. These features are strongly influenced by the depositional environment and subsequent post-depositional processes, particularly diagenesis and compaction.

Shales are heterogeneous porous materials consisting of inorganic minerals and carbonaceous organic matter (Hazra et al., 2024). Shales have three kinds of pore spaces- *(i)* pores within organic matter; *(ii)* those in between mineral grains, and *(iii)* those within discrete mineral grains (Hazra et al., 2024). The minimum *total organic carbon* (TOC) content in shale in order to consider it prospective for hydrocarbon was earlier stated to be 0.5 % by weight, however, others have considered different schemes (review in Hazra et al., 2019). Pores in nano- and micro-scales as well as fractures in shales are the places where hydrocarbon remain stored (Tucker and Jones, 2023). Middle East's bituminous shales of Jurassic and Cretaceous are richly petroliferous (Tucker and Jones, 2023). Reservoir properties of shales are dependent on its quartz content (Nie et al., 2024). Biogenic quartz has a relation with the TOC (Nie et al., 2024).

Organic matter occurs in black shale as fixed carbon and also as bituminous hydrocarbon (Dunber 1957). The primary and the secondary organic matter in shale is not always possible to distinguish. The organic content can be fragments of some taxa or amorphous substances from indeterminate sources (Tucker and Jones, 2023). The TOC of shales are uslally > 1 % (review in Sharma et al., 2019). The minimum TOC in shale in order to consider it prospective for hydrocarbon was earlier stated to be 0.5 % by weight, however, others have considered different schemes (review in Hazra et al., 2019). For example, Tucker and Jones (2023) state that 3–15 % TOC can be found from carbonaceous and bituminous mud and black shales. The range is 1–15 % as per Yaalon (1978) and 1–20 % in Doyele and Bennett (1999). Bates and Jackson (1980) and Friedman (2003) referred that black shales contain ≥ 5 %. organic matter. Few authors did not mention the minimum percent of organic matter that exists in black shales (e.g., Allaby, 2013). The reason is that in nature shale can have a wide range of organic matter. It appears that 0.5 % should not be counted as the high percentage of organic matter in shale, since marine mud can contain 0.35 wt% of C (Keary, 1994). Worldwide, the productive portion of shale is usually 2–5 m thick (review in Sharma et al., 2019).

Grains in black shales are dominantly silt and clay (Swanson, 1961; Tourtelot, 1979). The variation in its chemical and mineral constituents and proportion during burial diagenesis alters the color of the rock. Shales can also be red, brown, green and yellow (Morse and Mackenzie, 1990). Black shales are fine-grained organic-rich strata formed in suboxic to anoxic, and euxinic conditions (oxygen-deficient bottom waters) (Soua, 2015). Shale with an organic carbon content of 5–8 % can easily be identified due to their intense black color (Paproth, 1986; Duba et al., 1988). ~~They are important natural fuel resources.~~ Black shales containing 5 % organic matter have a low resistivity than a shale with no organic matter (Duba, 1988). They are laminated, enriched with pyrite, contains Type II marine organic matter with 1–20 % total organic carbon (TOC) and 350–850 mg Hc g^{-1} HI (Soua, 2015). The North African Lower Palaeozoic black shales are the most productive source rocks of the world (Armstrong et al., 2009).

Shales with carbon content were deposited in an environment where the rate of organic productivity was high (Tucker and Jones, 2023). Note that there are other terms in geoscience, for example "sapropel" that represent dark-coloured sediments rich in organic carbon up to 30 wt% (Gornitz, 2009), which are not necessarily shale. "Biopelite" is very fine sediment definining calcareous shale usually occurs as the coal seam's top portion (Bates and Jackson, 1980).

Shales besides being organic-content rich, can be enriched in chlorite, kaolinite, siliceous materials, chert or diatom. Black shales are commonly enriched in V, As, Mo, Pb, Cu, Ni, Zn and U (Yaalan 1978; also see Mukherjee et al., 2023). B, V and Cr are usually more abundant in marine shales than the continenta deposits and near shore deposits of clay (Yaalon, 1978).

Black shales are deposited in starved basins, in abyssal depths in marine environment where anoxic condition (0–1 ml l^{-1} of O_2 in H_2O: Doyele and Bennett, 1999) prevails, and in shallower waterbodies where circulation of water is for some reason stopped, such as cooling and ice formation at the top of the water layer (Weller, 1960). Black shales can also be of even non-marine origin. An example of this is the "roofing slate" layer in between coal seams. Such coal-bearing areas might have developed in swamp, bog or a lake environment (Dunber 1957). Black shales can also develop in fjors or in a geosyncline (Dunber 1957). Previous idea that fine-graned sediments such as those for shale deposit in a quet water condition has changed. Bottom current dynamics of various sorts such as turbidity, storm-induced and tidal currents can develop thick deposition of mud (Tucker and Jones, 2023).

Not all organic-rich shales generate hydrocarbon (Silva et al., 2015). Since shale has very low porosity, usually < 5 %, and ultra-low

Table 1
Modified World Shale Oil and Gas prospective basins and their reservoir properties [Source: EIA ARI World shale gas and shale oil assessment, 2013 (Attachment D) and USA EIA, 2014].

Continents	Countries	Basin	Shale Formation	Shale Reservoir	Geological Age	Depositional Environment
Asia	China	Sichuan	Qiongzhusi	Gas	Lower Cambrian	Marine
			Longmaxi		Lower Silurian	
			Permian		Permian	
		The Yangtze Platform	Lower Cambrian		Lower Cambrian	
			Lower Silurian		Lower Silurian	
		Jianghan	Niutitang/Shuijintuo	Gas	Lower Cambrian	
			Longmaxi	Oil and Gas	Lower Silurian	
			Qixia/Maokou		Permian	
		Greater Subei	Mufushan	Gas	Lower Cambrian	
			Wufeng/Gaobiajian	Oil and Gas	Upper Ordovician-Lower Silurian	
			Upper Permian		Upper Permian	
		Tarim	Xiaoerbulake	Gas	Lower Cambrian	
			Lianglitage (O$_3$)		Lower Ordovician	
			Yijianfan (O$_2$)/Hetuao (O$_{1}$-$_{2}$)	Oil and Gas	Middle-Upper Ordovician	
			Ketuer		Late Triassic	Lacustrine
		Junggar	Pingdiquan/Lucaogou	Oil and Gas	Permian	
			Triassic		Triassic	
		Songliao	Qingshankou		Cretaceous	
	India	Cambay	Cambay Shale	Gas	Upper Cretaceous-Tertiary	Marine
		Rajasthan	Permian Karampur	Oil and Gas	Neoproterozoic	
		Vindhyan	Hinota, Pulkovar,	Gas	Proterozoic	
		Upper Assam	Barail Group		Upper Eocene-Oligocene	
		Krishna-Godavari	Permian-Triassic		Permian-Triassic	
		Cauvery	Sattapadi-Andimadam		Cretaceous	
		Damodar Valley	Barren Measure		Permian-Triassic	
	Pakistan	Lower Indus	Sembar		Lower Cretaceous	
			Ranikot		Paleocene	
	Indonesia	C. Sumatra	Brown Shale	Oil and Gas	Paleogene	Lacustrine
		S. Sumatra	Talang Akar		Eocene-Oligocene	
		Kutei	Balikpapan		Middle-Upper Miocene	
		Tarakan	Meliat		Middle Miocene	
			Tabul		Late Miocene	
			Naintupo	Gas	Upper Miocene	
		Bituni	Aifam Group		Permian	Marine
	Jordan	Hamad	Batra		Silurian	
		Wadi Sirhan	Batra	Oil and Gas		
	Mongolia	East Gobi	Tsagaantsav		Late Cretaceous	Lacustrine
		Tamtsag				
	Oman	S. Oman Salt	Thuleilat Shale		Lower Cambrian	Marine
			Athel			
			U Shale			
		N. Oman Foreland	Natih		Middle Cretaceous	
		Rub' Al-Khali/Oman	Sahmah Shale		Silurian	
	United Arab Emirates (U.A.E)	Rub' Al-Khali/U.A.E.	Diyab		Upper Jurassic	
			Shilaif		Middle Cretaceous	
			Qusaiba	Gas	Silurian	
	Russia	West Siberian	Bazhenov Central	Oil and Gas	Upper Jurassic-Lower Cretaceous	Marine
			Bazhenov North			
	Thailand	Khorat	Nam Duk	Gas	Permian	Marine
	Kazakhstan	North Caspian (North Basin Margin/ SE Basin Margin)	Tournaisian		Late Carboniferous	Marine
			Lower Serpukhovian, Vereiskiy, Gzelian-Kasimovian		Middle-Upper Carboniferous	
			Visean		Late Carboniferous	
		Mangyshlak	Karadzhatyk		Late Triassic	
		South Turgay	Karagansay		Middle Jurassic	Lacustrine
			Abaleen		Late Jurassic	
Africa	Algeria	Ghadames/Berkine	Fransnian	Gas and Oil	Upper Devonian	Marine
			Tannezuft		Silurian	
		Illizi	Tannezuft		Silurian	
		Timimoun	Fransnian	Gas	Upper Devonian	
			Tannezuft		Silurian	
		Ahnet	Fransnian	Gas and Oil	Upper Devonian	
			Tannezuft	Gas	Silurian	
		Mouydir	Tannezuft		Silurian	
		Reggane	Fransnian	Gas and Oil	Upper Devonian	
			Tannezuft		Silurian	
		Tindouf	Tannezuft		Silurian	
	Chad	Termit	Late Cretaceous	Gas and Oil	Late Cretaceous	Lacustrine
			Upper Cretaceous		Upper Cretaceous	
		Bongor	Late Cretaceous		Late Cretaceous	
		Doba				

(*continued on next page*)

Table 1 (*continued*)

Continents	Countries	Basin	Shale Formation	Shale Reservoir	Geological Age	Depositional Environment
		Doseo				
	Egypt	Abu Gharadig Alamein Natrun Shoushan-Matruh	Khatatba	Gas and Oil	Middle Jurassic	Marine
	Libya	Ghadames/Berkine	Fransnian Tannezuft	Gas and Oil	Upper Devonian Lower Silurian	Marine
		Sirte	Sirte/Rachmat Etel		Upper Cretaceous	
		Murzuq	Tannezuft		Lower Silurian	
	Morocco/ Western Sahara/ Mauritania	Tindouf Tadla	Lower Silurian	Gas and Oil Gas		Marine
	South Africa	Karoo	Prince Albert Whitehill Collinghan	Gas	Lower Permian	Marine
	Tunisia	Ghadames/Berkine	Fransnian Tannezuft	Gas and Oil	Upper Devonian Silurian	Marine
North America	British Columbia (Canada)	Horn River	Muskwa/Otter Park Evie/Kua	Gas	Devonian	Marine
		Cordova Liard	Muskwa/Otter Park Lower Besa River			
		Deep Basin	Doig Phosphate		Triassic	
	Mexico	Burgos	Eagle Ford Shale Tithonian	Gas and Oil Gas	Middle – Upper Cretaceous Upper Jurassic	Marine
		Sabinas	Eagle Ford Shale Tithonian		Middle – Upper Cretaceous Upper Jurassic	
		Tampico	Pimienta	Gas and Oil	Jurassic	
		Tuxpan	Tamaulipas Pimienta		Lower-Middle Cretaceous Jurassic	
		Veracruz	Maltrata		Upper Cretaceous	
South America	Northern South America (Colombia and Western Venezuela)	Middle Magdalena Valley	La Luna/ Tablazo	Gas and Oil	Upper Cretaceous	Marine
		Llanos	Gacheta			
		Maracaibo/Catatumbo	La Luna/ Capacho			
	Argentina	Neuquen	Los Molles Vaca Muerta	Gas and Oil	Middle Jurassic Upper Jurassic – Lower Cretaceous	Marine
		San Jorge	Aguada Bandera	Gas	Upper Jurassic – Lower Cretaceous	Lacustrine
			Pozo D−129	Gas and Oil	Lower Cretaceous	
		Austral-Magallanes	Lower Inoceramua-Magna Verdes			Marine
		Parana	Ponta Grossa		Devonian	
	Brazil	Parana Solimoes Amazonas	Ponta Grossa Jandiatuba Barreirinha	Gas and Oil	Devonian	Marine
	Bolivia/ Chile/ Paraguay/ Uruguay	Parana	Ponta Grossa Cordoboes	Gas and Oil	Devonian	Marine
		Chaco	Los Monos			
		Austral-Magallanes	Estratos con Favrella		Lower Cretaceous	
Antarctica	Data not available					
Europe	Turkey	SE Anatolian Thrace	Dadas Hamitabat	Gas and Oil	Silurian-Devonian Middle – Lower Eocene	Marine
	Eastern Europe (Bulgaria, Romanis, Ukraine)	Carpathian Foreland	Late Silurian	Gas	Late Silurian	Marine
		Dniepr-Donets	Late Carboniferous	Gas and Oil	Late Carboniferous	
		Moesian Platform	Late Silurian Etropole		Late Silurian Late Jurassic	
	France	Paris Basin	Lias Shale Permian-Carboniferous	Gas and Oil	Late Jurassic Permian-Carboniferous	Marine Lacustrine
	United Kingdom	North UK Carboniferous Shale	Carboniferous Shale	Gas	Carboniferous	Marine
		South UK Jurassic Shale	Lias Shale	Gas and Oil	Late Jurassic	
	Spain	Basque-Cantabrian	Jurassic	Gas and Oil	Late-Middle Jurassic	Marine
	Poland	Baltic/Warsaw Trough Podlasie	Llandovery	Gas and Oil	Late Silurian-Ordovician-Upper Cambrian	Marine
		Lublin		Gas		
		Fore Sudetic	Carboniferous		Carboniferous	Lacustrine
	Lithuania/ Kaliningrad	Baltic	Llandovery	Gas and Oil	Late Silurian-Ordovician-Upper Cambrian	Marine
	Germany	Lower Saxony Basin	Toarcian Posidonia	Gas and Oil	Late Jurassic	Marine

(*continued on next page*)

Table 1 (*continued*)

Continents	Countries	Basin	Shale Formation	Shale Reservoir	Geological Age	Depositional Environment
			Wealden		Late Cretaceous	
	Netherlands	West Netherlands Basin	Namurian Epen		Upper Carboniferous	Marine
			Namurian Geverik			
			Toarcian Posidonia		Late Jurassic	
	Scandinavia	Scandinavia Region	Alum Shale-Sweden	Gas	Cambro-Ordovician	
			Alum Shale-Denmark			
Australia	Australia	Cooper	Nappamerri	Oil and Gas	Permian	Lacustrine
			Patchawarra			
			Tenappera			
		Maryborough	Goodwood/Cherwell Mudstone	Gas	Cretaceous	Marine
		Perth	Caryngina	Gas	Upper Permian	
			Kockatea	Gas and Oil	Late Triassic	
		Canning	Goldwyer	Oil and Gas	Middle Ordovician	
		Georgina	Dulcie Trough		Middle Cambrian	
			Toko Trough			
		Beetaloo	Middle Velkerri		Precambrian	
			Lower Kyalla			

permeability- 100–1 mD, hydraulic fracturing (Sahai, 2022) and horizontal drilling (review in Hazra et al. 2024) becomes important to extract hydrocarbon from them. In order to crack the rock and liberate natural gas or oil, hydraulic fracturing/ fracking is the process of injecting chemicals, sand and water under high pressure into shale deposits (Yin et al., 2024). For unconventional petroleum system this fracking technology is required, which is not needed for conventional systems. Shale with brittle mineral content > 40 % is required to propagate fracture during fracking (Tucker and Jones, 2023).

Since most of the targeted carbon sequestration sites have a topseal of very fine graned rocks (> 60 % are shale: Olabode et al., 2012), study of shales worldwide has gained enormous attention (Tucker and Jones, 2023). Weller (1960) stated that ~ 70 % of the global oil mineral resources come form the Mesozoic black shales. North America witnesses *"shale revolution"* since around 2015 (Tucker and Jones 2023). About 32 % of the worldwide natural gas are in shales (Khosrokhavar et al., 2014). Shales after formation can reduce anisotrpy by loosing their laminations due to bioturbations, which are commonly found in the boundaries of parasequences (Tucker and Jones, 2023). This can change the mechanical property of shales.

Dong et al. (2022) reported that supercritical CO_2 (i.e., CO_2 at temperature and pressure, > 31.1 °C and 7.38 MPa, respectively) can replace hydrocarbons from shale's organic materials, and that in this process shale's microstructures change. In an independent study by Yang and Pan (2023) revealed that the supercritical CO_2 reduces compressive strength and elastioc modulus of the shale. Sharma et al. (2021) discussed the feasibility of injecting CO_2 in shale, the long (10^4 Yr) and the short-term chemical changes. Supercritical CO_2 fracturing leads to more complex and rougher fractures than hydraulic fracturing, and produce greater permeabilities (review in Han et al. 2024). However, chemical changes alter the reservoir property (Lyu et al., 2021). Chen et al. (2016) through numerical modelling proved that as the stress-sensitivity coefficients (indices of adsorption and Knudsen diffusion) elevate, the CO_2-storage capacity in shale reservoirs increases.

Hazra et al. (2022) demonstrate that the uniaxial compressive strength, Young's modulus and tensile strength of shales fall as the supercritical CO_2 saturation elevates. Hazra te al. (2022) in their Table 1 reviewed how supercritical CO_2 injection alters the pore structures in shales. Zhou et al. (2022) found through numerical modelling that changes in pore structures are primarily controlled by precipitation/dissolution of minerals and swelling in shale samples. The volume of CH_4 recovered and CO_2 stored rises with injection pressure of CO_2 (Huo et al. 2017). A recent work by Wang et al. (2023) proved that the total pore volume and the total specific surface diminish in shales with exposures of supercritical CO_2. Geosceicne of CO_2 injection in shale formations are summarizd in Khosrokhavar et al. (2014). Xhan et al. (2020) reviewed CO_2 sequestration in shales. They pointed out that the adsorbation power of CO_2 in shale depend on the type of organic materials in shale, content of moisture, TOC, clay content and composition, pore structure and burial depth. Jia et al. (2019) through modelling explained that continuous gas flooding would be needed when the matrix permeability exceeds 0.01 mD. On other hand, cyclic gas injection/ huff-n-puff scheme is to be applied on shales with ultra-low permeability.

Kerogens with large areas of surfaces such as in shales have greater capability of adsorbtion of CO_2 (Bashir et al., 2024). In case of physical adsorption, CO_2 is contained within the structure of the shale. On other hand, in chemisorption, CO_2 is attached by chemical bonds. The later has a reuced risk of leakage. Satic and capillary or residual trapping of CO_2 is involved in physical trapping mechanism in shales (review in Bashir et al., 2024).

Unlike conventional reservoirs, shale reservoirs have no separate "trap" structure. Marine shales are prone to fracturing by hydraulic means. In contrast non-marine shales have more clay content, are more ductile, and hence are less favourable to hydraulic fracturing. Another observation is that more hydrocarnon recovery is possible from shales deposited in a transgressive environment than those found from the regressive system (review in Ahmed and Meehan, 2016).

Out of the different kinds of storage of CO_2 within shale, viz., tructural space storage, bound space storage, dissolution storage, and mineralization storage, the later kind of storage is the most long-lasting (Wang et al., 2023). Liquid oil production from gas condensate reservoirs is the prime target from shale reservoirs (Sheng 2015). Shales are useful porous media for CO_2 storage with ~ 5–10 kg t^{-1} capacity, or 1 million tons km^{-2} in adsorption capacity (review in Wang et al., 2017).

A confusion may arise between *shale oil* and *oil shale*. Shales with oil content > 3.5 % is designated internationally as oil shales (Zou, 2017). For more than a century, organic-rich shales and mudstones (oil shale) with substantial hydrocarbons have been explored. By heating such sediments in vessels, synthetic / shale oil and gas were produced (Boak and Kleinberg, 2020). In other words, any type of shale from which substantial oil can be extracted by heating is termed as 'oil shale' whereas the heat reaction and degradation of the kerogen found in oil shales results in shale oil (Pettijohn, 2004; Zendehboudi and Bahadori, 2017). Problems and prospects in shale oil development can be found in Feng et al. (2020).

Oil shales are found in rocks of Cambrian, Ordovician, Devonian, Carboniferous, Mesozoic and Paleogene ages (Zou 2019). Zou (2019) presented characteristics of Paleozoic and Mesozoic oil shales. Highest (71 %) oil shales occur in USA (Zou 2019). Oil shales contain > 10 % of organic matter and is called 'kerogen' (Hughes, 1978). This can have a source from algal and terrestrial humic matters (Selley 1985). Gas in shales can be located within bands and in fractures (Selley 1985). Coal types such as tobanite/bog head/canal coal and tasmanite are also made

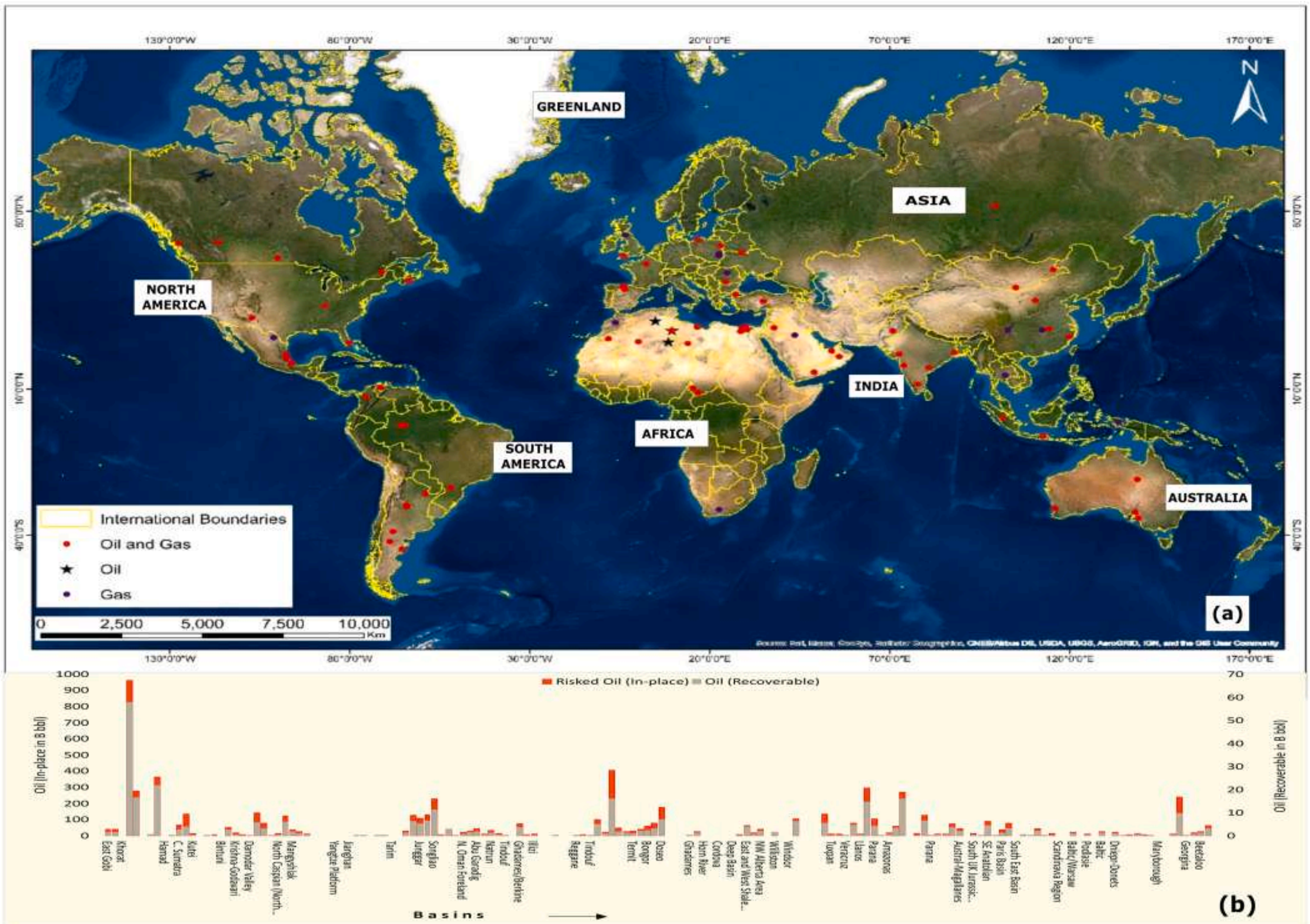

Fig. 1. **a.** Location of the world shale oil and gas basins using Arc GIS platform and Google Earth Pro. **b.** Global risked In-place and recoverable shale Oil Resources (Bbbl mi^{-2}) (Data Source: USA EIA, 2013).

up of algal matter (Selley 1985). Oil shales do not contain free liquid oil (Allaby, 2013). A generalized definition of oil shale in industry is that it is any rock from where oil can be extracted (Hughes, 1978). If a significant amout of gas is released upon heating a shale sample, it can be called as a gas shale (Tucker and Jones, 2023). For pure shale formations, shale oil migrates too little. On the other hand, for sandwitch-type shale oil, the migration is maximum. The chemical composition of individual laminations in layered shale offer different types of flow pathways (Gao et al., 2024). Thermal extraction techniques are used to separate the shale oil from oil shale (Ramirez-Corredores, 2017). Shale gas refers to thermogenic or biogenic gas produced from organic-rich fine-grained low permeability sedimentary rocks e.g., shales, mudstones, mudrocks and the associated lithofacies (Suriamin and Ko, 2022). However, definitions of 'shale', 'mud' and 'mudstone' might differ (review in Hazra et al., 2019).

For more than a century, organic-rich shales and mudstones (oil shale) with substantial hydrocarbons have been explored. By heating such sediments in vessels, synthetic / shale oil and gas were produced (Boak and Kleinberg, 2020). In other words, any type of shale from which substantial oil can be extracted by heating is termed as 'oil shale' whereas the heat reaction and degradation of the kerogen found in oil shales results in shale oil (Pettijohn, 2004; Zendehboudi and Bahadori, 2017).

Thermal extraction techniques are used to separate the shale oil from oil shale (Ramirez-Corredores, 2017). Shale gas refers to thermogenic or biogenic gas produced from organic-rich fine-grained low permeability sedimentary rocks e.g., shales, mudstones, mudrocks and the associated lithofacies (Suriamin and Ko, 2022). Oil shale's history of business is presented by Zou (2017). Within 2035, shale gas is expected to have half the share in total enegy generation in USA (review in Sharme et al., 2019). Geopolitical aspects of shale gas have been reviewed in Jaffe (2016). Shale gas consists mostly of CH_4, and ethane, butane and propane make up the remainder (review in Dayal and Mani 2017). In shale gas reservoir, gas can occur in three ways- *(A)* free gas (in pores and joints; calcite veins with hydrocarbon- Liang et al. 2024; also see Zoback and Kohli, 2019), *(B)* adsorbed gas (within organic materaisl and clays) and *(C)* dissolved gas (in organic matters). Free gas also can occur in hydraulic fractures or within pore networks (Aguilera, 2016).

Strong plasticity of organic matter will mean that the pores are sustanible to collapse (Jiang et al., 2023). Shale with 1–1.1 % R_o (a measutre of vitrinite reflectance) indicates that the organic material is mature adequately to produce hydrocarbon (review in Zendehboudi et al., 2017). These reservoirs usually have 1–100 nano-Darcy of permeability (ultra-tight and low permeability reservoir type), < 10 % porosity, 2 nm to 2 μm pore size, moderate thermal maturity, and are found in gentle slopes, areas under pressure and in the basin margins. These reservoirs are characterized by low production (~ 10,000 m^3d^{-1}) and even in absence of water injection, are capable of 30–50 years of production (review in Taghavinejad et al., 2022). Oil-enriched shales that have crossed the oil and gas generatuning windows have very low HI but with much high TOC values (Wood and Cai,2022).

The mineralogy of clay in shale matters much in hydrocarbon geoscience and in gas storage. For example, *(i)* a correlation between smectite abundance and TOC has been made in few Late Archean-Early

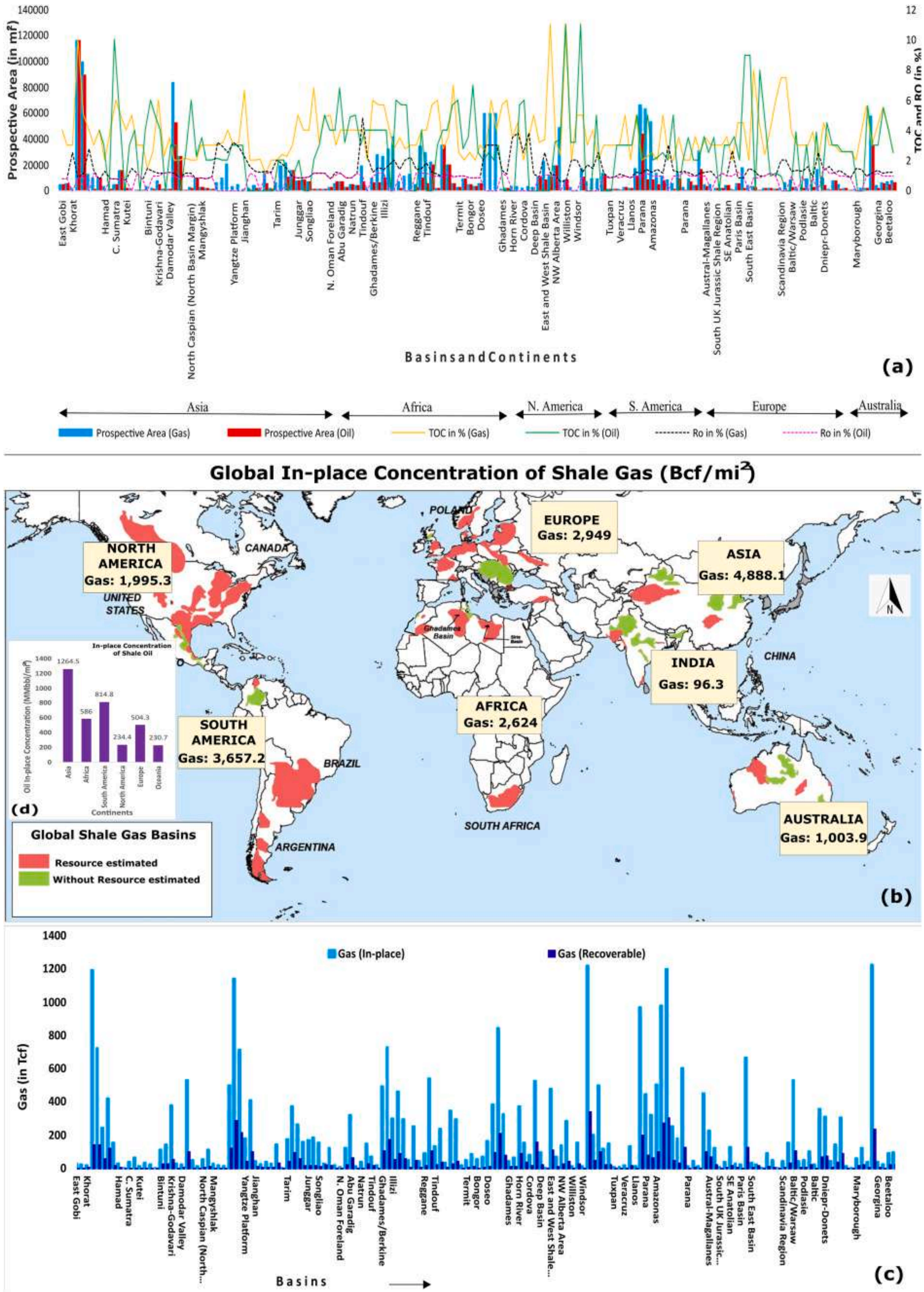

Fig. 2. a. Graphical representation of the world shale basin prospective area with respective TOC and Ro content. **b.** Global In-place concentration of Shale Gas Resources (Bcf mi^{-2}) (Source: modified after Soua, 2014). **c.** Global risked shale gas In-place and risked recoverable of Resources (Tcf). **d.** Global In-place concentration of Shale Oil Resources (MMbbl mi^{-2}) of the continents (Data Source: USA EIA, 2013).

Table 2
Methods for assessing shale quality and its basin characteristics.

Sl. no.	Analysis/ techniques	Formula and uses	References
1.	Optical microscopic analysis of thin sections	Assessing the mineralogy and petrology of shale samples	De et al. (2020)
2.	Spectral gamma ray log (SGR)	analyses the clay mineralogy, geochemical, depositional environment and the thickness of the shale formation	De et al. (2020)
3.	Scanning electron microscopy (SEM)- Energy Dispersive X-Ray analysis (EDS)	Identifying the characteristics of organic porosity	Mark et al. (2012); Camp et al. (2013); Goergen et al. (2014); Jiao et al. (2014); Cardott et al. (2015); Hackley and Cardott (2016)
4.	X-ray diffraction (XRD)	Studies the ratio of major minerals at relative intensities and scanning range	Rani et al. (2020)
5.	X-ray fluorescence (XRF)	assess the concentration of **major** oxides	Hupp and Donovan (2018)
6.	Total Organic Carbon (TOC)	Asses the degree of organic richness in the prepared sample and its potential resource	Bonis et al. (2009); Jarvis et al. (2010); Wang and Carr (2012)
9.	$\mathbf{T_{max}}$ index	determines **thermal maturity of source rock. See review by** Hazra et al. (2024) **for limitation of $\mathbf{T_{max}}$ in such interpretations**	Diasty et al. (2017)
10.	Vitrinite reflectance (VR)	**Helps in determining the thermal maturity**	Huang et al. (2012); Jarvie (2012); Silva et al. (2015)
11.	Organic pore size dimension	characterizes the quality of the shale rock to study its pore size.	Armstrong et al. (2009)
	12. Rock-Eval pyrolysis	**Measures TOC, HI, OI, $\mathbf{T_{max}}$ and hydrocarbon generation potential of a rock**	
13.	Fourier transform infrared spectroscopy (FTIR) pyrolysis	determines the decomposition zones of the shale sample and investigates the compounds produced at different temperatures during thermal degradation	Tong et al. (2011); Hazra et al. (2016); Baruah et al. (2018)
14.	Seismic inversion technique	It is a subsurface modelling technique that produces the geological structure of a basin from seismic data and well log data	Oadfeul and Aliouane (2016a,b); Haris et al. (2017); Mahmood et al. (2018); Sohail et al. (2020)
15.	P-**impedance**	Density $\times$ P-velocity	
16.	S-**impedance**	Density $\times$ S-velocity	
17.	Hydrocarbon saturation (Shc)	suggest the best patch for hydraulic fracturing	Deshmukh et al. (2020)
18.	X-ray computed tomography (XCT)	provides 3D data geometries and properties of the solid shale reservoirs in different scales (mm-nm)	Health et al. (2011); Lin et al. (2017)
19.	Young's modulus (E)		Bazunu et al. (2015)
20.	Capillary suction time (CST)	It states the nature of the shale zone. Mainly applicable during reservoir drilling.	Gale and Baskerville (1967); Wilcox and Fisk (1983); Sliaupa et al. (2020)
21.	Entropy weight Method (EWM)	Multi-Criteria decision making statistical analysis. $\mathbf{weighted\ vector(wj)} = (\mathbf{i} - \mathbf{ej})/\sum(\mathbf{i} - \mathbf{ej})$ Where ej is the range of the entropy value between 0 and 1.	

Cambrian basins, *(ii)* dry smectite has a greater adsorbtion pontential than kaolinite, and *(iii)* transformation from smectite to illite creates microcracks hence increase permeability (Zhao et al., 2023).

CO_2 can be injected cyclically in unconventional shale reservoirs and can lead to a high oil recovery rate (*"huff-n-puff"*, review in Fakher et al. 2020). CO_2 can efficiently undergo physical adsorbtion in shale in a voluminous amount due to van der Waal force without the need of any catalyst (review in Fakher et al. 2020). Shale oil and gas plays have become the target areas with increasing population and energy consumers, for economic (oil and gas industries) and societal development after the success of the U.S. shale development (Han et al., 2024). For example, the "hot shales" of the Upper Ordovician-Lower Silurian organic carbon (OC) with TOC reaching 15 % in ~ 20 m thick layer within the succession in North Africa and Arabia give ~ 30 % of the world's oil production (Lüning et al., 2000, 2006; Armstrong et al., 2009). More than 48 countries have over 90 potential shale basins that might be exploited for shale oil-gas resources. Nearly 2.9 trillion barrels of oil can be recovered from the world shale basins (Dyni, 2004; 2006).

This review article discusses the qualitative and quantitative prospective shale basins of the world (Fig. 1a-c; Table 1) with special reference to hydrocarbon-bearing organic-rich black shale. The discussion includes source rock characters, geochemistry, reservoir potential and carbon capture and sequestration (CCS) issues for the basins based on the available literature. Countries and the respective continents (excluding Antarctica) have been studied. Asia, the largest continent, is mentioned at the outset. Nations have been reviewed in descending order based on their total recoverable shale gas and oil output. For instance, China is one of the most potential shale gas and oil producing nations in the Asia. This is followed by Russia, the United Arab Emirates, Pakistan and India *(Repository File 1;* Fig. 1*)*. Few previous authors made such review (e.g., Kennedy et al., 2016). Shale gas mainly comes from USA, China and Canada at present (Aybar et al. 2015). However, an up to date review was not available, and this article fills up this gap.

2. Workflow

The 1931–2023 literature *(Repository File 1;* Fig. 2 *a-b)* discusses the physical extent, reservoir properties and commercial resource of shale and shale plays including the CCS potential for the shale basins. The literature also includes various methods for assessing the quality of the shale samples collected from the basins and other sources (Table 2).

In the published literature, the shale samples for analysis were either collected by drilling or fieldworks. Optical microscopic studies of thin-sections have been the primary/basic criterion in assessing the mineralogy and petrology of the shale samples. Spectral gamma ray log (SGR) analyses were used along with clay mineralogy and geochemistry. The log measures and enables various cross-plots of uranium (in ppm), thorium (in ppm), and potassium (in %) in the well (e.g., De et al., 2020). This analysis is further verified by SEM-EDS and XRD. Scanning electron microscopy (SEM) is performed in industries to decipher the porosity and mudstone reservoirs (e.g., Passey et al., 2010; Loucks et al., 2010, 2012; Heath et al. 2011; Josh et al., 2012; Klaver et al., 2012, 2015; Camp et al., 2013; Goergen et al., 2014; Jiao et al., 2014; Cardott et al., 2015; Hackley and Cardott, 2016). The samples are dried using a hot air oven, crushed using a ball mill to minimize the grain size below 0.75 mm. They are polished and leveled using dry emery paper, mounted to SEM stubs using carbon coating with gold and palladium to provide a conductive topography. The SEM images states the surface detail such as pore spaces, organic matter, inorganic minerals, fractures etc. at 2.5 nm resolution (Lei et al., 2021).

The Backscattered electron (BSE) images obtained during SEM can identify kerogen by its darker gray-scale value. Further, Energy Dispersive X-Ray analysis (EDS) can be used to validate the BSE (Mark et al., 2012). X-ray diffraction (XRD) studies the ratio of major minerals at relative intensities and scanning ranges. It determines mineral composition. Sample preparation is the crucial part of the analysis. The samples are powdered to < 0.075 mm size using an agate mortar and pestle or a ball mill, dried in hot-air oven and mounted on glass slide for analysis. The strongest peak of the minerals is identified followed by its weaker peaks (Rani et al., 2020). It poses a major challenge in the identification of minerals, particularly in shales, since being deposited in a marine or lacustrine environment, shale contains several phases of clay-minerals, micas, carbonates, aluminosilicates, sulfide group of minerals, quartz and organic matters.

For a more accurate assessment of shale samples, X-ray fluorescence (XRF) is applied to assess the concentration of major elements in terms of oxides. These oxide concentrations are used to estimate the underlying mineralogy of the samples (Hupp and Donovan, 2018). TOC represents the degree of organic richness in the prepared sample and its potential resource. It measures the quality from rock records (Wang and Carr, 2012). It also evaluates the recoverable shale gas content. The TOC content of any sediment can be obtained by substracting total inorganic carbon (TIC) from total carbon (TC) (Bonis et al., 2009, Jarvis et al., 2010).

The TOC of the mature reservoirs ranges between ~ 2–10 % (Alexander et al., 2011; Silva et al., 2015). The scatter plot between hydrogen index (HI) and oxygen index (OI), and HI with T_{max} determines the kerogen type (Van Krevlen, 1961). Thermal maturity represents the degree to which a shale sample has undergone heating or thermal alteration over time. Higher the thermal maturity, more advanced is the process of hydrocarbon generation. This can help in determining whether a shale is in the oil window, gas window, or past its productive phase. Vitrinite reflectance (VR) is an optical parameter indicating thermal maturity (Allen and Allen, 2013). The vitrinite group of macerals appears to vary smoothly and predictably with temperature (Sweeney and Burmnham, 1990). The thermal maturity of mature shale ranges 0.6–1.1 % (representing the oil window zone) and in potential gas from 1.1 % to 3.0 % (Huang et al., 2012; Jarvie, 2012, Silva et al., 2015). Immature kerogen content has a vitrinite reflectance level of < 0.6 %. Advanced thermal maturity and presence of hydrocarbons generated from kerogen determines the organic porosity (e.g., Behar and Vandenbrouke, 1987; Driskil et al., 2013a,b; Pommer and Milliken, 2015). Higher TOC and higher maturity of usually lead to greater porosity (review in Aybar et al. 2015). Organic pore size dimension of shale samples and their connectivities are the two important parameters that characterize the quality of the shale rock. Shale oil/gas of commercial production exists within there are abundant pore spaces in shale samples. Nanopores constitute ~ 88 % of porosity of shales and it can increase with increasing thermal evolution (Zou, 2017).

Rock-Eval pyrolysis can quantify hydrocarbons in the rock. Pyrolysis yields four parameters. The volatilization of hydrocarbons that are free in the rock while sampling gives the S_1 peak. The S_2 peak connotes hydrocarbons and tars created by thermal cracking and other non-hydrocarbon (kerogens) organic matter reactions (Teichmuller and Durand 1983). The S_2 peak infers the temperature (T_{max}) at which the greatest amount of hydrocarbon production occurs. S_3 indicates the CO_2 produced (Geel et al., 2013). The HI and the OI are obtained by dividing the values indicated by the S_2 and the S_3 peaks with the organic carbon, respectively (Langford and Valleron, 1990). As a specific example, Armstrong et al., (2009) in his article on black shale deposition in southern Jordan conducted the pyrolysis using a Delsi Oil Show Analyser. Further advancement in this direction was made by Hazra et al. (2021a, 2021b) who used $S4T_{peak}$ to represent thermal maturity of shales.

Further, Fourier transform infrared spectroscopy (FTIR) analysis determines the decomposition zones of the shale sample and investigate the compounds produced at different temperatures during thermal degradation (e.g., Tong et al., 2011; Hazra et al., 2016; Baruah et al., 2018). Seismic inversion using high lateral resolution seismic data is widely used to characterize unconventional hydrocarbons and the source rock. It is a subsurface modelling technique that produces the geological structure of a basin from seismic ~~data~~ and well log data

Table 3
Modified World black shale oil and gas prospective basins with quantitative details after EIA ARI, 2013 [Source: EIA ARI World shale gas and shale oil assessment, 2013 (Attachment C) and 2014]**.** The yellow shaded formation states lowest and the green shaded formation states highest hydrocarbon content among the black shale Formations of the world.

Continent	Country	Basin	Formation	In-place Gas	Recoverable Gas	In-place Oil	Recoverable Oil
Asia	Indonesia	C. Sumatra	Brown Shale	41.5	3.3	69.4	2.77
		Bintuni	Aifam Group	114.3	28.6	0	0
	India	Cambay	Cambay Shale	145.6	29.5	54.3	2.71
	Kazakhstan	North Caspian (North Basin)	Tournaisian, Radaevskiy-Kosvinkskiy	14.1	2.3	1.3	0.06
			L. Serpukhovian, Vereiskiy, Gzelian-Kasimovian	55.3	7.6	14.9	0.75
		North Caspian (SE Basin)	Visean	116.3	11.6	125.3	6.26
	China	Sichuan	Qiongzhusi	499.6	124.9	0	0
			Longmaxi	1146.1	286.5	0	0
			Permian	715.2	214.5	0	0
		Yangtze Platform	L. Cambrian	181	45.2	0	0
			L. Silurian	414.7	103.7	0	0
		Jianghan	Niutitang/Shuijintuo	45.7	11.4	0	0
			Longmaxi	28	6.5	0.8	0.04
			Qixia/Maokou	40.1	9.8	5	0.24
		Greater Subei	Mufushan	29	7.3	0	0
			Wufeng/Gaobiajian	143.9	36	4.5	0.23
			U. Permian	7.7	2	1	0.05
		Tarim	L. Cambrian	175.9	44	0	0
			L. Ordovician	377.5	94.4	0	0
			M.-U. Ordovician	265.1	61.4	31.1	1.55
			Ketuer	161.2	16.1	129.5	6.47
		Junggar	Pingdiquan/Lucaogou	172.4	17.2	108.9	5.44
			Triassic	187.5	18.7	134.1	6.7
		Songliao	Qingshankou	155.4	15.5	229.2	11.46
Africa	Egypt	Abu Garadig	Khataba	325.7	65.1	47.1	1.88
		Alamein	Khataba	16.7	1.3	14.4	0.58
		Natrun	Khataba	41.6	3.3	35.9	1.43
		Shoushan-Matruh	Khataba	151.2	30.2	16.8	0.67
	Libiya	Murzuq	Tannezuft	18.6	1.9	26.9	1.34
	South Africa	Karoo	Whitehill	845.4	211.3	0	0
North America	Mexico	Sabinas	Eagle Ford Shale	501	100.2	0	0
			Tithonian La Casita	118.1	23.6	0	0
South America	Venezuela/Colombia	Middle Magdalena Valley	La Luna/Tablazo	134.6	18.3	79.2	4.76
		Maracaibo/Catatumbo	La Luna/Capacho	970	201.9	296.7	14.83
	Brazil	Parana	Ponta Grossa	449.6	80.5	107.1	4.29
		Solimoes	Jandiatuba	322.6	64.6	7.1	0.28
		Amazonas	Barreirinha	507.2	99.9	19.4	0.78
	Argentina	Neuquen	Los Molles	982	275.3	61	3.66
			Vaca Muerta	1201.9	307.7	270.4	16.22
		Golfo San Jorge	Aguada Bandera	254.2	50.8	0	0
			Pozo D−129	184	34.8	16.7	0.5
		Austral-Magallanes	L. Inoceramus-Magnas Verdes	605.5	129.5	131.2	6.56
		Parana	Ponta Grossa	16.3	3.2	0.3	0.01
	Bolivia, Chile, Paraguay, Uruguay	Parana	Ponta Grossa	46.5	8.2	13.6	0.55
			Cordobes	13.3	2.1	14.3	0.57
		Chaco	Los Monos	456.9	103.5	75.1	3.76
		Austral-Magallanes	Estratos con Favrella	227.5	69.1	47	2.35
Europe	United Kingdom	North UK Shale Region	Carboniferous Shale	125.6	25.1	0	0
		South UK Shale Region	Lias Shale	8	0.6	17.1	0.69
	Spain	Basque-Cantabrian	Jurassic	41.8	8.4	2.9	0.14
	Paris	Lias Shale	L. Jurassic	23.8	1.9	38	1.52
	France	South East Basin	Lias Shale	37	7.4	0	0
	Scandinavia	Scandinavia Region	Alum Shale-Sweden	48.9	9.8	0	0
	Poland	Baltic/Warsaw	Llandovery	532.1	105.2	24.6	1.23
	Lithuania/Kaliningrad	Baltic	Llandovery	24.5	2.4	28.9	1.45
	Bulgaria/Romania/Ukraine	Carpathian Foreland	L. Silurian	362.5	72.5	0	0
		Dniepr-Donets	L. Carboniferous	312.5	75.9	22.9	1.14
		Moesian Platform	L. Silurian	48.3	9.7	1.6	0.08
			Etropole	148.2	37.1	7.9	0.4
Oceania	Australia	Maryborough	Goodwood/Cherwell Mudstone	63.9	19.2	0	0
		Canning	Goldwyer	1227.2	235.4	243.7	9.75
		Georgina	L. Arthur Shale (Dulcie Trough)	40.6	8.2	2.9	0.12
			L. Arthur Shale (Toko Trough)	26.6	4.6	21.6	0.87
		Beetaloo	M. Velkerri Shale	94.3	22.2	27.8	1.39

(Sohail et al., 2020). It converts the seismic data into organic geochemical data producing synthetic seismogram (Oadfeul and Aliouane, 2016a,b; Haris et al., 2017; Mahmood et al., 2018; Sohail et al., 2020). Further, the analysis of seismic attributes includes trace envelope, instantaneous phase and frequency, seismic trace inversion and amplitude *vs.* offset (AVO) from the seismic trace date through statistical evaluation approaches such as linear regression and conventional crossplotting. The Multilayer feedforward neural network (MLFN) and Probabilistic neural network (PNN) are applied for predicting well log properties (i.e., porosity, TOC and density) (Hampson et al., 2001; Deshmukh et al., 2020). The MLFN access is less susceptible to noise because to the non-linear relationship between the input data and the destination data (Deshmukh et al., 2020).

One of the purposes of geomechanical modeling is that it constrains the brittleness index (BI) of a rock to assess its capacity to conduct hydraulic fracturing. The P-impedence (density*P-wave velocity) and S-impedence (density*S-wave velocity) are the input data to generate 3D models/volumes of the shale properties. The TOC and hydrocarbon saturation (Shc) volume of samples suggest the best location for the hydraulic fracturing (Deshmukh et al., 2020). X-ray computed tomography (XCT) provides 3D data geometries and properties of the solid shale reservoirs at different scales (nm-mm) (e.g., Health et al., 2011; Lin et al., 2017). The mechanical properties of the rock viz., tensile, comprehensive and shear strength, and degree of brittleness can be measured by Young's modulus *(E)*, Poisson's ratio *(v)*, shear strain and elastic modulus *(G)* applying both the static and dynamic methods (Bazunu et al., 2015). For decision-making among the explored shale formations producing both shale oil and shale gas, the entropy method is implemented. Here, the recoverable shale oil and gas from shale formations are considered as the indicators or input factors (Zou et al., 2006; Zhao et al., 2018). This method has been conducted in global-scale for the explored black shales.

$$\text{Weighted vector(wj)} = (\text{i} - \text{ej})/\in(\text{i} - \text{ej}) \tag{1}$$

Here ej: range of the entropy values (0−1). *Repository file 1, Section 2* details the entropy method.

3. General points

Shale basins are one of the most significant unconventional natural resources and targets for exploration. Critical parameters for assessing hydrocarbon production and CO2 storability from shales are *(i)* kerogen type/quality; *(ii)* amount and its thermal maturity; *(iii)* inorganic matter; *(iv)* pore attributes, *(v)* depth of shale deposit and *(vi)* thickness of shale layer (review in Hazra et al. 2024). Shale basins contain shales deposited between the Neoproterozoic to Tertiary Periods. Hydrocarbons were generated worldwide during the Caledonian, Hercynian and the Himalayan orogenies (Wu et al., 2023). At several places in North Africa, a major sea-level rise during the Late Ordovician and Early Silurian Periods after the Late Ordovician glaciation of Gondwana led deposition of the shale units (Hasany and Khan, 2012; Yang wt al., 2016). Transgressive black shales all over the world are deposited presumably during or after the retreat of glaciers. The coastal upwelling with the melt of the Hirnanthian (Late Ordovician) ice sheet in North Africa and Arabia deposited organically rich black shales (Heron et al., 2009).

Shale reservoirs are extensively explored presently for hydrocarbon in several countries- the United States and Canada are the two leading countries (Sahai, 2022). Asia has an estimated highest recoverable shale resource with 1948.2 Tcf of recoverable shale gas (wet gas/condensate, dry gas) and 170.43 B bbl of recoverable shale oil (oil/associate) (calculated in this work from Fig. 6 and Table 3). The West Siberian Basin of Russia is the largest shale basin (2201,489.89 km^2) of the world (U.S. Energy Information Administration E.I.A, 2013). The Sirte basin of Libiya and the Illizi basin of Algeria together contains 80 % and 85 % of shale gas and oil, respectively, in North Africa (Macgregor, 1996; Yahi et al., 2001). Since 2013, the United States has been the world's largest producer of petroleum and natural gas (~ 616 Tcf of shale gas and 102 B bbl of shale oil) (Andrews et al., 2009). Almost, every potential shale reservior in North America with potential organic carbon and thermal maturity windows are explored. Amongst them, the Bakken (Montana and North Dakota) and the Eagle Ford tight oil fields (Southern Texas) and Marcellus (Appalachian Basin), Barnett (Texas), and Haynesville (Louisiana, Arkansas, and Texas) shale gas fields rank highest in oil and gas reserves (Hackley and Cardott, 2016). The three basins (Middle Magdalena Valley and Llanos Basin of Colombia, the Maracaibo of Venezuela and the Catatumbo Basin of Colombia) of South America have great prospects of shale oil and gas potential from the Upper Cretaceous marine shales. The Cretaceous La Luna Shale of Maracaibo and Catatumbo Basin are some of the richest petroleum basins having an extensive potential for oil and gas (Comet and Martinez, 2006; Escalona and Mann, 2006). The Bakken shales have remarkable capability of adsorbing CO_2, which is up to 17 mg g^{-1}. Additionally, 15–65 % of hydrocarbon can be extracted from Bakken shales (Jin et al., 2017).

Gas was first extracted from shale in 1825, but interest in shale reservoir grew since 1970s. Shale revolution was accelerated in 2000s in the U.S. (as referred in Sahai, 2022). About 77 % of the world's oil shale resource are found in USA with richest area in Green River deposits of Utah, Colorado and Wyoming (Council, 2010; Kang et al., 2020). As per Claypool et al. (1978), the oil explored from the Phosphoria black shales of Western Interior United States (western Wyoming and adjacent states) is limited to the Cretaceous. ŦThe United States' shale oil and gas production grew from about 11.2104 tonnes of oil equivalent per day (toe/d) to over 300.0104 toe/d between 2007 and 2023 (Mcmahon et al., 2024). The Aguada Bandera and Pozo D-129 Formation of the Golf San Jorge Basin (Argentina) is a Late Cretaceous lacustrine shale with high clay content and is prospective for shale gas (Patrica 1996). According to Kama and Kuchler (2019) and EUOGA (2020), Europe has 49 shale deposits in 82 hydrocarbon basins. These deposits are spread over 21 countries amongst which 15 contain shale gas and oil, 26 and eight basins hold only shale gas and shale oil resources, respectively (Kama and Kuchler, 2019). Poland has a bigger territory of organic-rich shale basins and a good potential in developing a shale industry in Europe (Salygin et al., 2019). The Baltic basin is most prospective in Europe with a high TOC (3.9 %). The Goldwyer Shale (Australia) is the highest shale gas producing unit from the Canning basin.

The Aguada Bandera and Pozo D-129 Formation of the Golf San Jorge Basin (Argentina) is a Late Cretaceous lacustrine shale with high clay content and is prospective for shale gas (Patrica 1996). The Austral or Magallanes Basin in Chile contains Lower Cretaceous marine black shale. According to Kama and Kuchler (2019) and EUOGA (2020), Europe has 49 shale deposits in 82 hydrocarbon basins. These deposits are spread over 21 countries amongst which 15 contain shale gas and oil, 26 and eight basins hold only shale gas and shale oil resources, respectively (Kama and Kuchler, 2019). Poland has a bigger territory of organic-rich shale basins and a good potential in developing a shale industry in Europe (Salygin et al., 2019). The Baltic basin is most prospective in Europe with a high TOC (3.9 %). The Goldwyer Shale (Australia) is the highest shale gas producing unit from the Canning basin.

As per Wu et al. (2023), black shales formed between the Neoproterozoic and the Cambrian Periods are the significant hydrocarbon source rocks in the world. The Chattanooga Late Devonian and Early Mississippian marine black shale contributes to 5 gallons of oil per ton shale and extends for thousands of square miles of North America with 40 ft (12.19 m) of average thickness (Swanson, 1960). The 15 ft (4.57 m) thick Gassaway Member along the Eastern Highland Rim in Tennessee yields 5–17 gallons of oil per ton. The black shale of Los Molles (Middle Jurassic) and Vaca Muerta Formation (Upper Jurassic-Lower Cretaceous) in the Neuquen Basin (Argentina) is a thick organic-rich marine-shale (Capelli et al., 2021). Its total organic carbon

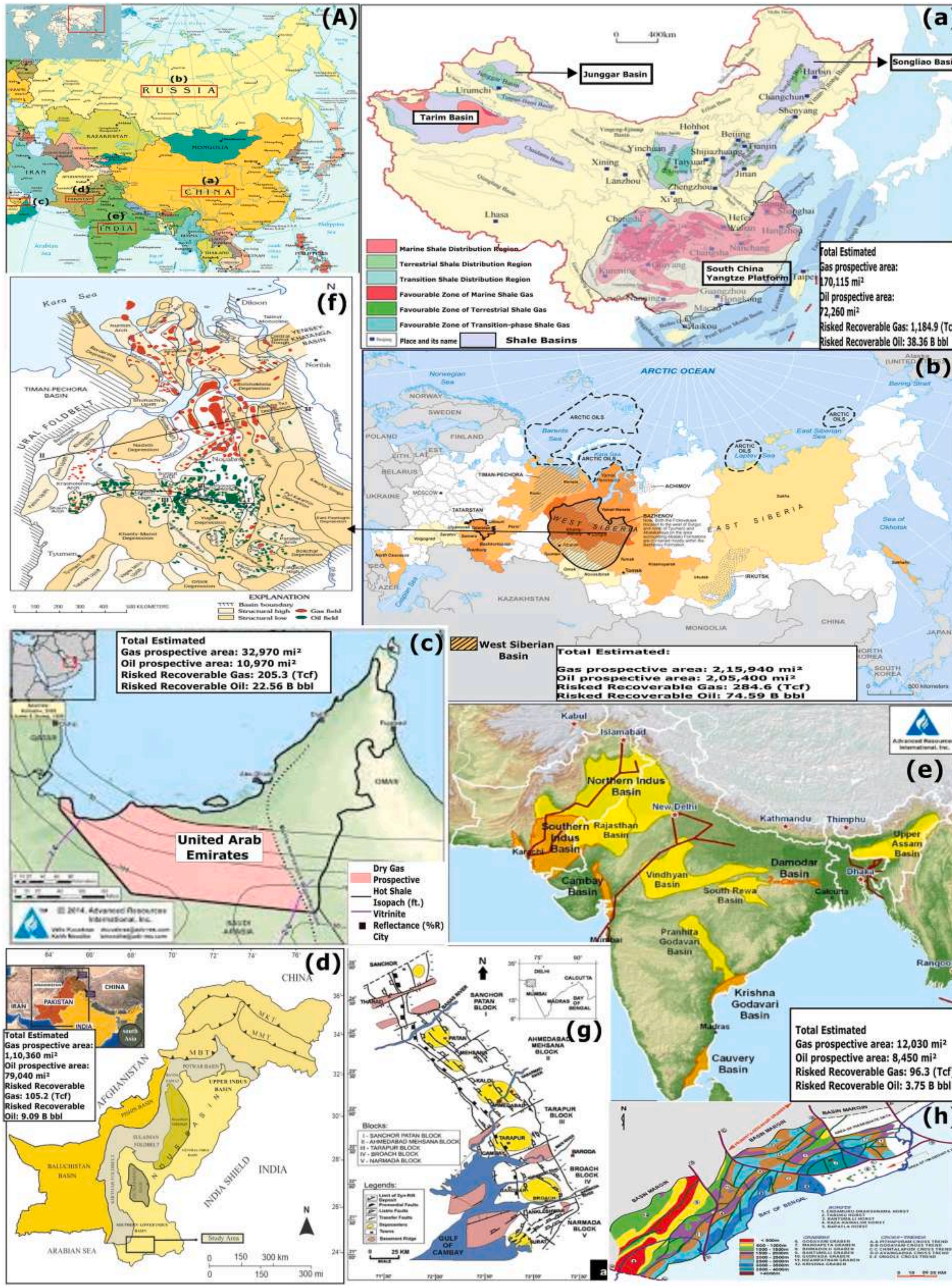

Fig. 3. A. Location details of China, Russia, UAE, Pakistan, and India in the map of Asia (CIA, 2013). **a.** Distribution of different types of shale and prediction of favourable shale gas zones in China (Source: Modified after Dong et al#, 2016). **b.** Location map of Western Siberian Basin in Russia (Source: Modified after Gordan and Sautin, 2013). **c.** Location of the prospective area for Silurian Qusaiba "Hot Shale" in the UAE (USA EIA, 2014). **d.** Location of the Sedimentary basins in Pakistan (Ali et al#, 2021). **e.** Assessed prospective shale gas and shale oil basins in India (Kuuskraa et al#, 2011). **f.** Structural map of West Siberia (Ulmishek, 2003). **g.** The Cambay Basin including the tectonic blocks (Source: Sharma and Sircar, 2020). **h.** Time structure map on top of basement depicting tectonic elements of Krishna Godavari Basin (Source: Gupta, 2006).

(TOC) ranges between 2 and 5 wt% with a thermal maturity of 0.85–2.20 %. The 3300 ft (1005.84 m) thick Los Molles Formation is the source rock for conventional oil and gas deposits in the basin. Its depth ranges from 8,000-14,500 ft (2438.4 – 4419.6 m) with a maximum of 16,000 ft (4876.8 m) in the basin center. It is one of the most prolific resource in South America.

In the Early Jurassic, the Toarcian marine anoxic event played a significant role in sequestrating CO_2 in the shale reservoirs. For example, a lake system in Sichuan Basin with hydrocarbon shale reservoir in China was produced (Xu et al., 2017). The mid Devodian Marcellus black shale in the eastern United States has a total CO_2 storage of 1.6 Mt km^2 (Godec et al., 2013).

The detailed quality and the quantity of the shale deposits are reviewed in Fig. 2a-d. As per Tao and Clarens (2013), Marcellus shale alone can store 10.4–18.4 Gt of CO_2.

4. Specific examples

4.1. Asia

4.1.1. China

It is one of the world's most promising shale gas and oil producing countries, with seven possible shale basins (Sichuan, the Yangtze Platform, Jianghan, Subei, Tarim, Junggar and Songliao) (Fig. 3A). It is estimated to have world's largest shale gas reserves (Boosari et al., 2015). Chinese pre-Devonian shales usually consist of lamalgnites, bituminites and Types II and III TOC (Luo et al., 2025). In Chinese shales, Precambrian to Upper Paleozic examples attainbed maturity in gas window, shallow Quaternary ones have gas potentials and Mesozoic-Cenozoic varieties have shale gas potential, and are in oil window (Jiang 2016). Jian (2016) Chinese shales and conclude that the country's most potential shales are the marine ones with high maturity for gas generation, and lacustrine shanples have low maturity and have gas generation potential. Most non-Chinese oil shales are of marine facies and are mainly of Types I and II varieties (Zou, 2017).The marine deposits of the Sichuan, Jianghan, Subei Basin and the Yangtze platform of Cambrian and Silurian age are known as the South China Shale Corridor. These organic-rich black shale formations occur in south-central and eastern China. Complex folding and faulting define these gas-prone, thermally over-mature basins (Yongsheng, 2020). The Paleozoic shales have the most resource potential in the South China Shale Corridor. The basins in China has an estimated 4 billion tons of storage capacity of natural gas (Wei et al., 2015).

- *Sichuan Basin:* The Sichuan province has ben described as the shale corridor of the SW China (Jiang et al. 2017). These shales are either structurally disturbed or are buried deeper than 4000 m. The shale gas resources in the Sichuan Basin is $\sim 41.5 \times 10^{12}$ m^3, which ranks first for shale gas reserves in China (as referred in Lai et al. (2022). This basin is therefore called as the *Super Gas Basin.* The southwestern zone of the tectonically uplifted petroliferous basin (~ 192, 954 km^2) is the most suitable site for exploration due to its being structurally and tectonically less complex, stable, thermally mature, and thick with suitable depth (Zou et al., 2015; Mengjun et al., 2016). The Tongwan tectonic movement in the Sinian Epoch deposited Sichuan shale within 2000–7000 m depth (Jinliang et al., 2012; Yang et al., 2015). The fine-grained (clay-rich) nature of the shale rock along with its waxy and low permeable nature and high adsorption capacity makes the basin often requires hydraulic fracturing. The natural shear fractures formed under tectonic stress increase the deliverability of shale gas in the basin (Zhao et al., 2023).

  The 1000 ft (304.8 m) thick Longmaxi Formation (Lower Silurian) consists of organic-rich mudrock/shale formations (siliceous to cherty) with 0.77–8.7 % porosity (Liang et al., 2014), $\leq$ 4 % TOC (increases up to 5.35 % with burial depth containing Type I and II kerogen), and 2.4–3.6 % R_O (Chen et al., 2011; Liu et al., 2017; Morozov et al., 2021). It is over-matured in the Changning section of the basin with Ro = 2.8–3.3 % is a source to typically dry gas (Ziqi et al., 2016; Zhang et al., 2017). The shale predominantly consists of clay (30–65 % illite/smectite, illite and chlorite), quartz, carbonates, graptolites with feldspar, and pyrite (Liang et al., 2014; Shu et al., 2019; Wang et al., 2019). The significant gas resource lies in the 50 m thick layer of shale at the bottom of the formation (Chen et al., 2011). The Longmaxi Formation of the Sichuan basin has an estimated 286.5 Tcf of recoverable shale gas and 0.04 B bbl of recoverable shale oil (USA EIA, 2013).

  The 230–600 m thick Qiongzhusi Formation contains organic-rich black shale deposited in a deep-water lacustrine anoxic environment ranging from black-dark grey sandy shales to dark grey-grey silty shales (Jinliang et al., 2012). It has a high-temperature gradient with an average TOC of 2.0 % and thermal maturity ranging from 2.5 % to 5 % (Wang et al., 2014). However, commercial-scale recovery for shale oil has been slow compared to other global shale oil plays due to technical challenges. It is a shallow marine Cambrian deposit containing 120 m thick hot shale with ample fractures. Radioactive shales are termed as "hot shales" (Gluyas and Swarbick, 2004). It has an estimated 287 Tcf of recoverable gas out of 1146 Tcf of risked gas (USA EIA, 2013). The 314 ft (95.71 m) Qiongzhusi black shale is the source rock for the Weiyuan gas field in the southern Sichuan Basin, which extends from the central to the SE portion of the Sichuan Basin. Dry gas is the major resource of this formation, with an average R_O of 2.5 % and a TOC of 4 % (Zhang et al., 2022). It has a potential of 500 Tcf risked shale gas. The Permian formations of the basin estimate 215 Tcf of recoverable gas out of 715 Tcf of estimated total gas.

  CO_2 entrapped within the Sichuan Basin happened since thermal decomposition of the carbonates ($\delta^{13}C_{CO2} = 0 \pm z3$ % ranging from -5.45 to -16.99 %) during tectono-thermal events involved organic matter within the Wufeng-Longmaxi Formation shale (Tang et al., 2015; Yin et al., 2017). According to Zhao et al. (2020), CO_2 is naturally present and is distributed evenly within the middle layers of the shale reservoir. It is distributed unevenly within the upper and bottom layers due to its heterogeneous properties, e.g., pore orientation and connectivity. The Wufeng-Longmaxi Formation has a shale gas resource of $\sim 3.78{*}10^{12}$ m^3 (as referred in Wang et al., 2024). The abandoned shale gas wells in Sichuan basins have been targeted for injection of CO_2 (Lai et al., 2022). The carbon sequestration is highest within 1280–1300 m depth (Liu et al., 2020; Zhao et al., 2020). The carbon capture in this basin exhibits the Toarcin oceanic anoxic event (~ 183 Ma) in a super-large lake system where CO_2 got trapped during the greenhouse warming due to excessive weathering of the Ca-Mg silicates (Xu et al., 2017). CCS potential of Sichuan basin has been estimated to be 348 Gt of CO_2 (as referred in Wang et al., 2024). It is interesting to note that the highest adsorption capacity of the Sichuan shale is primarily controlled by the shale's TOC content, whereas the clay content has a negligable effect (Hu et al., 2022).
- *The Yangtze Platform:* The structurally complex and tectonically stable basin of 1582,482.74 km^2 has strata of ages such as Silurian, Ordovician, Cambrian that got deposited in an anoxic environment (Holland, 1990; Cai et al., 2016; Zhang et al., 2019). The platform extends across the Sichuan, Yunnan, Guizhou, Hubei and western Hunan provinces of South China. It consists of several potential shale gas basins. These consist of Doushantuo and Liuchapo Formations (Ediacaran/Upper Sinian), Xiaoyanxi Formation (Lower Cambrian), Niutitang Formation (Early Cambrian), Jiumenchong Formation, Bianmachong Formation, Palang and Wufeng Formation (Ordovician), Longmaxi Formation (Lower Silurian), and Longtan Formation (Upper Permian) with an average TOC of 2.7 %, porosity of 5.84 % (pore size < 2 nm), 38.3 % of quartz, and 36.2 % clay and micas (Chen et al., 2017; Zhang et al., 2019; Wang et al., 2019). Brittle shale formations developed natural fractures (Tan et al., 2014),

which are beneficial for hydraulic fracturing-related operations (Zhang et al., 2019).

The upper Yangtze Platform in South China has a high shale gas potential, with TOC ranging between 0.92 % and 4.96 % in the Lower Silurian and high biogenic quartz (30.6–69.5 %) and clay content (24.1–51.2 %) (Tan et al., 2014; Chen et al., 2017). The Lower Silurian (Longmaxi Formation) strata is composed of marine black shale deposited during a significant marine transgression in the Early Silurian (Ji et al., 2019). Its adsorption capacity increases with increasing TOC% (Tan et al., 2014). The Early Cambrian Niutitang Formation has a massive deposition of carbon-rich black marine shale at 3251–3436.08 m depth with a TOC ranging between 0.18 % and 9.73 % with Type I kerogen, Ro > 2.5 %, porosity between 0.8 % and 6.2 % and a sedimentation rate of ~ 0.09 ± 0.03 mm yr^{-1} (Wu et al., 2016; Li et al., 2016; Li et al., 2020). The siliceous shale has larger pore structures that stores shale gas (Wang et al., 2017).

The Lower Cambrian black shales located in the Xiang-Qian back-arc of the central Yangtze platform were formed in a subtidal environment dominated by current and low-energy (Xiaofeng et al., 1998). The 100-m-thick Late Cambrian black shale of the Xiaoyanxi Formation or Shuijingtuo platform is composed of siliceous minerals with moderate clay content (Tan et al., 2014). It has an average TOC of 7.5 % by weight. The platform has so far remained unmapped in (sub)surface. It has an estimated 149 Tcf out of 596 Tcf of recoverable gas (USA EIA, 2013). The platform covers the entire drainage basin of the Yangtze River, including the southern portion of the Yellow Sea (Holland, 1990). The Paleozoic section in the platform is tectonically deformed and partly eroded. The Doushantuo Shale of the Middle Yangtze Platform has recently attracted attention due to its unique kerogen, bitumen pore structure and methane adsorption potential (Wei et al., 2021).

The Early Cambrian transgression on the Yangtze Plate developed organic carbon pool and carbon capture by photosynthetic microorganisms. Cyanobacteria, algae and archaea were the main contributors (Wu et al., 2016). The biomarkers for terpenoids and steranes show that algae constitute a significant source of organic matter. These indicates a sedimentary environment within a deep anoxic maritime shelf. As a result, the redox environment of the Upper Yangtze shallow sea during the Early Cambrian favoured burial of organic materials (Wu et al., 2016; Yang and Pan, 2023).

- *Jianghan Basin:* The Jianghan Basin is a pre-Cretaceous salt-bearing rift basin covering the central part of the Yangtze Platform near Wuhan. It is bounded by faults and has ~ 37554.828 km^2 area (Peng et al., 2013). The basin got faulted during the Cretaceous-Paleogene due to the Yanshan movement. It has gone through two fault depression cycles, primarily leading to the development of the Xingouzui Formation and Qianjiang Formation source and reservoir series (Zhang et al., 2021). The basin has ~ 4–5 km of thick Lower Paleozoic shale. The Lower Silurian Longmaxi (120 m) and the Permian Qixia Formation are marine Paleozoic source rocks, occurring at a shallow depth of 9000 ft (2743.2 m), and are dry-gas-prone, with TOC 2.0 % and thermal maturity ~ 1.5 %. The Lower Silurian consists of black, thin-to-moderate siliceous shale layers. It has an estimated 7 Tcf and the Permian has 10 Tcf of recoverable shale gas. The Qixia Formation has a potential oil reservoir with an estimated recoverable oil of 0.1–1 B bbl. The Lower Cambrian Shuijintuo Formation is the deepest (13,000 ft, 3962.4 m) dry-gas prone unit. The dry-gas in the formation is found at 11,500 ft (3505.2 m) depth. The R_O ranges from 1.5 % to 2.5 % and indicates an overmature unit in the northwest with 3.5–5 % of R_O. It is best matured in the central and southeast Sichuan Basin, with a height of 314 ft (95.71 m), TOC 2–6 %, and R_O 2.0–3.0 %. It has an estimated 46 Tcf recoverable gas out of 149 Tcf (USA EIA, 2013).

The Upper Eocene saline lacustrine Qianjiang shale Formation is formed in the Qianjiang depression (2500 km^2) by several hundred of cyclotherms, resulting in alternate bedding of salt and mudstone (Li et al., 2018; Zang et al., 2018).The inter-salt oil play's reservoir properties and production have been of interest to many researchers in recent times (Zang et al., 2018).The silica-rich carbonate and siliceous mudstones contain an average TOC of 3.5 % with an Ro between 0.8 % and 1.3 %, HI index between 31 and 259 mg HC g^{-1} TOC, porosity ranging from 2.8 % to 30.6 %, average Tmax of 432 ^{0}C and oil-prone kerogen (Hou et al., 2017; Ma et al., 2019). The oil shale is the main hydrocarbon reservoir of the formation with laminated glauberite (Li et al., 2018). The third round of the Chinese National Petroleum Resource Assessment estimated 9.078 billion tons of oil in the basin, out of which only 5 % could be recovered (Li et al., 2018).

As the basin rocks has rich carbonate and low clay content, the rocks are brittle. In the Qianjiang depression, the presence of widespread cracks, tectonic fractures developed a flow-path network (Li et al., 2022). Large inorganic pores and intense micro-factures contribute to the pore network, resulting in a saline shale reservoir with a reasonably high porosity (2.8–30.6 %) and permeability (0.045–6.27 md), which might improve the flow ability and storage capacity of oil (Hou et al., 2017).

The CO_2 in the basin was sequestrated in deep saline aquifers, invaded into the cap-rock and flows through open fractures of deflection, branching and approaching types (Tian et al., 2013; Zhang et al., 2019). Salt acts as a seal that precludes vertical movement of hydrocarbons and initiates lateral migration (Hou et al., 2017). An excessive pressure gradient often aggravates leakage between the storage and the overlaying geologic unit (Qi et al., 2014).

- *The Great Subei Basin:* The basin is located near the shore in Jiangsu Province, north of Shanghai, East China, in the lowest part of the Yangtze Platform, covering ~ 3625.983 km^2 area (Peng et al., 2023). The Mesozoic-Cenozoic basin is structurally complex, consisting of major faults and the deposition of sedimentary layers. The Jiangsu Basin is the largest conventional oil field among all shale in the Upper Permian, Lower Silurian and Lower Cambrian Periods in the Changxing/Talung, Gaojiabian, Wufeng, Funing and Mufushan Formations of the basin (Qi, 2002).

The Funing Formation, located in the transgressive system tract (deep lake), has layers of thick, black shale that accumulated related to active fault depression (Wang et al., 2023). The 2363 m thick Lower Cambrian Mufushan Fm (prospective area: 5283.576 km^2, 2040 mi^2) consists of low to moderately organic-rich black shale with an average thickness of 120 m, TOC of 2.1 % with gas-prone kerogens of Types I and II at 4–5 km depth. It has an estimated 7 Tcf of recoverable gas. The Lower Silurian siliceous shale in the Gaojiabian Formation (38, 823.922 km^2, 14,990 mi^2) has a lower TOC (0.6–1.3 %) and is gas-prone at 3.5–5 km depth. The Upper Ordovician 4–214 m thick Wufeng Fm consists of grey and black siliceous shales and fossiliferous mudstones (Wang et al., 2019). The formation is thick and has an estimated average of 36 Tcf of risked shale gas. The siliceous shale of the Upper Permian Changxing/Talung is gas-prone at 1–2.5 km depth. It holds a potential of 8 Tcf gas and 1 B bbl of oil in the poorly defined formation.

The generation of veins, dissolution pores, and fractures formed during successive tectonic episodes such as Wubao and Sanduo movements is observed in the shale sequences (Su et al., 2022; Wang et al., 2023). The basin has a capacity to store ~ 21 Mt. of CO_2 in 108 hydrocarbon oil fields (Pearce et al., 2011).

Tarim Basin: Sharing a border with eastern Kyrgyzstan, the basin is located in the far northwest of China's Xinjiang Autonomous Region, between 36 and 42° N and 75 and 93° E. Between the orogenic belts of Tianshan and Kunlun, it is the biggest superimposed onshore diamond-shaped sedimentary basin in China (Wang, 1992; Liu et al., 2017). The Altun Fault defines the basin's southeast border. It features ~ 200 km long shear zone. The North Kunlun and Karakoram mountains' compressional and transpressional fault systems define the W and SW limits (Tian, 1983; Wang et al., 1992). The southern boundary of the basin is overridden by the South Tianshan Thrust and the Kurutktag transpressional slip fault in the west (Nishidai and Berry, 1988; Wang et al., 1992). According to Jia and Wei (2002), the basin contains seven structural depression zones running from north to south, viz., Kuqa, Tanan Uplift, Tabei Uplift, North Depression, Tazhong Uplift, Southwest and Southeast Depressions. According to the USA EIA (2013), these raised zones have good potentials for commercial shale production. As per USA EIA (2013), these raised zones have good potentials for commercial shale production with the entire basin having 215.9 Tcf of recoverable gas and 8.02 B bbl of recoverable shale oil.

The Cambrian and Ordovician marine black shales are the most potential source rocks in the Tarim basin (Cai et al., 2009). These rocks contain kerogen, macerals (vitrinite-like) and bitumen through the TOC, which varies in the depression (7 %) and the uplift (1–2 %) zones. The 28,308.57 km^2 (10,930 mi^2) Heituao (O_{1-2}) Formation of the Upper Ordovician Period is 48–63 m thick and brittle with TOC 0.63–2.51 %, T_{max} ranges 382–523̊ ^{0}C, porosity 0.067–1.304 % and thermal maturity 0.9 % with Type III kerogen (Jiang et al., 2018; Zhao et al., 2021). The Heituao shale in Tadong's low uplift has the potential for shale gas production, and the BI ranges between 0.28 and 0.99 (average = 0.85) (Zhao et al., 2021). The 10–30 m thick black marine mudstone of Middle Ordovician Yijianfang (O_2) Formation measures TOC 0.56–2.86 % (Lan et al., 2009). The 50,297.569 km^2 (19,420 mi^2) Lower Ordovician Lianglitage unit (O_3) with 20–80 m thickness consists of carbonate-rich shale with TOC 0.93 % (average) and a thermal maturity of 1.8 %. The unit is located in the Central Tarim, Bachu and Tabei areas of East China. The formation holds a potential of 1.6 B bbl of recoverable oil out of 3 B bbl of shale oil and 94 Tcf recoverable gas out of 377 Tcf shale gas (USA EIA 2013).

The entire Ordovician group of the Tarim basin, with R_O ranging from 2.0 % to 2.6 % is prone to dry-gas (Lan et al., 2009). The Lower Cambrian Xiaoerbulake (16,886.72 km^2, 6520 mi^2 prospective area) consists of 120–415 m thick shales and siliceous rocks with 2.6–2.9 % in the dry-gas thermal maturity window (Qiao et al., 2019). It has an estimated 44 Tcf out of 176 Tcf of recoverable shale gas. The 41, 232.611 km^2 (15,920 mi^2) Late Triassic Ketuer Formation is oil-gas-prone at ~ 400 ft (121.92 m) depth measuring high TOC and 0.9 % R_O. It has an estimated 6.5 B bbl of recoverable shale oil out of 129 B bbl and 16 Tcf out of 161 Tcf of shale gas in-place (USA EIA, 2013). The Middle-Upper Triassic Taliqike Formation, the Hauangshanjie Formation and the Karamay Formation shales in the Kuqa Depression of the basin are the new targets for shale gas exploration. Cumulatively, they measure an average TOC of 2.68 % and Ro > 1 % from a 260 m thick Type III kerogen (Wang et al., 2014). The TOC of the Jurassic black shale in the foreland Kuqa Depression ranges ~ 0.08–28.48 %, Ro within 0.52–1.57 % and is in the form of kerogen Type III with abundant micro-pores suitable to adsorb gas (Jiang et al., 2018; Qu et al., 2019). The estimated volume of shale gas is $6.04 * 10^{12}$ m^3 (Wang et al., 2014).

The Jurassic terrestrial black lacustrine shale in the northern Kashi Sag is > 100 m thick and has an average TOC content of 2.77 % (Yong, 1983; Wu et al., 2021). The Lower Jurassic shale organic matter is in the early-mature stage, according to the vitrinite reflectance values (1.3–1.8 %), whereas the Middle Jurassic is in the mature to highly mature stage (TOC ranging upto 13.5 %) (Li et al., 2015). Additionally, organic matter mostly belongs to kerogen types II and III. Illite is present in the entire shale. The BI is 38.63 % on average (Wang et al., 2013; Wu et al., 2021). The Jurassic shales have well-developed nanoscale pores, including intergranular pores, dissolution pores and organic pores, together with microcracks. According to Wu et al. (2021), the Jurassic terrestrial shale has good-to-excellent shale gas exploration potential and development prospects.

According to Wu et al. (2023), the Neoproterozoic-Cambrian Tabei type, black shale is in the early stages of producing oil and gas with Ro between 1.0 % and 1.5 %. The thickness ranges from 10 to 25 m (TOC 2–17 %) in the Aksu region and ~ 180 m in the Kuruktag region. The water conditions around the carbonated platform in Tabei (the transpormation of Tabei uplit to the carbonated platform during the late Sinian and early Cambrian) initiated black shale deposition (Wu et al., 2021 a, b; 2022 a, b). The depth of the formation varies from 4400 to 6400 m in its western section and is > 8000 m in the northern slope.

Regarding feasibility of carbon sequestration in the Tarim Basin, no specific studies have been undertaken so far. With the enormous shale gas deposits in this basin, however, it can be stated that the carbon sequestration in the structural depression zones is due to the burial of the plants at different tectonic episodes.

Junggar Basin: The second largest asymmetric saline cratonic basin is situated in the Xinjiang region of NW China at the intersection of the Kazakhastan, Siberian, and Tarim plates (Cao et al., 2016; Ma et al., 2021). The inland basin gently dips towards the north, west, and east, with an overthrust defining the southern margin (Bian et al., 2010). The gentle dip with few faults characterises the basin as more structurally simpler than the other basins of China. The majority of the southern edge of the basin has a moderate slope and with lesser number of faults. Such a basic structure is thought to be advantageous for the production of shale gas and oil (Qiu et al., 2008). The static BI varies in the basin. According to Feng et al. (2018), the reservoir exhibits good brittleness when the static BI exceeds 85 and the Poisson's ratio is < 0.2. The reservoir displays mild brittleness when the static BI and Poisson's ratio are equal to each other, thus making it favourable for shale oil and gas exploration.

4.1.1.1.

The middle Permian Formation is the prime source rock, followed by the Triassic, covering ~ 19,165.91 km^2 area. They are mainly deposited in the inland fluvial environment of the Jimsar sag (Wang et al., 2019). The liquid-rich Permian rock is considered the richest source rock in the world with TOC ≤ 20 % (average of 3.49 % and highest in the shales bedded with organic matter of Type I and II kerogens), R_O = 0.7–1.3 %, T_{max} = 428–454̊ C, HI = 213–587 mg/g, and over-pressured at a depth of 2–5 km (Carroll, 1998; Luo et al., 2018; Pang et al., 2018; Wu et al., 2019). The lacustrine, 1200 m thick Permian Pingdiquan/Lucaogou Formation consists of oil shales between 50 and 650 m depth, characterised by different oil-bearing grades (oil trace, oils pot and oil stain) (Wang et al., 2019). The shale porosity ranges from 1.1 % to 13.9 % (Xiaoqi et al., 2015; Hu et al., 2017). The mudstone and shale of the formation estimate 5.4 out of 109 B bbl of shale oil. The Pingdiquan Formation holds 17 Tcf of 172 Tcf recoverable gas. The southeastern part of the Junggar Basin consists of non-commercial thick and > 5 km deep Permian and Jurassic shales. The Jurassic Xishanyao shale formation has an average TOC of 1.54 %, T_{max} ranging between 429 and 443̊ ^{0}C with high contents of clay and quartz (Liu et al., 2021). The 820 ft (249.94 m) thick Triassic formation at ~ 10,000 ft (3048 m) measures TOC 4 % and R_O 0.85 % in the oil window. It has an estimated 6.7 B bbl out of 134 B bbl of recoverable shale oil and 19 Tcf out of 187 Tcf of recoverable shale gas (USA EIA, 2013).

The basin has recorded several tectonic events, marine to terrestrial sedimentary environment and paleoclimatic evolutions. An average of 11.2 Gc m^{-2} yr^{-1} of organic carbon burial for ~ 3 Ma has been deciphered from the Lucaogou Formation (Gao et al., 2019). The Permian strata recorded the evolution of stratified saline to fresh lake environments and carbon sinks in the large Permian lakes. It is accompanied by a dry and humid climate in the Early and Mid-late Permian with slow tectonic subsidence (Gao et al., 2019).

About 60 m thick mudstone / shale dominated Donggou Formation can act as a caprock for CO_2 storage in saline aquifers. Rocks with low shale content can be used as reservoirs of CO_2 (Ma et al., 2021).

Songliao Basin: It is the largest non-marine, intracontinental oil potential basin of NE China with 279,718.716 km^2 (1,08,000 mi^2) area (Gao et al., 2015). An entire Cretaceous lacustrine continental predominantly fine-grained clastics with 86 Ma of duration of deposition makes the basin unique (Wang et al., 2017; Han et al., 2022). The basin in structurally complex. Tectonically, it contains six structural units (the northern plunge, the central downwrap, the NE uplift, the SE and SW uplift and the western slope) (Bian et al., 2010; Feng et al., 2010). The main oil-gas-producing potential rocks lie in the central-downwrap unit (Wang et al., 2015). According to Han et al. (2022), the shale interval in this basin measures an average BI of 55.10 %, average porosity of 45.8 %, where the majority of pores are inorganic intergranular meso-pores, dissolved pores and microcracks devoid of organic pores (Wang et al., 2022). The Qingshankou Formation of the basin underwent 133 drilling until 2020, of which 68 had oil and gas indications and 30 had significant oil flow with a maximum daily output of 40 m^3 d^{-1} (Liu et al., 2021c).

The Daqing complex of the unit produces ~ 800,000 B bbl $d^{-1}$of oil (USA EIA, 2013; Wang et al., 2015). The Lower Cretaceous Nenjiang, Yaojia and Qingshankou Formations (Qing I member) in the Gulong Sag consist of deep-water lacustrine black mudstone and shale with layered gray siltstone containg a high proportion of clay (Zhang et al., 2020). Their pore volumes are directly related to the TOC of the formations, < 50 nm diameter of the meso-pores, average porosity of 7.57 %, with high hydrocarbon fractions ranging between 48 % and 89 % (Wang et al., 2015; He et al., 2019; Liu et al., 2019; Cao et al., 2020). The formation has a low N_2 (2–80 nm), low CO_2 (< 2 nm) adsorption and mercury injection capillary pressure of > 80 nm (Han et al., 2019; Han et al., 2020). The formation holds 229 B bbl of shale oil in-place. It is prospective of 155 Tcf gas in-place (USA EIA, 2013).

The Nenjiang and the Qingshankou Formation are 70–240 and 80–420 m thick, respectively, at a depth of 300–2500 m with TOC ≤ 13 %, T_{max} ranging between 410 and 459̊ ^{0}C and pore volume within 0.045–0.131 cm^3 g^{-1} (Caineng et al., 2010; Liu et al., 2019; Liang et al., 2021). The Nen I and II Member act as caprock /seal for the Heidimiao and Sa'artu oilfield payzones, whereas the Qinqshankou mudstones are the caprock that seals the carbon sequestrated in the formation (Pearce et al., 2011). The Qingshankou Formation is thermally mature (0.43–1.5 %) and within the oil to wet gas windows, measuring HI between 639 and 934 mg g^{-1} with Type I and II kerogens (Huang et al., 2013; USA EIA, 2013; Liu et al., 2018; Hou et al., 2020). As per Zhang et al. (2015), the southern section of the basin is the shale oil sweet-spot, characterized by extensive fracturing and with ~ 2880 km^2 area. It can be an ideal location for shale oil exploration. The Early Cretaceous Shahezi Formation consists of dark gray-grayish black muddy shales. It is clay-rich within 78–477 m depth with TOC ranging between ~3.61–4.01 %, T_{max} between 433 and 445̊ C and consists of Type III kerogen (Wang et al., 2016; Liu et al., 2019).

With the total CO_2 storage capacity between 457.5 and 5114.5 m (mineral trapping), the CO_2 in the deep saline aquifers of the Songliao basin was potentially sequestrated for an extensive time period (Jin et al., 2017). The basin contains the largest oil and gas fields. Daqing and Jilin, the two locations, have geologic carbon storage capacities of 593 Mt and 71.2 Mt, respectively (Pearce et al., 2011). The emergence of Quanton Formation-Nenjiang Formation and Yaoji Formation (first member) and Qingshankou Formation (first-third member) formed strata during the expansion, shrinkage and leakage issues of the lake in the basin. Between these strata are the delta sandbodies and carbon capture pits (Jin et al., 2017). Within the paleolake, ~ 318 m thick dark mudstones and sand bodies are the storehouses of CO_2 with the mudstone as the caprock (Jin et al., 2017). A huge amount of CO_2 can be sequestrated, which decreases with increasing solubility during migration and diffusion of the CO_2 plume (Zhang et al., 2009).

4.1.2. Russia

The West Siberian basin is the largest petroleum basin in Russia with ~ 2201,490 km^2 (850,000 mi^2) area bounded by the Ural Mountains, Yenisey River, the Kara Sea and Kazakhstan in the west, east, north and south, respectively (Salygin et al., 2019) (Fig. 3b). The O-C rich siliceous shale of the West Siberia basin is the potential source rock of hydrocarbon production in Russia at a depth of 2220–2500 m (Shaldybin et al., 2017). It is dominated by biogenic silica from radiolarite and carbonate minerals with hydraulic characteristics, i.e., siliceous low-clay with 4.81–15.17 % porosity and 0.05–2.66 md permeability (Khamidullin et al., 2012; Balushkina and Kalmykov, 2016; Shaldybin et al., 2017). The reservoir belt is situated along fault planes. The primary oil movement was concentrated at the fault zone bordering fracture networks (Lopatin et al., 2003).

The Upper Jurassic Bazhenov shale is divided into two zones: North Bazhenov and Central Bazhenov (Gocharov et al., 2014). The northern Bazhenov region (Fig. 3c) of 258,325.41 km^2 (99,740 mi^2) area contains oil and wet/dry gas at ~ 16,400 ft (4998.72 m) depth with an average thickness of 110 ft (33.528 m). It has an average TOC of 2.1–20 %, R_O 0.7–1.3 %, HI = 233–794 mg, Tmax between 429 and 446° ^{0}C with a high-temperature gradient, and low clay content (Kontorovich et al., 1975; Skvortsov et al., 2016). Highest organic carbon is found from the Koltogory trough, the Frolov, Nadym and Yungan basins (Zumberge et al., 2014). The Central Bazhenov (300957 km^2, 1,16,200 mi^2) is oil-prone with an average TOC of 10 %. It measures 13 MM bbl mi^{-2} of oil, 4 MM bbl mi^{-2} and 42 Bcf mi^{-2} of wet/condensate gas window and 66 Bcf/mi^2 in the dry gas window (USA EIA, 2013). The European Union depends on Russia for shale oil and gas resource (Salygin et al., 2019). The REPowerEU actions in the European commission states a decrease in its dependency on Russian fossil fuels to support Ukraine.

Data for carbon sequestration is not available from the Russian basins.

4.1.3. United Arab Emirates (UAE)

The Rub' Al-Khali is the most important prospective basin for shale oil and gas sourced from the Qusaiba, Diyab and Shilaif Formation (Fig. 3d). Located at the base of the Qalibah Formation at 14,000 – 16,400 ft (4267.2–4998.72 m) deep, the Lower Silurian Qusaiba 'hot' shale developed in an anoxic marine setting. It encompasses 33722 km^2 (13,020 mi^2) area with 25–150 ft (7.62–45.72 m) thickness in the north to the south-central UAE. Its kerogen is type II with TOC between 4 % and 12 %, and Ro > 2.6 % (Ba Geri et al., 2019). According to Alghamdi et al. (2023), the primary variables controlling the micro-scale pore systems within the studied samples from Qusaiba shale are intergranular inorganic. Their fracture pores are regulated by the input of siliciclastic and mica. It has an estimated 248 Tcf of dry gas where 62 Tcf is technically recoverable (USA EIA, 2014).

The Upper Jurassic marine Diyab Formation consists of organic-rich "tight" carbonate argillaceous lime mudstone in the central UAE. The eastern UAE Diyab Formation consists of low organic packstones and grainstones (Al-Suwaidi et al., 2000). The topmost unit of the lower member of the formation placed in the eastern portion of the onshore UAE is the organic-rich source rock of the formation. The lower member of the formation consists of dark grey limestone and calcereous shale. The formation consists of Type II kerogen that is amorphous in nature including marine sapropelic kerogen in the prospective area of 9,500-13, 000 ft (2895.60–3962.40 m) (Al Hassani et al., 2023). The TOC ranges from 2 % to 3 % with a dry gas in the center and a wet gas window in the SE and northern part of the basin (Baig et al., 2017). The Ro varies, >1.3 % and 0.7–1.3 %, in both the windows, respectively, with a decrease towards offshore. The temperature gradient in the unit ranges from 1.5 to 2.5° F per 100 ft (= −0.54 to −0.55 ^{0}C m^{-1}). Around 123 Tcf of shale gas out of 409 Tcf and 0.5 Bbl of recoverable oil/condensate out of 11 MM bbl/mi^2 have been recovered (USA EIA 2014).

The Middle Cretaceous marine organic-rich Shilaif Formation is characterized by laminated bituminous carbonaceous marl and pelagic lime mudstone and are deposited in a deeper intra-shelf basin (USA EIA 2014, Laer et al. 2019). It is a member of the Wasi Group with an onshore prospective area of ~ 25,045.19 km^2 (9670 mi^2) at a depth range of 3,500-11,000 ft (1066.8–3352.8 m) (Alzabi et al., 2018). The geologic setting of the basin is inherited from the NW-SE compression by Indian plate's drift from Late Cretaceous to Early Eocene. The NE-compression reactivated during Late Tertiary Epoch. This resulted in anticlines and synclines. The synclines of Abu Dhabi have a thermal maturity of 1.1 % (Laer et al. 2019, Lazreq et al. 2020). It has a TOC value of 1–6 % on an average, Ro 0.6–0.8 %, and a thermal gradient of 1.5–2.5° F per 100 ft. The folds host 58 MM bbl mi^{-2} of oil and 157 Tcf of gas (USA EIA 2014).

According to Ye et al. (2023), geologic CO_2 storage potential exists in the Saudi Arabia's depleted oil and gas reserves. Structures such as the Wajid graben were produced during the Ediacaran to Early Cambrian extension. These basins plausibly contain continental clastics and volcanics. Continental to marine siliciclastic deposits accumulated all across the Arabian platform between the Cambrian and the Devonian Periods. Enormous hydrocarbon resources are found in the Phanerozoic deposits of the Arabian platform.

4.1.4. Pakistan

Pakistan has been facing challenges in meeting its growing energy with the rising demand due to its increasing population. The southern and the central portion of the Indus Basin (235,688.92 km^2, 91,000 mi^2) are the main hydrocarbon potential shale oil and shale gas basins in Pakistan (Fig. 3e). It is bordered by the Indian shield at east and Sulaiman mountain in the west. The Lower Cretaceous Sembar Formation, developed under an open-marine environment, is the primary source rock for shale oil and gas exploration (Quadri and Shuaib, 1968). It is 250 ft (76.2 m) (net) thick and consists of shale, silty shale and marl at the western and north-western sections of the basin.

The mineral composition of the formation is composed of quartz (42 %), clay (47 %), calcite (10 %) and pyrite (1 %) (Ahmad et al., 2013). It contains TOC of 1–4 %, thermal maturity > 1.35 % for dry gas, 1.0–1.3 % for wet gas/condensate, and 0.7–1.0 % for oil with type II and III kerogen (Sheikh et al., 2017; Aziz et al., 2018; Ghulam et al., 2020). Its porosity ranges up to 10 % (Sohail et al., 2020). 101 Tcf out of 531 Tcf shale gas in-place and 5.8 B bbl out of 145 B bbl of shale oil in-place is estimated to have recovered (USA EIA, 2014).

The Cretaceous Talhar Shale in Badin is the prospective shale gas reservoir in the Indus basin. It is a part of the Lower Goru Formation. This stratigraphic unit has also been documented in India in the Mesozoic basins of western Rajasthan (Dasgupta et al., 2022). Badin is located in the Sindh monocline. It was deposited in a deltaic setting and comprises of Type II and III kerogen with 0.5–3.5 % TOC, porosity of 0.02–15.7 %, level of maturity index is 0.54 and 0.5–0.55 % Ro (Ehsan et al., 2016; Abid et al., 2021). SSS It is 24 m thick in the SE and 80 m in the SW of the Badin Block at 2,700-3500 m depth (Haider et al., 2012; Mahmood et al., 2018). The Talhar Shale is at the onset of oil generation, and holds significant potential as a source in the study area (Ehsan et al., 2016).

The lacustrine Patala Formation in the Kotah-Potwar Plateau is a fossiliferous prospective shale gas reservoir with several tectonic events making it structurally complex. According to Ali et al. (2017), the basin experienced rapid subsidence from 60 Ma (initial stage) till 35 Ma and then uplited at an average rate of 123 m Ma^{-1} between 35 and 26 Ma. Subsidence during 26–23 Ma and from 11 Ma up to the recent initiated depositions of sediments and increase in temperature forming the hydrocarbon-rich 3738 m deep Lower Sakaser and 3967 m deep Patala Formation (Javed et al., 2023). With the rapid subsidence and temperature rise (64° C), mature hydrocarbons (as oil) generated within the Patala Formation (Ali et al., 2017). It has tight limestone strata with < 3 % porosity, low permeability, high density, and > 30 m thickness at < 2500 m burial depth. It has > 2 % TOC and a high thermal maturity (416–445 °C) (Yasin et al. 2021).

The shales of the Paleocene Ranikot Formation consist of dolomitic shale and becomes the Korara shale with deep marine deposition (Asghar et al., 2022). Dominated by sandstone and shale facies, it encompasses an area of 69,359.882 km^2 (26,780 mi^2), a net thickness of 200 ft (60.96 m), and is oil prone with Ro of 0.7–1.7 % and TOC of 0.65–37.62 % with an average TOC of the Ranikot shale of 4.6 %, Ro of 0.7–1.7 % and II-III kerogen type (Ahmad et al., 2005; Haider et al., 2012). (Ahmad et al., 2005; Haider et al., 2012). It has an estimated 17 Bcf mi^{-2} of wet gas and 25 MM bbl mi^{-2} of shale oil/condensate out of which 4 Tcf of wet shale gas and 3.3 B bbl of shale oil/condensate is recovered (USA EIA, 2014). The Laki Formation in the southern section of the Indus Basin is a prospective of hydrocarbon resource with TOC ranging from 0.53 % to 2.66 %, Type III kerogen. It is brittle with high content of quartz and carbonates (Asghar et al. 2021).

Carbon sequestration in the basins are observed in the tight carbonate rocks with ~ 3 % porosity (Mahesar et al., 2020).

4.1.5. India

India has the four most potential hydrocarbon thermally matured shale basins with recoverable shales gas 96.3 Tcf of shale gas and 3.75 B bbl of shale oil (Singh et al., 2018). As per a 2017 report, 8.5–59.5 trillion m^3 of shale gas reserve is present in India (as referred in Sharma et al., 2019). These four basins- the Cambay, the Krishna-Godavari, the Cauvery, and the Damodar valley shale basin (Fig. 3f) are structurally complex. Cambay and the Cauvery are extensively normal faulted and consist of a series of horst and graben structures. Sharma et al. (2019) have reviewed geochemical data of shales from Cambay, Krishna-Godavari, Cauvery and Damodar basins.

- *Cambay Basin:* It is a narrow NNW-SSE elongated, rift sag and an intra-cratonic Tertiary basin found along the western continental rifted margin of India in Gujarat extending between latitudes 21°00'/25°00' and longitudes 71°15'/73°30' (Biswas et al., 2013; Mukherjee, 2015; Kumar et al., 2018; Surabhi et al. 2024). The evolution of this petroliferous onshore basin in the Late Cretaceous is related to the breakdown of the Gondwana supercontinent resulting in half rift-grabens. The basin, characterized by N-E to NNW-SSE trending listric normal fault and transfer faults with ENE-WSW to NE-SW trend is sub-divided into Mehsana-Ahmedabad (prospective for shale oil), Tarapur (prospective for shale oil and wet gas), Broach (prospective for shale oil and wet/dry gas), and Narmada (likely immature) tectonic blocks. These blocks parted from each other by the faults-oriented transverse to the N-S axis/cross strike faults (Banerjee et al., 2000) (Fig. 3g). The Deccan Trap forms the basement of the basin bounded by Saurashtra uplift (Kutch-Saurashtra arc) and Aravalli- Delhi unit from W to NE and Deccan uplift at SE. The Late Paleocene is separated from the Deccan Trap by the Lower Paleocene Olpad Formation.

  The Cambay shale formation (Late Paleocene to Early Eocene; Hafiz et al., 2020) is divided into the Older Cambay Shale (OCS) and the Younger Cambay Shale (YCS). The Early Eocene black shales (50, 245.769 km^2, 19,400 mi^2) are marine deposits with Ro ranging from 0.7 % to 2.0 %, high thermal gradient (3 °F per 100 ft) (16.1 °C per 30.48 m) (Wandrey, 2004). The Early Eocene black shale is in the hydrocarbon window at depths 1828.8 m (oil), 3352.8 m (wet gas) and 3962.4 m (dry gas), respectively. respectively. A 1000 ft (304.80 m) thick wedges consisting of non-marine clastic shale of the Kadi and Kalol Formation lies within the intervals of the Cambay Black Shale in the north Mehsana-Ahmedabad Block (Bhandari and Chowdhary, 1975). It consists of Type II and III kerogens with 2–4 % TOC (Kumar et al., 2017). The Cambay black shale measures BI > 0.48 (0.21–0.66) with high proportion of kaolinite and chlorite (De et al., 2020). It has an estimated 228 Bcf mi^{-2} shale gas, 170 Bcf mi^{-2} of wet gas, and 80 MM bbl of shale oil (USA EIA, 2013) and 3.23 MM bbls per 60 acers of shale in-place (Kumar et al., 2017). According to the Government of India- Ministry of Mines Indian Bureau of Mines (2018), Cambay Basin in Gujarat has 84 oil and gas fields. Out of these, private/joint venture companies hold 38 oil and gas fields.

  The hydrocarbons are trapped in the structural blocks in the reserviors between Paleocene and Miocene with maximum carbon sequestration potential in the Eocene shales of the basin. The petroleum system lies in the north (Kalol and Kadi shale formation) and south (Cambay-Hazard) of the basin (Kumar et al., 2018). Cambay

Shale overlying the Oplad Formation are the major hydrocarbon sources of the basin.

- *Krishna-Godavari (KG) Basin:* The Krishna-Godavari Basin is a petroliferous pre-cratonic rifted margin basin with ~ 20,201.91 km^2 area. It was formed during the Indian and Australia or Antarctica (East Gondwanaland) plate divergence and oblique extension between Late Jurasic (160 Ma) and Early Cretaceous (130 Ma) (Nanda et al., 2019). The KG basin is divided into sub-basins and comprises of a series of horsts and grabens at the extended eastern coast of India (Fig. 3h) bounded by the Kakinada in the NW and Ongole at SW (state: Andra Pradesh). It is juxtaposed orthogonally to the NW-SE trending Pranhita Godavari Gondwana graben at north (Gupta, 2006).

The basin is a delta plain. Fault ridges divide it into several sub-basins (Rao, 2001). En-echelon grabens are filled due to ~ 3 km thick Permo-Carboniferous syntectonic sedimentation (Kala et al., 2021) in two phases. Shales of Pennar Formation (Early Cretaceous) are the sources for hydrocarbon for the overlying the Krishna Formation in the Krishna and the Mahanadi basins (review in Galushkin et al., 2016). Chintalapally Formation shale (Late Cretaceous) acts as the source rocks for the hydrocarbon in Tirupati sandstone. The Paleocene shales in the KG basinconsists of kerogens of Type III with TOC = 1.4 % (referred in (review in Galushkin et al., 2016). Thick clastic sediments are transported by the river Krishna (102 million tons yr^{-1}), Godavari (150 million tons yr^{-1}) and their tributaries from the Early Permian till the Recent (Sharma, 2002; Gupta, 2006). The deposited sediment facies is > 7 km thick (Bastia et al., 2006; Solomon et al., 2014). The basin contains organic-rich fluvial-lagoonal, deltaic-lacustrine and transitional marine-lagoonal sediments (Kala et al., 2021). Kommugudem Shale of Permian age, Triassic Mandapeta shale and Cretaceous Raghavapuram shale (Rao, 2001) are the key units for hydrocarbon production. The variation in the depositional environment are the result of the paleoclimatic shifts in the Lower Gondwana and continental-marine transition along the eastern margin of the peninsula (Kala et al., 2021).

Their Ro ranges from 0.7 % to 2 %. The 900–1000 m Kommuguden Shale is hard dense silty and carbonaceous with the presence of glauconite and pyrite (Padhy et al., 2013). Their colour varies from dark grey to black, and ocassionally shows alternate layers of sandstone and coal (Padhy et al., 2013). The Kommuguden Shale consists of 2–8 % of TOC, Ro between 0.8 % and 1.5 %, Tmax from 440 to 580 ^{0}C with kerogen type II and III (USGS, 2011; Padhy et al., 2013; Mani et al., 2017). The average value of 2.65 obtained using the fractal Frenkel-Halsey-Hill (FHH) approach reveals that the pore surfaces are rough and have a heterogeneous pore structure (Kala et al., 2021). The Mandapeta graben is the most exploited region for shale oil and gas in the basin (Khan et al., 2000). The oil potential of 4,000-16,400 ft (1219.2–4998.72 m) thick Permian-Triassic shale has the wet/condensate gas at 8000 ft (2438.4 m) depth. The dry gas prospective area is at 13,000 ft (3962.4 m) depth. The Permian-Triassic shale is 330–1300 ft (100.58–396.24 m) thick. The TOC ranges from 0.4 % to 11 %. It has an estimated 205 Bcf mi^{-2} of dry gas, 58 Bcf mi^{-2} of wet gas, and 18 MM bbl mi^{-2} of oil (USA EIA 2013). Only 57 Tcf of shale gas and 0.6 B bbl of shale oil are recoverable (USA EIA 2013).

The Cretaceous Raghavapuram shale is thermally immature with thermal maturity < 0.7 %. It matures at ~ 10,600 ft (3230.88 m) depth and is oil-prone. The TOC in this shale unit ranges from 0.8 % to 6.4 %, between 60 % and 80 %, T_{max} from 450 to 465 ^{0}C, kerogens of type II-III, brittleness index > 40 %, porosity > 10 % and class IV amplitude vs. offset (AVO) anomaly in the carbon-rich zones indicating suitable hydraulic fracturing (Deshmukh et al., 2020). The presence of vanadium and nickel enrichment in the organic matter of the Raghavapuram Shale suggests that the algal-derived organic matter was exposed to anaerobic conditions early in its deposition or burial process. Furthermore, slow sedimentation rates likely maintained an open sediment system (Mani et al., 2016).

The presence of gas hydrate and cold seeps in the K-G basin were identified from the topographic mounds by the multi-channel seismic data from the National Gas Hydrate Programmes –01 (NGHP-01) expedtion (Mazumdar et al., 2009; Ramana et al., 2009; Dewangan et al., 2010; Lorenson et al., 2018). Gas hydrates were found to be captured in fractures and the fossils in the form of carbonate nodules (Nanda et al., 2019). During the NGHP, analysing the composition of the carbon isotopes of the samples portrayed the history of natural sequestration of carbon in the basin. The sulphate reduction from degraded organic matter and methanogenesis produced authigenic carbonate in the basin (Solomon et al., 2014; Kocherla et al., 2015). The organoclastic sulfate (SO_4^{2-}) reduction, anaerobic oxidation of methane (CH_4) and methanogenesis precipitated authigenic carbonates in the K-G basin (Teichert et al., 2014).

- *Cauvery Basin*: The southernmost NE-SW trending basin (onshore area on the east coast: 23,568.89 km^2, 9100 mi^2), offshore area: 23,309.89 km^2/ 9000 mi^2) along the eastern margin of Indian subcontinent consists of numerous horsts and grabens and organic source rock. It was formed during a sheared-rift's extension during the Late Cretaceous rifting related to the Gondwana break-up (Watkinson et al., 2007; Bharktya et al., 2008; Nagendra and Eddy, 2017; Mukherjee et al., 2025). In the onland area, the northern part of this basin is more active neotectonically than the southern part (review in Mukherjee et al., 2025). The basin contains several fault-controlled depressions or sub-basins viz., Nagapattnam, Tranquebar, Ariyalur-Pondichery, Tanjavur and Mannar (Chakraborty et al., 2018; Biswas et al. submitted). The Ariyalur-Pondichery and the Thanjavur sub-basin in the north and center of the basin contain hydrocarbon-rich mature shales. The Lower Cretaceous Andimadam and Sattapadi Shale deposits of the Ariyalur-Pondichery Depression (1605.8 km^2, 620 mi^2) have an average depth of 10,000 ft (3048 m) and thickness of 1000 ft (304.8 m). The Andimadam and Sattapadi Shales of the Thanjavur sub-basin (1010.1 km^2, 390 mi^2) is ~ 9500 ft (~2895.6 m) deep with 500 ft (152.4 m) sediment. The thermal maturity ranges between 1.0 % and 1.3 %, and TOC between 2 % and 2.5 % with type III kerogen and hydrogen indices (HI) ranging from 100 to 280 (Chandra et al., 1991; also see Mogali et al. 2024). The basin has undergone minimum lateral erosion. This is evident from the close-by occurrence of the hydrocarbons and the mature source rock (Narasimha Chari et al., 1995). From Cauvery basin, 8 B bbl of shale oil in-place is there out of which 5 Tcf of shale gas and 0.2 B bbl of shale oil is recoverable (USA EIA, 2013).
- *Damodar Valley Basin:* Besides the Cambay Basin, Damodar Valley Basin is the most promising Indian basin for the exploration of shale gas. The basin is a portion of the four basins of Gondwana, viz., Satpura, Pranhita-Godavari, Son-Mahananda and Damodar valley basin. It occurs within the suture zone and was a part of the rift channel in the NE of the Gondwana supercontinent. The basin is characterized by faults formed along the Precambrian lineaments during deposition and consists of Carboniferous to the Lower Cretaceous thick sedimentary deposits (Mukhopadhyay et al., 2010; Mani et al., 2015). The organic content of the marine deposited Permian Barren Measure shale is microporous and thermally mature up to the gas window (Turlapati et al., 2020). Along E-W, Hutar, Daltonganj, Auranga, Karanpura, Ramgarh, Bokaro, Jharia and Raniganj sub-basins fall within it (also see Srivastava et al., 2025).

The shales have a thermal maturity of 1.0–1.3 % and TOC between 3 % and 6 % (Mishra and Cook, 1992; Chawla, 2010). It lies in the gas/condensate window. The prospective area of the formation is 2797.19 km^2 (1080 mi^2) and is constricted to the Bokaro (285 km^2, 110 mi^2), Karanpura (829 km^2, 320 mi^2), and the Raniganj (1683.49 km^2, 650 mi^2) sub-basins with a gross thickness of 2000 ft (609.6 m) and organic matter thickness of 283 ft (86.26 m), respectively (Veevers and Tewari, 1995; Mendhe et al., 2018). According to the samples studied by Mukhopadhyay et al. (2021) from the Damodar Valley basin, the TOC content of the Barren Measure Formation ranges 4.24–9.78 % where variation in T_{max} values from 437 to 447 ^{0}C and porosity value ≥ 13 % (Mukhopadhyay et al., 2021). The HI ranges from 110 to 211 mg HC g^{-1} TOC and OI between 3 and 36 mg HC g^{-1}. The TOC indicates a mixture of Type II/III kerogens (Mukhopadhyay et al., 2021). The mineral composition of the shales in the basin consists of feldspar (2–9 %), quartz (25–63 %), muscovite and illite (7–29 %), kaolinite (24–41 %), siderite (9–15 %), and dolomite (2–30 %) (Mani et al., 2015; Bakshi et al., 2020). The basin resource estimates 63 Bcf mi^{-2} wet shale gas, 300–2100 tcf of shale gas-in-place, 12 MM bbl $mi^{-2}$of condensate shale and 5 B bbl of shale oil (Jain et al., 2012; USA EIA, 2013). The Barakar Formation of the basin consists of thick organic-rich shale with 4.40–8.29 % of TOC (Sain et al., 2014).

- The other potential Indian shale basins are located at Upper Assam, Pranhita-Godavari basin, Vindhyan basin and in the state Rajasthan. *The Upper Assam basin* is located in the NE part of India. It is one of the foremost shale oil and gas exploration areas of the country. It consists of an organic-rich Upper Eocene-Oligocene Barail Group of coals and shales (Sahoo and Gogoi, 2010). The source rock is composed of feldspar (1.0–2.0 %), quartz (6–45 %), muscovite-illite (11–66 %), kaolinite (10–43 %), and dolomite (Bakshi et al., 2020). It contains a TOC between 1 % and 2 % and Ro ranging 0.5–0.7 %. The oil window is at its early mature stage. The thermal maturity increases with the basin depth mainly towards S-SW (Sain et al., 2014). The organic-rich Permian Puram and Khanapur Formations of the Pranhita-Godavari Basin are located in eastern India. The Jai Puram and the Khanapur Formations are organic-rich and contain Type III kerogen with 0.67 % Ro, favorable for gas generation (Sain et al., 2014).

Pranhita-Godavari Basin: The basin is an intracratonicrift Proterozoic sedimentary basin deposited in the galcio-lacustrine to highly sinuous fluvial environment extending the states of Andhra Pradesh and Maharashtra (Chaudhuri et al., 2003; Sharan et al., 2016). The P-G basin has the potential to contain shale gas specifically in the lower Gondwana group, the P-G basin's shale features include a TOC from 3.58 % to 6.4 %, a VRo of 0.47–0.67 %, and a kerogen type of III (Sharan et al., 2016). The organic-rich Permian Puram and Khanapur Formations of the *Pranhita-Godavari Basin* are located in eastern India. The Jai Puram and the Khanapur Formations are organic-rich and contain Type III kerogen with 0.67 % Ro, favorable for gas generation (Sain et al., 2014).

The Vindhyan Basin is a stable intracratonic basin situated in north-central India (extending from Sasaram to Agra) (Krishnan et al., 1959; Bose et al., 2001). The basin comprises of several Proterozoic shale units (Arangi, Koldaha, Rampur, Bijaygarh, Rewa and Sirbu shale) altogather measuring TOC 0.29–8.44 %, Tmax ranging from 292 to 607̊ C, Oxygen Index (OI) ranges from 11 to 178 mgHC/g TOC, and the Hydrogen Index (HI) ranges from 1 to 44 mgHC/g TOC (Singh et al., 2023). Few of these series such as the Hinota and the Pulkovar are organic-rich and are ~ 6000 m thick (Sain et al., 2014). The basin contains shallow marine deposits with TOC ranging from 0.5 % to 3.8 % (Dayal et al., 2014).

The Rajasthan basin located in the NW part of India encloses a large onshore area structurally complex with numerous fault blocks (e.g., Biswas et al. 2024). Tectonically, the Rajasthan shelf is divided into four distinct units: the Jaisalmer Basin, the Bikaner-Nagaur Basin, the Barmer-Sanchor Basin, and the Pokaran-Nachna High (Pandey et al., 2012). Permian Karampur Formation is thermally mature and consists of type III kerogen. For reservoir age in Rajasthan basins, see Dasgupta and Mukherjee (2017) and Dasgupta et al. (2024). The TOC of Kapurdi carbonaceous shales are 10.24–22.42 % (Kumar et al. 2022). The Barmer Hill Formation has a TOC of 14 % and an HI ~ 1000 (Dolson et al., 2015). In the Jaisalmer basin, from the Jaisalmer-Mari high, the source rock has a TOC = 1.63–5.3 % (Pandey et al., 2019). TOC > 2.0 wt % has been deciphered from the for the Baisakhi–Bhadesar Formation, Jaisalmer basin (Kumar et al., 2024). In the Bikaner-Nagau basin, the Bilara–Hanseran rocks have 5–6 % TOC (Yasin et al., 2022). The discovery of reservoirs of Neoproterozoic age in the *Bikaner–Nagaur basin* of Rajasthan, western India, during the early nineties, marked one of the most significant milestones in the history of oil and gas exploration in India (Raju et al., 2014). Marine deposited bituminous shale from the Gurha mines studied by Singh et al. (2020) of the *Bikaner–Nagaur basin* stated a Tmax of the samples <430̊ C and VRo <0.40 %, high TOC varies from 18.23 % to 36.23 % with type II kerogen and classified the shale in the immature stage of the oil window determining the Tmax and VRo value. *The Paleogene lignitic shales of the Barmer basin* from the Giral lignite mine was studied by Kar et al. (2022) and measured TOC ranging from 0.76 % to 49.83 %, Tmax varying from 320 to 608̊ C with Type III heterogenous kerogen. The Mesozoic shales of the Jaisalmer Basin are the hydrocarbon rich source rock of the basin (Singh et al., 2006; Kumar et al., 2024).

In the Andaman and Nicobar island, up to 1200 m thick carbonaceous shale of Oligocene Port Blair Formation overlying the Bartang Formation is presumably the source rock after adequate burial in the eastern part at a shallow marine depth (Dangwal et al., 2009).

The Kerala-Konkan region in the southern part of Indian western offshore (Chatterjee et al., 2024) consists of Miocene marine stata within the intracontinental basin. The marine deposits of Santonian to Maastrichtian age consists a sequence of calcareous sandstones, shales and siltstones facies (Singh et al., 1999; Raju, 2018). The southern portion of the basin consists of a hydrocarbon reservoir (Das et al., 2008; Peters and Das, 2008).

4.1.6. Oman

The progressive breakup of the Gondwana during the Late-Precambrian-Cambrian Period affected the source rocks and their depositional history. Gondwana rocks in Oman is the world's significant producers of hydrocarbons. Oman has three distinct shale oil and shale gas basin viz., the South Oman Salt Basin, the North Foreland Basin and the south-eastern longitudinal edge of the Rub' Al-Khali Basin. Fahud and Ghaba salt basins are the prospective/promising shale basins of Oman for future exploration and development. These two basins are considered potential due to its geological characteristics and other favourable conditions for unconventional hydrocarbon reserves. It also consists of two shale prospective basins viz., Fahud and Ghaba Salt Basins. In these three basins, a total of 48 Tcf of shale gas and 6.2 B bbl of shale oil exist (USA EIA, 2014).

- *South Oman Salt:* The South Oman Salt Basin is located in the south-central between 30,000 and 15,000 ft (9144–4572 m) depth. The deformation mechanism and orientation of the local stress in the basin are governed by salt halokinesis resulting in several folds and faults (Al-Kindi and Richard, 2014). The western margin of the basin is characterised by complex transpression deformation fronts and thins towards the eastern margin of the basin (Amthor et al., 2005). The saline Ara A4 Formation/Group of the Huqf Super Group (c. 725–540 Ma) formed between Neoproterozoic and Early Cambrian Period are the Lower Cambrian Thuleialat, Silicilyte and U Shale source rock deposited under anoxic environment and covers ~ 3833.18 km^2 (1480 mi^2) (Terken et al., 2001; Roussel et al., 2020). Carbonate-evporites alternate layers make the basin an ideal geologic setting for carbon capture and storage since c. 547–540 Ma (Amthor et al., 2005; Allen, 2007).

  Silicilyte, a shallow-marine rift saline deposit bounded by carbonate platforms is the primary source rock of the basin generating voluminous oil at a lower temperature (Rajaibi et al., 2014). It ranges from 6,500-15,000 ft (1981.2–4572 m) and is trapped by a series of salt domes (Ramseyer et al., 2013). It generates kerogen Type between II-I with a TOC ~3.2 % and a Ro of 1.0–1.3 %. Based on the reservoir properties, 2.9 B bbl of shale oil and 18 Tcf of wet gas is recoverable. The Thuleiat Shale with an organic-rich thickness of 293 ft (89.31 m) contains Type I/II kerogen with TOC 2.5–10.4 %, and thermal maturity (Ro) of 1.0 – 1.3 % (Grosjean et al., 2008; Kukla et al., 2012). It has an estimated 31 Tcf of wet gas and 11 B bbl of oil. The prospective 11,000 ft (3352.8 m) deep U Shale with a rich organic thickness of 195 ft (59.44 m) has a TOC from 3.5 % to 6.4 % and Ro 1.0–1.3 %. It generated matured Type I/II kerogen. The recoverable shale oil can be estimated as 0.3 B bbl of oil and 2 Tcf of wet gas (USA EIA, 2014).

- *North Oman Salt basin*: The Middle Cretaceous marine Natih shale is the most efficient source rock of the foreland basin. It is enclosed by the Oman Mountain Thrust Front in the east, the Peripheral Bulge, Fahud fault in the south, and United Arab Emirates (U.A.E) border in the north. The compression from the Oman Mountain Thrust Front in the east and the Fahud Fault in the south made the basin structurally complex. It is 1300 ft (396.24 m) thick and consists of seven carbonate litho-stratigraphic units A to G (Terken, 2001; USA EIA, 2014). The B and E units consist of hydrocarbon-rich organic shale with Type I/II kerogen. The 3000 – 9000 ft (914.4–2743.2 m) deep Naith B Shale encompasses an area of 6164.17 km^2 (2380 mi^2). The TOC ranges from 2 % to 15 % and thermal maturity 0.7–0.9 % (Terken, 1999) with a concentration of 20 MM bbl of oil and 8 Tcf of shale gas. The Naith E Shale is not resourceful due to its lower TOC content (USA EIA, 2014). The Natih E Shale is thinner (rich resource rock lies between 1042 and 1037 m) than Natih B resource rock and is not resourceful. The organic matter is structureless and load-bearing resulting in a moderate quality shale with TOC < 2 % (Terken, 1999).
- *Rub' Al-Khali (Oman)*: The basin extends from SE Saudi Arabia to west-central Oman and often known as the Su'aydan Platform (Svendsen, 2004). Here, we discuss the extended portion of the Rub' Al-Khali basin of United Arab Emirates (UAE). The Lower Silurian Sahmah Shale formed in a marine setting. It is an organic-rich world-class hot shale with a hydrocarbon potential area of 24345.89 km^2 (9400 mi^2), which is 9,000-13,000 ft (2743.2–3962.4 m) deep and consists of 55 m thick sediment (Jamal and Belhadj, 2015). Tectonically, it has experienced subsidence, uplit and erosion. The basin is characteized by the presence of sub-horizontal Hercynian unconformity produced during Paleozoic and Cretaceous obduction (Svendsen, 2004; Searle, (2019). It has Type I and II kerogen and TOC from 0.8 % to 9 %. This section of the basin in Oman is thermally mature (vitrinite reflectance 1.4 %) and gradually over-matures and thickens towards Saudi Arab into North Africa (Madi et al., 2015). It has an estimated 19 Tcf of wet gas and 9 B bbl of condensate gas (USA EIA, 2014).

The Oman shale storage reservoir has a poor permeability and is only moderately thick (30 m) (Chen, et al., 2021). Shuaiba limestone deposit, which is covered by the impermeable Nahr Umr Shale and serves as the principal oil reserve for the whole foreland basin, has been divided by faults into several isolated blocks with different dips and is geologically ideal for carbon sequestration (Al Hadhrami, et al., 2018). The caprock for the Shuaiba and Naith Formation are made up of the Fiqa and Umr shale Formation (Al-Anboori et al., 2010). In Rub'Al-Khali basin (Oman), the Early and the Late Paleozoic cycles including the Hercynian produced regional unconfirmities, subsidence with rise in temperature, deglaciation, rise in sea level resulting thick sedimentary strata and carbon sequestration (Jaju et al., 2016).

4.1.7. Indonesia

The country has an extensive shale oil and gas reservoir formed in lacustrine setting of the Mesozoic and Cenozoic Eras. It has the five most potential dispersed basins (Central Sumatra, South Sumatra, Kutei, Tarakan and Bintuni) bordered by the Indian Ocean. It has an estimated 46 Tcf and 7.6 B bbl of recoverable shale gas and shale oil out of 303 Tcf and 234 B bbl of shale oil gas and oil in-place (USA EIA, 2013). According to the USA Energy Information Administration (EIA) report (2013), MIGAS (upstream oil and gas regulator of Indonesia) estimated 574 Tcf of shale gas resource in the country. Being the fourth most populous country in the world, the consumption of oil (3.1 million bbl d^{-1}) exceeds its production (2.5 million bbl d^{-1}) and therefore oil is imported.

Sumatra Basins: The north, south and the central portion of the Sumatra are the largest hydrocarbon producers of Indonesia. It is shale oil and gas potential (Haris, 2018). The North Sumatra basin formed during the Early Oligocene has a series of N-S trending grabens. The Lower Baong and Belumai calcareous shale of Middle – Early Miocene, and Bampo black shale of the Late Oligocene (Ryacudu and Sjahbuddin, 1994; Musu et al., 2015) are the source rocks of the basin. The Lower Baong Shale has three facies amongst which the siliceous calcareous mudstone has a strong potential for shale gas, with 2–3.5 % TOC, brittle index of 0.48, kerogen of type II, maturity depths ~ 2300 m, and sweet spot thicknesses of 350–425 m. (Bahesti et al., 2014). As per Haris et al., (2017), this shale layer is characterized by early mature phase and type II kerogen based on the estimated Tmax ($\mathring{435}$ $-\mathring{470}$ ^{0}C), indicating that it has the potential to produce oil.

- Since the reservoir is shallow, young, ductile and contaminated with clay (smectite), CO_2, and H_2S; it is not considered as a prospective basin of the Sumatra.

  The Central Sumatra Basin is a potential oil prospective trans-tensional pull-apart basin formed during Late Cretaceous to Early Tertiary Period, encircled to the north and south by major strike-slip fault. It has N-S trending fault-bounded troughs parted by horst blocks (USA EIA, 2013). The sedimentation in the troughs began with non-marine sediments followed by the marine cycle. The lacustrine Brown Shale of the Paleogene Period has the most shale oil potential of the basin. The 295 ft (89.92 m) thick and 6,600-10,500 ft (2011.68–3200.4 m) deep organic-rich facies of the brown shale with TOC 1–15 % consist of Type I and II kerogen. It has an estimated 3.3 Tcf and 2.8 Bbl of recoverable shale gas and shale oil (USA EIA, 2013). The resource potential deep-water shale of the southern Sumatra basin is gas-prone. The Mid-Upper Miocene Talang Akar Formation of the basin consists of coaly shales. It is 1300 ft (396.24 m) thick, 6,000 ft (1828.8 m) deep with TOC ranging from 1.7 % to 8.5 %, thermal maturity 0.5–0.9 % (J and Cheng et al., 2006). It holds a potential of 68 Tcf and 136 B bbl of shale gas and shale oil where only 6 % of the shale gas and 3 % of the shale oil are recovered (USA EIA, 2013).
- *Kutei Basin:* The Kutei basin is 93,239.57 km^2 (36,000 mi^2) surrounded by the eastern part of the Kalimantan coast. It was formed by rifting and syn-rift deposition of deep marine lacustrine sediments during the Middle–Late Eocene Period (USA EIA, 2013). Mid-Late Miocene mudstones and carbonaceous shales of shallow fluvial-deltaic deposits are the source rocks for oil and gas production. The Balikpapan lacustrine formation of Mid-Upper Miocene is of Type III kerogen with TOC ranging from 2 % to 20 %. The oil-producing region on its onshore is 9,000 ft (2743.2 m) deep with R_O 0.7 % and TOC 4.0 %, while the overmatured gas-producing region in the eastern Kalimantan coast and Mahakam Delta are found below 19,000 ft (5791.2 m) depth. The basin has an estimated 1.3 Tcf and 0.7 B bbl of recoverable shale gas and shale oil (USA EIA, 2013).

  The source rocks for the oil and gas resources in the Lower Kutei Basin are carbonaceous shales and coals from the Middle to Late Miocene Epoch, which are connected to the delta plain to the delta front depositional settings (Paterson et al., 1997). According to the geochemical investigations mentioned by Lin et al. (2005), the carbon got stored in the deepwater Kutei Basin originate from allochthonous land-plant organic matter. Lin et al. (2005) and Sallar et al. (2006) also stated that the plant leaf fragments, woody debris, and less commonly resin bodies and recycled coaly particles constitute mostly the organic matter within the turbidities. The top of the hard overpressure zone is considered to be the base of the effective hydrocarbon range. The significant potential for trapping stems from the fact that trap development happened before hydrocarbon migration (Paterson et al., 1997).

- *Tarakan Basin:* It is located in western Indonesia bordered by Malaysia in the north and northeastern Kalimantan coast in the west and south. It contains fluvio-deltaic-shallow marine Miocene shale that got deformed by NE-SW trending folds (Noon et al., 2003). The basin has three important Formation (Naintupo of Early Miocene, Meliat of Middle Miocene and Tabul of Late Miocene) containing the source rock producing shale oil and shale gas (Laksono et al., 2021). The TOC of Naintupo (1828.8–4876.8 m) ranges from 1.6 % to 12.1 % with Type II and III kerogen. The R_O in the dry gas window ranges from 1.3 % to 2.0 % estimating 5 Tcf shale gas (Widyanita et al., 2018; Laksono et al., 2021). The Meliat (1005.84–3048 m) has an interbedded layer of shales and claystones with sandstones, coal, and dolomites with R_O 0.7–1.3 % and an estimated 4 Tcf recoverable shale gas (Subroto et al., 2005; Indrajaya et al., 2016). Around 1005.8 m thick Late Miocene Tabul Formation formed in an anisotropic environment consists of coaly shale with TOC 0.5–4 %, R_O ~0.7 % of Type II and III kerogens at 3,300-6600 ft (1005.84–2011.68 m) depth (Ronoatmojo et al., 2018). It has an estimated 0.2 Tcf and 0.3 B bbl of recoverable shale gas and oil, respectively (USA EIA, 2013).
- *Bintuni Basin:* Located in the eastern part of Indonesia, Bintuni is a Permian marine basin, bounded by Lengguru folds with potential shale prospects. The Aifat and the Ainim Formation of the Aifam Group consist of the main source rock of the consisting black marine calcareous shale. The Aifat, lower member of the Aifam Group is 3500 ft (1066.8 m) thick and 12,000 ft (3657.6 m). The organic-rich part of the Ainim Formation is 2400 ft with an average depth of 10,000 ft (3048 m) with R_O 1.2–1.8 %, and 0.66 % at its transition zone. It has an estimated 29 Tcf of recoverable gas out of114 Tcf of gas-in-place (USA EIA, 2013; also see Chevallier and Bordenave, 1986; Pratama and Paramitha 2013; Utomo et al., 2015; Wisesa et al., 2017). The Jurassic Tipuma Formation (1219.2–2438.4 m) and Lower Miocene Tomori Formation (152.4–304.8 m) consists of carbonaceous shale (Harahap, 2012) with TOC ranging from 4.5 % to 7.6 % and 2–4 %, respectively. The Tomori Formation consists of Type II and III kerogen with R_O > 1.0 % at a depth of 11300 ft (3444.24 m) (Chevallier et al., 1986; USA EIA, 2013).

The transgression towards the end of the early Miocene developed the western deltaic Indonesian basins. Between the Mid-Miocene to the Pliocene, the Sumatra, Natuna and Java basins saw regressive sedimentation and compression and inversion tectonic processes or volcanic eruptions Satyana (2022). Post-collision molassic sedimentation into the foreland basins is a characteristic of the Mid-Miocene to Pliocene epoch, which is often referred to as the Neogene Period. Satyana (2022) asserts that during the Neogene Period, hydrocarbon trap developed.

4.1.8. Kazakhstan

It is one of the major oil producers of the world located in central Asia. It is bordered at north by Russia, at south by Kyrgyzstan and Uzbekistan, at east by China, and at west by the Caspian Sea. The major petroleum basins of the country are situated in its western part (Parkhomchik and Syrlybayeva, 2016). The North Caspian, South Mangyshlak, South Turgay, Chu-Sarysu and North Ustyurt are the significant hydrocarbon basin of Kazakhstan (Effimoff, 1999).

- *North Caspian Basin:* The large basin of 549077.48 km^2 (2,12,000 mi^2) is located in western Kazakhstan; bordered by the Russian Platform on the north, Northern Ustyurt Block on the southeast, Karpinski inverse rift on the southwest, the Ural Mountains at east and Kazakhstan and Russian border at west. The complex regionally structured basin is also known as the Pre-Caspian or the Pricaspian Basin (Bealessio et al., 2020). The primary hydrocarbon source rocks are found at 16,400 ft (4998.72 m) depth with ~ 20,000 m thick marine sedimentary deposition (including shale sequence) formed during the Carboniferous Period (USA EIA, 2014). Only the shallower portion of the basin is assessed.
- The deformed Lower Permian Kungurian salt formation in the basin divides the sediments of the basin into subsalt and suprasalt strata at intervals. The subsalt strata consist of thick organic-rich anoxic black shale facies are deposited during the Upper Devonian and Carboniferous Periods (USA EIA, 2014; Zholtaev et al., 2019). This large and geologically complex basin is divided into two parts: *(i)* north basin margin, and *(ii)* south-east basin margin. The north basin margin contains one of the thickest hydrocarbon facies (5300 ft, 1615.44 m) of the world (Ulmishek, 2011). It has five distinct marine shale rocks of the Devonian and Carboniferous Period with Ro ranging from 0.7 % to 1.3 %.

  The Lower Carboniferous Tournaisian Formation is the deepest and one of the prime source rocks shale rocks deposited at ~ 15, 600 ft (4754.88 m) depth in the North Caspian Basin with a thickness of 630 ft (192.02 m) (with 34 % shale content). They contain Type II kerogen with TOC > 2 %. The Tournaisian Formation has patches of organic-rich area with estimated dry gas, wet gas/condensate and oil with 259 km^2 (100 mi^2), 518 km^2 (200 mi^2), and 26 km^2 (10 mi^2) areas, respectively. The 1250 ft (381 m) thick Radaevskiy-Kosvinskiy (R-K) lies above the Tournaisian Formation at 14,400 ft (4389.12 m) depth. The R-K has 60 % shale content. The Lower Carboniferous Formation in the NE portion encloses ~ 130 km^2 (50 mi^2) having type II and III kerogens rich in oil and wet gas/condensate. The Lower Serpukhovian located along the basin's southern margin contains Type II-III kerogen with TOC 2–3 %. It is in the oil window and gradually extends towards the dry gas and wet gas/condensate in the center of the basin. It has an estimated area with dry gas for 777 km^2, 1192 km^2 for wet gas/condensate, and 2901 km^2 for oil (USA EIA, 2014). The Vereiskiy Formation of the Middle Carboniferous Period with Type III kerogen and low TOC value has a dry gas and wet gas/condensate prospective area of 155 km^2 respectively including 316 km^2 for oil.
- The Gzelian-Kasimovian (G-K) deposited over Myachkovskian Formation holds Type II kerogen with TOC between 2 % and 3 %. T_{max} varies from 428 to 462 ^{0}C. This formation is matured for oil (Ro ranges 0.7–0.8 %) covering an area of 673 km^2 (Huvaz et al., 2007). The Lower Carboniferous shales (Tournaisian and R-K) with 933 km^2 estimates 52 km^2 for oil and associated gas, 622 km^2 for wet gas/-condensate, and 259 km^2 for dry gas. Whereas, the Middle/Upper Carboniferous shales (G-K, Vereiskiy, Lower Serpukhovian) cover an area of 6164 km^2. It has estimates of 932 km^2 for dry gas, 1347 km^2 for wet gas/condensate, and 3885 km^2 for oil and associated gas. The E-SE basin margin covers ~ 25900 km^2 area of the North Caspian Basin. The SE margin identifies Middle Carboniferous black shales with TOC ranging from 6.1 % to 7.8 % with Type II kerogen (Arabadzhi et al., 1993; Dalyan, 1996; USA EIA, 2014). It thickens towards the basin center. They are in the phase of early oil generation window with Ro of 0.8 % at 10,500–13,200 ft (3200.4–4023.36 m) depth (Yensepbayev et al., 2010). The Early Permian source rocks have the oil window within 6,000-13,200 ft (1828.8–4023.36 m) depth. The margin has an estimated 40 MM bbl/mi^2 of oil and 37 Bcf/mi^2 for the associated gas (USA EIA, 2014).
- *South Mangyshlak Basin*: It is situated in the eastern part of the Middle Caspian Basin with ~ 77700 km^2 (30000 mi^2) area. It is bordered by the Mangyshlak fold belt at north, Caspian Sea and Uzbekistan border at west and east, and Turkmenistan border including the Karabogaz regional basement high at south. The collision between the Mangyshla and Ustyurt plates in the Triassic formed a series of linear mega-scale anticlines and synclines (USA EIA, 2014). The Triassic shales are the main hydrocarbon zones placed in the Bekebashkuduk Anticline and Zhetybay Step (2500 ft, 762 m thick) in the NE portion Peschanomys Uplift (800–1000 ft, 243.84–304.8 m

thick) in the western portion of the basin. The TOC ranges from 1 % to 4 % dominated by Type II kerogen. It consists of 39 MM bbl mi^{-2} of oil and 32 Bcf mi^{-2} of associated gas in a 2460 mi^2 prospective area for hydrocarbons (Ulmishek, 1990; Popkov et al., 2023).

- *South Turgay Basin:* It is a triangular intracontinental rift basin in central Kazakhstan. It is bordered by the Lower Syr-Darya Arch and the Main Karatau strike-slip Fault (MKF) at SW, Minbulak Saddle at north, and Ulutau Massif at east. It comprises of Lower Jurassic Sazimbai and Aibaleen shales, Middle Jurassic Karaqansay Shale and the Upper Jurassic Akshabulak Shale. The Karaqansay and the Aibaleen Shale are the most prospective organic-rich shales of the basin. The Turgay basin encompasses Ariskum, Akshabulak, Sarylan and Bozingen grabens with high-quality algal-rich Type I-II kerogens and TOC. The TOC ranges from 0.01 % to 3 % in the Lower Cretaceous section and 2–3 % in the Jurassic section (Madisheva et al., 2024). The Karaqansay shalesis in the oil generation phase below 7, 300-10,000 ft (2225.04–3048 m) and the Sazimbai and Aibaleen shales is in the wet gas window at the base of the graben (USA EIA, 2014). The Middle Jurassic Karaqansay estimates 38 MM bbl mi^{-2} of oil and 29 Bcf mi^{-2} of associated gas. It enters the oil window in the deeper section of the grabens. The Lower Jurrasic Aibaleen shales have resource potential of 43 MM bbl mi^{-2} of oil and 48 Bcf mi^{-2} of associated gas. It enters the oil window in each of the four grabens (USA EIA, 2014).
- *The North Ustyurt and Chu-Sarysu Basins* are the prospective basins of the country that are not yet assessed for hydrocarbon potential. The North Ustyurt (56,000 mi^2, 145039.33 km^{-2}) has a chain of shallow, heavy oil fields (Jurassic-Cretaceous) along with the western edge of the basin. The Chu-Sarysu contains the oil and gas field of Middle Carboniferous Visean and Early Permian subsalt in the southern section of the basin (Zhao et al., 2016). The Tournaisian and Permian shales of the Lower Carboniferous and the Permian age are the principal source rocks (e.g., Bykadorov et al., 2003; Zhao et al., 2017).

Oil and gas reservoirs, saline aquifers and unmineable coal seams are the most suitable geologic formations suitable for the CO_2 storage. Such regimes are found in sedimentary basins (Abuov et al., 2020). When the Kungurian salt seal was in place and thick orogenic molasse clastics deposited, the main stage of hydrocarbon production occurred presumably in the basin's peripheral shallower regions. Hydrocarbon was produced significantly from local depressions adjacent to the expanding salt domes (Huvaz et al., 2007).

4.1.9. *Jordan*

The country has the two most promising hydrocarbon basins (Hamad and Wadi Sirhan Basin) of the Silurian Period. The marine deposition of black shale of the Batra Member of Mudawwara Formation has potential of producing shale oil and shale gas lying in the sub-surface of the hydrocarbon basins. According to Armstrong et al. (2005), It is formed due to the last deglacial transgressive succession that in-filled an existing low stand glacial continental shelf topography. The formation expanded during the transgression that split the sub-basin and the interfluves. It has an estimated 35 Tcf and 4 Bbl of shale gas and oil in-place with 7 Tcf shale gas and 0.1 B bbl of shale oil is recoverable (USA EIA, 2013). The ~ 8000 ft (2438.4 m) deep and 160 ft (48.77 m) thick Hamada Formation (3300 mi^2) of Hamad Basin is an organic-rich marine Upper Ordovician Black Shale where the TOC ranges from 0.5 % to 2.0 % and $R_O \geq 1.2$ %. The O-C unit in the basin is called the *"Upper Hot Shale"* along the Iraq border. The gas prospective area of 1050 mi^2 has a gas window that estimates 33 Tcf mi^{-2} in-place. The Wadi Sirhan Basin consists of 3300 mi^2 of *"Lower Hot Shale"* or Lower Batra Shale deposited at its base having an oil window with an average height of 5500 ft (1676.4 m). The TOC ranges from 1.5 % to 9 % and R_O 0.7–1.0 %. It has an estimated 9 MM bbl mi^{-2} of oil and 2 Tcf shale gas in-place.

Jordon has ~ $5*10^{10}$ tons of unexplored oil shale reservoir and resembles compositionally with the shales of western Colorado, USA (Jaber and Probert, 1997; Hrayshat et al., 2008). The central Jordan has significant unexploited deposits of oil shale with an average organic conent of 9–13 % (MEMR, 1991–1996; NRA, 1985–1995; Jaber and Probert, 1999).

No detail study is available regarding carbon sequestration from these basins.

4.1.10. *Mongolia*

East Gobi and the Tamtag basins are the two most thermally mature prospective shale resource basin of Mongolia. It has an estimated 4 Tcf out of 55 Tcf of shale gas and 3.4 B bbl out of 85 B bbl of shale oil.

- *East Gobi Basin:* It is a 25,000 mi^2 rift basin located in SE Mongolia adjacent to the Zuunbayan and Tsagaan Els oil fields (Prost, 2004). It is a narrow and elongated basin formed by rifting and several tectonic episodes between Jurassic to Cretaceous Period with several close-spaced faults (Prost, 2004; Graham et al., 2014). It contains sand and shale deposits in a fluvial-lacustrine environment during the Jurassic to Early Cretaceous period (Johnson, 2004). It is oil-prone in the deep troughs. The East Gobi basin comprises of four sub-basins (Unget, Zuunbayan, Khovsgol and Sainshand) containing thick lacustrine mudstone of the Middle Jurassic to Tertiary period. The sub-basins are the potential targets for shale oil in the East Gobi basin. The Tsagaantsav Formation overlaying the Sharlyn Formation contains thick O-C oil shale of Type I and II kerogen with TOC 1.5–15 % and with an average Ro = 0.8 % (Prost, 2004). It has ~ 29 Tcf and 43 B bbl of shale gas and shale oil in-place.
- *Tamtsag Basin:* It is located on the eastern part of Mongolia and is a part of Hailar-Tamtsag basin extended over China and Mongolia (Jia et al., 2014). The Tamtsag basin is a structurally complex (6700 mi^2) intra-continental rift basin comprising several fault-bounded WSW-ENE trending troughs. It consists of volcanic sedimentary rocks of the Mid-Jurassic to Tertiary period (Henk et al., 2007). The Lower Cretaceous Nantun Formation is the main hydrocarbon reservoir of the basin. It consists of fluvio-deltaic conglomerate, sandstone, and deep-water lacustrine shale. According to Liu et al. (2023), the basin has 250 ft (76.2 m) O-C rich lacustrine shale at a depth of 7000 ft (2133.6 m). It has an average TOC of 3.0 % with thermal maturity 0.8 %. It has ~ 26 Tcf of shale gas and 43 B bbl of shale oil in-place from which 2.1 Tcf and 1.7 B bbl of shale gas and oil could not be extracted for commercial use (USA EIA, 2015).

No detail study is available regarding carbon sequestration from these basins.

4.1.11. *Thailand*

The southeast Asian countries has no explorations in unconventional shale resource though it has remarkable potential of shale gas reserves. The Khorat basin, located south of the Khorat Plateau, NE Thailand, the basin of 90650 km^2 (35000 mi^2) is estimated to have the world's best potential shale gas reservoir. It lies on the Indochina microplate parted from the Sakon Nakhon Basin to the north by the Phu Phan anticline (Koyasamram and Comrie-Smith, 2011; USA EIA, 2013). The basin comprises of Permo-Carboniferous, Mesozoic and Quaternary deposits of Late Cambrian through recent sequences interrupted by unconformities. The Nam Duk Formation is the notable shale gas target of the basin. Due to insufficient data, it is assumed to be 1000 ft (304.8 m) thick with an average depth of 9000 ft (2743.2 m), TOC 3 %, pressure gradient 0.6 psi ft^{-1}, and $R_O > 2.5$ %. It has an estimated 22 Tcf shale gas in-place with 5 Tcf of recoverable shale gas (USA EIA, 2013).

The Central Plains Basin and its sub-basin, e.g., Phitsanulok Basin and Suphan Buri Basin are prospective of Early Miocene lacustrine shale. It is mature and oil-prone but several normal faults may hinder the resource development. The Mae Sot and Fan- Sub-Basin of the Northern Intermontane Basin comprises of organic-rich grey-green Miocene lacustrine shale and are prospective of thermally mature shale oil in near future. More assessments are necessary for the commercial exploration of shale oil and gas from these basins. The mudstones in Hui Hin Lat Triassic Formation in the western margin of the Khorat Plateau is evaluated as a potential shale gas play (Chenrai et al., 2022). It is formed in anoxic to suboxic marine environment. According to Chumkratoke et al. (2015), the samples measure an average 4.9 % porosity. The higher content of quartz and carbonate makes it suitable for hydraulic fracturing.

No detail study is available regarding carbon sequestration from these basins.

4.2. Africa

4.2.1. Algeria

The Silurian Tannezuft and the Devonian Frasnian Shale are the two significant shale formations of Algeria in seven potential hydrocarbon basins (Ghadames/Berkine, Illizi, Timimoun, Ahnet, Mouydir, Reggane and Tindouf) (Boote et al., 1998). The evolution of these seven basins results due to the breakup and collision of the Laurasia and the Gondwanaland from the single massive basin of North Africa in the Paleozoic (Klett, 2000). The Silurian and the Late Devonian marine transgression had deposited the organic-rich sediments in these basins.

- *Ghadames/Berkine Basin:* It is a large intra-cratonic depression covering eastern Algeria, Southern Tunisia and western Libya (Echikn, 1998). It constitutes a chain of reverse faults, structural traps and uplifted fault blocks (in the basin center) formed during the Cambrian and Ordovician Periods. The basin has two significant formations- the Silurian Tannezuft lying below the Rhuddanian and the Upper Devonian Frasnian, in the country's eastern section (Emme et al., 1991; Underdown and Redfern, 2008). The Silurian Tannezuft Formation ranging from 10,000 to 16,000 ft (3048–4876.8 m) in thickness (from the eastern and northern edge to the basin center) and net organic-rich thickness of 248 ft (75.59 m), increases its thermal maturity (1.3–2 %) towards the center or the dry gas portion of the basin. The Ro changes towards the basin edge (1.0–3 %) placing these portions in the wet gas and condensate window (Wang et al., 2019). The average TOC values are 5.7 % with 15 % towards the lower portion of the formation. It contains Type II kerogen with an estimated HI of 600 mg Hc g^{-1} of TOC (Dadi et al., 2019).

  It has an evaluated resource concentration of 43 Bcf mi^{-2} of wet gas, 3 MM bbl mi^{-2} of condensate, and 55 Bcf mi^{-2} of dry gas. The Upper Devonian Frasnian Shale deposited above the Tannezuft are thermally less mature (Ro = 0.7 %; TOC = 3–10 %: Rahamani et al., 2012) with a depth ranging from 8,000-16,000 ft (2438.4–4876.8 m) with a gross thickness of 50–500 ft (15.24–152.4 m). The center portion of the prospective area (5010 mi^2) with Ro ranging from 1.3 % to 2 % is in the dry gas window. The northern, eastern and southern outer ring of the area with Ro ranging from 0.7 % to 1.0 % is in the oil window. In between the dry gas and oil window lies in the wet gas condensate window with Ro between 1.0 % and 1.3 %. It has an estimated resource concentration of 111 Bcf mi^{-2} of wet gas, 44 MM bbl mi^{-2} of oil, 10 MM bbl mi^{-2} of condensate, and 134 Bcf mi^{-2} of dry gas.

  These structural traps in the basin are the convenient sediment depositional traps for shale oil and gas. Approximately, 60–63 mW m^{-2} of heat flow in and around the folded structures between the Late Cretaceous and Tertiary Periods accompanied by Herciniyan event sequestrated carbon in the basin (Yahi eta la., 2001). The deposited thick shallow marine sediments in the Early Jurassic have captured carbon sealed by the salt and anhydrite sediment beds (Boudjema, 1987; Yahi et la., 2001).
- *Illizi Basin:* It is an intractratonic sag basin located south of the Berkine Basin bounded by the Tihemboka Arch on the east, Hoggar Massif on the south and Amguid-Hassi Toureg structural axis on the west, which separates the basin from the Mouydir Basin. The Illizi Basin is separated from the Ghadames/Berkine by a hinge line in the slope of the baseme nt rock. This hinge line controls the migration and accumulation of petroleum in these two basins (Keltt, 2000). The gross thickness of the formation is 30–330 ft (9.144–100.584 m). It contains Type II kerogen with TOC ranging from 2 % to 10 %. The Ro varies from 1 to > 2 % in the basin prospective area exceptionally between 1 % and 1.3 % in the wet gas and condensate window region (English et al., 2016). The wet gas and condensate are placed in the north-central portion of the basin with the deeper sections in the dry gas window. The basin estimates a resource concentration of 51 Bcf mi^{-2} of wet shale, 6 MM bbl $mi^{-2}$of shale oil and condensate, and 61 Bcf mi^{-2} of dry gas (USA EIA, 2013).

  Timimoun Basin: It is located in central Algeria bordered by the Beni Abbes Saddle on the west, Djoua Saddle on the south, and structural uplift on the north and the east. The erosion process along the structural highs of the basin differs with the basin depth and sedimentation. The primary source rocks (shale) for dry gas are the Silurian Tannezuft Shale that covers almost the entire part of the basin except its NW section. The depth ranges from 5,000-15,000 ft (1524–4572 m), from basin edge to the basin center, with net organic-rich pay of 90 ft (27.432 m). It has an estimated resource concentration of 36 Bcf mi^{-2} of dry gas. The Upper Devonian Frasnian Shale has a dry gas area covering the two-third portion in the eastern part of the basin. Its net organic-rich thickness is 180 ft. It has an estimated a resource concentration of 73 Bcf mi^{-2} of dry gas (USA EIA, 2013). It has a TOC ~ 3 % and Ro > 1 % (Luning et al., 2003).

  The fine-grained siliciclastic sedimentary units of the Timimoun Basin are the caprocks that captured and sealed the carbon in the basin with 1.8 % porosity. Minerals such as quartz, muscovite, chlorite, illite and detrital mica compacted and reduced the porosity initiating trap of carbon (Armitage et al., 2010).
- *Ahnet Basin:* The N-S trending basin is placed in the Sahara Desert Platform bounded by the Timimoun Basin at south and Mouydir Basin at west (Kadri et al., 2018). Tectonic compression had led to the evolution of numerous large elongated anticlines and domes. The basin contains Paleozoic sediments including the Silurian Tannezuft and the Devonian Frasnian shales. The potential area for shale gas and oil reservoirs are the Tannezuft and the Frasnian that lies in the northern sector of the basin (Kadri et al., 2017). The depth of the Tannezuft shale ranges between 6,000-10,500 ft (1828.8–3200.4 m) with a thickness between 150 and 500 ft (45.72–152.4 m). The TOC ranges from 1.5 % to 3 % with Type II/III kerogens (Lueing et al., 2003; Mezzar et al., 2024). The Ro exceeds 1.3 in the dry gas area. It has an estimated resource concentration of 109 Bcf mi^{-2} of dry gas in the basin. The Devonian Frasnian Formation is within 3300–9500 ft (1005.84–2895.6 m) depth with thickness ranging from 60 to 275 ft (18.28–83.82 m). The dry gas prospective area prevails in the deeper section and the wet gas/condensate in the shallower portion of the basin. The shale has a TOC ranging from 3 % to 12.6 %, Ro >1.0 % with Type III kerogen (Kadri et al., 2017). It has ~ 22 Bcf mi^{-2} of dry gas as the concentrated resource (USA EIA, 2013).
- *Mouydir Basin:* Situated in central Algeria bounded by the Illizi Basin on the west and Timimoun and Ahnet Basin on the east contains the Silurian Tannezuft Shale and Upper Devonian Frasnian Shale. Several upthrust structural ridges separate these basins (Wendt, 2006). The source rocks are found deepest in the northern section of the basin. An outcrop of the formation is visible in the southern portion of the basin. Here, the Tannezuft Shale is assessed as the most prospective formation within 5,000-10,000 ft (1524–3048 m) depth with a gross organic-rich shale thickness from 20 to 120 ft (6.1–36.58 m). The TOC ranges from 2 % to 4 % with Ro > 1.3 % and is placed in the dry gas window. It has an estimated resource concentration of 19 Bcf mi^{-2} of dry gas (USA EIA, 2013).

- *Reggane Basin:* It is an asymmetric synclinal basin placed on the Sahara Desert section of central Algeria. It is bordered by a sequential reverse fault on the north and is parted from the Timimoun Basin by the Ougarta Ridge. The depth of the Silurian Tannezuft is 16000 ft (4876.8 m) on the north to 5000 ft (1524 m) on the south with a gross organic-rich thickness between 130 and 230 ft (39.62–70.10 m) (Arab et al., 2011). The TOC ranges between 3 % and 5 % with Ro from 1.0 % to 1.3 % into the wet gas and condensate window and > 1.3 % in the dry gas window (Kaced et al., 2012). The wet gas and the condensate lie in the shallow region of the southern section of the basin whereas the dry window lies deep in the northern section of the basin. It has an estimated 94 Bcf mi^{-2}of dry gas, 38 Bcf mi^{-2} of wet gas, and 4 MM bbl mi^{-2} of oil and condensate concentrated unconventional resource (Boudjema et al., 1990). The depth of the Upper Devonian Frasnian Formation ranges from 5500 to 16000 ft (1676.4–4876.8 m) with the thickness of the hydrocarbon producing shale between 260 and 330 ft (79.25–100.58 m) (Logan and Duddy, 1998). The TOC ranges from 2 % to 4 % (Rahmani et al., 2012). The Ro in the wet/condensate window in the shallow area and the dry gas window in the deeper section of the basin exceed 1. It has an estimated a resource concentration of 97 Bcf mi^{-2} of dry gas, 104 Bcf mi^{-2} of wet gas, and 11 MM bbl mi^{-2} of oil/condensate (USA EIA, 2013).

- *Tindouf Basin:* It is situated in the SW part of Algeria surrounded by Morocco on the west and by Mauritania. The Devonian Frasnian Shale is relatively thin where thickness ranges from 3 to 4 ft (0.91–1.22 m) with a TOC of 1 %. Thus, the formation is excluded from hydrocarbon quantitative assessment. The Silurian Tannezuft is the potential and primary source rock with a prospective area lying in the northern portion of the basin. Its depth ranges from 6600 to 14000 ft (2011.68–4267.2 m) with a net hydrocarbon producing shale thickness of 54 ft (16.46 m). The TOC value is > 2 %, and the Ro is > 1.0 % with Type III kerogen (Belhameche and Saadallah, 2007; Ramahari et al., 2012). The Silurian is in the wet gas/condensate and dry gas window. It has an estimated a resource concentration of 24 Bcf mi^{-2} of dry gas, 19 Bcf mi^{-2} of wet gas, and 1.7 MM bb mi^{-2} of oil and condensate.

4.2.2. South Africa

The *Karoo* is one of the massive and promising sedimentary basins of South Africa. It comprises of continuous sedimentary sequences from the Pennsylvanian to Mid Jurassic, documenting the postglacial sediments of central Gondwana to the Triassic Hothouse extremes (Montanez et al., 2007; Sun et al., 2012; Scotese, 2016; Gotz et al., 2018; Nolte et al., 2019). The Permian postglacial sediments deposited ∼ 300–183 Ma ago during the Gondwanaland breakup between ca. 280–180 Ma (Geel et al., 2013; de Kock et al., 2017; Gotz et al., 2018). It contains organic-rich thick black shales covering 612272 km^2 (2,36,400 mi^2) area, which approximates two-third portion of the country. The southern section of the basin has a potential gas reservoir and is known as a foreland trough. It is formed by the gentle slope subduction of the paleo-Pacific plate beneath the Gondwana supercontinent, which formed the wide Cape Fold Belt (CFB) (Geel et al., 2013). Prince Albert, Whitehill and Collingham of the Lower Permian age are the primary source rock of the Ecca Group.

The Ecca Group is divided into Upper Ecca and Lower Ecca is 10,000 ft (3048 m) thick in the southern part of the basin. The Upper Ecca is a geologically complex shallow marine deposition of 5000 ft (1524 m) thick. The TOC ranges from 1 % to 2 % with a thermal maturity of 0.9–1.1 %, defining the area in the oil and wet gas window (Raseroka, 2009). The basalt intrusion occupied ∼ 25899 km^2 (10, 000 mi^2) area in the center of the resourceful area and extensive igneous thick sills obstructs the exploration of shale resources in the Upper Ecca Group.

The Fort Brown and the Waterford are the two rock formations of the Upper Ecca unit. The Fort Brown Shale covers a hydrocarbon producing area of 82103 km^2 (31,700 mi^2) with an average depth of 6000 ft (1828.8 m). It has a net productive shale thickness of 3000 ft (914.4 m) with a TOC value from 1 % to 2 % and an average Ro of 1.1 %. The Waterford Shale has a resource area of 53870 km^2 (20,800 mi^2) with an average depth of 4500 ft (1371.6 m) and a net productive shale thickness of 100 ft (30.48 m). The TOC values range from 1 % to 2 % with an average Ro of 0.9 %. These Formations are below the criterion for resource assessment thus not accounted as a hydrocarbon resource. The Lower Ecca estimates a shale resource area of 155865 km^2 (60,180 mi^2) defined by the Lower Ecca Group shales on the NE and the Upper Ecca Group on the other sides. It is in the dry gas window. The Lower Ecca contains three distinct shale formations (the Prince Albert Formation overlain by the Whitehill and Collingham Formations) located in the central and the southern part of the basin (Johnson, 2009).

The Prince Albert of Lower Permian is a potential shale gas reservoir overlaying the glaciomarine Dwyka tillites with a depth ranging from 6,000- 10,000 ft (1,828.8-3048 m) and thickness from 200 to 800 ft (60.96–243.84 m) (net organic-rich thickness is 120 ft, 36.58 m). The northern basin is composed of olive-dark grey silty shale with intruded laminated sandstone layers whereas, the southern shales are dark grey with pyrite, chert, phosphatic nodules and lenses (Cole, 2005). The TOC values from 1.5 % to 5.5 % and Ro ranges from 2 % to 4 % (Ro is high in the dry gas window) with a high thermal gradient. The organic content loses its properties near the igneous intrusion where the shale has converted into graphite and CO_2. It has an estimated 385 Tcf of shale gas in-place out of which 77 Tcf is recoverable.

The Whitehill Formation of Lower Ecca Group contains hydrocarbon producing mature black shale widely spread in the southern section of the basin (Branch, 2007). The Formation was deposited in a deep-marine anoxic environment (Steffen et al., 2019). It contains sediments, minor sandy interbeds, from distal turbidities and storm deposits. The black shales are composed of quartz, illite, muscovite and chlorite with lesser plagioclase and pyrite (Geel et al., 2015). With 5,500-10, 000 ft (1,676.6-3048 m) depth and 100–300 ft (30.48–91.44 m) thickness, it is one of the prime shale gas targets of South Africa. The TOC ranges from 3 % to 14 % and Ro 2–4 %. The shale is presumably over pressured and it lies within the dry gas window. The Whitehill Shale is composed of quartz, pyrite, calcite and chlorite. It holds Type I and II kerogens. It has an estimated 845 Tcf shale gas in-place out of which 211 Tcf is recoverable (USA EIA, 2013). The Lower Permian Collingham Formation is deposited in a deltaic environment with a net organic-rich thickness of 80 ft (24.38 m) and an average depth of 7800 ft (2377.44 m). The formation is composed of thin dark grey shale with an alteration of very thin tuff layers (Johnson et al., 2006). The TOC ranges from 2 % to 8 % and an average Ro of 3 %. It has a concentration of 328 Tcf of shale gas out of which 82 Tcf is recoverable (USA EIA, 2013).

4.2.3. Libya

Geologically, Libya can be divided into two distinct provinces with several sedimentary basins. The northern province is situated on an unstable shelf including the Pelgian shelf, Sirte Basin, and Cyrenaica Platform from west to east. The southern section of the country lies within a stable cratonic area. It includes Ghadames, Muzuruk and Kuffra Basins. The Ghadames, Sirte and Muzuruk basins have an estimated 942 Tcf shale gas and 613 B bbl of shale oil in-place (USA EIA, 2013). Sirte is the prime productive hydrocarbon resource basins of North Africa with 16 giant oil and gas fields.

- *Ghadames (Berkine) Basin:* It is a massive intracratonic basin extending from east Algeria to south Tunisia encompassing ∼ 217559 km^2 (84,000 mi^2) area in NW Libya. The interval results in two sequences are separated by the Caledonian and the Hercynian unconformity (Dardour et al., 2006). The basin contains 600 m thick sediments of Paleozoic and Mesozoic Periods (Echikh, 1998). The distribution of shale oil and gas field are highly influenced by the

Silurian-Devonian succession in Libya. The Silurian Tannezuft Formation (57938 km^2, 22,370 mi^2) and the Upper Devonian Frasnian contain the primary source rock of the basin. The *"hot shale"* Tannezuft Formation in Libya contains an organic-rich basal stratum within 10,000–14,500 ft (3048–4419.6 m) depth towards the center. Its thermal maturity increases towards the basin's center. The dry gas area (2580 mi^2) in the center has a Ro ranging from 1.3- >2 % and the oil window (16,440 mi^2) between 0.7 % and 1.3 %. Out of 42 Tcf of wet and dry shale gas, it has an estimated 54 Bcf mi^{-2} of dry gas and 43 Bcf mi^{-2} of wet gas. It comprises of 12 MM bbl mi^{-2} of shale oil *in-situ* (USA EIA, 2013).

The Frasnian Shale is thermally less mature here with an average depth of 8500 ft (2590.8 m). The source area covers 5102 km^2 (1970 mi^2) of the basin in Libya. The eastern, northern and the southern boundaries have a minimum Ro 0.7 %. The outer ring of the area (1570 mi^2) is in the oil window with Ro ranging from 0.7 % to 1.0 %. Only 30 mi^2 (77.7 km^2) in the center of the formation with Ro > 2 %, is in the dry gas window. In between these lies the wet gas and condensate area of 370 mi^2 (958.3 km^2) with Ro ranging from 1.0 % to 1.3 %. The TOC value of the Formation ranges from 3 % to 10 %. It has an estimated 31 MM bbl mi^{-2} of oil, 7 MM bbl mi^{-2} of condensate, 8 Bcf mi^{-2} of wet gas, and 93 Bcf mi^{-2} dry gas from the prospective area of 1970 mi^2 (USA EIA, 2013).

- *Sirte Basin:* It is a pericratonic basin located between the Cyrenaica and the Zelten-Defa Platform extending from the Gulf of Sirte in the south to central Libya covering ~ 445478 km^2 (1,72,000 mi^2) area (Gumati, 1992). It is bounded by the Cyrenaica platform, the Ghadames basin and the Kuffra Basin to the east and northeast, west and south. The evolution of the basin resulted from normal faulting and thrusting within the African plate during the Cretaceous Period (Brown et al., 1985; Almond, 1986; Gumati et al., 1996). This crustal extension produced a chain of normal faults dividing the basin into complex Cretaceous to Eocene horst and grabens trending NW to SE. These resulted from Cretaceous to Miocene crustal extension (Parsons et al., 1980). The basin has evidences of eight rifting episodes from Early Cretaceous to Early Eocene (Abadi et al., 2008). In the Early Cenomanian Period, the deposition of the oldest marine sediments occurred due to transgression. The carbonates, evaporites, terrigenous clastics and organic-rich green shales deposited in the graben whereas the horst blocks remained partly exposed (Selley, 1968; Gumati et al., 1996). The western part of the basin has observed high geothermal gradients in their Upper Cretaceous shallow-water sediments (Gumati and Schamel, 1988). The fault-defined trough from west to east are the Hon, Zella, Hagfa and Agedabia. These consist of the thickest, richest and hottest (due to crustal thinning) petroleum source rocks of the Upper Cretaceous and Palaeocene Periods (Selly, 1997). The Hameimat, Agedabia, Wadayat, Hagfa and Zella troughs contain the two significant hydrocarbon sources, Ramchat and Etel Formation.

The Upper Cretaceous Rachmat and Etel Shale Formations cover a prospective area of 35,240 mi^2 and 19,920 mi^2, respectively. The net organic-rich thickness of the Rachmat shale formation is 200 ft (60.96 m) with an average TOC of 2.8 % and thermal maturity ranging from 0.7 % to 1.0 % in the oil window. It has estimated an oil concentration of 29 MM bbl mi^{-2} and 350 Tcf of shale gas in-place out of which only 28 Tcf is recoverable (USA EIA, 2013). The Etel Formation underlying the Rachmat shale has a depth ranging from 11000 –16400 ft (335.28–4998.72 m) with a thickness of 600 ft (182.88 m) and net organic-rich thickness of 120 ft (36.58 m). It has a maximum TOC of 3.6 % with Ro ranging between 1.0 % and 1.3 %. It has ~ 6 MM bbl mi^{-2} of oil and 37 Bcf mi^{-2} of wet gas (USA EIA, 2013).

- *Murzuq Basin:* It is a 5670 mi2 (14685.23 km^2) Palaeozoic intracratonic basin that extends south into the Republic of Chad and is located to the southwest of Libya. It is encircled by the Tihembada Arch to the west and the Tibis ti Arch to the east. The Illizi Basin in Algeria is divided from this basin by Tibisti and Tihembada arch. The basin is divided from the Ghadames basin, which includes the borders of Libya and Chad at south, by the Qurcal arch at west. It consists of a series of troughs and rifts with high-angle reverse faults in the hangingwalls or tip-line folds above the faults (Davidson et al., 2000). The shale units were deposited during the post-glacial sea--level rise extending from Morocco to Oman along east-west across the northern Gondwanaland (Luning et al., 2000; Fello et al., 2006).

After the 1980s, the giant Elephant field and other smaller fields were discovered with an estimated resource potential of 5.4 B bbl of oil in-place. The Tannezuft Formation of the Lower Silurian and Awaynat Formation of the Middle Devonian Period are the two primary hydrocarbon source rocks of the basin. The Silurian Tannezuft is a marine deposited Formation containing dark grey to black graptolitic "hot" shales within 3300 – 10,000 ft (1005.84–3048 m) depth (Aziz, 2000). Though, the width of the basal "hot shale" unit ranges between 30 and 100 ft (9.14–30.48 m) with TOC ranging from 3.2 % to 23.1 % and Ro from 0.83 % to 0.95 %. The maturity of the shale increases towards the southern portion of the basin. It holds Type II kerogen with HI ranging between 220 and 400 mg HC g^{-1} (Luning et al., 2003; Belaid et al., 2010). The Upper Silurian Tannezuft Formation mainly consists of Type III kerogen with its maturity ranging from 0.6 % to 0.9 % (early to intermediate maturity), TOC 0.4–1.28 %, and T_{max} 432–445 °C (Luning et al., 2003; Hodairi and Philip, 2011). The shale has moderate organic content at the eastern margin of the basin with average TOC ranging between 0.07 % and 1.7 % and < 10 ppm concentration of uranium (Meinhold et al., 2013). Overall, it has an estimated 10 MM bbl $mi^{-2}$of oil and associate gas where 1500 MM bbl of oil is recoverable (Davidson et al., 2000). The Middle-Late Devonian Awaynat Formation is considered as a potential shale formation (Echik and Sola, 2000).

- *Kufra Basin:* It is a massive unexplored intra-cratonic sag basin in SE Libya covering ~ 4,00,000 km^2 area. Mostly due to its isolated location, the Kufra Basin has not seen much geological exploration (Luening et al., 1999). The basin has a sedimentary record from shallow marine to fluvial deposits of infracambrian to the Cretaceous period (Luning et al., 1999). The Lower Silurian Tannezuft Formation is present at the base on the western section of the basin with potential structural traps of hydrocarbon in the fault blocks with hot marine shales (Xiao et al., 2023). The basin has a TOC 0.21–0.84 % with low uranium concentrations (< 12 ppm) (Luening et al., 2010; Meinhold et al., 2021). T_{max} values of 422–426 °C and HI values of 242–252 mg S2/g show that the organic matter is immature (Meinhold et al., 2013). Few samples revealed that the RO is < 0.6 % for the Tanezzuft Formation connoting a marginally mature early-mature stage. The Ro within 2000–6000 ft succession ranges from 0.5 % to 0.6 % (marginally mature to peak oil window) (Almadhone et al., 2011).

4.2.4. Egypt

The organic-rich Middle Jurassic Khatatba Shale (Kabrit or Safa shale) is the prime source rock of the Abu Gharadig, Alamein, Natrun and Shoushan-Matruh hydrocarbon basins. These is a series of rift basins with thick sedimentary sequences (> 15,000 ft, > 4572 m deep) composed of marine deposits of Paleozoic through Tertiary strata situated in the north region of the Egyptian western desert. The Khatatba Formation is 0–2000 ft (0–609.60 m) thick. The TOC ranges from 3.6 % to 4.2 % and Ro from 0.7 % to 1.0 % in the oil window and 1.0–1.3 % (Younes, 2002) in the wet gas and condensate window with HI ranging from 63 to 261 mg Hc g^{-1} TOC (Shalaby et al., 2012; Younes, 2012). The T_{max} of the Khataba Shale is within 436–449 °C (El Diasty, 2015). It holds a mixed kerogen Type (II-III and III) (vitrinite-inertinite) of marginal marine and continental organic matter with 1–17 % porosity (Peters and Cassa, 1994; Shalaby et al., 2014). The other hydrocarbon producing rocks of the basins include the Silurian and the Cretaceous

Formation. The Silurian consists of thick strata of siltstones and sandstones including organic-rich shales in the NW portion of the western desert. The thickness gradually decreases towards south and east. The Silurian shales are not visible in the other part of the basin. The Cretaceous shales are of moderate quality with TOC < 2 % and thermally less mature for oil and gas generation (Moretti, 2010). It lies within the Alam El-Bueib and the Roash Formations extending the maximum portion of the Western Desert. Thus, lack of favorable reservoir properties, the Silurian and Cretaceous shales are not considered for resource assessment (USA EIA, 2013).

4.2.5. Chad

Chad is a large intracratonic depression in Central West Africa. It is a sub-division of the series of the African interior cratonic basins. It developed during the extension and subsidence of the Central African crustal blocks and separation of the Gondwanaland in the Cretaceous Period (Boboye and Abimbola, 2009). The country has six hydrocarbon prospective basins: Termit Basin in the west, Bongor, Doba, Doseo and Salamat basin in the south and the Erdis Basin, which is also known as Kufra Basin in Libya in the north.

- *The Termit Basin:* It is an asymmetric rift basin with ~ 11400 mi^2 area consists of Lower and Upper Cretaceous hydrocarbon source rock (Wan et al., 2014). The basin is enclosed by Cretaceous and Tertiary extensional rifts in the NE, SW and east; and Niger and Nigeria in the west. The lacustrine and marine deposited sediments of the Cretaceous Period are the commercial hydrocarbon source rocks in the shallower conventional oil fields (USA EIA, 2014). The Lower Cretaceous shale along the eastern boundary of the basin and the Upper Cretaceous shale along the eastern and western boundaries are oil-prospective. Both are gas prospective towards the basin center. These 2–10 km thick sediments deposited over the Precambrian basement. Thickness increases from the basin edge towards the center. The TOC in the Lower Cretaceous shales ranges 2–10 %, thermal maturity of 0.7–1.0 %, the temperature gradient of 1.4 °F per 100 ft with Type III kerogen. They range in thickness from 30 to 60 ft. The Upper Cretaceous (thickness: 6–20 ft, 1.83–6.09 m) contains TOC between < 0.36–23.32 %, Ro of 0.7–1.3 % on average, and HI values ranges from 29 to 822 mg Hc g^{-1} TOC with Type II and III kerogen (Wan et al., 2014). The basin is in the oil generating window at 8200–13000 ft (2499.36–3962.4 m) depth and the wet gas window between 13000 – 16400 ft and further below. The estimated resource concentration for the Lower Cretaceous shale is 58 MM bbl mi^{-2} of oil and 134 Bcf mi-2 of wet gas/condensate. A resource concentration of 22 MM bbl mi^{-2} of oil and 47 Bcf mi^{-2} of wet gas/condensate are estimated from the Upper Cretaceous units (USA EIA, 2014).
- The *Bongor Basin* is an elongated inverted rift depression covering ~ 21238 km^2 (8200 mi^2) area bounded by a series of deep-seated rift-influenced faults (Dou et al., 2020). The Lower Cretaceous deposited in the deep lacustrine anoxic environment is the primary hydrocarbon producing rock (Tan et al., 2017). Their type matches the Lower Cretaceous of the Termit Basin. The Tertiary sediments are directly deposited on the Precambrian basement with 2,000-5000 m thickness (USA EIA, 2014). The TOC ranges from 1 % to 19.51 %, thermal maturity 0.7–1.0 %, HI ranging from 222 to 889 mg/g, TOC with a mixture of Type I, II and III kerogens (Yang et al., 2018). It has ~ 62 B bbl mi^{-2} of shale oil and 58 Tcf of associated gas (USA EIA, 2014).

  The Doba Basin with ~ 9100 mi^2 area is located in the easternmost of the Central rift basins (in southern Chad) along the southern border of Chad and the Central African Republic. It is bordered by a chain of deep-seated faults at north, south and west. The Central African Fault Zone encloses the eastern border of the basin. The Lower Cretaceous primary source rock of the basin resembles those of the Termit and Bongor Basins. The sediment thickness ranges from 1,000-5000 m from north to the center of the basin. The source rock is in the middle to late oil window phase with an average temperature gradient between 1.4 and 1.6 °F per 100 ft (= 0.56–0.55 ^{0}C m^{-1}). It has an estimated shale oil concentration of 80 B bbl mi^{-2} of oil and 74 Tcf of associated gas (USA EIA, 2014).
- *The Doseo Basin* is flanked on the east by the Doba Basin divided and bordered by the Central African Fault Zone on the north. Though the Lower Cretaceous shales resemble its characteristics to the other mentioned basin, they are thick (2,500-3000 m) with TOC ranging from 2 to over 5 %. It reaches the oil window at a depth of 7500 to 16,400 ft (2,286- 4998.72 m) (Zhange et al., 2023). The temperature gradient of the reservoir is 1.5 °F per 100 ft (= −0.54 ^{0}C m^{-1}). It has an assumed 64 MM bbl mi^{-2} of oil and associated gas concentrated in the formation (USA EIA, 2014).

4.2.6. Tunisia

The deposition of Tunisian black shales is accompanied by initial transgression related to melting of ice or tectonics (Soua, 2014). The two most important prospective hydrocarbon producing basins are Ghadames and Pelagian. The Ghadames basin is of great interest for explorers due to its rather simple and stable geologic setting within the Saharan Platform. It is an intra-cratonic basin in the southern region of the country bounded by the Tunisia border in the east and Libya border in the south (Aissaoui et al., 2016). It is formed during the Paleozoic Gondwana tectonics (Soua, 2014). The Tannezuft and the Frasnian Formation of Silurian and Upper Devonian age of marine deposits are the two most notable hydrocarbon producing rocks of the basin. The Tannezuft Formation covers most of the North Africa and the Middle East section of the country with a prospective area of 3496 km^2 (1350 mi^2) with 7.2 % TOC (Rezouga et al., 2012; USA EIA, 2013). It contains organic-rich 'hot shale' due to its high uranium content. The source rock matured towards south of the basin and up to the gas window. The clay content increases towards its western and northern boundaries. The northern part of the basin has an estimated organic-rich area of 410 mi^2 with Ro ranging between 1.0 % and 1.3 % in the wet gas and condensate window. It has ~ 43 Bcf mi^{-2} of wet gas and 3.1 MM bbl mi^{-2} of condensate concentrated in the basin. The dry gas window covers ~ 940 mi^2 area with Ro > 1.3 %. It holds 54 Bcf mi^{-2} of dry gas.

The Frasnian hot shale is deposited above the Tannezuft source rock and beneath the Frasnian unconformity. These black shales hold a hydrocarbon producing area of 2140 mi^2 with thickness between 75 and 250 m. It thickens towards the SE and thins over the Ahara high to 4 m (Soua, 2014). This formation is thermally less mature at its northern boundary with Ro = 0.7 %. The formation is surrounded by Tunisia and Algeria border in the west, Tunisia and Libya border at its east and south. It has an oil window at its eastern and western parts of the shale formation with Ro = 1.0–1.3 %. It contains Type II kerogen with HI = 350–700 mg g^{-1} TOC (Acheche et al., 2001). Only 80 mi^2 prospective area in the SW section of the basin is in the dry gas window with Ro > 1.3 %. It is composed of quartz, pyrite, carbonate and low content clay with high content of brittle minerals (Soua, 2014). From the prospective area of 1970 mi^2, it has 31 MM bbl mi^{-2} of shale oil, 7 MM bbl mi^{-2} of condensate, 8 Bcf mi^{-2} of wet gas, and 93 Bcf mi^{-2} of dry gas (USA EIA, 2013).

Besides Ghadames basin, Tunisia has a less defined Pelagian shale basin in the east extending offshore. They consist of Jurassic-Cretaceous and Tertiary Petroleum System (Bou Dabbous). The Jurassic Nara Formation, the Early Cretaceous Fahdene Formation and the Late Cretaceous Bahloul Formation of the Jurassic-Cretaceous Petroleum System are composed of dark mudstone as the primary source rock (Klett, 2001). It contains Type III and II kerogens, respectively. The Ro ranges from 0.72 % to 0.87 % and for TOC it is 1–3 % (Hadded et al., 2021). The oil generated from the basin is light. The Bou Dabbous Shale Formation of the Tertiary Petroleum System extends from northern Tunisia up to the Libyan offshore. It contains Type I and II kerogen. The TOC is 0.4–4 % with a Ro indicating early mature to mature stage. The TOC is 0.4–4 % with a Ro (0.65–0.8 %), which indicates an early mature to

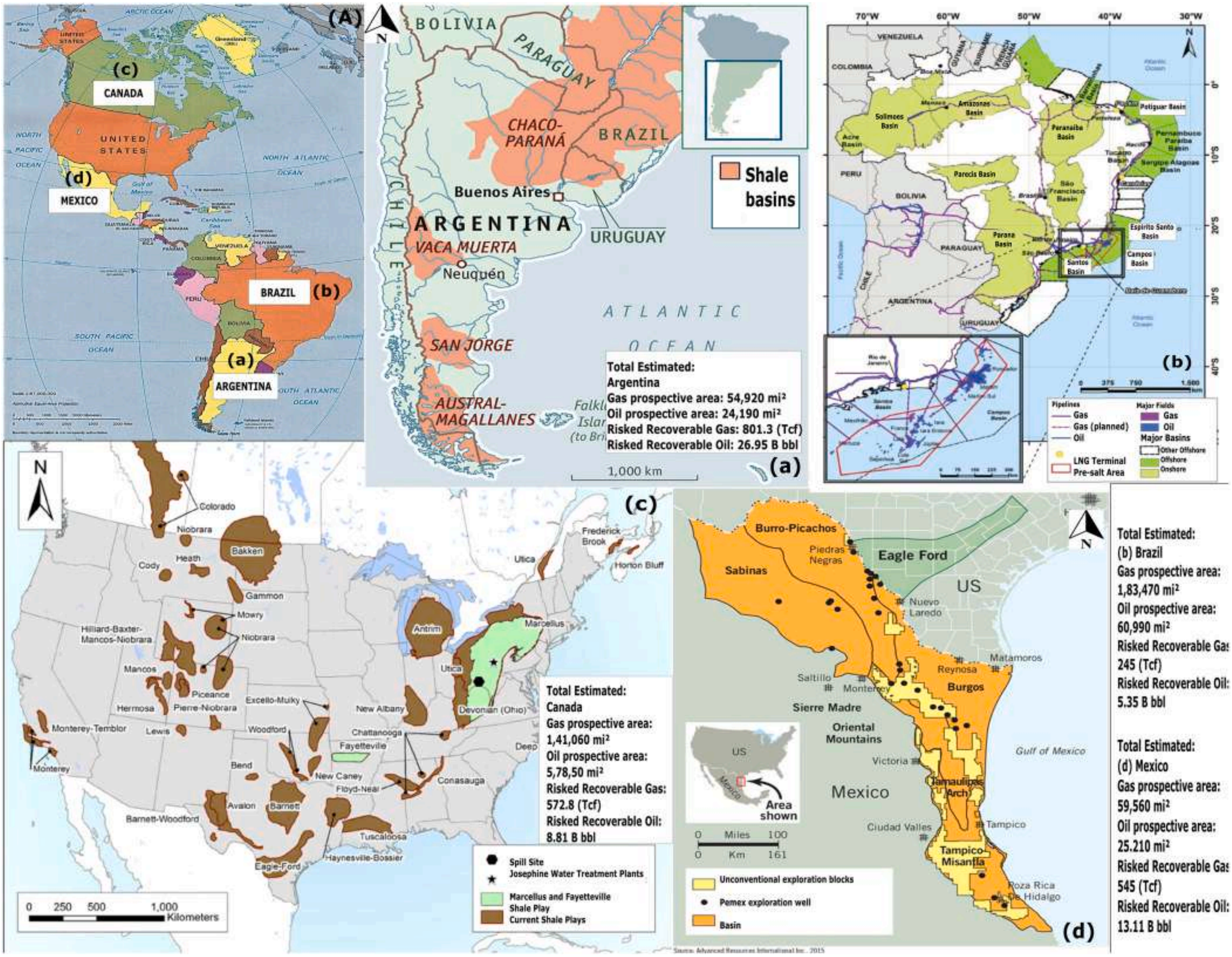

Fig. 4. **A.** Location of shale basins in Argentina and Brazil of South America, Canada and Mexico of North America (Source: Ms. Fairley's Site). **a.** The prospective shale oil and gas basins with commercial shale exploration activities (Source: Oil and Energy Trends, 2019). **b.** Map showing onshore and offshore Brazilian Basins for conventional and unconventional hydrocarbons (natural gas and oil) reserves (Rocha et al#, 2015). **c.** Shale Plays in United States and Canada mentioning the total estimated shale oil and gas resource with its prospective area (Warner et al#, 2014). **d.** The location map of potential shale basins in Mexico (Source: Stevens and Moodhe, 2016).

mature stage to the peak of the oil window (Bizerte region) (Klett, 2001; Arfaoui, 2024). The Bir M' Cherga basin in NE Tunisia has recorded thick organic-rich black shale formed during the Lower to Middle Cretaceous Period. It is placed at the E-NE at the end of the Tunisian furrow during the Barrimian-Albian Interval (Talbi et al., 2018). The T_{max} value ranges from 436 to 450 °C and thermal maturity from 0.5 % to 1 %. The average oil saturation index (OSI) of the basin is between 3 % and 23 % and TOC from 0.5 % to 1.24 %. The basin contains two "oil cross overs" and it had not exceeded the oil window. It consists of mini-reservoirs (Talbi et al., 2018).

4.2.7. Morocco, Western Sahara & Mauritania

The neighboring countries- Morocco, Western Sahara and Mauritania possess two organic-rich shale oil and gas potential reservoirs in the Tindouf and Tadla basins of Silurian and Devonian ages. The basin is composed of marine and organic-rich thin layers of Lower Silurian 'Hot Shale'. The Tadla and Tindouf have a concentration of 5 B bbl of shale oil/condensate and 95 Tcf of shale gas in-place (USA EIA, 2013).

- *Tindouf Basin:* It is the westernmost basin of North Africa surrounded by the Atlas Mountains and Ougarta Arch to the north and the Reguibate Massif in the south. The Tindouf basin covers ~ 81999 km^2 (31,660 mi^2) area. It is an asymmetric depression with a broad gentle southern wing. It has a steep-angled structurally deformed northern margin. It is a large depocenter of sediments from the Late Ordovician to the Carboniferous Period (Luning et al., 2000). The basin obtains its high maturity during the heat flow in the Carboniferous Period. The depth of the 'Hot Shales' ranges from 6,600-14,000 ft (2011.68–4267.2 m) with TOC ranging between 1 % and 7 % and Ro from 0.7 % to 3 % (Boote et al., 1998). The southern flank of the basin is 54 ft (16.46 m) thick. The three neighboring countries have an estimated 75 Tcf of shale gas and 5 B bbl of shale oil from the Tindouf Basin (USA EIA, 2013).
- *Tadla Basin:* It is an intra-cratonic basin located in central Morocco with a resource concentrated area of 4325 km^2 (1670 mi^2). The basin is enclosed by the Central Massif in the north, the Jebiliet Massif in the south, the Atlas Mountains in the east, and the Rehamna Massif in the west. During the Hercynian orogeny, the Fkih Ben Salah Fault divides the basin into SE and NW portions (Jabour and Nakayama, 1988). The SE section underwent a structuredby complex tectonics with substantial folding and faulting whereas the NW section possesses thick carboniferous units and isolated faults (Jabour and Nakayama, 1988). Numerous regional events during the

Hercynian and Alpine periods acted on the Silurian, Devonian and Ordovician hydrocarbon-rich shales of 16,500 ft (5029.2 m) sedimentary strata (Morabet et al., 1998). The depth of the "Hot Shales" in the Tadla Basin between 3,280-9840 ft (999.74–2999.23 m) and becomes shallower towards the east. The TOC ranges from 2 % to 12 % and Ro in the dry gas window from 1.5 % to 3 %. It has an estimated 20 Tcf of shale gas in-place with 3 Tcf recoverable shale gas resources (Kuuskraa et al., 2011). As per the USA EIA (2013) report, no shale gas has been explored from this basin.

As discussed, Morocco, Western Sahara, and Mauritania owe parts of the Tindouf and Tadla Basin. Morocco has a hydrocarbon prospective area of 1670 mi^2 containing dry gas of 56 Tcf in-place. Out of this 12 Tcf is recoverable. The Tindouf Basin in Western Sahara has a dry gas prospective area of 11344 km^2 (4380 mi^2), a wet shale gas/condensate prospective area of 12095 km^2 (4670 mi^2), and 5232 km^2 (2020 mi^2) prospective area for shale oil. It holds a resource concentration of 39 Tcf of shale gas (dry, wet and associated shale gas) in-place with 8 Tcf as recoverable (USA EIA, 2013). Mauritania possesses only 50 mi^2 prospective area with minor shale oil and gas in the Tindouf basin.

4.3. South America

4.3.1. Argentina

Argentina has the most potential and large shale oil and gas reservoir in South America. The Neuquen, Golfo San Jorge, Austral and Parana are the four significant sedimentary basins assessed for commercial shale oil and shale gas exploration (Di Sbroiavacca, 2021) (Fig. 4 A,a).

- *Neuquen Basin:* It is a continental rift basin located in west-central Argentina bounded by the Patagonian Massif in the north, Colorado basin in the SE and east and Andes Mountain in the west. It contains Late Triassic to Early Cenozoic depositions in a back-arc tectonic setting (Howell et al., 2005). It was formed during the differential intraplate stresses from the back-arc extension (Barredo and Stinco, 2013). The Los Molles and Vaca Muerta Formation in the basin consist of deepwater marine deposited organic-rich black shales from the Middle-Late Jurassic-Early Cretaceous Period. The Mid Jurassic Los Molles Shale has a thick deposition of ~ 3300 ft (10, 05.84 m) in the basin center at a depth ranging from 8000 to 16000 ft (2438.4–4876.8 m). The TOC ranges from 0.55 % to 5.01 %, thermal maturity from 0.3 % to 2 %, and varies horizontally and vertically (Sounders-Smith, 2001; Villar et., 2005; Martinez et al., 2008). The TOC and Ro are maximum in the basin center and in the dry mature window.

  The Late Jurassic to Early Cretaceous Vaca Muerta Shale is 200–1700 ft (60.96–518.16 m) thick organic-rich shallow to deep marine deposited strata of finely-layered bituminous dark grey shale and lime-mudstone in an anoxic environment (Monti et al., 2013). The northern and the western portions of the basin comprise of the thickest sediment strata and deepest in the basin center. The lithology of the Formation contains marls (claystones and siltstones interbedding with variable carbonate content) and are composed of solid bitumen and substantial amorphous materials (Soldo, 2015; Petersen et al., 2020). The TOC ranges from 2.9 % to 14.2 % and is highest northward. The thermal maturity ranges from 0.5 % to 2.5 % with kerogens of Type II and I (Soldo, 2015; Craddock et al., 2019). The oil window lies in the NE of the Huinchul Arch with Ro 0.8 %. The Los Molles Formation estimates a resource concentration of 49–303 Bcf mi^{-2} of shale gas and 23–78 MM bbl mi^{-2} for shale oil (USA EIA, 2013). The Vaca Muerta Formation estimates 554.9 Bcf mi^{-2} of gas and 100 MM bbl mi^{-2} of shale oil (USA EIA, 2013). The technically recoverable resource as estimated in 2018, ranges between 443 and 8992 MMm^3 (oil) and 223–3609 Bm^3 (gas) (Mayol et al., 2020).

- *Golfo San Jorge Basin*: It is an intra-cratonic extensional depression located in central Patagonia extending across southern Argentina, Andean foothills and the offshore Atlantic continental shelf in the west and east respectively. It is bounded in the south by the Deseado Graben and Massif, to the north by the Somuncura Massif, and in the west by the Andes transected by the San Bernardo Fold Belt (west-central). It evolved during the Gondwana breakup (Fitzgerald et al., 1990). The sediment deposition occurred during the end of the Jurassic period. These sediments are composed of mainly lacustrine black shales, fine grey sandstones, mudstone rocks, and occasionally limestones. The composite is defined as the Neocomian Aguada Bandera Formation. The Aguada is a gas-prone formation with a thickness of 15,000 ft (4572 m) in the SW, 1,000-5000 ft (304.8–1524 m) in the basin center, and decreases towards offshore in the east (0–2000 ft, 0–6,09.6 m) with a depth up to 20,000 ft (6096 m). It is shallower in the northern and western flanks of the formation and deepest in the east. The average TOC ranges from 1.44 % to 3.01 % and Ro up to 2.4 % (Rodriguez and Littke, 2001).

  It consists of 152 Bcf mi^{-2} of shale resources. The Early Cretaceous deep lacustrine black shale of the Pozo D-129 Formation is the most prospective shale reservoir of the basin with pyrite and dark laminations. The depositional environment was anoxic (Figari et al., 1999; Paredes et al., 2008). It is gas-prone with thickness ranging up to 4500 ft (1371.6 m). The thickness is maximum in the western section of the basin. The depth varies throughout the basin and ranges up to 15,900 ft (4846.32 m). The TOC ranges from 1.42 to > 3 % with Ro of 1.06 % (Caprioglio et al., 2020). The thermal maturity recorded at the basin center ranges from 2.49 % to 3.15 %. It drops in the south to 0.83 % and TOC of 0.84 % defining the region thermally immature. It has kerogen Types I and III (Caprioglio et al., 2020). It has 41–163 Bcf mi^{-2} of shale gas and MMbbl mi^{-2} of shale oil/condensate concentrated in the basin (USA EIA, 2013).
- *Austral Basin:* It is also called as the Astral-Magallanes basin. It is located in Patagonia covering ~ 13530 mi^2 area (4620 mi^2 in oil window, 4600 mi^2 in the wet gas/condensate window and 4310 mi^2 in the dry gas window). It consists of Upper Cretaceous and Tertiary sedimentary and volcaniclastic rocks with normal and thrust faulted eastern and western regions. The Early Cretaceous Lower Inoceramus or Palermo Aike Formations are the most prospective of all the stratigraphic units. It has a complex fault system that enhanced the productivity of the formation. It consists of N-S to NE-SE strike-slip faults and close-spaced normal faults resulting in a polygonal fault network (Belotti et al., 2013). It is 800–4000 ft (243.84 – 1219.2 m) thick from north to south, 8,000-13,500 ft (2438.4 – 4114.8 m) deep with TOC between 0.5 % and 2.5 %, pressure gradient of 0.46 psi ft^{-1}, and HI of 150–550 mg g^{-1} with Type I-II kerogen (Pittion and Arbe, 1999; Belotti et al., 2013). The porosity of the shale ranges from 5 % to 12 % with thermal maturity between 0.8 % and 2.0 %. Ro increases from the oil-prone to dry-gas section of the basin (Legarreta and Villar, 2011). It has an estimated resource concentration of 33–156 Bcf mi^{-2} of shale gas and 15–48 MM bbl mi^{-2} of shale oil/condensate.
- *Parana Basin:* The basin is located at the NE part of Argentina and the rest of the large basin lies in Brazil, Paraguay and Uruguay. The Ponta Grossa Formation in the basin consists of black organic-rich Devonian shale that is up to 600 m thick with a depth ranging from 11,000 to 14,000 ft (3,352.8- 4267.2 m). The TOC ranging up to 4.6 % (avg. 2.5 %), Ro from 0.85 % to 1.5 %, and Type II kerogen (Vesely et al., 2007). The basin is recorded thermally mature in the basin center with concentric oil-, wet gas-, and dry-gas window. It has an estimated a resource concentration of 35–57 Bcf mi^{-2} of shale gas and 8 MM bbl mi^{-2} of shale oil/condensate in the thermal maturity window (USA EIA, 2013).

4.3.2. Brazil

Brazil has 18 sedimentary basins among which three are the most significant and potential large shale rock reservoirs with prolific commercial shale oil and gas. The Devonian black shales deposited in the marine environment of Parana, Solimoes and Amazonas Basins are the main targets for shale gas and oil exploration in Brazil (Fig. 4b).

Parana Basin: It is a huge depositional intracratonic basin in the southern part of Brazil, with an extension in Paraguay, Uruguay and northern Argentina. It is bounded by the Asuncion Arch in the west, truncated in the east by the South Atlantic tectonic margin, and the basin onlaps the Precambrian basement in the north. The geology of the basin is structured by secondary folding, minor faults, a gentle syncline with numerous sills and dykes. The normal faults controlled by the older basement faults separate the undeformed tracts of the basin. Two-third of the basin is covered by flood basalts of Ordovician to Cretaceous Period (Weniger et al., 2010). The organic-rice, marine deposited Devonian (Frasnian) black shale of the Ponta Grossa Formation is the petroleum source rock of the basin. The thickness ranges up to 600 m in the center and a depth from 11000 to 14000 ft (3352.8–4267.2 m). The TOC ranges from 1.5 % to 4.6 %, porosity of 2 %, and thermally mature (0.85–1.5 %) in oil, wet-gas and dry-gas window at a considerable depth in the basin center. Thermal maturity was attained during the Late Jurassic to Early Cretaceous Period due to its moderate burial history and generation of heat from the intrusives (USA EIA, 2013; Martins et al., 2022).

- It hosts Type II kerogens. The Formation estimates a resource concentration of 26–91 Bcf mi^{-2} of shale gas and 11–27 M bbl mi^{-2} of shale oil in the thermally mature windows.

  The Irati Formation of the Early Permian Period consists of bituminious shale with TOC ranging from 8 % to 15.90 %. Its ~~type I/II~~ kerogen is considered as a noteworthy petroleum source rock (Carreta et al., 1985; Weniger et al., 2010). According to the USA ERI (2013) report, 124 petroleum wells have been drilled in the Brazilian part of this basin.
- *Solimoes Basin:* It is the most prolific productive onshore basin located in the northern part of Brazil and 90,6496 km^2 (3,50,000 mi^2) extended in the Amazon Rainforest. The Jandiatuba Formation underlying the Carboniferous Jurua Formation contains marine deposited Devonian "hot" black shale. The depth ranges from 7,500-12,000 ft (2,286-36,57.6 m) with an average thickness of 120 ft (36.58 m). The TOC ranges from 1 % to 4 %, Ro > 1.35 %, with a porosity of 4 %. The thermal maturity is more (> 1.35 %) in the dry gas window and lower (1–1.3 %) in the wet gas region in the east of the basin. It has an estimated a resource concentration of 20–36 Bcf mi^{-2} of shale gas and 5.5 M bbl mi^{-2} of shale oil in the basin.
- *Amazon Basin:* The 500 km^2 intercratonic basin is located in northern Brazil extended across the Amazon Rainforest bounded by the Purus and Garupa arches (Putzer, 1984). It is an ENE-WSW trending trough intruded by the Early Jurassic igneous rocks. Deformation in the Cenozoic Period includes strike-slip faulting, salt tectonics and extension. The petroleum system in the basin is similar to the Solimoes Basin in Brazil. The Devonian Barreirinha Formation of the Amazon Basin consists of marine deposited laminated black shale with a thickness of 195–225 ft (59.44–68.58 m) and 9,500-12,000 ft (2,895.6-3657.6 m) deep. The TOC ranges from 2 % to 5 %, the porosity of 4 % with Type II/III kerogen (Souza et al., 2021). Ro is low (0.3–1.8 %) in the shallower regions of the basin and increases with depth towards the basin center (Silva et al., 2015). It has an estimated a resource concentration of 15–70 Bcf mi^{-2} of shale gas and 9–18 M bbl mi^{-2} of shale oil.

Other promising sedimentary basins with shale deposits are the Potiguar, Parnaiba, Sergipe-Alagoa and Parecis in northeastern Brazil; Reconcavo in eastern Brazil, Sao Francisco in southwest Brazil, Taubate in southeast Brazil and Chaco-Parana in south Brazil. The Pimenterias Formation of Parnaiba Basin contains Devonian black shale and the Cretaceous Maceio Formation of Sergipe-Alagoas basin consists of black shales, marls, and calcilutites deposited in the lacustrine environment. The non-marine Oligocene Tremembe Formation of Taubate Basin and the Devonian marine deposited Rincon Formation of Chaco-Parana contains laminated black shales. These basins lack one or many favorable characteristics e.g., structural complexity, low TOC and thermal immaturity (USA EIA, 2013).

4.3.3. Colombia and Venezuela

The Middle Magdalena Valley, Llano's basins and the Maracaibo/Catatumbo basins are the three most potential reservoirs for shale oil and gas of the northern South America (Colombia and Venezuela). The basin consists of Cretaceous organic-rich marine deposits.

- *The Middle Magdalena* located in central Columbia between the Eastern and Central Cordilleras. The N-S trending intermontane basin is geologically complex with several thrust and extensional faults with the western part structurally overthrust, and flat surface topography in the basin interior. The La Luna Formation is the promising source rock of the basin characterized by thick organic-rich black shale within 4,000-12,000 ft (1,219.2-3657.6 m) depth and thickness between 12,000 and 18,000 ft (3657.6–5486.4 m) with Type II kerogen. Salada, Pujamana and Galembo are the three stratigraphic units of the Formation (Torres et al., 2012). Salada Member is the most organic-rich portion with 3–12 % TOC. It is ~ 150 m thick hard thin-bedded black shale with calcareous shale, and thin interbeds of black fine-grained limestones with pyrite veins (USA EIA, 2013). The Pujamana with low TOC consists of grey to black shales interbedded with limy shales. The Galembo is ~ 220 m thick and consists of black shales interbedded with argillaceous limestone and blue/black chert beds with moderate TOC. The Tablazo/Rosablanca Formation (480–920 ft, 146.30–280.42 m thick) below the Cretaceous rock is oil to wet gas prone with 0.6–1.2 %, thermal maturity 2–8 %, TOC, 8 % porosity and 30 % clay. The resource concentration estimated from La Luna and Rosablanca Formation are 135 Tcf of shale gas and 79 Bbl mi^{-2} of shale oil in-place. It has an estimated 135 Tcf of shale gas and 79 B bbl of shale oil in-place.
- The NE-trending *Llanos Basin* in eastern Colombia with a simple geologic structure and overthrusting on the western margin has a thick Cretaceous marine shale. The Gacheta, Los Cuervos, Carbonera and Leon Formations are the primary source rocks. Gacheta is the most significant potential Formation. With a depth of 2,000-15,000 ft (609.6–4572 m), from western to eastern margin, and 150–300 ft (45.72–91.44 m) thick, 1820 mi^2 (4713.78 km^2) in the depth-prospective area lies within the oil window. The TOC range from 1 % to 3 %, Ro from 0.3 % to 1.1 % with a mixed Type II and III kerogen and a high porosity of 7 % (ANH, 2007). The pressure gradient of the basin is 0.5 psi ft^{-1}. The basin has an estimated 18 Tcf of shale gas and 13 B bbl of shale oil and condensate in place (USA EIA, 2013).
- The *Maracaibo Basin* in western Venezuela and eastern Colombia contains marine organic-rich Cretaceous shales. The black calcareous La Luna/Catatumbo Formation with a depth of 5,000-15,000 ft (1,524-4572 m) (deepening from NE to SW) and thickness from 100-> 400 ft (30.48->121.92 m) has a TOC from 3.7 % to 5.7 % in the NW, 1.7–2 % in south and east (USA EIA, 2013), and reaches up to 16.7 % in the basin. The thermal maturity ranges from 0.7 % to 1.7 %, increases with the burial depth. The Catatumbo sub-basin has 200 ft (20.96 m) thick and 6,000-7600 ft (1,828.8-2316.48 m) deep La Luna Formation of dark-gray laminated shale with TOC of 4.55, average Ro of 0.85 % and Type II and III kerogens (Yurewicz et al., 1998). The Capacho Formation overlying the La Luna Formation in the Catatumbo sub-basin consists of dark greyish black shales and limestones with 590–1400 ft (179.83–426.72 m) thickness within 6,500-8500 ft (1,981.2-2590.8 m) depth. The TOC is measures from

1.5 % to 5 %, Ro from 1.22 % to 1.24 % with Type II and III kerogens. The dry gas window of 5840 mi^2 area in the La Luna and the Upper Capacho Formation lies at a depth of 12,000 ft (3657.6 m) and thickness of 500 ft (152.4 m) with an average TOC of 5 % and Ro of 1.6 %. It has an estimated 523 Tcf of shale gas in-place. The wet gas window with 4290 mi^2 area lies 1,1000 ft (3352.8 m) deep with an average Ro of 1.15 %. A number of zones in the basin with high fragility indices between 0.54 and 0.85 are noted. According to these brittleness indices, the formation can be suitable for hydraulic fracturing and unconventional exploration (Mendez et al., 2023). It has an estimated 264 Tcf of wet gas and 62 B bbl of shale condensate in-place. The oil window with 7280 mi^2 area located within 10, 000 ft (3048 m) is thermally less mature with an average Ro of 0.85 %. It has an estimated 235 B bbl of shale oil and 183 Tcf of shale gas in-place (USA EIA, 2013).

4.3.4. Bolivia, Chile, Paraguay and Uruguay

The four countries in South America share three large prospective shale basins for shale oil and gas exploration. The shale formations in the basin are marine deposited sediments in the Cretaceous and Devonian Periods.

- *The Parana Basin* is a large cratonic basin extended in Paraguay and Uruguay (south-central South America) with a prospective area of 24450 km^2 (9440 mi^2) and 10,153 km^2 (3920 mi^2), respectively (Fulfaro et al., 1997). It is bounded by the Asuncion Arch in the west and the South Atlantic tectonic margin in the east. The black shale of the Ponta Grossa Formation is the shale oil-bearing source rock of the basin with a depth of 10,500–12,500 ft (3,200.4-3810 m) in Paraguay and 4,000-6000 ft (1,219.2-1828.8 m) in Uruguay. The TOC of the basin ranges from 1.5 % to 4.6 % with Type II kerogen passes through the oil window into the gas window in the basin center with high thermal maturity. The Ro ranges from 0.85 % to 1.5 % and porosity ~ 4 %. According to the USA EIA (2013), the basin estimates 8 Tcf of shale gas and 0.6 Bbl of shale oil and condensate in Paraguay; whereas, 2 Tcf of shale gas and 0.6 B bbl of shale oil and condensate are estimated in Uruguay USA EIA (2013).

- The *Chaco Basin* extended over SE Bolivia and NW Paraguay is an intra-cratonic foreland basin separated from the Parana Basin by Ascuncion Arch. The basin is structured by numerous vertical normal faults. Ordovician and Cretaceous volcanic deposists are found within the basin (Veroslavsky et al., 2020). The basin has several sub-basins- Carandayty, Curupayty and Pirity troughs. The Silurian Kirusillas Formation and the Devonian Los Monos and Icla Formation are the significant shale formation. The San Alfredo Shales in Los Monos (in the Carandity and Curupaity sub-basin) is the most resource potential formation. The shales are thick and black, deposited in the shallow marine environment at a depth of 8200 −10,000 ft (2499.36 −3048 m) (in synclines) and 12,000 ft (3657.6 m) thick. The TOC ranges from 1.44 % to 1.86 % with a high geothermal gradient. Mineralogically, the shale is composed of calcite, dolomite, ankerite, albite, feldspar, rutile and pyrite, along with low clay content, viz., illite, kaolinite and chlorite (Kern et al., 2004). The temperature gradient varies in structural highs and sub-basin with 1.9 °F per 100 ft (= 0.53 $^0C\ m^{-1}$) and 1.0 °F per 100 ft (= 0.56 $^0C\ m^{-1}$), respectively (Bernard et al., 2012). The play is in the shale oil, wet gas and dry gas window estimating 28–141 Bcf mi^{-2} of shale gas and 19–46 million bbl mi^{-2} of shale oil (USA ERI, 2013).
- *The Magallanes Basin* in south Patagonia (Chile) consists of a foreland basin with 3,000-6000 ft (9,14.4-1828.8 m) thick strata of Upper Cretaceous and Tertiary sediments and volcanic rocks along its eastern coast (Biddle et al., 1986). The Jurassic and Early Cretaceous shales are deposited in an anoxic marine environment. The Early Cretaceous Estratos con Favrella Formation is the most prospective shale formation of the basin with TOC ranging up to 6 %, porosity ranging 6–12 %, pressure gradient of 0.46 psi ft^{-1}, and thermal maturity ranges between 0.7 % and 2.0 %. The depth ranges from 8,000-13,500 ft (2,438.4-4114.8 m) with an average thickness of 800 ft (243.84 m). The play estimates a resource concentration for shale gas of 33–156 Bcf mi^{-2} and shale oil of 15–48 million bbl mi^{-2}. The extensions of these basins lie in Argentina and Brazil.

4.4. North America

4.4.1. Mexico

Mexico has huge shale gas and oil reservoir along its onshore Gulf region. Mexico with large storage of shale gas and oil in its marine deposited shale, which correlates with notable Jurassic and Cretaceous hydrocarbon-rich shale deposits of the Eagle Ford and Haynesville shales (Stevens and Moodhe, 2015) (Fig. 4c). Maximum oil and gas fields is found in the narrow coastal area, which has conventional Miocene and Pliocene sandstone reservoirs. The genesis of hydrocarbon is associated with the compression and thrust faulting during the evolution of the Sierra Madra Ranges when the narrow coastal plain of Mexico was squeezed and created a chain of discontinuous sub-basins (Mello and Kamer, 1996). According to the geologic data from ARI's/EIA initial 2011, Mexico's prosperous areas of shale gas are structurally more complex. The Mexico's shale basins in the western portions are structurally more complex and overthrusts the less distorted eastern portions and adjoining shallower platforms. The onshore east Mexico has a chain of medium-sized basins, which carry organic-rich Jurassic and Cretaceous marine shales. The Upper Cretaceous (Turonian to Santorian), Lower-Mid Cretaceous (Albian-Cenomanian), and Upper Jurassic (Tithonian) are the three major Mesozoic source rocks that have been identified in Mexico's gulf coast basin by pyrolysis and studies of carbon isotopes and biomarkers (Guzman-Vega et al., 2001). The Tithonian appears to have the highest potential for shale gas development, contributing ~ 80 % of the conventional oil and gas discovered in this gulf region. The Burgos, Sabinas, Tampico, Tuxpan Platform and Veracruz basins are the most prospective shale gas and oil exploration targets (USGS, 2014; Stevens and Moodhe, 2015).

- *Burgos Basin:* With an unconventional shale oil and gas resource area of 44807 km^2 (17,300 mi^2), the southward extension of the Maverick Basin (Texas) is located in the NE Coahuila (south of Rio Grande River). The basin formed into a restricted carbonate platform during its expansion in the Early Jurassic. The basin consists of faults and tilt developed during the Cretaceous Laramide Orogeny. The Cretaceous Period Eagle Ford shale play and the Jurassic La Casita and Pimienta Formation are significant targets for shale oil and gas exploration in the basin (Araujo et al., 2015). The TOC ranges from 0.17 % to 4.47 % with Type II kerogen (Luque and Marcela, 2017). The TOC is estimated to be 3.10–5.74 %, depth-dependent thermal maturity ranges from 0.85 % to 1.6 %, pressure gradient of 0.65 psi ft^{-1} and a geothermal gradient of 23 °C km^{-1} (Luque and Marcela, 2017). It has an estimated 191 Bcf mi^{-2} of unconventional resource. The Tithonian Shale (La Casita and Pimienta) is the prime hydrocarbon source rock in the western portion of the basin (Stevens et al., 2015). It is 5,000-16,400 ft (1524 – 4998.72 m) deep with ~ 1400 ft (426.72 m) and net pay of 200 ft (60.96 m). The TOC ranges from 2.6 % to 4 %, Ro from 0.8 % to 1.70 % and consists of Type II kerogen (Ambrose et al., 2005; Zimbrick and Dolan, 2019). The gas-prone formation estimates a resource concentration of 100 Bcf mi^{-2} (USA EIA, 2013).

The 200–300 ft (60.96–91.44 m) thick Eagle Ford shale is the most significant hydrocarbon reservoir in the country. It was deposited in the Cenomanian and Turonian Stages during climate change, sea-level rise and extinction of Tethys ocean. The favourable sea water temperature (25–29 ℃) in a sluggish-saline water column promoted production and deposition of carbon in the strata from the *in-situ* fossils including both benthic amd epibenthic varieties (Schieber et al., 2016).

- *Sabinas Basin:* The onshore marine shale basin is situated in the northern part of the country with 9,2463 km^2 (3,5700 mi^2) area. The basin expanded and allowed sedimentation of ~ 5000 m thick sediment layer during the Jurassic Period and Late Cretaceous Laramide Orogeny (Antunano, 2001; Enciso-Cardenas et al., 2021). A series of NW-SE trending Sabinas Fold belts developed during the deformation of the basin related to the Laramide Orogeny, structuring development of basin complex. The Cretaceous Olmos (Maastrichtian) coaly unit, Eagle Ford Shale (Turonian) and the Late Jurassic (Tithonian) La Casita Formation of marine shales are the primary hydrocarbon shale reservoirs of the basin. The 400 ft (121.92 m) thick black Eagle Ford shale encompasses the NW, NE and central region of the basin. It has an estimated TOC of 0.2–4 %, thermal maturity of 1.50 %, pressure gradient of 0.35 psi ft^{-1}, and porosity of 5 % at ~ 9000 ft (2743.2 m) depth (Enciso-Cardenas et al., 2021). The gas-prone shale has an estimated 132 Bcf mi^{-2} of average resource concentration. The Tithonian La Casita is a deep-water marine organic-rich shale with 600–800 m thick, and 11, 500 ft (3505.2 m) deep with a TOC of 2.0–2.5 % and a porosity of 5 %. It is ~ 69 Bcf mi^{-2} of resource (USA EIA, 2013).
- *Tampico Misantla Basin:* The Pimienta Shale with an area of 35,224 km^2 (13,600 mi^2) is located onshore in the eastern central part of the country extending towards the shallow waters of the Gulf of Mexico (Daniel and Govela, 1978). It is bounded by the Sierra Madre Oriental and the fold-and-thrust belt in the west and the Tuxpan platform in the east. The Upper Jurassic Pimienta Shale is the prime hydrocarbon-rich rock of the basin within 1400–3000 m depth in the south defined by uplifted structures. The dry gas, wet gas and oil window are found from west to east respectively. Its thickness ranges from 200 to 10 m on paleo-highs with a TOC of ~ 0.25–3 % and Ro between 0.85 % and 1.45 % with Type II kerogen (Vega-Ortiz et al., 2020). The estimated shale gas concentration between 19 and 83 Bcf mi^{-2} and shale oil from 17 to 38 M bbl mi^{-2} has bee reported from this basin (USA EIA, 2013).
- *Tuxpan Platform:* The Early Cretaceous isolated carbonate platform known as the Tuxpan Platform evolved on a basement high and is located southeast of the Tompico Basin. (Salvador, 1991). The hydrocarbon-rich zone in the Le Mesa Syncline consitituies of thick organic-rich shales of the Pimienta (Tithonian) and Tamaulipus (Lower Cretaceous) Formations (Ambrose et al., 2005). This area is found ~ 50 km south of Tuxpan city, near Poza Rica. The Jurassic Pimienta Formation with a thickness of 500 ft (152.4 m) (net 200 ft, 60.96 m) and at a depth of 6,600-10,000 ft (2,011.68-3048 m) is the main source rock of the platform. It has an estimated TOC of 3 % and Ro of 0.9 %. It has an estimated 10 Tcf and 12 B bbl of shale gas and oil/condensate of risked shale resource in-place. The Lower Cretaceous Tamaulipas Formation consists of organic-rich interval thickness of 300 ft (91.44 m), at 6,000-9500 ft (1,828.8-2895.6 m) depth. The TOC measures 3.0 % and Ro of 0.85 %. It has an estimated 9 Tcf of shale gas and 13 B bbl of risked shale oil in place (USA EIA, 2013).
- *Veracruz Basin:* The Basin is located near Veracruz city of Mexico covering the onshore area of 23,389 km^2 (9030 mi^2). The Mesozoic carbonates of the Cordoba Platform and the Sierra Madre Oriental control the western part of this asymmetric basin. It is the deepest part along the western margin. It is formed by several major structural controls from west to east. The Upper Cretaceous (Turonian) Maltrata Formation is the hydrocarbon-rich rock composed of 300 ft (91.44 m) thick organic-rich shaly marine limestone with TOC of 0.5–8 % with an average of 2 %, and Ro ranging from 0.58 % to 1.4 % with Type II kerogen (Gonzalez et al., 2014). The oil window is present at 11,000 ft (3352.8 m) deep and a gas window at 11500 ft (3505.2 m). It has an estimated 21 Tcf and 7 B bbl mi^{-2} of risked shale gas and oil-in-place (USA EIA, 2013).

4.4.2. Canada

Canada has a series of hydrocarbon basins (Horn River, Cordova Embayment, Liard, Doig Phosphate Shale, Montey/Doig Resource Plays in British Columbia and Northwest Territories; Alberta Basin, East and West Shale Basin, Deep Basin, NW Alberta Basin, and Southern Alberta Basin in Alberta; Williston Basin in Saskatchewan and Manitoba; Appalachian Fold Belt and Windsor in eastern Canada) and formations where marine sediments got deposited (Fig. 4d). In Canada, ~28 Tcm gas-in-place is estimated from the shale formations (Khosrokhavar et al., 2014). See Zobac and Kohli (2019) for shale gas data from Canada and USA.

4.4.2.1. British Columbia and Northwest Territories. Located in northern British Columbia and the NW Territories, the Horn River Basin is encircled by the Bovie Fault on the west, Slave Point on the east. The shale deposits are thick and organic-rich in the west-central section of the basin, whereas it thins towards east. The Muskwa/Otter Park and Evie/Klua are the significant hydrocarbon shale strata with thick organic-rich Mid Devonian Shale characterized by high quartz and low clay content. The Muskwa/Otter shale deposited atop the Horn River Formation within 6,300-10,200 ft (1,920.24-3108.96 m) depth-range. The thickness of the net organic-rich shale is 380 ft (115.82 m). Due to high thermal maturity, the shale contains 11 % of CO2. It has ~ 151 Bcf mi^{-2} of shale gas (USA EIA, 2013). The Evie/Klua located 500 ft (152.4 m) below the Muskwa is thinner and the lowermost strata and dry gas prospective of the Horn River Formation. With Ro of 3.8 %, the CO_2 content is 13 %. It has an estimated 62 Bcf mi^{-2} of shale gas (USA EIA, 2013).

Cordova Embayment is located in the NE corner region of British Columbia. It is surrounded by organic-rich shale deposit platform and Horn Tiver basin. The embayment is known for its shale gas (British Columbia Oil and Gas report, 2015). The Muskwa/Otter Park is the target for shale gas exploration. It is 58 m thick in the center and decreases to ~ 20 m at the edge. It is moderately over-pressured at the basin center. The Muskwa/Otter Park basin has an estimated shale gas resource of 68 Bcf mi^{-2}. The Liard basin is located at the NW British Columbia separated by the Bovie Fault from the Horn River Basin at its eastern border. The basin is bounded by several structural folds in its west and south with organic-rich shale deposits. The Lower Besa River Shale of the Middle Devonian Period is the significant exploration target of the basin. The most hydrocarbon-rich area lies in the central portion of the basin within 6,600-13,000 ft (2,011.68-3962.4 m) depth with a net organic material-rich thickness of 600 ft (182.88 m). The TOC value ranges up to 5 %, average Ro of 3.8 % and with 13 % of CO2 content. The formation is quartz-rich, with an interval of dolomite and extensive clay. It has an estimated shale gas concentration of 319 Bcf mi^{-2} (USA EIA, 2013).

The Middle Triassic Doig phosphate shale/deep basin is located in British Colombia and in the deep basin of Alberta. The western and the central portions of the Deep Basin contain thick rich organic shale at 9250 ft (2819.4 m) deep with a net thickness of 150 ft (45.72 m). With Ro of 1.1 % and TOC of ~ 5 %, the shale is placed in the wet gas/condensate window. It is composed of higher content of quartz, low clay, pyrite and dolomite. This makes the formation favorable for hydraulic fracturing. It has an estimated wet gas concentration of 67 Bcf mi^{-2} (USA EIA, 2013). The Montney and Doig resource plays in the Deep Basin of British Columbia contain hydrocarbon deposition of the Triassic age. It is containing large volumes of dry and wet gas in tight sand and shale formations with a small prospective area for oil/condensate in the Montney resource play. The Canol Shale play in Central Mackenzie Valley, NW Territories is a prospective shale oil play. It is a shale oil exploration target in near future.

4.4.2.2. Alberta. Alberta Basin in Alberta, Canada hosts five hydrocarbon producing shale formations including the section part of the Doig

Phosphate Shale play. The Basal Banff and Exshaw shale, deposited in the southern region of the Alberta Basin, is bounded by the deformed belt in the west, the Alberta and Saskatchewan border in the east, U.S. and Canada border in the south, and the sub-crop erosional edge in the north. The upper and the lower strata of the shale are hydrocarbon-rich with 3–17 % TOC. The middle strata consist of a mixed lithology of calcareous sandstones, dolomitic siltstones, limestones, sands and siltstones. The shale unit is thinner in the western section of the basin. The prospective area target for shale oil exploration lies in the center of the basin play area. The formation has ~ 2.5 MM bbl mi^{-2} of oil and associated gas. The East and West Shale units deposited in central Alberta are confined by the Deformed Belt in the west, the Grosmont Carbonate in the east, the Peace River Arch in the north, and the Leduc Shelf in the south. It consists of the Upper and Middle Devonian Duvernay shale with 7,500-16,400 ft (2,286-4998.72 m) from east to west with a gross thickness ranging from 30 to 200 ft (9.14–60.96 m). The TOC ranges up to 11 % with Ro from 0.8 % to 2 % (Wust et al., 2013). The thermal maturity increases towards the basin center. It has an estimated 64 Bcf mi^{-2} of dry gas, 7.1 MM bbl mi^{-2} of oil and associated gas, 0.5 MM bbl mi^{-2} of condensate and 47 Bcf mi^{-2} of wet gas concentrated in the basin.

The Lower Jurassic Nordegg Shale in the Deep Basin of Alberta is a carbonate-rich marine deposit that lies at the base of the Fernie Formation. The shale includes cherty and phosphoric carbonates, siltstones and sandstones. The top of the shale unit lies 3300 ft (1005.84 m) below the ground surface in the NE and 15,000 ft (4572 m) in the south with thickness ranging from 50 to 150 ft (15.24–45.72 m). The TOC ranges over 11 % and Ro from 0.8 % to 1.3 %. They vary from north to south with depth. It has an estimated 56 MM bbl of oil mi^{-2} from the associated from oil prospective area, 0.4 MM bbl mi^{-2} of oil and 20 Bcf mi^{-2} of wet gas from the "wet gas and condensate prospective area" and 22 Bcf mi^{-2} of dry gas from the "dry gas prospective area". The Alberta portion of the Montney and Doig Resource plays is observed in the Deep Basin with low organic-rich pay, low TOC and low Ro content; thus, not assessed for quantitative analysis.

The NW Alberta basin consists of the large shale oil and gas prospective Muskwa Shale, which is a continuation of the Duvernay Shale in central Alberta and Otter Park Shale in the NE British Columbia. Geographically, the formation is bounded on the west by the Albert and British Columbia border, the Grosmont Carbonate Platform on the east, the Albert and the North-Western Territories border in the north, and the Peace River Arch on the south. The shale ranges in depth from 3,300-8200 ft (1,005.84-2499.36 m) in the NE and SW, respectively, with a net hydrocarbon producing shale thickness from 33 to 200 ft (10.06–60.96 m) (USA EIA, 2013). The TOC ranges from < 1 - > 10 % with Ro < 0.8 % in the east to 1.2 % in the west. ~~It matures with increasing depth.~~ It has an estimated 6 MM bbl mi^{-2} of oil and associated gas, 1 MM bbl mi^{-2} of shale oil and condensate, and 31 Tcf of shale gas. The Cretaceous Colorado Group of shale in the Southern Alberta basin is a prospective reservoir composed of sands, mudstones and shales. It is a thick organic-rich shale deposition defined by the Canadian Rockies Overthrust on the west, the U.S./Canada border in the south. The Fish Scale in the lower Colorado Group and the Second White Speckled (2WS) Shale in the Lower Colorado Group are the two most significant formations. The depth of the Fish Scale ranges from 5000 ft (1524 m) on the east to 10,000 ft (3048 m) in the west with a net thickness of 105 ft (32 m) where the formation is 200 ft (60.96 m) deeper than the 2WS. The TOC ranges from 2 % to 3 %, Ro between 0.5 % and 0.6 % and a pressure gradient of 0.3 psi ft^{-1}. The presence of low to moderate clay of 31 % makes the group favorable for hydraulic fracturing.

4.4.2.3. Eastern Canada. Eastern Canada has two major prospective shale basins, i.e., *Appalachian Fold Belt and Windsor*. The Upper Ordovician marine deposited Utica Shale Formation of the Appalachian Fold Belt lies within the St. Lawrence Lowland above the conventional Trenton-Black River Formation in Quebec (Ladeveze et al., 2018). It is bounded by the Yamaska, Tracy, Logna's Line and Brook faults and partitions the play. Extensive faulting and thrusting make the formation geologically complex (Rivard et al., 2018). The formation begins at a depth of 3,000-11,000 ft (914.4–3352.8 m) in the SW to NW boundaries and far deep along the eastern boundary. The shale is in the dry gas window with TOC ranges from 1.5 % to 3 % and more in the Upper Utica Shale and Ro from 1.1 % to 4 %. It has an estimated gas reserve of 134 Bcf mi^{-2}. The Carboniferous Horton Bluff Shale in the Windsor Basin is also a geologically complex formation located in north-central Nova Scotia, Canada. The depth of the shale in the prospective area ranges between 3,000-5000 ft (914.4–1524 m) with a thickness of organically rich net pay of 300 ft (91.44 m). The TOC ranges from 4 % to 5 % with Ro from 1.2 % to 2.5 % in the NW. It is thermally mature due to high heat flow as the Horton Bluff Shale Formation directly lies above the pre-Carboniferous igneous and metamorphic basement. It has an estimated a shale gas concentration of 82 Bcf mi^{-2} (USA EIA, 2013).

4.4.2.4. Saskatchewan/Manitoba. The large Canadian portion of the Late Devonian to Early Mississippian Bakken Shale lies in the *Williston Basin* of Canada with an area of 5,69,797 km^2 (2,20,000 mi^2) (Christopher et al., 1973). It is rich in shale oil and associated gas. The formation extends north from the Canada border into the southern section of Saskatchewan and SW of Manitoba. According to the National Energy Board, Canada (2011); shale oil has migrated from the deeper and mature section of the Bakken Formation into the South of Williston Basin. The Williston Basin is elliptical and intracratonic. It occurs in most of western North Dakota, northeastern Montana and parts of Canada. The Bakken Formation is one of the significant organic-rich formations in the Williston Basin with an average of 8 % (upper member) and 10 % (lower member) TOC (Liu et al., 2018). The marine shale has upper and lower units of hydrocarbon-rich units whereas the middle unit is made up of mixed lithologies with high porosity and permeability. Its depth ranges from 5,500-8800 ft (1676.4–2682.24 m) in the north to south with a net pay of 20 ft (6.09 m). It has ~ 22 Bbl mi^{-2} of shale oil and 16 Tcf of associated gas (USA EIA, 2013). The upper and lower Bakken Formation members have kerogen type is II/III and 0.85–0.98 % of Ro. (Smith and Bustin, 1995; Jin et al., 2015; Liu et al., 2018). The Middle Bakken is categorised as an unconventional reservoir rock since it is made up of fine-grained clastics and mixed carbonates, whereas the two members act as the source and seal for the hydrocarbons that are produced (Pitman et al., 2001; Liu et al., 2018). Its depth ranges from 5,500-8800 ft (1,676.4-2682.24 m) in the north to south with a net pay of 20 ft (6.09 m). It has ~ 22 Bbl mi^{-2} of shale oil and 16 Tcf of associated gas (USA EIA, 2013). Detail of Bakken Formation can also be found in Ostadhassan et al. (2018).

4.4.2.5. Other locations. The Fort Worth Basin: The Barnett Formation is a promising oil-prone hydrocarbon-rich Paleozoic deposited thermogenic black shale covering 1,2950 km^2 (5000 mi^2) area in the Newark East field, Texas in recent time formed due to the advancing of the Ouachita Thrust belt (Jarvie et al., 2005, 2007; Andrews et al., 2009). The Barnett Formation lies on the Ordovician-age carbonates (Ellenburger Group and Viola Formation), except in the western and southwestern parts of the basin, where it overlies a Mississippian-age limestone (Chappel Formation) (Henry, 1982; Rowe et al., 2008). It is found at a depth of 6,500-8500 ft (1,981.2-2590.8 m). It is thickest in the northeastern section of the basin and gradually thins as it extends south-southwest toward the Llano Uplift with Ro > 1.4 %, pressure gradient of 0.52 psi ft^{-1}, TOC ranging between 1.5 % and 2 % with Type II-III kerogen estimating 26.7 Tcf shale gas and 3 bcf d^{-1} of shale oil (Jarvie et al., 2005; Bowker, 2007; Loucks and Ruppel, 2007; Andrews et al., 2009; Romero-Sarmiento et al., 2013). According to Rodriguez et al. (2010), the gas produced from the Barnett Shale was formed within the condensate–wet gas window (1.3–2.0 % Ro) at a later stage compared to the hydrocarbons accumulated in the shallower reservoirs.

Folds, joints and faults are examples of local and regional characteristics that control the fracture porosity of the Barnette Shale and impact production potential on a variety of scales (Smith et al., 2010). At the core scale, the Barnett Shale exhibits a larger average pore size, higher porosity and a greater extent of natural fractures, all of which enhance its reservoir quality (Xiong et al., 2024). Most natural fissures are sealed, however artificial fracturing might improve the flow rates around a well by taking advantage of this (Bowker, 2007).

The carbon sequestration story of the basin states that with lithostratigraphic and petrographic studies stratigraphic bulk geochemical analyses by Rowe et al. (2008) suggest that the deposition environment was anoxic to euxinic, characterized by a lack of sediment and relatively high organic matter accumulation rates. The deeper foreland basin where the Barnett layers were deposited had little access to the open ocean for circulation. Because the bottom waters of the basin remained euxinic, organic matter was preserved, creating a rich source rock that allowed for the accumulation of a large amount of framboidal pyrite (Loucks et al., 2007).

Appalachian basin: Located in the northeastern United states, (West Virginia and W-NE Pennsylvania); the Middle-Devonian Marcellus Shale formation covers a hydrocarbon producing area of 24,6049 km^2 (9,5000 mi^2) (Andrews et al., 2009). The Northeastern Pennsylvania extent of the basin is extensively hydrocarbon productive area (Harper, 2008). It is found at 4,000-8500 ft (1,219.2-2590.8 m) depth and with 50–250 ft (15.24–76.2 m) thickness that hosts 30–300 Tcf of shale gas (US Department of Energy Office of Fossil Energy and National Technology Laboratory, 2009; Soeder, 2010; Lee et al., 2011). The Ro ranges between 1.16 % and 2.79 % and TOC between 0.71 % and 7.88 % (Song et al., 2019). The play has a vitrinite reflectance of 1.0–2.8 %, and 1.59–1.78 % VRo in the wet gas region (Deller et al., 2018). The Marcellus Shale is one of the most productive gas fields in the world, and the most abundant hydrocarbon play in the Appalachian Basin (Laughrey, 2013, 2022). Nine major mineral phases—quartz, muscovite, illite, pyrite, chlorite, albite, calcite, dolomite and barite dominate the shales of the Marcellus Formation reservoir (Hupp and Weislogel, 2018).

The Southeast Regional Carbon Sequestration Partnership (SECARB), incorporates 11 states. These are Alabama, Arkansas, Florida, Georgia, Louisiana, Mississippi, North Carolina, South Carolina, Tennessee, Virginia and east Texas. Tertiary coal of the Gulf of Mexico has a potential of 20–28 Gt of CO_2 storage capacity (Petrusak et al. 2009).

The Late Devonian Acadian and Pennsylvanian-Permian Alleghenian orogenies produced primarily clastic terrestrial deposits that dispersed throughout the basin and foreland in a wide, westward coalescing coastal plain, primarily due to sediment supply from the uplifting and eroding Appalachian Mountains. Both clastics and carbonates depositeddue to maritime intrusions during high eustasy and/or decreased sediment supply (Cristopher 2022).

Illinois Basin: The Late Devonian Albany shales located between south-central Illionis and SW Indiana is composed of up to 140 m thick black to greenish gray shales, Ro within 0.5–1.5 % and TOC between 10.77 % and 2.58 % in the gas-window with Type II kerogen (Liu et al., 2017). It has tight black shale reservoir with 13 % of biogenic quartz and is ideal for hydraulic stimulation (Liu et al., 2020). As per Liu (2017), the secondary nanopores in Albany black shale store hydrocarbons.

4.5. Europe

Counry wise shale gas status in Europe and USa is also available in the report of the EMD Shale Gas and Liquid Committee (2024).

4.5.1. Bulgaria, Romania & Ukraine

The Eastern European countries contain three potential sedimentary basins: the Dniepr-Donets, the Carpathian Foreland and the Mesozoic Platform. These the targets for shale oil and gas exploration. They are composed of Paleozoic and Mesozoic marine shales. The Carboniferous and Silurian of the Paleozoic contain organic-rich black shales whereas the mid-Jurassic shales of the Mesozoic are oil-gas-prone.

- *Carpathian Foreland Basin:* The largest foreland basin of Europe stretches from SE Poland up to the Black sea containing Silurian organic-rich black marine shales within the Paleozoic belt for 50–200 km (Sowizdzal et al., 2020). The thrust belt dips gently to the SW and widens further SE to west Ukraine and northern Romania getting structurally simpler with few faults. It enters into the Scythian Platform after a tectonic disturbance. The entire Paleozoic belt is separated from the Moesian Platform to the south by the North Dobrogea Orogen. (Seghedi, 2012). The basin covers a hydrocarbon producing area of 2,9837 km^2 (1,1520 mi^2) in Ukraine and 4560 mi^2 in Romania with a depth of 10,000 ft (3048 m). The basin also includes the Jurassic Kokhanivka (12 % TOC), L. Cretaceous Spas and Shypot (2–7 % TOC) and the Oligo-Miocene Lower Menilite Formation (20 % TOC). Whereas, the Silurian black shales, especially the 400–600 m thick Ludlow Member are the main exploration targets in the basin. It is in the dry gas window with Ro between 1.3 % and 3.5 %. The TOC weighs < 2 % with a porosity of 4 %, and a pressure gradient of 0.43 psi ft^{-1}. It has an estimated 52 Tcf of recoverable resources in Ukraine and 21 Tcf in Romania (USA EIA, 2013).

  There were three ~~times~~ periods of significant foreland subsidence: the Early Miocene, the Early Badenian, and the Late Badenian–Sarmatian (Perty et al., 2016). Terrestrial depositional habitats were present in the Early Miocene, but marine environments predominated in the Middle Miocene. During the first marine incursion, the oldest Neogene (Eggenburgian to Lower Badenian inclusive) strata deposited onto the mountain foreland and in the southern portion of the Inner Foredeep (Sowizdzal et al., 2020). Geologic timeframes may allow for the entrapment and storage of carbon dioxide (CO2) in shale formations due to their high organic matter content. It is considered to have transformed chemically into hydrocarbons after being buried for millions of years.
- *Dniepr-Donets Basin (DDB):* It is a Mid-Late Devonian 700 km long and 40–70 km extensional failed rift basin on the Eastern European Craton located in eastern Ukraine (Stephenson et al., 1993). Trending NW-SE, it comprises of half-graben bounded by large displacement faults (Stephenson, 1993). It extends into the Pripyat Trough of southern Belarus getting shallower. The basin consists of marine deposited Lower Carboniferous organic-rich black shales overlying the Devonian salt interval is potential for shale oil and gas. The Upper Visean Rudov Beds composed of black shales are the best significant shale rock of the basin for shale gas exploration. It is 70 m thick and best developed in the Sreben and Zhdanivske depressions. The Rudov Beds are organic-rich with TOC ranging 3–10.7 % and the Upper Visean lying above the Rudov measure TOC of 5 %. The bed contains both Type II and III kerogen with a maximum of Type III kerogen. The Ro ranges from 0.8 % to 3.0 % in the oil (in central and NW DDB) and dry gas window at SE, respectively. It has ~ 59 Tcf of risked recoverable shale gas out of 235 Tcf shale gas is in-place (USA EIA, 2013).
- *Moesian Platform:* A structurally simple foreland basin spread over southern Romania and north-central Bulgaria is an overthrust platform by the Balkan thrust system in the south. It is surrounded by the Carpathian thrust in the north and separated from the Carpathian Foreland Basin by the North Dobrogea Orogen. The Silurian and the Jurassic Etropole Shale are the main target zones of the basin. The Silurian shale ranges from 4,050-4200 m deep, 160 m thick and with a TOC of 3 % in the South Craiova Block (SW Romania) (Sterling Resources, 2012). It is 1–5 km deep and 650 m thick in the Bulgarian Arch in eastern Bulgaria. The lower portion (Stefanetz Member) of the Jurassic Etropole Shale in NW Bulgaria, at > 5 km depth, contains thick carbonate-rich black shales with 1.0–4.6 %, TOC, 1.0–1.5 % Ro and 0.78 psi ft^{-1} pressure gradient with Type II kerogen (TransAtlantic Petroleum ltd., 2011). The estimated

resource concentrations are 383 Bcf mi^{-2} and 13.9 MM bbl mi^{-2} of shale gas and oil, respectively (USA EIA, 2013).

4.5.2. Poland

Poland has got Europe's most prospective Lower Paleozoic (Silurian and Ordovician) shale basins for shale oil and gas exploration (Uliasz-Misiak et al., 2014). Nearly 700 km deep, it spreads along the western margins of the East European Craton (EEC) (Jarzyna, 2017). The four prospective shale oil and gas basins evolved with the Late Neoproterozoic rifting and the post-rift thermal depressions basins are the Baltic Basin/Warsaw Trough, Podlasie Depression, Lublin, and Fore Sudetic (Papiernik, et al., 2017). The extensive flexural foredeep basin consists of marine deposited thick organic-rich Paleozoic sediments. They are highly porous and brittle with low clay and high quartz content. Poland has the biggest shale gas deposits in Europe (Lutynski and Gonzalez, 2016).

- *Baltic Basin:* It is the most prospective basin in Europe located in northern Poland bounded by the NW-SE trending Trans-European Suture Zone (TESZ) in the SW, the Mazury-Belarus High in the east, and it extends into the Baltic Sea to the north. The flat-lying basin has the organic-rich thick deposition of marine sediments from Paleozoic to Mesozoic, with Paleozoic organic-rich shale separated by regional unconformities. The tectonically passive basin evolved during the Late Precambrian rifting and post-rift downwraping of the East European Platform in the Early Paleozoic. The Lower Paleozoic deposits consist of thick extensive dark grey to black organic-rich marine shales with Type II/III kerogen (Kosakowski et al., 2016). This combined sediment sequence is 1,000-3500 ft (304.8–1066.8 m) thick where the Silurian is the thickest (~ 3 km in SW near TESZ) interbedded with dolomitic limestone. The older western Baltic Basin basin is composed of high silica content (40–80 %) and thus brittle. The TOC on average is 3.9 % with a porosity of 4 % and pressure gradient of 0.50 psi ft^{-1} for the basin sediment. The Upper Jurassic and Lower Triassic shales being thermally immature with low TOC are not accounted for quantitative assessment. It has an estimated dry gas of 181 Bcf mi^{-2}, 109 Tcf of shale gas, 14 Bbl of shale oil-in-place in the wet gas window and 14 B bbl of shale oil from the prospective area.

  As per Wojcicki et al. (2021), the maximum CO_2 capture capacity in the Baltic basin depends on ~ 76 % sorption by the OM where pore space and fractures accounts for only ~ 24 % sorption. The main target shales are Cambrian, Ordovician and Silurian in the deep saline aquifers (Silaupa et al., 2008).
- *Lublin Basin:* Located in the SE extension of the Baltic Basin, it is geologically complex with several close-spaced faults and steep dips (Narkiewicz and Narkiewicz, 2008). The major fault system of the basin includes the Holy Cross faults, Izbeca-Zamosc, the NW-SE trending Knock and Ursynow-Kazimierz. The significant source rock reservoirs in the basin are the Devonian Bychawa Formation, the Silurian and the Ordovician shales (Kufrasa et al., 2021). The combined Lower Silurian, Ordovician and Cambrian thickness of shales range from 330 to 1100 ft (100.58–335.28 m); and the Lower Paleozoic is 415 ft (126.49 m) (avg.). The TOC value is 3.5 % and Ro ranges from 1.7 % to 2.7 % (National Geological Institute, 2012; Sliwa et al., 2021). A slightly high-pressure gradient and 5 % porosity are documented from the Devonian section. It holds Type I/II kerogen (Botor et al., 2002). It has an estimated a resource concentration of 91 Bcf mi^{-2}.
- *Podlasie Basin:* The basin resembels the Lublin basin. It is a SE extension of the Baltic Depression and geologically less complex than the Lublin Basin. The Lower Paleozoic with an average thickness of 540 ft (164.59 m), depth ranging from 7,500-12,500 ft (2286–3810 m) has a TOC of 3 %, the porosity of 5 %, and a pressure gradient of 0.5 psi ft^{-1}. The Ro value varies from the dry gas section to wet gas and the oil window. It consists of 122 Bcf mi^{-2} of dry gas in the dry gas window, 22 Tcf of gas and 3 B bbl mi^{-2} of condensate in-place in the wet gas window and 9 B bbl of oil-in-place in the oil window (USA EIA, 2013).
- *Fore-Sudetic Monocline:* The lacustrine thick non-marine Carboniferous units are at 2–5 km depth. It is a significant source rock of the basin for shale gas exploration (Krzywiec, 2006). The Carboniferous is a mixed sequence of tight sandstones, deep coal seams, and shales and lies below the Rotliegend sandstone. The Carboniferous sequence is similar to the Relative Element Magnitude (REM) of the Cooper Basin, Australia. The basin is structurally simple, overpressured, and rich in clay and silica (20–60 %), porous (2–8 %) and ductile (San Leon Energy, 2012). The TOC ranges from 2.0 % to 2.5 % and Ro from 1.3 % to 1.8 % (Poprawa, 2015). The monocline has ~ 67 Bcf mi^{-2} of shale gas (USA EIA, 2013).

4.5.3. France

The Paris and the South-East basins are the two promising shale oil and gas basins potential for resource exploration. The Paris basin is an intra-cratonic depression extending nearly throughout the northern portion of the country. It is surrounded by the Vosges Mountains in the east, the Armorican Massif in the west, the Central Massif in the south and the English Channel in the north.

The Lower Jurassic Lias Shale and the Permian-Carboniferous Shale are the two shale plays of the basin. The black marine Jurassic Lias Dhale Formation (up to 650 ft, 198.12 m thick with 105 ft, 32 m of net shale and 4,000-10,000 ft, 1219.2–3048 m deep) is composed of three shale Groups: the Hettangian-Sinemurian Shale (Lower Lias), the Pliensbachian Shale (Middle Lias), and the younger Toarcian Shale (Schistes Craton). The shale is composed of calcite (10–30 %) and quartz (5–20 %) with medium clay content. The Ro ranges from 0.7 % to 1.0 %, TOC of 4 %, and T_{max} of 435 °C placing the shale in the oil window (Chungkham, 2009). As per the Torcian shale samples considered by Romero-Sarmiento et al. (2015), the T_{max} ranges 441–442 °C. The TOC is highest in the Toarcian Shales (3–12 %) with HI of 500–750 mg Hc g^{-1} of TOC and it is lowest in the Lower Lias (Hollander et al., 1991). It has an estimated 13 MM bbl mi^{-2} of shale oil and gas occurrence.

The Permian-Carboniferous gas play is situated in the eastern and southern part of the basin contains a stratum of tight sands, shales and methane-charged coals. It further includes the Lower Permian Autunian Unit, the Upper Carboniferous Namurian Unit and the Stephanian and Westphalian units with interbedded bituminous shales. The sediments are fluvial deposited in a lacustrine environment containing a higher percentage of clay and less brittle by nature with a mixture of Type II/III kerogen. It is gas-prone and ranges between 6,000-16,400 ft (1828.8–4998.72 m) deep; 7000 ft (2133.6 m) in the oil window, 10,000 ft (3048 m) in the wet/condensate gas window, and 14200 ft (4328.16 m) deep in the dry window with a net thickness of 83–160 ft (25.3–48.77 m) thick (USA EIA, 2013). The TOC ranges from 2 % to 15 %. The basin has an estimated resource of 20 MM bbl mi^{-2} of oil, 46 B bbl mi^{-2} of wet gas/condensate and 61 B bbl mi^{-2} of dry gas window stages. In 2011, Government has banned hydraulic fracturing for the extraction of shale gas and shale oil.

Carbon sequestration occurred when the Lower Jurassic White Lias, Lower Lias, Middle and Upper Lias strata were deposited as a result of the Lower Jurassif Rhaetic transgression, which was caused by the thermal subsidence linked to a block faulting during the mid Mesozoic (Barshep et al., 2021).

4.5.4. Scandinavia

The Alum Shales covering a prospective area of 8100 mi^2, extended over Scandinavia, Sweden, Denmark and Norway, are the main hydrocarbon exploration targets of the countries. The Alum Shale of the Cambrian-Ordovician Period is bounded by the tectonically active Caledonia Deformation Front in the west and Lower Paleozoic depositional limits in the east (Leventhal, 1991).

The depth of the basin ranges 3,300-15,000 ft (1,005.84-4572 m) from the southern part of Sweden to the northern portion of Denmark with 200 ft (60.96 m) thick layer containing hydrocarbon. Alum shale has a significant potential for total organic carbon and often appears gray-black in colour. It also has a high concentration of clay minerals, pyrite, and carbonate beds (Rexer et al., 2020; Thickpenny, 1984). The marine Alum shale consists of an average TOC of 7.5 % and an average Ro of 0.5–2.4 %, HI of 600 mg Hc g^{-1} (Dahl et al., 1989; Buchardt, 1990; Ghanizadeh et al., 2014). The organic matter is composed of liptinite group of macerals, viz., alginate (Samuelsson and Middleton, 1998). It has an estimated a resource concentration of 77 Bcf mi^{-2} of shale gas in Sweden and 110 Bcf mi^{-2} shale gas in Denmark (USA EIA, 2013).

In Alum Shale formation, during the Middle Cambrian to Early Ordovician age, abundant organic elements of marine origin were deposited offshore at a minimum depth of 100 m (Anderson et al., 1985). This facilitated the formation of a stable, bottom euxinic layer and a stratified water column (Leventhal 1990). The Alum Shale has been divided into two facies, each represents a different depositional environment (Fig. 3A,B). In the Furongian, the inner paleoshelf is distinguished by a greater amount of primary limestone and carbonate concretions in > 30 % of section thickness. The deepest portions of the shelf exhibited very monotonous mud deposition (Schulz et al. 2015).

4.5.5. Netherlands

The West Netherlands Basin is the main hydrocarbon exploration target. It is located in the SW part of the country extending into the shore. It is an inverted basin with complex geologic setting consisting of several NW-trending faults (De Jager et al., 1996). The Upper Carboniferous lacustrine-deltaic deposited Epen Formation, the open-marine deposited Geverik Member and the marine deposited Late Jurassic Posidonia Shale are the hydrocarbon source rocks of the basin. The Epen Formation lying above the Geverik Member has a hydrocarbon-rich area of 6009 km^2 (2320 mi^2) ranging between 3,300-16,400 ft (1, 005.84-4998.72 m) deep with a net shale thickness of 450 ft (137.16 m). Its Ro lies between 0.7 % and 1.3 % and TOC between 1 % and 15 % with Type III kerogen. The shale is over-pressured (Balen et al., 2000; Muntendam-Bos et al., 2009; USA EIA, 2013). It has an unconventional resource of 199.8 Bcf mi^{-2} of shale gas and 79.4 MM bb mi^{-2} of shale oil/condensate.

The depth of the underlying Geverik Shale ranges between 5,000-16,400 ft (1,524-4998.72 m) with a net organic-rich thickness of 135 ft (41.15 m). Its TOC ranges from 2 % to 7 % and Ro between 1.0 % and 1.3 % with Type II kerogen (Bergen et al., 2013). It is over-pressured and has a low to medium clay content. It has an estimated a resource concentration of 48.5 Bcf mi^{-2} of shale wet gas and 6.1 MM bbl mi^{-2} of condensate. The Posidonia Shale is shallower than the Epen and Geverik shales and overlies them. It is found at a depth between 3,300-12,500 ft (1,005.84-3810 m) with a net organic-rich thickness of 98.42 ft (29.99 ft) (Bergen et al., 2013). The Ro ranges between 0.7 and 1.3, TOC < 1–16 %, HI of 800 mg Hc g^{-1} TOC and porosity of 5–9.5 % along with Type II marine kerogen (Herber and Jager, 2010; Bergen et al., 2013). It is slightly overpressured with low to medium clay content. It has an estimated of 48.7 Bcf mi^{-2} of shale wet gas/associate and 17.3 MM bbl mi^{-2} of shale oil/condensate (USA EIA, 2013).

The Upper Jurassic and Lower Cretaceous fluvial to shoreface sandstones and lower Paleogene shallow-marine sandstones in the West Netherlands Basin are the most promising traps in synclinal structures involving the Lower Cretaceous Vlieland Sandstone Formation, which formed during Late Cretaceous tectonic inversion (Siebels et al., 2022).

4.5.6. Turkey

Turkey is a mountainous country bounded by Bulgaria in NW, Greece to the west, Armenia, Azerbaijan, and Iran to the east, Georgia to the NE, Syria to the south and Iraq to the SE. The country's dependency on natural gas is rapidly increasing with ~ 40 billion m^3 annually whereas it produces only ~ 1.5 % of the consumption (Kok and Merey, 2014). By 2035, the country's demand is estimated to reach 5 trillion m^3 (Bayramoglu and Ari, 2015). Hence, its dependency on unconventional energy resources is increasing. It has the two most potential shale basins: the SE Anatolia Basin in the south and the Thrace Basin in the west.

- *SE Anatolian Basin:* The basin covers an area of 3,2100 mi^2. It is an active oil-prone basin. It is situated in the eastern region of the Aegean's extended area, in SE Turkey surrounded by the Zagros suture zone on the north, the Syria and Iraq borders on the south, Iran border on the east. Being a part of the Gondwana supercontinent (its northern edge), the basin was affected by several vertical strike-slip and normal faults due to active graben tectonics (Ozdemir et al., 2020). In the Early Paleozoic, the Silurian shale was deposited throughout the northern Gondwana supercontinent (North Africa and the Middle East in present-day) in an anoxic environment. The deep Silurian Dadas, the Late Cretaceous Karabogaz and the Jodi Group of the Triassic and Jurassic Period are the three primary source rocks of the basin (USA EIA, 2013).

  The Silurian Dadas is the most hydrocarbon producing shale oil and gas reservoir of the basin containing hot shale at 6,000-13,000 ft (1,828.8-3962.4 m) depth and with 100–1000 ft (30.48–304.8 m) gross thickness. The shale is oil-prone and presumably wet gas-prone at deeper depth in the basin's north-central section (Hosgor et al., 2022). Carbon isotope studies reveal that frequent changes in the global carbon cycle (Early Silurian glaciation to greenhouse), the ocean-atmospheric influence. Alternate periods of carbonate production in the Silurian developed abundant reefs and carbonates (Cramer et al., 2007). The central area of the basin with 3540 mi^2 is oil-prone and the northern 500 mi^2 of the basin is prospective of wet gas and condensate shale. It measures T_{max} of 455 °C and I Ro from 1 % to 1.2 % (Kok and Merey, 2014). The Dadas I hot Shale contains Type II kerogen with TOC ranging from 2 % to 7 %, porosity from 6 % to 7 % with low water saturation and oil generation window (Kok and Merey, 2014; Sen and Kozlu, 2020). It has an estimated resource concentration of 41 MM bbl mi^{-2} of oil and associated gas from 3540 mi^2, and 91 Bcf mi^{-2} concentration of wet gas including 14 MM bbl mi^{-2} of condensate from 500 mi^2 (1295 km^2) area.
- *Thrace Basin*: The Tertiary age intermontane trough is the most significant gas-producing reservoir of the country covering an area of 16,835 km (6500 mi^2). It is located in the European portion of Turkey. The basin provides 80 % of the country's gas production. The basin is bounded by the Istranca Massif in the north, the Rhodope Massif in the west and the Sakarya Massif in the south. The basin was first investigated in the 1930s (Coskun, 1997). The Middle Eocene Hamitabat and the Lower Oligocene Mezardere are the two prime shale reservoirs of the basin with shallow marine and deltaic deposits, respectively. The marine deposited Hamitabat is the deepest, oldest and thermally mature shale formation at 14,000–16, 400 ft (4,267.2-4998.72 m) depth in the dry gas window. The Ro ranges from 1.3 % to 2.5 % and TOC from 1 % to 4 % (Aydmir, 2010). The basin has 104 Bcf mi^{-2} dry shale gas, 82 Bcf mi^{-2} wet shale gas and 34 MM bbl mi^{-2} shale oil concentrated reserve. The Mezardere shale formation comprises of 600 m thick alternating extensive dark-grey black shales, siltstones and laminated sandstone with low TOC content (Coskun, 1997). Thus, this formation is not quantitatively assessed (USA EIA, 2013). Due to its high quartz concentration (18–39 %), Dadas I shales are thought to be relatively brittle, which makes hydraulic fracturing more successful (Anatolia Energy Corp, 2012).
- The other prospective shale basin not assessed for commercial shale oil and gas exploration are Himmentoglu oil shale basins, Beypazari, Seyitomer, Goynuk, Taurus, Black Sea Basin, Sivas, and Salt Lake basins. As per Dogan and Uysal (1996), Himmentoglu oil shale gives better oil yield with Tmax 700 °C than Beypazari (400 °C) and Seyitomer (550 °C). The Paleocene Kabalar Formation of Goynuk Basin in Bolu deposited in a lacustrine environment. They are organic-rich oil potential formation with type I kerogen derived from

algae, i.e., Botryococcus and Tasmanites. The TOC ranges between 1 % and 10 % and HI from 751 to 953. The ratio between H/C and O/C are 1.52 and 0.19, respectively (Putun et al., 1988). The T_{max} values range from 432 to 442 °C stating from immature to early mature for oil generation (Hepbasli, 2004; Sari and Aliyev, 2005).

Data on geological carbon sequestration in Turkey shale reservoirs are not available.

4.5.7. United Kingdom (UK)

The UK is the country with the second-largest oil and gas potential. It has an extensive stratigraphic sequence of organic-rich shales. The older shales are mature and contain thermogenic gas whereas the shallower and younger shales are conventional hydrocarbon source rocks containing biogenic shale gas (Selley, 2005). The country has two most potential regions of isolated sub-basins with shale oil and gas reservoirs within the Carboniferous and Jurassic Periods extending the northern, central and southern section of the country. These Formations are Carboniferous and Jurassic marine black shales (Selley, 1987, 2012; Smith et al., 2015). The basins are structured by small fault-bound sub-basins and are structurally complex. It has been > 35 years since researchers have been evaluating the potential of UK shale gas and are at an early stage in developing the shale gas industry (Selley, 2012; Cooper et al., 2018). The Upper Paleozoic to the Mesozoic rocks of the country consists of shale gas window (Selley, 2012). The Carboniferous Lower Namurian and the Lower Jurassic Lias Formations are the main targets for shale exploration.

- *North UK shale region:* North England and southern Scotland contain thick, O-C, carboniferous shale covering 10,000 mi^2 area. The area is structurally complex with several isolated troughs. These troughs act as the main shale reservoirs. The examples are, the Bowland sub-basin of Lancashire representing the petroliferous East Irish Sea Basin, Cleveland Basin- an onshore extension of the Southern North Sea gas basin located east of Bowland, Cheshire, West Lancashire, Northumberland, East Midlands, Gainsborough, Midland Valley and others of the greater Pennine Basin. The Pennine Basin is considered to be UK's significant prospective basin.

  According to Hennissen et al. (2017), in the Pennine Basin, prograding deltas were the outcome of the gradual infilling of the Visean-created basin topography during the Namurian epoch. The deltaic successions exhibit a unique cyclicity as a result of repeated marine incursions: dark-colored limestone rich in marine fossils, often goniatites, sits over sandstone and/or shale with less fossils (Gross et al., 2014, Martinsen et al., 1995). The appearance of new ammonoid species, each of which is capped by a large ammonoid group (Ramsbottom, 1979), indicates longer-term marine invasions. The marine bands (Maynard and Leeder, 1992) and mesothems are linked to an eccentricity driving of glacio-eustatic sea level oscillations. These maritime bands represent the greatest flooding surfaces and can be considered as parasequences and carbon sequestration detail in the basin (Posamentier et al., 1988).

  The Bowland sub-basin located in the west of the Pennine Basin of NW England contains thick organic-rich gas-bearing shale. The western section of the moderately faulted Bowland sub-basin is an important 20–120 m thick shale exploration target. It measures TOC > 4 %. The UK shale region is in the dry gas window (i.e., Cleveland Basin and Bowland Basin). The Bowland Shale measures TOC 3.63 %, Ro 1.26 % at 2246 m depth in the dry gas window (Dart Energy, 2013). The Bowland shale is often defined as *"hemipelagic mudstone deposited in deep water"* and has an estimated higher potential for both shale oil and gas in the basin center (Palci et al., 2020). The eastern portion of the sub-basin extending towards Gainsborough is 300 m thick with minor geologic control. The lower rich-hydrocarbon part of the Bowland and Holywell are ~ 300 ft (~ 91.44 m) thick and deposited at ~ 8000 ft (~ 2438.4 m) depth with an average TOC of 3.0 % (De Pater and Baisch, 2011). The Ro measures 1.3 % in the wet condensate gas window. The Bowland, Edale, Holywell and the uppermost part of the Craven Group are known as the early Namurian shale units. These marine shales are 450–1400 m thick organic-rich strata at the outcrop and TOC values > 4 %.

  The Bowland sub-basin of the North UK shale region formed late ca. 330 Ma is the only commercial shale drilling region in the country (Walker et al., 2023). The lower part of the Bowland and Holywell Shale is the target shale region. The target is 8000 ft (2438.4 m) deep and 300 ft (91.44 m) thick with an average TOC of 3.0 % in the Bowland Sub-basin. At 3 km depth, it has 4 % porosity. The magnitude is 5–10 % at < 1 km depth with Ro 1.3 % in the dry gas window (Emmingns et al., 2022; Walker et al., 2023). It is the sole active shale drilling region of the country with five shale exploration wells. The main operators are the companies Cuadrilla Resources, IGAS Resources and Dart Energy (USA EIA, 2013). Lodhia et al. (2023) reported a 10 % recovery factor, and the resource potential of the Bowland shale is 6.4–13.1 Tcf. The Midland Valley Basin (MVB) is a massive ENE trending graben. It extends in south Scotland and is encompassed by the Highland boundary fault and the Southern Upland Fault to the NW and SE, respectively, comprising of small faulted sub-basins (e.g., the Kinkardine Basin). It is structurally complex due to Late Carboniferous to Early Permian extensive igneous intrusion (Underhill et al., 2008). The Visean Oil shale of MVB, Scotland has a TOC ≤ 30 %. The Lower Carboniferous oil source rocks are deposited in the Midlothian-Leven Syncline. Due to the structural complexity of the region, only 4635 mi^2 out of 10,200 mi^2 area is prospective. 25 Tcf out of 126 Tcf of shale gas in-place is recovarable (USA EIA, 2013).
- South UK Jurassic Shale Region: It extends throughout southern part of England with the two most prospective oil-producing onshore basins- Wessex and Weald. These basins stretch offshore into the English Channel. These are Jurassic-Triassic marine carbonate black shale reservoirs (Greenhalgh, 2016). The Wessex, located in Hampshire and Dorset, is the largest onshore basin of the UK. It produces 500 M bbl of oil from Wytch Farm oil field of Lower Lias (Ebukanson and Kinghorn, 1986b). It comprises of post-Variscan extensional sedimentary troughs and intra-basinal highs sequentially. The Pewsey, Mere-Portsdown, Dorset and Channel are the four small half-grabens in the basin.
- *The Weald Basin:* consists of synclines located in Sussex, Surrey and Kent. Both the Wessex and the Weald basins are regarded as a single oil-producing area separated by the Hampshire-Dieppe High. They are geologically simple with gentle dip. The Weald basin in southern England consists of Jurassic rocks. The faults trend E-W lying in the eastern part of the basin (Andrews, 2014). The Lower Carboniferous to Tertiary sedimentary rocks is 10,000 ft (3048 m) thick whereas the Lower Jurassic organic-rich shales are 7000 ft (2133.6 m) deep in the Weald Basin. It comprises of potential unconventional shale play which includes, the Kimmeridge Clay, the Corallian, the Lower Oxford Clay, the Upper Lias and the Middle Lias (USA EIA, 2013). The thermal maturity is highly variable in the Lias (Type II kerogen), Kimmeridge (Type III kerogen), and Oxford clays (mixed Type II/III kerogen). It increases towards the center of the Weald and Wessex basin.

The Jurassic shales are the main shale oil exploration targets in the South UK region. The Lower Lias Clay (rock) is significant in contributing unconventional resource with TOC ranging from 0.5 % to 7 % and Ro from 0.8 % to 0.9 % in Lias. It is mature for oil generation in the 'core mature area' (Andrews, 2014). The Lias Shale/Lias Black Shale has an average thickness of 600 ft (182.88 m) and 5000 ft (1524 m) in both basins. Its average TOC is 3 %, porosity ranges 7–30 % in various samples (Smith et al., 2010). The shale was under a geothermal gradient of 33 °C km^{-1}. Both the basins (Wessex and Weald) have an estimated

0.7 Bbl of recoverable shale oil and risked 0.6 Tcf of shale gas (USA EIA, 2013). The Wessex and the Weald are the largest onshore shale oil potential basins of the country.

The carbon sequestration in the Weald Basin started from the Early Jurassic. According to Barshep et al. (2021), in the end of the Early Jurassic, deposition of marine mudstones and limestones of the Oxford Clay Formation, Corallian Group, Kimmeridge Clay Formation, and Portland Group occurred as a result of tectonic uplift and the ongoing rifting, thermal subsidence and transgression from the Middle Jurassic (Callovian) to Lower Cretaceous (Sellwood 1986). The coarse clastic Upper Oxfordian and Portlandian sandstones, which were thought to have originated from the London Brabant Massif, to the north of the basin, broke up the deposition of these maritime mudstones and limestones. Clastic sediments of the Valanginian Wealden Group from the continent were deposited after the sea level dropped. Originating from the previous Variscan thrusts, the Upper Jurassic to Lower Cretaceous rifting created E-W trending extensional trapping geometries along low-angle faults. Some have proposed that in the Early Cretaceous, the Lower Jurassic source rocks acquired maturity and released hydrocarbons (Butler et al., 1990; Radley et al., 2006). The release of hydrocarbons ended as the source rocks cooled, inverted and the Cenozoic fault reactivated (Hansen et al., 2002).

4.5.8. Germany

The Lower Saxony Basin in NW Germany is the main hydrocarbon reservoir of the country. It covers ~ 10,000 mi^2 (25,900 km^2) area and is bounded by the Hanz Mountains in the south, Pompecky Block in the north, Hercynian Uplift in the east and Central Netherland High in the west. The basin is a subsided graben filled with sediments during the Late Jurassic and Early Cretaceous Period. It has a complex geologic setting with reverse faults. The two significant source rocks of the basin are the marine deposited Jurassic Posidonia Shale extending across the basin and the lacustrine-deltaic Lower Cretaceous Wealden Shale across the western portion of the basin (Kockel et al., 1994). The Ro of the basin on average ranges from 0.7 % to 1.3 %. It increases from the area with rich oil resource towards the dry gas window.

The Jurassic Posidonia Shale containing marine organi-rich marlstones ranges in depth from 3,300-16,400 ft (1,005.84-4998.72 m) where the oil window area lies at an average 8000 ft (2438.4 m) deep, wet gas/condensate window at 11,500 ft (3505.2 m) deep, and dry window at 14,500 ft (4419.6 m) deep with a net shale thickness of 90 ft (27.43 m) (Bruns et al., 2014). The TOC measured is 2–18 %, Ro 0.4–0.8 %, T_{max} 421–443°C and has type II kerogen (Bouw and Lutgert, 2012; Song et al., 2015). The Formation contains an average of 30 % carbonates in the SW and NW Germany including the place Luxembourg (Song et al., 2015). It has an estimated a resource concentration of 56 Bcf mi^{-2} of dry gas, 44 Bcf mi^{-2} of wet gas, 4 MM bbl mi^{-2} of condensate and 13 million bbl mi^{-2} of oil in their respective windows (USA EIA, 2013). The formation is yet explored in the country (Heege et al., 2015). The Wealden black shale is in the oil window and is mature for oil generation. It has a TOC ranging between 1 % and 18 % and Ro between 0.7 % and 1.0 %, HI within 344–719 mg HC g^{-1}, TOC with Type I and II kerogens (Rippen et al., 2013; Ziegs, 2015; Froidl et al., 2021). It has an estimated a resource of 10 MM bbl mi^{-2} (USA EIA, 2013).

According to Luders et al. (2021), tectonic forces generated hot hydrothermal fluids that were overpressured during the Late Cretaceous inversion of the Lower Saxony Basin, supplying a substantial volume of CO_2. The movement of CO_2-rich fluids was recorded by fluid inclusions in minerals from fracture-fill mineralization in the Devonian, Upper Carboniferous and the Ca2 strata. Deeply buried Devonian sequestrated carbonates underwent a high-temperature metamorphism, which released CO_2, which rose and reached particular Ca2 reservoirs through deep-reaching faults and hot hydrothermal fluids.

4.5.9. Spain

Spain has moderate deposits of commercial shale oil and gas (Torrente and Galan, 2000). The Mesozoic-Early Cenozoic Basque-Cantabrian Basin in northern Spain is the most important potential shale oil and gas basin of the country. The basin with an area of 6620 mi^2 consists of hydrocarbons potentially in Silurian-Ordovician, Jurassic and Cretaceous shales. During the Pyrenean orogeny, the basin underwent folding and thrusting in the Tertiary (Quesada et al., 1997). The Ordovician and Silurian shales are well established in the outcrops and the boreholes in Spain. The Formigoso and the Sueve Formation of the Lower Silurian and Ordovician have TOC < 1 % with Type IV kerogen (Mio et al., 2011).

The Cretaceous Valmaseda Formation containing Enara Shale estimates 185 Bm^3 of shale gas based on the 13 wells in the Gran Enara field. San Leon Energy estimates that the average TOC of the formations is 1 % (USA EIA, 2013). The Jurassic thick black shales contain potential wet gas and condensate reservoir. It includes 2100 mi^2 of prospective Lias Shale below the Lower Jurassic prospective shales. The Jurassic/Liassic black shale has a net thickness of 30–50 ft (9.14–15.24 m). The TOC of the formation ranges from 2 % to 8.7 %, Ro of 1.2 %, HI = 760, and S2 = 56.5 mg g^{-1} (Quesada et al., 1997). The Cadiolos-1 well touched Lower Jurassic unit at 9500 ft (2895.6 m) and a net thickness of 100 ft (30.48 m) with 2 % TOC and Ro = 1.1 %. As per USA EIA (2013), the Basque-Cantabrian basin containing organic-rich Jurassic-Liassic Formation has ~ 42 Tcf of wet shale gas and 3 B bbl of shale condensate out of which 8 Tcf and 0.1 B bbl, respectively, are recoverable. The Liassic shales are the only source of the Ayoluengo oils, the sole onshore commercial oil field in Spain (Comet, 2018).

Other shale basins include the Badenas Formation, the Ebro basin, and the Puertollano oil shale. The Badenas located in central Spain consists of Silurian graptolite black shales with Type III kerogen (Pozo et al., 2017). The lacustrine Puertollano of the late Stephanian age is located in the south La Mancha, Central Spain. It consists of bituminous shales and high volatile bituminous coal (Rio et al., 1994). The Ebro basin in NE Spain consists of 50–100 m thick shale sequence at 1, 650-4000 m depth. It has Ro ranging from 1 % to 2 % whereas a very poor TOC = 1 %. Due to the presence of low TOC, the Ebro basin is not considered for shale oil and gas assessment. Despite having some shale formations, such as the Cantabrian Mountains and the Ebro Basin, Spain has faced challenges and public opposition to hydraulic fracturing because to concerns about the consequences on the environment, e.g., water pollution and artificial seismicity. Therefore, hydraulic fracturing laws in Spain have been strict, with some regions passing outright bans or moratoriums on the practice (Costa et al., 2017; Buono et al., 2018).

Data on geological carbon sequestration in Spain shale reservoirs are not available.

4.5.10. Lithuania/ Kaliningrad

The Llandovery shales are the NE extension of the Baltic basin in Lithuania. The basin has experienced sedimentation during prolonged subsidence between Cambrian and Quaternary (Sliaupa et al., 2020). A deep-marine environment was created in the west of the basin (Alcalde et al., 2013). The TOC ranges from 1 % to 1.7 % (Poprawa, 2010; Hosgor et al., 2022). The Raikkula shales in the lower Silurian has the maximum TOC of 21 %. The TOC decreases in the Upper Silurian shales (Silaupa et al., 2016; 2020) It has an estimated 6 B bbl of shale oil and 4 Tcf of associated shale gas in-place (USA EIA, 2013). The Llandovery basin is the NE extension of the Baltic Basin into the Kaliningrad Oblast, Russia, similar to the Lituania basin in Europe. The main shale targets are the Cambrian, Ordovician and Silurian as is the case for the the Baltic basin. Being an extension of the Baltic Basin, the lithounits resemble characteristics and properties with the Basin in Poland. The Llandovery shales estimates 23 B bbl of shale oil and 4 Tcf of shale gas in-place (USA EIA, 2013).

In the basin, the Ireviken Excursion is characterized by a four-stage glaciations and climate change. Thermohaline circulation during low sea-level intiated sequestration of carbon in shallow sea (Cramer et al., 2007).

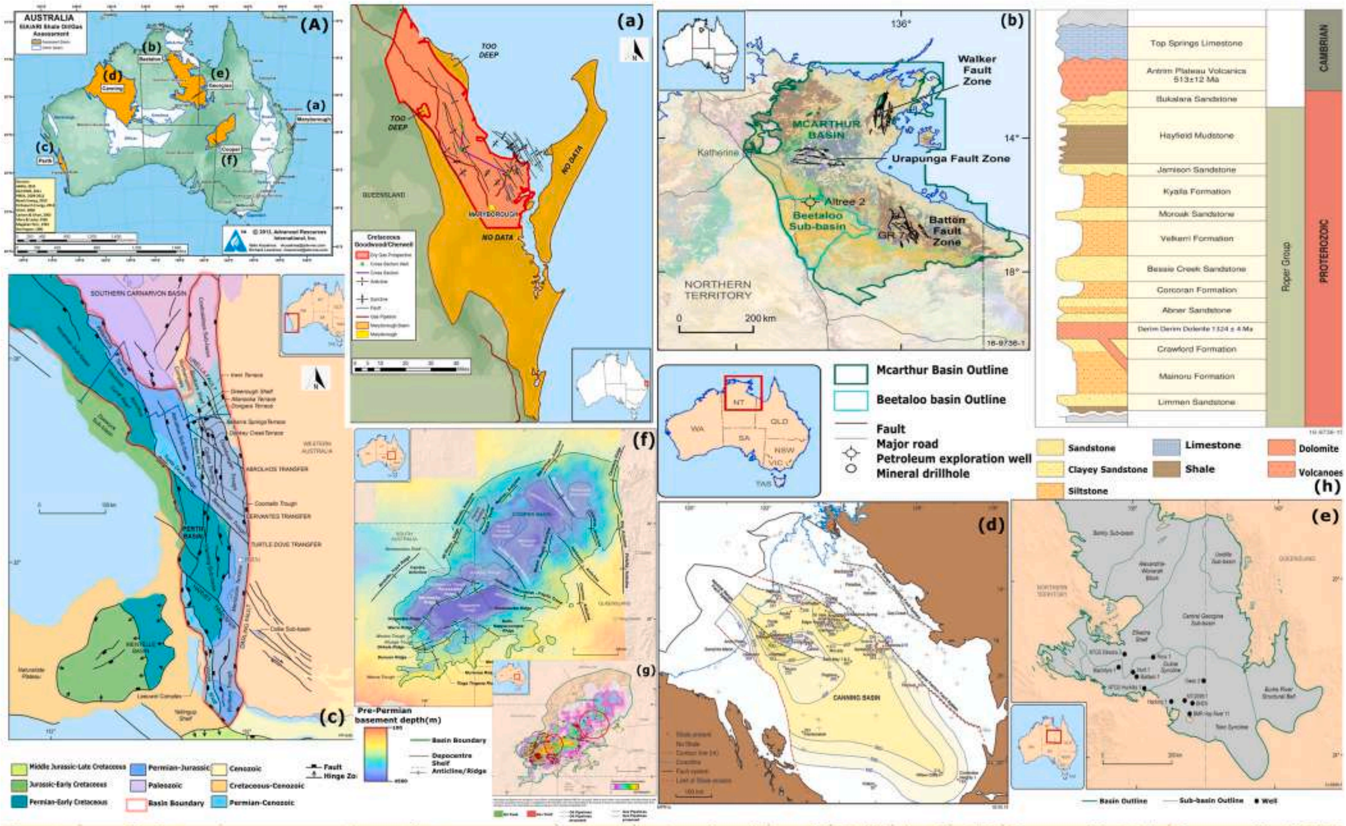

Country	Basin	Formation	Prospective Area (in mi²) Gas	Oil	Avg. TOC (%) Gas	Oil	Avg. Ro (%) Gas	Oil	Recoverable (Tcf) Gas	Recoverable (B bbl) Oil
Australia	Cooper	Roseneath-Epsilon-Murteree (Nappamerri)	4705	1180	2.6	2.6	1.333	1	89.2	0.99
		Roseneath-Epsilon-Murteree (Patchawarra)	2330	2160	2.6	2.6	1.1	1	3.6	0.44
		Roseneath-Epsilon-Murteree (Tenappera)	200	200	2.6	2.6	0.85	0.85	0.1	0.13
	Maryborough	Goodwood/Cherwell Mudstone	1540	0	2	0	1.5	0	19.2	0
	Perth	Carynginia	2200	0	4	0	1.4	0	24.8	0
		Kockatea	1890	1890	5.6	5.6	1	1	7.9	0.54
	Canning	Goldwyer	57380	34520	3	3	1.133	1	235.4	9.75
	Georgina	L. Arthur Shale (Dulcie Trough)	4210	2260	4.25	3	1.325	1.15	8.2	0.12

Fig. 5. **A.** Australia's assessed prospective shale gas and shale oil basins (Source: USA EIA, 2013). **a.** Maryborough basin prospective shale gas area (USA EIA, 2013). **b.** Beetaloo Basin defined as a sub-basin of Mcarthur Basin (Source: Jarrett et al#, 2013). **c.** Structural elements of the Perth Basin (modified after Hashimoto et al#, 2018). **d.** Map of the Canning Basin showing wells that intersect shale [Source: Department of Mines, Industry, and Safety (Petroleum), Govt. of Western Australia, 2013]. **e.** Sub-basins of southern, central and eastern Georgina Basin. Inset: Location of the Georgina Basin in Australia (Source: Smith et al#, 2013). **f.** Structural elements of the Cooper Basin overlain on a structure contour map of the top pre-Permian basement surface (Source: modified after Kuske et al#, 2015). **g.** Map of the combined modelled volume of hydrocarbons generated from all Permian source rocks (MMboe km^{-2}) (Source: modified after Kuske et al#, 2015). **h.** Generalised stratigraphy of the Proterozoic Roper Group (Figure adapted from Jarrett et al#, 2019). **i.** Assessment of properties and quantity of substantial shale formations in Australia (Data source: USA EIA, 2013).

4.6. Oceania

4.6.1. Australia

The success of the U.S. in the exploration of shale gas and oil reservoirs has triggered a focus on the shale plays in Australia for the past 10 years or so. It has ~ 30–40 sedimentary basins amongst which only six have major exploration potential (Ahmad, 2014). These are the shale oil and gas sedimentary basins: Cooper, Maryborough, Perth, Canning, Georgina and Beetaloo (ICF International, 2014) (Fig. 5A). The age of the shale units in the sedimentary basins of Australia varies from the Proterozoic to the Cretaceous in age. They contain 2046 Tcf of risked shale gas, 429 Tcf of recoverable shale gas and 403 B bbl of risked shale oil (USA EIA 2013, 2017).

- *Maryborough Basin:* Located in SE Queensland, 250 km north of Brisbane, the Cretaceous Marine Goodwood/Cherwell Mudstone Formation has two potential gas shale targets (Fig. 5a). The Mesozoic basin encompasses an onshore area of 11,136.95 km^2 (4300 mi^2) and a thickness of 8500 ft (2590.8 m) (Lipski, 2001). Formed in the fluvial and deltaic environment and influenced by various marine transgression, the basin is an asymmetric half-graben bounded by the Electra fault at the west along with numerous normal and reverse faults (Marshall et al., 2015). The Goodwood Mudstone, Woodgate Siltstone and Cherwell Mudstone Formation of the basin consist of mudstones, siltstones and minor shales. The dry gas prospective Goodwood Mudstone Shale is 2000 ft (609.6 m) thick and 5,000-15,000 ft (1,524-4572 m) deep with ~ 2.0 % TOC and < 1.5 % R_O. The underlying Cherwell Mudstone Black Shale is 17,000 ft (5181.6 m) deep. The organic-rich pay in the two shale intervals is at 250 ft (76.2 m). This dry gas-prone basin has an estimated 111 Bcf mi^{-2} of dry gas from the Goodwood and Cherwell mudstone troughs. The southern half of the basin is unexplored due to unavailable data and assessment.
- *Beetaloo Basin:* It is one of the northernmost Precambrian rift shale basins of Australia. It covers an area of 36,259.834 km^2 (14,000 mi^2), enclosed by the Walton High, the Helen Springs High, the Batten Trough, and the Daly Waters Arch, to the north, south, east and west, respectively (Fig. 5b). The Velkerri and Kyalla shale reservoirs are the organic-rich marine formations of the Beetaloo Basin. The Velkerri is composed of black mud shale (TOC 4–6 %) and laminated gray-green shale (TOC < 2 %) interbedded with thin sandstone and siltstone (Warren et al., 1998). The depth of the resource hydrocarbon rich Velkerri Formation ranges from 3300 −8700 ft (1,005.84-2651.76 m). The maximum TOC content is

12 %. Within 3,300-5000 ft (1,005.84-1524 m) depth, the formation gets in the oil window with R_O from 0.7 % to 1.0 %. At a greater depth of 5000 ft (1524 m) and 7000 ft (2133.6 m), it enters the gas/condensate window (1.0–1.3 %), and dry gas window (Ro > 1.3 %), respectively. It has dry and wet gas area of 6423 km^2 (2480 mi^2) and 5517 km^2 (2130 mi^2), respectively.

- The basin has an oil potential area of 6863 km^2 (2650 mi^2). It holds 22 Tcf shale dry/wet gas and 28 B bbl of shale oil. The upper and the lower section of Kyalla Shale is separated by thin Kyalla Sandstone with a combined thickness of 600–2500 ft (182.88–762 m). The lower section of the formation is resourceful whereas the upper section eroded from west to east. The shale has an average TOC of 2.5 % and 9 % in the center of the basin (Silverman and Ahlbrandt, 2011). It is in the oil window from 3,300-5000 ft (1,05.84-1524 m), a gas window from 5,000-6000 ft (1,524-1828.8 m), and a dry gas window below 6000 ft (1828.8 m). The unit has 1310 mi^2 area of dry gas, 2400 mi^2 of wet gas/condensate, and 4010 mi^2 for shale oil. It has an estimated 100 Tcf of dry and wet gas, recoverable 65 B bbl of shale oil, and 3.3 B bbl of condensate shale (USA EIA 2013).
- *McArthur Basin:* The Velkerri Formation of the Rooper Group (1280 Ma) consists of the most potential organic-rich shale reservoir in the McArthur Basin (Kralik, 1982, Mukherjee et al., 2017). The basin in the northern Austalia is formed during the mid-Proterozoic and in a marine environment (Jackson et al., 1988). The black dolomitic shale of Barney Creek Formation is a prospective hydrocarbon-rich reservoir. According to Crick et al. (1988), the source rock is deposited in lacustrine environment with TOC ranging from 0.6 to 7.6, and an HI < 100–740 of Type I-II kerogen. The Lynott Formation of the Caranbirini Member consists of organic-rich shales. It is > 300 m thick overmature lacustrine deposited formation with TOC = 0.2–3.4 and HI < 143 (Jackson et al., 1988; Crick et al., 1988). Nearly 2.91 bcf km^{-2} of recoverable shale gas is extracted from the basin (ACOLA, 2013).
- *Perth Basin*: It is an active petroleum onshore and offshore basin situated in the SW of Western Australia with rich-organic Carynginia and Kockatea marine shale (Fig. 5c). It is a NNW-trending half-graben favorable for oil and gas formation. The basin formed as the Australia rifted from India during the Permian to the Early Cretaceous Period (Playford et al., 1976; Harris, 1944; Cawood and Nemchain, 2000). The sedimentary strata of the Perth Basin include the Permian Lower Carynginia shales, non-marine shoreline siliclastics to shelf carbonates of Upper Permian and Triassic to Lower Cretaceous Kockatea Shale. The Carynginia underlies the Kockatea Shale. The on-shore basin of 20,000 mi^2 constitutes Dandaragan and Bunbury trough separated by the Harvey Ridge. The thickest and the deepest Dandaragan sub-basin have potential shale oil and shale gas development. The other marine shale formation e.g., Triassic Woodada and Jurassic Cadda, Yarragadee Formation and the Cretaceous South Perth Formation hold unfavorable conditions for shale oil and shale gas reservoirs. The shallow-marine deposited dark Kockatea Shale is the main hydrocarbon seal in the basin with a wet gas prospective area of 2667 km^2 (1030 mi^2) estimating 59 Bcf mi^{-2} (Cawood and Nemchain, 2000; USA EIA, 2013). It has a maximum thickness of 3500 ft (1066.8 m) with 8 % TOC at the most organic-rich site (Hovea Member) in the basin. The 160 ft (48.77 m) thick Hovea Member has an average clay content of 33 %. The TOC of Kockatea Basin ranges from 2.31 % to 7.65 % consisting of Type III kerogen. The Dongara Trough of the Basin contains a thermally matured shale gas reserve. Estimated shale oil from the oil and condensate prospective area are 19 and 6 MM bbl mi^{-2}, respectively. The Carynginia Shale of 800–1100 ft (243.84–335.28 m) thick is a deep-water shale unit with 5698 km^2 (2200 mi^2) dry gas area. It is in the dry gas window with 4 % average TOC and Type III kerogen. It has an estimated 94 Bcf mi^{-2} resource where 25 Tcf of shale gas is recovered (USA EIA, 2013). The middle zone of the Carynginia Shale is more prosperous with an estimated 1–4 % of TOC, lower clay content with 3–6 % porosity at its depth of 7,780-7960 ft (2, 371.34-2426.21 m).
- *Canning Basin*: It is the biggest sedimentary basin in Western Australia with an area of 60,606 km^2 (23,400 mi^2) (Fig. 5d). It is an intracratonic rift-basin containing Ordovician to Cretaceous sedimentary rocks. A Precambrian arch separates the basin from the Amadeus Basin at east having a series of NW trending fault-bounded troughs. The organic-rich Ordovician Goldwyer trough, deposited in open marine is highly fossiliferous. It is 1300–2414 ft (396.24–735.79 m) thick and 16,500-3000 ft (5,029.2-914.4 m) deep (Bailey et al., 2021). Grayish-green to black Goldwyer shale was deposited in an anoxic reducing condition. It has an oil reserve on the uplifted platforms and terraces, whereas it is gas-prone in the adjacent troughs. Its TOC value ranges from 1 % to 10 %. The upper portion of the formation has 6.40 % of TOC. The source rock is in the Southern Basin and mid-basin platform within the oil window whereas the dry gas window lies in the thermally mature Kidson sub-basin at 10,500 ft (3200.4 m) deep Goldwyer Shale estimating 109 Bcf mi^{-2} of dry gas. According to the Department of Mines and Petroleum (2014), (2017), the sedimentary succession of the Canning basin is thin and less deformed but the deep crustal seismic data from the Geoscience Australia indicates 6.4 km thick sedimentation in the Kidson Sub-basin (Southby et al., 2020). The wet gas and condensate window lie between 7,200-10,500 ft (2, 194.56-3200.4 m). The Goldwyer Shale contains oil and condensate potential of 41 MM bbl mi^{-2} and 10 MM bbl mi^{-2}, respectively. The wet gas concentration in the Kidson sub-basin is 67 Bcf/mi^2 (USA EIA, 2013).
- *Georgina Basin:* It is the largest Neoproterozoic-Paleozoic basin on the North Australian craton formed by moderate folding and faulting (Fig. 5e-f). The southern margin of the basin has experienced over-thrusting having conjugate fault and NE-trending joints (Kruse et al., 2001). It is a large unexplored basin of 3,30,000 km^2 area, located in North Australia extending to the border of North Queensland (Tenthorey and Alying, 2020). The Toko and the Dulcie troughs of Middle Cambrian are the major Shale oil and gas syncline depo-centers of the basin. At the southern margin, these deep synclines consist of downfaulted half-grabens and Cambrian to Devonian rock units of 7200 ft (2194.56 m). It shallows northward to < 3000 ft (914.4 m) depth. The lower section of the Cambrian sediments contains black pyritic-carbonaceous ‘hot’ black shale. The shale is characterized by high porosity (22 %) clastic and carbonate intervals. The TOC ranges from 2 % to 16 % and is prone to Type I and II kerogens. The northern portions of Dulice and Toko have a vitrinite reflectance (R_O) of 0.7 %. These troughs and their surrounding areas are prospective of shale oil and gas. Total risked wet and dry gas is estimated at 67 Tcf and oil/condensate at 25 B bbl (USA EIA, 2015).
- *Cooper basin:* This intracratonic Gondwana basin is a NE-trending up to 4.5 km deep structural depression formed under mild compression (Apak et al., 1997; Lindsay, 2000). It is a part of the Gondwanaland detached from the overlying extensive Eromanga Basin by a major unconformity at 970–2800 m depth (Reynolds et al., 2006). The Cooper Basin is the main mature non-marine onshore oil and gas reservoir of Australia formed in strata between Late Carboniferous and Middle Triassic Periods (Bazunu et al., 2015) (Fig. 5g,h). It spans the South Australia and Queensland border with 130,000 km^2 area. The South Australian part of the Cooper Basin consists of numerous NE and SW ridges and troughs. These depocenters include an organic-rich deep lacustrine Nappamerri, Patchwarra and Tenappera shale trough/formation of the Permian Period (Reynolds et al., 2006; Hill, 2010). These troughs are large, thermally mature, over-pressured and separated by faults at 5,000-13,000 ft (1, 524-3962.4 m) depth at the southern end to the centre (Fig. 5i). More than 200 wells have been drilled in the basin for exploration and production of shale oil and gas (Backe et al., 2011).

Table 4
Commercial, Potential and Speculative shale basins of the world.

Country	Shale plays/Formations			References
	Established	Potential	Speculative	
China	Sichuan Basin, Tarim Basin, Junggar Basin, Songliao Basin, Bohai Bay Basin, Ordos Basin	Bohai Bay Basin, Turpan-Hami Basin, Qinan Basin, Jianghan Basin, Qaidam Basin, Beibuwan Basin, Liaohe Basin, Bohai Gulf Basin, South Yellow Sea Basin, Yinggehai Basin	Sichuan Basin extension, Yanshan Basin, South China Basin, Erlian Basin, Pearl River Mouth Basin, Songliao Basin Extension, Juggar Basin Extension, Bohai Bay Basin Extension	Li et al. (2023); Hansheng et al. (2023); Zhao et al. (2022); Peng et al. (2022); Feng et al. (2021); Li et al., (2019); Zhang et al., (2019)
Russia	Volga-Ural Basin, Pechora Basin, West Siberia Basin, Timan-Pechora Basin, Yenisei-Khatanga Basin	East Siberian Basin, Khadum Formation	No relevant data	James et al. (1985); Lindquist (1999); Prischepa et al. (2011); Vernikovsky et al. (2018).
United Arabian Emirates	No Data	Al Ain Basin, Rub' Al-Khali Basin, North UAE basin	No Data	Alzabi et al. (2018), Hassani et al. (2023)
Pakistan	No Data	Indus Basin, Ranikot Shale, Sakesar Shale, Kohat Basin	Bannu Basin	Khan et al. (2017); Ashgar et al. (2022); Mir et al. (2023)
India	Cambay Basin, Damodar Valley Basin, Gondwana basin	Barmer Basin, Krishna-Godavari (KG) Basin, Cauvery Basin, Indo-Gangetic Basin, Spiti basin, Rajasthan Basin, Sayrashtra Basin, Son Valley Basin, Mahanadi Basin, Narmada Basin, Satpura Basin, Mumbai off-shore basin, Andaman Basin, Kerela Konkan Basin, Manipur-Nagaland Basin, Bhima Basin, Cuddapah Basin, Rajmahal Basin, Assam Shelf Basin	Kapurdi mine, Kachchh offshore basin, Vindhyan Basin, Deccan Syneclise Basin, Eastern Himalayan Basin	Sain et al. (2014), Bakshi et al. (2020), Kumar et al. (2022); Hakimi et al. (2023)
Oman	Rub' Al-Khali	South Oman Salt, North Oman Salt	No data	Grosjean et al. (2008); Al-Kindi and Richard (2014)
Indonesia		Sumatra Basin, Kutei Basin, Tarakan Basin, Bintuni Basin	No data	

(*continued on next page*)

Table 4 (*continued*)

Country	Shale plays/Formations			References
	Established	Potential	Speculative	
Kazakhstan	North Caspian Basin	South Mangyshlak Basin, South Turgay Basin, The North Ustyurt Basin, Chu-Sarysu Basin, Uralsk Basin, Zaysan Basin	No data	Huvaz et al. (2007); Nurbekova et al. (2023)
Jordan	Not yet explored	Hamad Basin, Wadi Sirhan Basin	No data	Armstrong et al. (2005); Hrayshat et al. (2008);
Mongolia	East Gobi basin	Zhesi Formation, Upper Permian Linxi Formation, Tamtsag basin	No data	Hu et al. (2022); Zhanping et al. (2023); Liu et al. (2023);
Thailand	Not yet explored	Khorat basin, The Central Plains Basin, Na Pho Song and Sap Phlu Basins	No data	Koyasamram et al. (2011); Chumkratoke et al. (2015); Chenrai et al. (2022)
Algeria	Tindouf Basin	Ghadames Basin, Illizi Basin, Timimoun Basin, Ahnet Basin, Mouydir Basin, Reggane Basin,	Taoudeni Basin, Oued Mya Basin	Baouche et al. (2023)
South Africa	Karoo Basin	Orange basin, Parana Basin	Tuli basin, Bredasdorp Basin	Adekola et al. (2012); Kock et al. (2017); Akintola et al. (2021); Afolayan et al. (2023);
Libya	Murzuq Basin	Ghadames Basin, Sirte Basin	Kufra Basin	Aziz (2000); Xiao et al. (2023);
Egypt	No data	Western Desert Basin, the Nile Delta Basin, Abu Gharadig, Alamein, Natrun and Shoushan-Matruh	Kom Ombo basin	El Diasty (2015); Hakimi et al. (2023)
Chad	Not yet explored	The Termit Basin, Bongor Basin, Salamat Basin, Erdis Basin.	Doba Basin, Doseo Basin	Zhang et al. (2023),
Tunisia	Ghadames Basin, Pelagian Basin	Kerkennah Basin	No data	Talbi et al. (2018); Gottlich et al. (2023);
Morocco, Western Sahara, Mauritania	Not yet explored	Tindouf Basin, Tadla Basin, Taourirt Basin	Senegal_Mauritania basin, Anti-Atlas Basin, Essaouira-Agadir Basin	Kassab et al. (2023); Bouayachi et al. (2023)
Argentina	Vaca Muerta Basin, Chaco Basin, Los Molles Basin, South Atlantic Basin, Tarija Basin	Neuquen Basin, Golfo San Jorge Basin, Austral Basin, Parana Basin, Austral-Magallanes Basin, Cuyo Basin, Northwest Basin, Chubt Basin, Salta Basin Colorado Basin, Canadon Asfalto Basin,	Central Basin, San Julian Basib, Cuenca del Colorado Basin, Northwest Basin extension, Sub-Andean Basins, Other Extensional basins	Martinez et al. (2008); Legarreta and Villar (2011); Caprioglio et al. (2020)

(*continued on next page*)

Table 4 (*continued*)

Country	Shale plays/Formations			References
	Established	Potential	Speculative	
		Malargue Basin, Cuenca del Golf San Jorge Basin, Los Monos Basin, Precordillera Basin		
Brazil	No data	Parana Basin, Solimoes Basin, Amazon Basin, Potiguar, Parnaiba, Sergipe-Alagoas, Parecis, Reconcavo, Sao Francisco, Taubate, Chaco-Parana	Potiguar Basin	Weniger et al. (2010); Ferreira et al. (2023)
Colombia and Venezuela	Not yet explored	The Middle Magdalena, Llanos Basin, Maracaibo Basin, Orinocco Belt	No data	Torres et al. (2012); Mendez et al. (2023);
Bolivia, Chile, Paraguay, Uruguay	Not yet explored	Parana Basin, Chaco Basin, Magallanes Basin, Sub-Andean Bolivian basin	No data	Fulfaro et al. (1997); Veroslavsky et al. (2020)
Mexico	Burgos Basin	Sabinas Basin, Tampico-Misantla Basin, Tuxpan Platform and Veracruz basins	Chihuahua Basin, Sonora Basin, Oaxaca Basin	Guzman-Vega et al. (2001); Luque and Marcela (2017); Enciso-Cardenas et al. (2021);
British Columbia and Northwest Territories	Montney Formation	Muskwa/Otter Park basin, Horn River Basin, Liard Basin, Cordova Embayment, Nechako Basin,	No data	Dixon et al. (2002); Yuan et al. (2023)
Alberta	Duvernay Formation	Alberta Basin	No data	Wust et al. (2013);
Eastern Canada	No data	Appalachian Fold Belt, Windsor	No data	Pashin et al. (2023);
Saskatchewan/ Manitoba	No data	Williston Basin	No data	Gelman et al. (2023)
USA	Permian Basin, Eagle Ford Shale, Bakken Formation, Marcellus Shale, Haynesville Shale, Utica Shale, Niobrara Formation	Illinois Basin, Appalachian basin, The Fort Worth Basin, Monterey Shale	Anadarko Basin, Fayetteville Shale, Powder River Basin, Tuscaloosa Marine Shale, Collingwood-Utica Shale, Mancos Shale	Wust et al. (2013); Elturki et al. (2023); Malki et al. (2023)
Bulgaria, Romania, Ukraine	Not yet explored	Moesian Platform, Dniepr-Donets Basin, Carpathian Foreland Basin,	Dobrudzha	Karpenko et al. (2023); Krezsek et al. (2023);

(*continued on next page*)

Table 4 (*continued*)

Country	Shale plays/Formations			References
	Established	Potential	Speculative	
Poland	Not yet explored	Baltic Basin, Lublin Basin, Podlasie Basin, Fore-Sudetic Monocline, Caledonian Foredeep Basin, Lower Silesia Basin, Greater Poland Basin	No data	Khufrasa et al. (2021), Wojcik et al. (2022); Haluch et al. (2023)
France	Not yet explored	Paris Basin, South East Basin	Grands Causses Basin, Mowry Shale	Bomou et al. (2022); French et al. (2022)
Scandinavia	Not yet explored	Alum Shale, Olso Graben, Baltic Basin	No data	Ghanizadeh et al. (2014); Zengh et al. (2023);
Netherland	Not yet explored	Namur Synclinorium, Campine Basin, West Netherland Basin, Lower Saxony Basin	No data	Wei et al. (2023), Buijze et al. (2023)
Turkey	Not yet explored	Thrace Basin, Southeastern Anatolia Basin, Central Anatolia Basin, Sakarya Basin, Himmentoglu oil shale basins, Beypazari, Seyitomer, Goynuk, Taurus, Black Sea Basin, Sivas, and Salt Lake basins	Tekman-Karayazı Basin	Ayyildiz et al. (2023), Celen and Develi (2022); Hosgor et al. (2022)
United Kingdom	Bowland basin	Weald basin, North Wales, Welsh Borders, East Irish Sea Basin, Cleveland Basin, Pennine Basin, Scottish Midland Valley Basin	East Anglia, Humber basin, Solway Basin, Isle of Wight Basin, Lancashire Basin, Northern Ireland	Walker et al. (2023); Oye et al. (2023); Michel et al. (2023);
Germany	Not yet explored	Rhineland Basin, Saxony Basin, Silesian Basin, Northwest German Basin, Posidonia Shale in the Hils Syncline	North German Basin, Molasse Basin, Saar-Nahe Basin, Hamburg Embayment, Thuringian Basin	Horsefield et al. (2010); Scheeder et al. (2023)
Spain	Onshore Cantabrian basin	Basque-Cantabrian Basin, Ebro basin	Valencia Trough, Central Iberian Zone	Maillard et al. (1992); Abeger et al. (2003);
Lithuania/ Kaliningrad	Not yet explored	Baltic basin	Baltic basin	Sliaupa et al. (2016); Ma et al. (2017)
Australia	Cooper Basin	Surat basin, Maryborough basin,	Canning Basin, Adavale Basin	Hichton and Hays (1971); Ruth et al. (2004); O'Leary et al. (2008), Faiz et al. (2020)

(*continued on next page*)

Table 4 (*continued*)

Country	Shale plays/Formations			References
	Established	Potential	Speculative	
		Gunnedah basin, Bonaparte basin, Canterbury basin, Galilee Basin, Isa Superbasin, Bowen Basin, Adelaide Rift, Bass Basin, Carnarvon basin, Browse Basin, Beetaloo basin, Georgina basin, Mcarthur Basin		

The Roseneath Shale, Elipson Shale and Murteree Shale units of the Cooper Basin are known as REM with gross pay of 300 ft (91.44 m) in the gas and 150 ft (45.72 m) in the oil reserve area. The Roseneath shale of Cooper basin os 120–330 ft (36.58–100.58 m) thick in the Nappamerri Trough. The low permeable Elipson is the fluvial-deltaic deposit and the dark Murteree Shale is a lacustrine deposition during a tectonically quiet period. It contains the highest volume of dispersed organic matter with ~ TOC of 2.5 %, and vitrinite reflectance of 0.3–4 % across the Cooper Basin (Stuart, 1976; Thornton, 1979; Smyth 1983; Apak et al., 1997; USA EIA, 2013; Bazunu et al., 2015). The Murteree shale and Roseneath shale have 30.5 % and 39 % porosity, respectively (Ahmad, 2014). It is 150–250 ft (45.72–76.2 m) thick in the Nappamerri Trough. The REM source rocks are Type III kerogen. These source rocks have lower thickness in the Patchwara and Tenappera troughs (Pokalai et al., 2015; Iqbal et al., 2017). The shales are rich in paraffin and generate medium to light gravity oil. It is mineralogically composed of quartz and feldspar (50 %), carbonate, mainly iron-rich siderite (30 %) and clay [predominantly illite (20 %)] ranging from 25 % to 48 % (Bazunu et al., 2015). REM rock units are oil-prone with R_O between 0.7 % and 1.0 % and gas-prone with $R_O > 1.3$ % in the deeper sections of Nappamerri and Patchwara troughs. The Nappamerri records a high-geothermal gradient [3.42 °F at 100 ft ((= 0.52 ^{0}C m^{-1}))] due to the presence of radioactive granite basement and overpressured regional hydrostatic pressure gradient (0.7 psi foot^{-1}) at 9,000-12,000 ft (2, 743.2-3657.6 m) depth.

The hydrocarbon-rich shale deposits in the basin is characterized by a minimum depth and a thickness of 6500 ft (1981.2 m) and 50 ft (15.24 m), respectvelty, with vitrinite reflectance < 1.0 % and porosity ranging from 0.93 % to 4.78 % in the electron microscope. It has an estimated shale dry and wet gas potential of 88–100 Bcf mi^{-2} in the Nappamerri and 16–19 Bcf mi^{-2} in Patchwarra trough (Bazunu et al., 2015). The Tenappara trough has an oil concentration of 22 MM bbl mi^{-2} (USA EIA, 2013).

The source rock characteristics and carbon capture in the basin are significantly influenced by periodic glaciation and upwelling of the Panthalassan ocean water. Water circulation brought rich marine flora and fauna that took part in the development of Permian Sydney, Bowmen and Nappamerrie shale strata (Ahmad, 2014).

5. Synthesis: Worldwide assessment on organic-rich black shale

Global black shale deposition [oceanic anoxic event 1a (OAE1)] during the Lower Cretaceous has been associated with methane hydrate dissociation and extensive igneous area volcanism (Arthur, 1979; Hernendez et al., 2014). One of the most important outcomes of the global driving mechanisms throughout the Cretaceous is the global deposition of sediments with varying carbonate contents. These sediments have been connected to anoxia (OAE1) and extreme oxygen shortage conditions in the ocean (Schlanger and Jenkyns, 1976). Depending on the physiography and the severity of the global driving factors, organic-rich marine deposits accumulated under oxygen-depleted environments across a variety of time periods and to varying degrees.

Black shale as an economic hydrocarbon source rock is found in diverse terrains. According to USA EIA (2013), there are 63 prospective shale gas and 44 shale oil formations composed of black shales amongst 156 shale formations in 21 countries worldwide for commercial shale gas and shale oil exploration (Table 3). Repository File 2 presents compilation of global data. Asia includes four countries- China, India, Kazakhstan, and Indonesia, and with 12 basins containing black shales. The Silurian marine deposited Longmaxi Formation of the Sichuan Basin (China) with TOC of 3.2 % and Ro of 2.9 % has got 1146.1 Tcf of risked in-place shale gas and 286.5 Tcf of risked recoverable shale gas resource in Asia. The lacustrine Cretaceous Qingshankou Formation of the Songliao Basin (China) produces the highest risked recoverable shale oil (11.46 Bbl) and risked shale oil in-place (229.2 B bbl) in Asia. Shale in this basin consists of TOC of 4 % and Ro of 0.9 %.

Table 5
a. The countries leading risked shale gas in-place and risked recoverable shale gas shale Formations in respective continents [Source: EIA ARI World shale gas and shale oil assessment, 2013 (attachment C and D) and 2014]. **b.** The countries leading risked shale oil in-place and risked recoverable shale oil shale Formations in respective continents (Data source: ARI, 2013 and 2014).

Continent	Country	Basin	Formation	Geological Period	Depositional environment	Prospective area (mi^2)	TOC (in %)	Ro (in %)	Risked In-place (Tcf)	Risked Recoverable (Tcf)
Asia	China	Sichuan	Longmaxi	Lower Silurian	Marine	10070	3.2	2.9	1146.1	286.5
Africa	South Africa	Karoo	Whitehill	Lower Permian	Marine	60180	6	3	845.4	211.3
North America	Mexico	Sabinas	Eagle Ford Shale	Middle – Upper Cretaceous	Marine	9500	4	1.5	501	100.2
South America	Argentina	Neuquen	Vaca Muerta	Upper Jurassic – Lower Cretaceous	Marine	11660	5	1.17	1201.9	307.7
Europe	Poland	Baltic/ Warsaw	Llandovery	Late Silurian- Ordovician- Upper Cambrian	Marine	8580	3.9	1.27	532.1	105.2
Oceania	Australia	Canning	Goldwyer	Middle Ordovician	Marine	57380	3	1.13	1227.2	235.4

Continent	Country	Basin	Formation	Geological period	Depositional environment	Prospective area (mi^2)	TOC (in %)	Ro (in %)	Risked In-place (B bbl)	Risked Recoverable (B bbl)
Asia	China	Songliao	Qingshankou	Cretaceous	Lacustrine	6900	4	0.9	229.2	11.46
Africa	Egypt	Abu Garadig	Khataba	Middle Jurassic	Marine	6840	4	1.15	47.1	1.88
South America	Venezuela/ Colombia	Maracaibo/ Catatumbo	La Luna/ Capacho	Upper Cretaceous	Marine	11570	5	1	296.7	14.83
	Argentina	Neuquen	Vaca Muerta	Upper Jurassic – Lower Cretaceous	Marine	8110	5	1	270.4	16.22
Europe	Paris	Lias Shale	L. Jurassic	Late Jurassic	Marine	5670	9	1.2	38	1.52
Oceania	Australia	Canning	Goldwyer	Middle Ordovician	Marine	34520	3	1	243.7	9.75

Egypt, Libya and South Africa in Africa have six potential basins with black shale formations. Among them, the Whitehill Formation of Karoo Basin (South Africa) consists of both risked shale gas in-place and recoverable shale gas. The Abu Garadig Formation of Egypt has the highest risked shale in-place and recoverable shale oil in the continent. Table 4

The Eagle Ford Shale Formation of Mexico, the Vaca Muerta Formation of Argentina, the Llandovery Formation of Poland and the Goldwyer Formation of Australia have the highest risked shale gas in-place and risked recoverable shale gas in North America, South America, Europe, and Oceania, respectively. Table 5 a and b present the highest shale oil and gas producing black shale Formations in the respective continent. Only North America does not have shale oil resources from black shale Formations in the continent. Their TOC ranges from 3 % to 6 % (in shale gas) and 3–9 % (in shale oil) in the prospective areas. The Ro ranges from 1.13 % to 3 % (in shale gas) and 0.9–1.15 % (in shale oil) in the prospective areas. The prospective hydrocarbon content lies within an average depth from 3,300-16,500 ft (1,005.84-5029.2 m) (Fig. 6a-c).

The Solimoes Basin (Jandiatuba Formation) of Brazil has the highest prospective area for shale gas (66,490 mi^2) and shale oil (43,650 mi^2) with 64.6 Tcf and 0.28 B bblof risked recoverable shale gas and oil, respectively. It is followed by the Amazonas basin (63,310 mi^2) of Brazil, and the Sabinas basin (60,180 mi^2) of Mexico (Fig. 6b). The Tournaisian, Radaevskiy-Kosvinkskiy Formation of North Caspian Basin (Kazakhstan) has the least shale gas (360 mi^2) and shale oil (260 mi^2) prospective areas with 2.3 Tcf and 0.06 B bbl of risked recoverable shale gas and oil, respectively, when compared globally.

The black shale in South America has the highest production of risked recoverable shale resources. The average TOC of the black shales in South America lies between 2 % and 5 % and Ro between 1 % and 1.34 %. The Tannezuft Formation of Murzuq Basin (Libya) measures a maximum average TOC of 7 % with 18.6 Tcf of risked shale gas and 26.9 B bbl of shale oil in-place. The Wufeng Formation of the Greater Subei Basin (China) measures the least TOC of 1.1 % on an average with 143.9 Tcf of risked shale gas and 4.5 B bbl of shale oil in-place. The Qiongzhusi Formation of the Sichuan Basin (China) has the highest average Ro of 3.2 % with 499.6 Tcf of risked shale gas in-place. The least Ro of 0.8 % is measured in Brown Shale of Central Sumatra, Indonesia and Visean Formation of the North Caspian (SE Basin), Kazakhstan with 41.5 Tcf and 116.3 Tcf of risked shale gas in-place. The basins measure 69.4 B bbl and 125.3 B bbl of risked shale oil in-place, respectively.

The marine deposited Vaca Muerta Formation of Neuquen Basin (Argentina) of South America with an average depth ranging from 3,000-10,000 ft (914.4–3048 m) and net organic-rich thickness of 325 ft (99.06 m) has the highest hydrocarbon reservoir in the world. It has an average TOC of 5 % and Ro between 1 % and 1.5 %. Whereas, the 14,500–16,400 ft (4,419.6-4988.72 m) deep marine Tournaisian, Radaevskiy-Kosvinkskiy Formation of North Caspian Basin (Kazakhstan) with a net organic-rich shale thickness of 225 ft (68.58 m) has the lowest hydrocarbon reservoir of black shales as source rocks in the entire world. They estimated 1201.9 Tcf of risked shale gas and 270.4 B bbl of risked shale oil in-place and 14.1 Tcf of risked shale gas and 1.3 B bbl of risked shale oil in-place, respectively. The Vaca Muerta Formation has the highest risked recoverable shale oil (16.22 B bbl) and (307.7 Tcf) shale gas in-place (Fig. 6a-c).

Applying the entropy method on both recoverable shale oil and shale gas for the hydrocarbon producing 44 basins with black shale, we find that the Ponta Grossa Formation of Parana basin (Argentina) has the highest weighted vector (0.0368). This is followed by the Solimoes basin (Brazil), Jianghan and Greater Subei basins (China) and the Amazonaz basin (Brazil) (Table 6a). These five basins amongst the 44 shale oil and shale gas explorable basins with black shale formations is significant in terms of the recoverable resource. Table 4 represents all the commercial, potential and speculative shale basins of the world including black shale plays/basins/formations.

6. Conclusions

Shale is an important source rock for unconventional gas exploration. We study the worldwide distribution of oil shale basins with a focus on various key parameters (TOC, Ro, HI, T_{max}, depth, thickness,

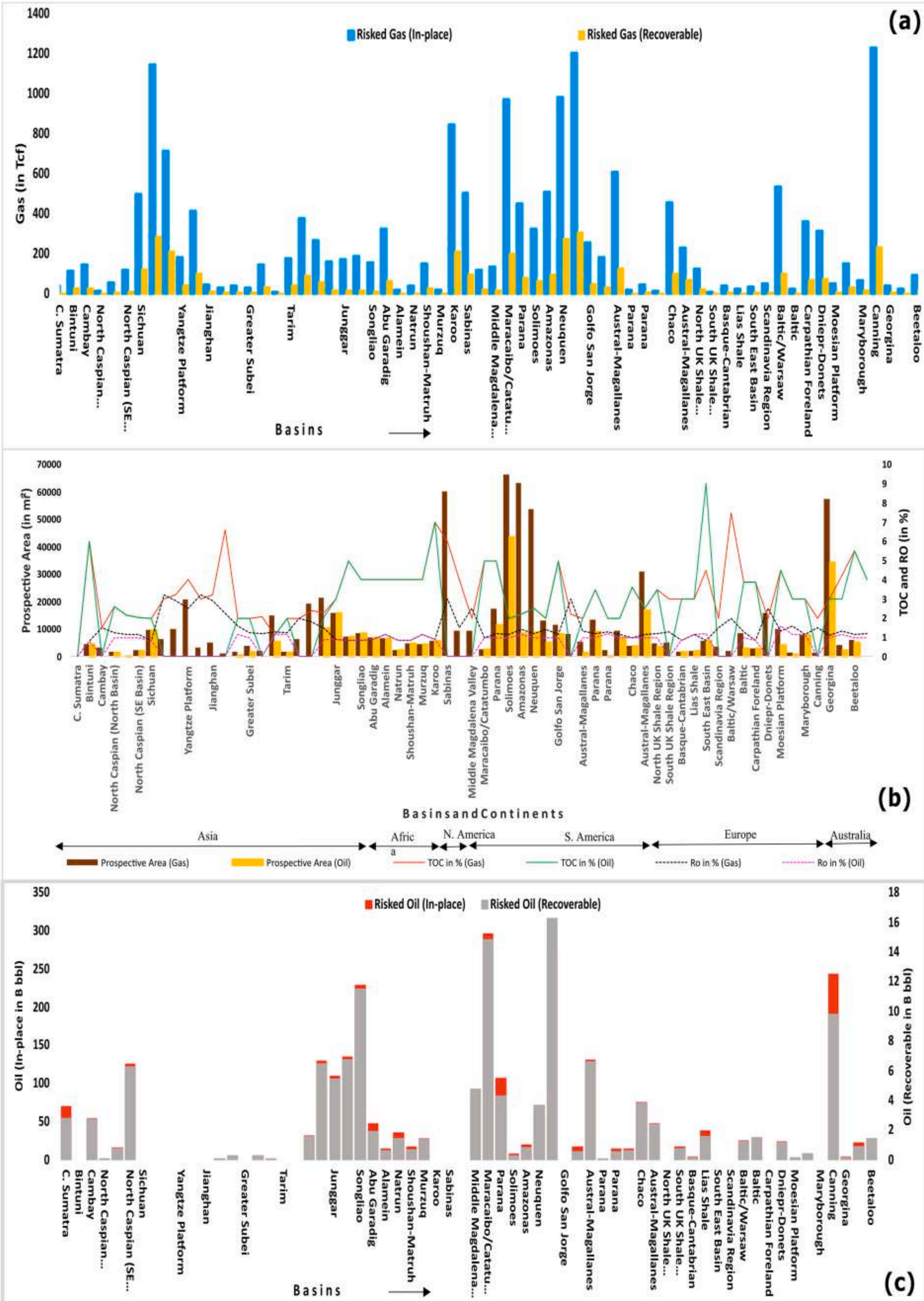

Fig. 6. a. Global risked shale gas In-place and risked recoverable of Resources (Tcf) from black shale. **b.** Graphical representation of the world black shale basin prospective area with respective TOC and Ro content. **c.** Global risked In-place and recoverable shale Oil Resources (B bbl) from black shale (Data Source: USA EIA, 2013).

Table 6
a. Weighted vector derived from the entropy method for the explored world black shale formations potential in producing both shale oil and shale gas.

Continent	Country	Basin	Formation	Weight vector
South America	Argentina	Parana	Ponta Grossa	0.036802
Africa	Brazil	Solimoes	Jandiatuba	0.036435
Asia	China	Jianghan	Longmaxi	0.035916
Asia	China	Greater Subei	Wufeng/ Gaobiajian	0.035852
South America	Brazil	Amazonas	Barreirinha	0.035473

Continent	Country	Basin	Formation	Weight vector
Africa	Algeria	Ghadames/Berkine	Tannezuft	0.009604956
Africa	Algeria	Tinduof	Tannezuft	0.009602743
Africa	Algeria	Reggane	Frasnian	0.009572347
Africa	Tunisia	Ghadames	Tannezuft	0.009514972
South America	Brazil	Solimoes	Jandiatuba	0.009471349

geological and sediment depositional setting) along with their natural geologic carbon sequestration history. The different qualitative and quantitative measures of shale are associated with geologic time scale, with the spatial distribution of shale as the major hydrocarbon source rock and thieir physio-chemical properties.

Hydrocarbon-rich shales deposited from the Cambrian to the Cretaceous Period. The Ro of hydrocarbon basins increases with depth. The highest thermal maturity is observed in the dry gas windows. Most of the potential hydrocarbon reservoir discussed in this work has high Ro in the basin centre. Asymmetric synclinal Algerian Reggane Basin is an exception where the Ro increases from the shallow southern portion to the deep northern part of the basin. The matured hydrocarbon for exploration is found at a depth ranging from 3,280-16,500 ft (999.74–5029.2 m) (e.g., Perth, Canning, Betaloo Basin in Australia; Middle Magdalena Valley, Solimoes Basins of South America; Vaca Muerta Formation of Neuquen Basin in Argentina). The thickness of the net organic-rich shale ranges between 54 and 500 ft (16.46–152.4 m), worldwide. Cases of thin shales such as those within the Stassfurth Carbonate of the Upper Permian Period in Lower Saxony Basin (Germany) are not included in resource assessment. The Devonian Los Monos Formation of Chaco Basin (SE Bolivia and NW Paraguay, South America) contains exceptionally thick organic-rich shale deposits of ∼ 2000 ft (609.6 m).

The Bazhenov Central Formation of the West Siberian Basin (Russia) has the largest sedimentary basin covering a hydrocarbon rich shale potential area of 300957 km^2 (1,16,200 mi^2 in the world. It has an average TOC of 10 % and Ro of 0.85 % with the world's highest risked recoverable shale oil (57.89 B bbl) and risked shale oil in-place (964.8 B bbl). The large gentle uplifted anticlines formed related to the N-S trending faults during the Triassic Period and acted as structural hydrocarbon traps/pools. The basin leads the hydrocarbon reservior of the world in quantity. The Goldwyer Shale of the Canning Basin (Australia) has the highest risked shale gas (1227.2 Tcf) in-place. Here only 235.4 Tcf of the gas is recoverable. Argentina has the world's most shale gas and oil potential reservoir. The Vaca Muerta Formation of the Neuquen Basin (Argentina) estimates the world's highest risked recoverable shale gas (307.7 Tcf) from 1201.9 Tcf risked shale in-place. The Tenappera Formation of the Cooper Basin (Australia) is the least hydrocarbon prospective reservoir in the world. This is because it has the lowest (1.2 Tcf) amount of risked shale gas in-place and only 0.1 Tcf of risked recoverable shale gas with an average TOC of 2.6 % and Ro of 0.85 %. Table 5b presents the Ghadames, Tinduof, Reggane and Ghadames basins (Africa), and Solimoes basin (South America) presents the highest significant basins contributing recoverable shale oil and shale gas when all basins are compared worldwide.

With increasing global warming and demand for unconventional shale oil and gas, injection and sealing of CO_2 in depleted potential hydrocarbon reservoirs have attracted and researchers around the globe besides the natural geologic carbon sequestration in shales. The complexity of the geology, technical difficulties, political climate, regulatory issues, environmental concerns and technological advancements, however, prevent the commercialization of all the viable shale basins for unconventional resources.

CRediT authorship contribution statement

Paul Ankita: Writing – review & editing, Writing – original draft. **Mukherjee Soumyajit:** Writing – review & editing, Writing – original draft, Conceptualization. **Biswas Mery:** Writing – review & editing, Supervision.

Declaration of Competing Interest

We have no conflict of interest with anybody regarding this manuscript.

Acknowledgements

CPDA (IIT Bombay) grant supported SM. We apologize if we missed relevant references, it was unintentional. An anonymous reviewer and the Chief Editor Mimmo Palano are thanked for providing detail comments.

Appendix

Abbreviations

AI	Acoustic impedance
AVO	Amplitude vs. offset
Bbl	Billion barrels
Bcf	Billion cubic feet
Bcm	Billion cubic metres
BI	Brittleness index
CFB	Cape Fold Belt
CO_2	Carbon dioxide
DDB	Dniepr-Donets Basin
EEC	East European Craton
EDS	Energy dispersive X-Ray
ENE	East North East
EUOGA	European Unconventional Oil and Gas Assessment
F	Fahrenheit
ft	feet
FTIR	Fourier transform infrared spectroscopy
HC	hydrocarbon
HI	Hydrogen Index
ICF	International Cablemakers Federation
IGAS	L'Inspection générale des affaires sociales
km	kilometre
m	metre
Ma	Million years ago, or megaanni
mg	milligram
mi^2	square mile
mm	millimetre
nm	nanometre
NW	Northwest
O-C	Organic-Carbon
OI	Oxygen Index
PSC	The UK People with Significant Control
psi	Pressure gradient
R_o	Vitrinite reflectance
SE	Southeast
SEM	Scanning electron microscopy
Tcf	Trillion cubic feet

Tmax	the temperature at which the maximum release of hydrocarbons occurs during pyrolysis while cracking of kerogen.
TOC	Total Organic Carbonic
USA EIA	United States Energy Information Administration
WSW	West South West
XCT	X-ray computed tomography
XRD	X-ray power diffraction
XRF	X-ray fluorescence

Appendix A. Supporting information

Supplementary data associated with this article can be found in the online version at doi:10.1016/j.rines.2025.100088.

Data availability

Data will be made available on request.

References

Abdulbaset, M.A., Jan-Diederik, W., Paul, M.D., Sierd, A.P.L.C., 2008. Tectonics and subsidence evolution b of the Sirt Basin, Libya. AAPG Bull. 92, 993–1027.

Abuov, Y., Seisenbayev, N., Lee, W., 2020. CO2 storage potential in sedimentary basins of Kazakhstan. Int. J. Greenh. Gas. Control 103, 103186.

Acheche, M.H., M'Rabet, A., Ghariani, H., Ouahchi, A., Montgomery, S.L., 2001. Ghadames basin, southern Tunisia: A reappraisal of Triassic reservoirs and future prospectivity (E & P Notes). AAPG Bull. 85, 765–780.

ACOLA (2013) Engineering energy: Unconventional gas production. Australian Council of Learned Academies URL: 〈http://www.acola.org.au/PDF/SAF06FINAL/Final%20Report%20Engineering%20Energy%20〉 June%202013.pdf.

Aguilera, R., 2016. Shale gas reservoirs: Theoretical, practical and research issues. Pet. Res. 1, 10–26.

Ahmad, N., 2014. Petrophysical and mineralogical evaluation of shale gas reservoirs: a Cooper Basin case study. Thesis(Ph.D.) – University of Adelaide. Australian School of Petroleum.

Ahmad, N., Mateen, J., Chaudry, K.S., Mehmood, N., Arif, F., 2013. Shale Gas Potential of Lower Cretaceous Sembar Formation in Middle and Lower Indus Basin, Pakistan. Pak. J. Hydrocarb. Res. 23, 51–62.

Ahmed, U., Meehan, D.N., 2016. Characterists of Unconventional Oil and Gas Resources. In: Ahmed, U., Meehan, D.N. (Eds.), Unconventional Oil and Gas Resources Exploration and Development. CRC Press, 3-1 to 3-17. ISBN-13: 978-1-4987-5941-0.

Aissaoui, M.N., Bédir, M., Gabtni, H., 2016. Petroleum assessment of Berkine–Ghadames Basin, southern Tunisia. AAPG Bull. 100, 445–476.

Al-Anboori, A., Kendall, J.M., Johnston, D.H., 2010. Passive seismic monitoring of reservoirs: A case study from Oman. In: Johnston, D.H., et al. (Eds.), Methods and Applications in Reservoir Geophysics. Spciety of Exploration Geophysicists, pp. 441–450. ISBN 978-0-931830-46-4.

Alcalde, J., Martí, D., Juhlin, C., Malehmir, A., Sopher, D., Saura, E., Carbonell, R., 2013. 3-D reflection seismic imaging of the Hontomín structure in the Basque–Cantabrian Basin (Spain). Solid Earth 4, 481–496.

Alexander, T., Baihly, J., Boyer, C., Clark, B., Jochen, V., Calvez, J.L., Lewis, R., Miller, C. K., Thaeler, J., Toelle, B.E., 2011. Shale Gas Revolution, Oilfield Review. Schlumberger, USA.

Ali, A., Salman, M., Ahmad, R., 2021. Smectite illitization of the Talhar shale, Lower Goru Formation, Southern Indus Basin, Pakistan. J. Pet. Explor Prod. Technol. 11, 2315–2325.

Al-Kindi, M.H., Richard, P.D., 2014. The main structural styles of the hydrocarbon reservoirs in Oman. In: Rollinson, H.R., Searle, M.P., Abbasi, I.A., Al-Lazki, A., Al Kindi, M.H. (Eds.), Tectonic Evolution of the Oman Mountains, 392. Special Publications, Geological Society, London, pp. 409–445.

Allaby, M., 2013. A Dictionary of Geology and Earth Science, 69. Oxford University Press, p. 527.

Allen, P.A., 2007. The Huqf Supergroup of Oman: Basin development and context for Neoproterozoic glaciation. Earth-Sci. Rev. 84, 139–185.

Allen, P.A., Allen, J.R., 2013. Basin Analysis. Published by John Wiley and Sons, Ltd, Printed in Malaysia. ISBN 978-0-470-67376-8.

Almadhone, A.A., Gruenwald, R.M., Rodriguez, A.M., 2011. Tawengi, K. S. Review of the Elements of the Northern Kufra Basin Petroleum System. SE Libya. 5th North Afr. Mediterr. Pet. Geosci. Conf. Exhib. Tripoli, Libya.

Al-Suwaidi, A.S., Taher, A.K., Alsharhan, A.S., Salah, M.G., 2000. Stratigraphy and Geochemistry of Upper Jurassic Diyab Formation, Abu Dhabi, UAE. In: Alsharhan, A. S., Scott, R.W. (Eds.), Middle East Models of Jurassic/Cretaceous Carbonate Systems, 69. Society of Sedimentary Geology (SEPM) Special Publication, pp. 249–271. ISBN 1-56576-075.

Ambrose, W.A., Wawrzyniec, T.F., Fouad, K., Sakurai, S., Jennette, D.C., Brown, L.F., Guevara, E.H., Dunlap, D.B., Talukdar, S.C., Garcia, M.A., Romano, U.H., Vega, J.A., Zamora, E.M., Ruiz, H.R., Hernández, R.C., 2005. Neogene tectonic, stratigraphic, and play framework of the southern Laguna Madre–Tuxpan continental shelf, Gulf of Mexico. AAPG Bull. 89, 725–751.

Amthor, J.E., Ramseyer, K., Faulkner, T., Lucas, P., 2005. Stratigraphy and sedimentology of a chert reservoir at the Precambrian-Cambrian Boundary: The Al Shomou Silicilyte, South Oman Salt Basin. GeoArabia 10, 89–122.

Andrews, A., Folger, P., Humphries, M., Copeland, C., Tiemann, M., Meltz, R., Brougher, C., 2009. Unconventional Gas Shales: Development, Technology, and Policy issues. CRS Rep. Congr., Congr. Res. Serv. 1–12.

Andrews, I.J., 2014. The Jurassic Shales of the Weald Basin: Geology and Shale Oil and Shale Gas Resource Estimation. British Geological Survey for Department of Energy and Climate Change, London, UK.

Antunano, S.E., 2001. The Western Gulf of Mexico Basin: Tectonics, Sedimentary Basins, and Petroleum Systems. In: Bartolini C., Buffler R.T., Cantú-Chapa A. (Eds) The American Association of Petroleum Geologists 75, 241-270..

Apak, S.N., Stuart, W.J., Lemon, N.M., Wood, G., 1997. Structural Evolution of the Permian–Triassic Cooper Basin, Australia: Relation to Hydrocarbon Trap Styles. Am. Assoc. Pet. Geol., Bull. 81, 533–555.

Arabadzhi, M.S., Bezborodov, R.S., Bukharov, A.V., et. al, 1993. Prediction of Petroleum Potential of the Southeastern North Caspian Basin (Prognoz neftegazonosnosti yugo-vostoka Prikaspiyskoy sineklizy): Moscow, Nedra, 160 p.

Arfaoui, I., 2024. Assessment of Unconventional Reservoirs Potential in Tunisia: A Multidisciplinary Study of Silurian Hot shales and Ypresian limestones Source Rocks. URL: file:///C:/Users/Prof%20S%20Mukherjee/Downloads/Comit%C3%A9_de_th%C3%A8se-pr%C3%A9sentation-2024.pdf (Accessed on 12-Jan-2025).

Armitage, P.J., Worden, R.H., Faulkner, D.R., Aplin, A.C., Butcher, A.R., Iliffe, J., 2010. Diagenetic and sedimentary controls on porosity in Lower Carboniferous fine-grained lithologies, Krechba field, Algeria: A petrological study of a caprock to a carbon capture site. Mar. Pet. Geol. 27, 1395–1410.

Armstrong, H., Abbott, G., Turner, B., Makhlouf, I., Muhammad, A., Pedentchouk, N., Peters, H., 2009. Black shale deposition in an Upper Ordovician–Silurian permanently stratified, peri-glacial basin, southern Jordan. Palaeogeogr., Palaeoclimatol., Palaeoecol. 273, 368–377.

Armstrong, H.A., Turner, B.R., Makhlouf, I.M., Weedon, G.P., Williams, M., Smadi, A.A., Salah, A.A., 2005. Origin, Sequence Stratigraphy and Depositional Environment of an Upper Ordovician (Hirnantian) Deglacial Black Shale, Jordan. Elsevier, Paleogeography, Paleoclimatology, Paleoecol. 220, 273–289.

Arthur, M.A., 1979. North Atlantic Cretaceous Black Shales: The Record at Site 398 and a brief comparison with other occurrences. In: Sibuet, J.-C., Ryan, W.B.F., et al. (Eds.), Initial Reports of the Deep Sea Drilling Project, v. 47. Part 2: Washington (U.S. Government Printing Office), pp. 451–468.

Asef, M.R., Farrokhrouz, M., 2013. Shale engineering: Mechanics and mechanisms. Boca Raton, Fla: CRC. ISBN: 9780415874199.

Asghar, H., Khan, M.S., Abbas, S., Hussain, G., Ahmed, W., Ali, A., Ali, M., Hassnain, M., 2021. Geochemical Investigation of The Early Eocene Laki Formation Shales in The Selected Regions of Southern Indus Basin Pakistan. Earth Sci. Malays. 5, 27–32.

Asghar, H., Abbas, S., Khan, M.S., Jahandad, S., Hanif, M., Mughal, M.S., Hussain, G., 2022. Organic geochemistry and mineralogical characterization of the Paleocene Ranikot Formation shales in selected areas of Southern Indus Basin Pakistan. Kuwait J. Sci. 49, 1–20.

Aybar, U., Eshkalak, M.O., Wood, D.A., 2015. Advances in practical shale assessment techniques. J. Nat. Gas. Sci. Eng. 27, 399–401.

Aydmir, A., 2010. Potential Unconventional Reservoirs in Different Basins of Turkey. Presented at the AAPG European Region Annual Conference. Kiev, Ukraine. October 17.

Aziz, A., 2000. Stratigraphy and Hydrocarbon Potential of the Lower Paleozoic Succession of License NC-115, Murzuq Basin, SW Libya. Geological Exploration in Murzuq Basin, Chapter 16. Elsevier Science B.V., pp. 349–368

Aziz, O., Hussain, T., Ullah, M., Bhatti, A., S, Ali, A., 2018. Seismic based characterization of total organic content from the marine Sembar shale, Lower Indus Basin, Pakistan. Mar. Geophys. Res. 39, 491–508.

Ba Geri, Mohammed, Ellafi, A., Flori, R., Belhaij, A., Alkamil, E.H.K., 2019. New Opportunities and Challenges to Discover and Develop Unconventional Plays in the Middle East and North Africa. Crit. Rev. https://doi.org/10.2118/197271-MS.

Bahesti, F., Subroto, E.A., Manaf, N.A., & Sadirsan, W., 2014. Integrated Basin Analysis and Geomechanics Study of Lower Baong Shale for Preliminary Shale Gas Prospectivity in the North Sumatra Basin.

Baig, M.Z., Van Laer, P., Leyrer, K., Makrachev, G., Al Marzooqi, H., Al Suwaidi, S., Raina, I., Dasgupta, S., 2017. Assessing Reservoir Quality of the Diyab Source Rock in UAE. Paper presented at the Abu Dhabi International Petroleum Exhibition & Conference. Abu Dhabi, UAE. https://doi.org/10.2118/188433-MS.

Bailey, A.H.E., Jarrett, A.J.M., Tenthorey, E., Henson, P.A., 2021. Understanding present-day stress in the onshore Canning Basin of Western Australia. Aust. J. Earth Sci. 68, 1–18.

Bakshi, T., Vishal, V., Prusty, B.K., Pathak, K., 2020. Carbon dioxide and methane sorption characteristics of Damodar Valley and Upper Assam shale, India. Energy Clim. Change 1, 100002.

Balen, R.T.V., et al., 2000. Modelling the hydrocarbon generation and migration in the West Netherlands Basin, the Netherlands. Geol. En. Mijnb. / Neth. J. Geosci. 79 (1), 29–44.

Balushkina, N.S., Kalmykov, G.A., 2016. Cavity structure in oil-saturated Bazhenov and Abalak shale rock in the Western Siberian basin. Mosc. Univ. Geol. Bull. 71, 71–80. https://doi.org/10.3103/S0145875215050026.

Banerjee, A., Jha, M., Mittal, A., Thomas, N., Misra, K., 2000. The effective source rocks in the north Cambay Basin, India. Mar. Pet. Geol. 17 (10), 1111–1129. https://doi.org/10.1016/s0264-8172(00)00049-0.

Barredo, S., Stinco, L., 2013. A Geodynamic View of Oil and Gas Resources Associated to the Unconventional Shale Reservoirs of Argentina, 12-14 August 2013 Unconv. Resour. Technol. Conf., Denver, Colo.. https://doi.org/10.1190/urtec2013-087.

Baruah, B., Tiwari, P., Thakur, P., Kataki, R., 2018. TGA-FTIR analysis of upper assam oil shale, optimization of lab-scale pyrolysis process parameters using RSM. J. Anal. Appl. Pyrolysis 135, 397–405.
Bashir, A., et al., 2024. Comprehensive review of CO_2 geological storage: Exploring principles, mechanisms, and prospects. Earth-Sci. Rev. 249, 104672.
Bates, R.L., Jackson, J.A., 1980. Glossary of Geology. In: Second Edition, 433. American Geological Institute, Leesburg, pp. 573–574.
Bayramoglu, T., Ari, Y.O., 2015. Global Economic Observer. pp. 5. ISSN 2343 – 9742.
Bazunu, G., Rahman, Sheik S., Zhou, F.D., Wang, L., 2015. Geomechanical Characterization of Shale Gas Reservoir Rocks for Design and Planning of Stimulation Treatment: A Cooper Basin Case Study. doi:10.15530/urtec-2015-2152935.
Bealessio, B.A., Blánquez Alonso, N.A., Mendes, N.J., Sande, A.V., Hascakir, B., 2020. A review of enhanced oil recovery (EOR) methods applied in Kazakhstan. Petroleum 7, 1–9.
Beckmann, B., Flögel, S., Hofmann, P., Schulz, M., Wagner, T., 2005a. Orbital forcing of Cretaceous river discharge in tropical Africa and ocean response. Nature 437, 241–244.
Behar, F., Vandenbrouke, M., 1987. Chemical modelling of kerogens. Org. Geochem 11, 15–24.
Belaid, A., Krooss, B.M., Littke, R., 2010. Thermal history and source rock characterization of a Paleozoic section in the Awbari Trough, Murzuq Basin, SW Libya. Mar. Pet. Geol. 27, 612–632.
Belhameche, F., Saadallah, N., 2007. Hydrocarbons Potential of the Tindouf Basin (Algeria). SONATRACH EXPLORATION, Boumerdes, Algeria. AAPG Search and Discovery Article #90072, American Association of PetroleumGeologists. European Region Conference, Athens, Greece.
Belotti, H., Pagan, F., Mazas, A.Perez, Agüera, M., Rodriguez, J., Porras, J., Köhler, G., Weiner, G., Conforto, G., Cagnolatti. M., 2013.Geologic Interpretation and Assessment of Early Cretaceous Shale Oil and Gas Potential in Austral Basin, Santa Cruz. doi: https://doi.org/10.1190/urtec2013-094.
Bergen, F.V., Zijp, M., Nelskamp, S., Kombrink, H., 2013. Shale Gas Evaluation of the Early Jurassic Posidonia Shale Formation and the Carboniferous Epen Formation in the Netherlands. Critical Assessment of Shale Resource Plays. Memoir 103, AAPG Special Volumes, pp. 1–24.
Berry, J.L., Nishidai, T., 1988. Hydrocarbon potential of part of the margin of the Tarim Basin from Landsat: a case history. Proc. 6th Themat. Coi2f: Remote Sens. Explor. Houst. Tex. 1, 49–64.
Bhandari, L.L., Chowdhary, R., 1975. Stratigraphic Analysis of Kadi and Kalol Formations, Cambay Basin, India. AAPG Bull. 59, 856–871.
Bharktya, D.K., Bhaskaran, B., Goswami, P., Nagaraj, M., Satyanarayana, K., 2008. Deep water sedimentary processes with special reference to bottom currentreworking for Eocene sediments in Nagapattinam (North) sub basin. In: Kapoor, P.N. (Ed.), CauveryBasin, 3. Association of Petroleum Geologists Bulletin, pp. 145–156.
Bian, W., Hornung, J., Liu, Z., et al., 2010. Sedimentary and palaeoenvironmental evolution of the Junggar Basin, Xinjiang, Northwest China. Palaeobio Palaeoenv 90, 175–186.
Biswas, M., Raha, A., Mukherjee, S., Kotak, V.S., 2024. Geomorphic Imprints of Active Tectonics of the Bikaner-Nagaur Petroliferous Rift Basin and its Surroundings (western Rajasthan, India). J. Geol. Soc. India 100, 377–390.
Biswas, S.K., Ariketi, R., Dubey, R., Chandra, S., 2013. Shale Gas Evaluation of Cambay Shale Formation in Tarapur Syncline, Cambay Basin, India – A Seismo-geological approach. 10th Biennial International Conference & Exposition, Kochi, pp. 1–4.
Boak, J., Kleinberg, R., 2020. 4-Shale Gas, Tight Oil, Shale Oil and Hydraulic Fracturing, Editor(s): Trevor M. Letcher. Future Energy (Third Edition). Elsevier, pp. 67–95. https://doi.org/10.1016/B978-0-08-102886-5.00004-9.
Boboye, O.A., Abimbola, A.F., 2009. Hydrocarbon Potential of the Lithostratigraphic Units in Late Cenomanian-Early Paleocene Shale, Southwestern Chad Basin. Southwest. Chad Basin. J. World Appl. Sci. 7.
Boggs, S.J.R., 2016. Principles of Sedimentlogy& Stratigraphy, 5th Edition. Pearson Education India. ISBN-13978933257095.
Boosari, S., Aybar, U., Eshkalak, M., 2015. Carbon Dioxide Storage and Sequestration in Unconventional Shale Reservoirs. J. Geosci. Environ. Prot. 3 7–15.
Boote, D.R.D., Clark-Lowes, D.D., Traut, M.W., 1998. Palaeozoic Petroleum Systems of North Africa. In: Macgregor, D.S., Moody, R.T.J., Clark-Lowes, D.D. (Eds.), Petroleum Geology of North Africa. Geological Society, 132. Special Publication, London, pp. 7–68.
Bose, P.K., Sarkar, S., Chakrabarty, S., Banerjee, S., 2001. Overview of the Meso-to Neoproterozoic evolution of the Vindhyan basin, central India. Sediment. Geol. 141, 395–419.
Botor, D., Kotarba, M., Kosakowski, P., 2002. Petroleum generation in the Carboniferous strata of the Lublin Trough (Poland): an integrated geochemical and numerical modelling approach. Org. Geochem. 33, 461–476.
Boudjema, A., 1987. Evolution structurale du bassin pe´trolier Triasique du Sahara Nord-Oriental (Alge´rie): Ph.D. thesis, Universite´ Paris-Sud, France, 290 p.
Boudjema, A., Hamel, M., Mohamedi, A., Lounissi, R., 1990. Petroleum potential of the Reggane basin, Algeria. AAPG Bull. 74, 616.
Bouw, S., Lutgert, J., 2012. Shale Plays in The Netherlands. Pap. Presente SPE/EAGE Eur. Unconv. Resour. Conf. Exhib., Vienna, Austria. https://doi.org/10.2118/152644-MS.
Bowker, K.A., 2007. Barnett Shale gas production, Fort Worth Basin: Issues and discussion. AAPG Bull. 91, 523–533.
Bradely, W.H., 1931. Origins and Microfossils of the Oil Shale of the Green River Formation of Colorado and Utah. United states Department of the interior. Volume 168 of U. S. Geological Survey. Prof. Pap. 168, 1–54.
Buchardt, B., 1990. Reflectance of Vitrinite-Like Macerals as a Thermal Maturity Index for Cambrian-Ordovician Alum Shale, Southern Scandinavia. The American Association of Petroleum Geologists. Bulletin 74, 394–406.
Buono, R.M., Mayor, B., López-Gunn, E., 2018. A comparative study of water-related issues in the context of hydraulic fracturing in Texas and Spain. Environ. Sci. Policy 90, 193–200.
Busch, A., Alles, S., Gensterblum, Y., Prinz, D., Dewhurst, D., Raven, M., Krooss, B., 2008. Carbon dioxide storage potential of shales. Int. J. Greenh. Gas. Control 2, 297–308.
Bykadorov, V.A., et al., 2003. Ordovician-Permian palaeogeography of central Eurasia: Development of Paleozoic Petroleum-bearing basins. J. Pet. Geol. 26, 325–350.
Cai, C.F., Li, K.K., Ma, A.L., Zhang, C.M., Xu, Z.M., Worden, R.H., Wu, G.H., Zhang, B.S., Chen, L.X., 2009. Distinguishing Cambrian from Lower Ordovician Source Rocks: Evidence from SulfurIsotopes and Biomarkers in the Tarim Basin. Org. Geochem. 40, 755–768.
Cai, Z., Huang, Q., Xia, B., Xiang, J., 2016. Differences in shale gas exploration prospects of the upper Yangtze Platform and the lower Yangtze Platform: Insights from computer modelling of tectonic development. J. Nat. Gas. Sci. Eng. 36, 42–53.
Caineng, Z., Dazhong, D., Shejiao, W., Jianzhong, L., Xinjing, L., Yuman, W., Denghua, L., Keming, C., 2010. Geological characteristics and resource potential of shale gas in China. Pet. Explor. Develoipment 37, 641–653.
Camp, W.K., Diaz, E., Wawak, B., 2013. Electron microscopy of shale hydrocarbon reservoirs. 1AAPG Mem. 102, 260.
Cao, X., Gao, Y., Cui, J., Han, S., Kang, L., Song, S., Wang, C., 2020. Pore Characteristics of Lacustrine Shale Oil Reservoir in the Cretaceous Qingshankou Formation of the Songliao Basin, NE China. Energies 13, 2027.
Cao, Z., Liu, G., Kong, Y., Wang, C., Niu, Z., Zhang, J., Geng, C., Shan, X., Wei, Z., 2016. Lacustrine tight oil accumulation characteristics: Permian Lucaogou Formation in Jimusaer Sag, Junggar Basin. Int. J. Coal Geol. 153, 37–51.
Capelli, I.A., Scasso, R.A., Cravero, F., Kietzmann, D.A., Vallejo, D., Adatte, T., 2021. Late-diagenetic clay mineral assemblages in carbonatized ash beds of the Vaca Muerta Formation (Neuquén Basin, Argentina): Insights into the diagenetic formation of chlorite. Mar. Pet. Geol. 132, 105207.
Caprioglio, P.A., Jarque, G., Irigoyen, M., Maiztegui, G., Luz, N., D'Agostino, A., Casal, M., Villalba, D., Villar, H.J., 2020. Pozo D-129 Formation: The Case of a Recent Shale Oil Discovery in a Lacustrine Source Rock in El Huemul Field, Golfo San Jorge Basin, Southern Argentina. SPE/AAPG/SEG Lat. Am. Unconv. Resour. Technol. Conf. ⟨https://doi.org/10.15530/urtec-2020-1521⟩.
Cardott, B.J., Landis, C.R., Curtis, M.E., 2015. Post-oil solid bitumen network in the Woodford Shale, USA—a potential primary migration pathway. Int. J. Coal Geol. 139, 106–113.
Carroll, A.R., 1998. Upper Permian Lacustrine Organic Facies Evolution. South. Junggar Basin,NW China Org. Geochem. 28, 649–667.
Chakraborty, N., Mandal, A., Choudhuri, A., Mandal, S., Sarkar, S., 2018. Indigenous siliciclastic and extraneous polygenetic carbonate facies in the Albian-Turonian Karai Shale, Cauvery Basin, India. Carbonates Evaporites 33, 561–576.
Chandra, K., Philip, P.C., Sridharan, P., Chopra, V.S., Rao, B., Saha, P.K., 1991. Petroleum source-rock potentials of the cretaceous transgressive-regressive sedimentary sequences of the Cauvery Basin. J. Southeast Asian Earth Sci. 5, 367–371.
Chatterjee, S., Ansari, K., Biswas, M., Mukherjee, S., Kavitha, B., 2024. Morphometry and active tectonics of the Konkan coast, western India. In: Evolving Earth, 2, 100041.
Chawla, S., 2010. Pre-Confrence on Shale Gas.Presentation presented at the Petrotech 2010, New Delhi, India. URL: ⟨http://www.petrotech.in/pre-conference-shale-gas-tapping-india%E2%80%99s-shale-gas-potential⟩ (Accessed on 17-May-2023).
Chen, L., Jiang, Z., Liu, K., Gao, F., Wang, P., 2017. A Combination of N_2 and CO_2 Adsorption to Characterize Nanopore Structure of Organic-Rich Lower Silurian Shale in the Upper Yangtze Platform, South China: Implications for Shale Gas Sorption Capacity. Acta Geol. Sin. 91, 1380–1394.
Chen, M., Al-Maktoumi, A., Rajabi, M.M., Izady, A., Al-Mamari, H., Cai, J., 2021. Evaluation of CO2 sequestration and circulation in fault-bounded thin geothermal reservoirs in North Oman using response surface methods. J. Hydrol. 598, 126411.
Chen, S., Zhu, Y., Wang, H., Liu, H., Wei, W., Fang, J., 2011. Shale gas reservoir characterisation: A typical case in the southern Sichuan Basin of China 36, 6609–6616.
Chen, Z., Liao, X., Zhao, X., Dou, X., Zhu, L., 2016. Development of a trilinear-flow model for carbon sequestration in depleted shale. SPE J. 21, 1386–1399.
Chevallier, B., Bordenave, M.L., 1986. Contribution of geochemistry to the exploration in the Bintuni Basin. Irian Jaya 439–460.
Christopher, J.E., Kent, D.M., Simpson, F., 1973. Saskatchewan and Manitoba. Future Petroleum Provinces of Canada. Their Geol. Potential — Mem. 1, 121–149. ⟨https://archives.datapages.com/data/cspg_sp/data/001/001001/121_cspgsp0010121.htm⟩.
Chungkham, P., 2009. Paris Basin offers opportunities for unconventional hydrocarbon resources. first Break 27.
Claypool, E., Love, A.H., Maughan, E.K., 1978. Organic Geochemistry, Incipient Metamorphism, and Oil Generation in Black Shale Members of Phosphoria Formation, Western Interior United States. AAPG-Bull. 62, 98–120.
Cole, D.I., 2005. Prince Albert Formation. In: Johnson, M.R. (Ed.), Catalogue of South African lithostratigraphic units. South African Committee for Stratigraphy, Pretoria, pp. 33–36.
Comet, J.N., 2018. Ayoluengo's history – Spain's only onshore oil field. In: Craig, J., Gerali, F., Maculay, F., Sorkhabi, R. (Eds.), Geological Society, 465. Special Publications, London, pp. 333–344.
Comet, J.N., Martinez, A.A., 2006. September. Cretaceous and Tertiary petroleum systems in the Catatumbo basin (Colombia). 9th Simposio Bolivariano-Exploracion Petrolera en las Cuencas Subandinas (pp. cp-111). European Association of Geoscientists & Engineers.

Conybeare, C.E.B., 1979. Lithostratigraphic analysis of sedimentary basins. Academic Press, New York, pp. 410–411.
Cooper, J., Stamford, L., Azapagic, A., 2018. Economic viability of UK shale gas and potential impacts on the energy market up to 2030. In: Applied Energy, 215, pp. 577–590.
Coskun, B., 1997. Oil and gas fields—transfer zone relationships, Thrace basin, NW Turkey. Mar. Pet. Geol. 14, 401–416.
Council W.E., 2010. Survey of energy resources. London, UK: World Energy Council. URL: ⟨https://www.worldenergy.org/assets/downloads/ser_2010_report_1.pdf⟩ (Accessed on 18-May-2023).
Craddock, P.R., Mossé, L., Bernhardt, C., Ortiz, A.C., Gonzalez Tomassini, F., Saldungaray, P., Pomerantz, A.E., 2019. Characterization and range of kerogen properties in the Vaca Muerta formation, Neuquén basin, Argentina. Org. Geochem. 129, 42–44.
Crick, I.H., Boreham, C.J., Cook, A.C., Powell, T.G., 1988. Studies on petroleum geology and geochemistry of the middle Proterozoic McArthur Basin, Northern Australia II: Assessment of source rocks. Am. Assoc. Pet. Geol. Bull. 52, 1747–1763.
Dadi, K., Ahmadi, R., Ouali, J.A., 2019. Organic Geochemical Assessment and Shale Gas Potential of Lower Silurian Organic Rich Shale. In: The Ghadames Basin, 36. North Africa. Oil Shale, pp. 337–352.
Dahl, J., Chen, T., Kaplan, I.R., 1989. Alum Shale Bitumen Maturation and Migration: Implications for Gotland's Oil. J. Pet. Geol. 12, 465–476.
Dalyan, I.B., 1996. Tectonics of Subsalt Rocks of the Eastern Margin of the North Caspian Basin in Connection with Petroleum Potential. Geol. Neft. i Gaza 6, 8–17.
Dangwal, V., Waraich, R.S., Sengupta, S., Srivastava, D.K., Sathe, A.V., Asthana, M., 2009. Volcanic Intrusions and their implication on Petroleum System in Andaman Basin, India. Assoc. Pet. Geol. Bull., GEO India Expo. XXI, Noida, N. Delhi.
Dart Energy, Corporate Presentation, March 1, 2013.
Dasgupta, A., 2017. An Introduction to Earth Science. The World Press Private Limited. Kolkata. ISBN: 978-93-82878-00-1.
Dasgupta, S., Mukherjee, S., 2017. Brittle shear tectonics in a narrow continental rift: asymmetric non-volcanic Barmer basin (Rajasthan, India). J. Geol. 125, 561–591.
Davidson, L., Beswetherick, S., Craig, J., Eales, M., Fisher, A., Himmali, A., Jho, J., Mejrab, B., Smart, J., 2000. In: Sola, M.A., Worsley, D. (Eds.), The structure, stratigraphy and petroleum geology of the Murzuq Basin, Southwest Libya. Geological Exploration in Murzuq Basin, Elsevier, pp. 295–320. ISBN 9780444506115.
Dayal, A.M., 2017. Shale. In: Dayal, A.M., Mani, D. (Eds.), Shale gas exploration and environmental impacts. Elsevier, Amsterdam, pp. 1–11. ISBN: 978-0-12-809573-7.
Dayal, A.M., Mani, D., Madhavi, T., Kavitha, S., Kalpana, M.S., Patil, D.J., Sharma, M., 2014. Organic geochemistry of the Vindhyan sediments: Implications for hydrocarbons. J. Asian Earth Sci. 91, 329–3383.
De, S., Aastha, Sengupta, D., 2020. Depositional environment and geomechanical properties of Cambay Shale: potential reservoir for shale oil and gas in India. Arab. J. Geosci. 13, 455.
De Jager, J., Doyle, M.A., Grantham, P.J., Mabillard, J.E., 1996. Hydrocarbon habitat of the West Netherlands Basin. In: Rondeel, H.E., Batjes, D.A.J., Nieuwenhuijs, W.H. (Eds.), Geology of Gas and Oil under the Netherlands. Springer. Dordrecht. ⟨https://doi.org/10.1007/978-94-009-0121-6_17⟩.
De Pater, D.J., Baisch, S., 2011. Geomechanical Study of Bowland Shale Seismicity: Synthesis Report. Rep. Prep. Cuadrilla Resour., Ltd. November 2, 71.
Department of Mines and Petroleum, 2014. Western Australia's Petroleum and Geothermal Explorer's Guide, 2014 Edition.
Department of Mines and Petroleum. Department of Mines and Petroleum, 2017. Summary of Petroleum Prospectivity: Canning Basin, February 2017. Department of Mines and Petroleum.
Deshmukh, S., Omer, S., Tomor, P.S., Harilal, 2020. Shale Gas Sweet Spot Identification Using Quantitative Seismic Interpretation (QSI) and Neural Network in Krishna-Godavari Basin, India. SPE/AAPG/SEG Unconv. Resour. Technol. Conf. https://doi.org/10.15530/urtec-2020-2710.
Dewangan, P., Ramprasad, T., Ramana, M.V., Mazumdar, A., Desa, M., Badesab, F.K., 2010. Seabed morphology and gas venting features in the continental slope region of Krishna–Godavari basin, Bay of Bengal: Implications in gas–hydrate exploration. Mar. Petrol. Geol. 27, 1628–1641.
Di Sbroiavacca, N., 2021. Shale Oil and Shale Gas in Argentina. State of Situation and Prospective. Oil and Natural Gas Economy in Argentina. The Latin American Studies Book Series. Springer, Cham. https://doi.org/10.1007/978-3-030-65520-4_4.
Diasty, W.Sh, El, Beialy, S.Y.El, Anwari, T.A., Peters, K.E., Batten, D.J., 2017. Organic geochemistry ofthe Silurian Tanezzuft Formation and crudeoils, NC115 Concession, Murzuq Basin, southwest Libya. Mar. Pet. Geol. 86, 367–385.
Dolson, J., et al., 2015. The discovery of the Barmer Basin, Rajasthan, India, and its petroleum geology. AAPG Bull. 99, 433–465.
Dong, D., Zou, C., Dai, J., Huang, S., Zheng, J., Gong, J., Wang, Y., Li, X., Guan, Q., Zhang, C., Huang, J., Wang, S., Liu, D., Qiu, Z., 2016. Suggestions on the development strategy of shale gas in China. J. Nat. Gas. Geosci. 1, 413–423.
Dong, M., Gong, H., Sang, Q., Zhao, X., Zhu, C., 2022. Review of CO2-kerogen interaction and its effects on enhanced oil recovery and carbon sequestration in shale oil reservoirs. Resour. Chem. Mater. 1, 93–113.
Dou, L., Cheng, D., Wang, J., Du, Y., Xiao, G., Wang, R., 2020. Petroleum Systems of The Bongor Basin And The Great Baobab Oilfield, Southern Chad. J. Pet. Geol. 43, 301–321.
Doyele, P., Bennett, M.R., 1999. Interpreting paleoenvironment from fossils. Unlocking Stratigr. Rec.: Adv. Mod. Stratigr. Wiley Chichester 441–469.
Driskill, B., Walls, J., Sinclair, S.W., DeVito, J., 2013a. Micro-scale Characterization of the Eagle Ford Formation Using SEM Methods and Digital Rock Modeling. Unconv. Resour. Technol. Conf. Pap. https://doi.org/10.1190/urtec2013-165.
Driskill, B., Walls, J., Sinclair, S.W., DeVito, J., 2013b. Applications of SEM imaging to reservoir characterization in the Eagle Ford Shale. In: Camp, W., Diaz, E., Wawak, B. (Eds.), Electron Microscopy of Shale Hydrocarbon Reservoirs AAPG Memoir, 102. south Texas, U.S.A, pp. 115–136.
Duba, A., Huenges'f, E., Nover, G., Will, G., 1988. Impedance of black shale from Munsterland 1 borehole: an anomalously good conductor? Geophys. J. Int. 94, 413–419.
Dyni, J.R., 2004. Oil Shale. In: Cleveland, C.J. (Ed.), Encyclopedia of Energy. Elsevier, pp. 739–752. ISBN: 978-0-12-176480-7.
Dyni, J.R., 2006. Geology and resources of some world oil-shale deposits. U. S. Geol. Surv. Sci. Investig. Rep. 2005–5294.
Echikh, K., 1998. Geology and hydrocarbon occurrences in the Ghadames Basin, Algeria, Tunisia, Libya. In: Mac-Gregor, D.S., Moody, R.T.J., Clark-Lowes, D.D. (Eds.), Petroleum Geology of North Africa. Geological Society, 132. Special Publication, London, pp. 109–129.
Effimoff, I., 1999. Future Hydrocarbon Potential of Kazakhstan. In: Petroleum Provinces of the 21st Century, 83. Second Wallace E. Pratt Conference, January San Diego, Calfornia. AAPG.
Ehsan, M., Gu, H., Akhtar, M.M., Abbasi, S., Ullah, Z., 2016. The identification of hydrocarbon potential of Talhar Shale: Member of Lower Goru Formation by using well logs derived parameters, Southern Lower Indus Basin, Pakistan. J. Earth Sci. 29, 587–593.
El Diasty, W.S., 2015. Khatatba Formation as an active source rock for hydrocarbons in the northeast Abu Gharadig Basin, north Western Desert, Egypt. Arab J. Geosci. 8, 1903–1920.
English, K.L., Redfern, J., Corcoran, D.V., English, J.M., Cherif, R.Y., 2016. Constraining burial history and petroleum charge in exhumed basins: New insights from the Illizi Basin, Algeria. AAPG Bull. 100, 623–655.
Escalona, A., Mann, P., 2006. An overview of the petroleum system of Maracaibo Basin. AAPG Bull. 90, 657–678.
Fakher, S., Abdelaal, H., Elgahawy, Y., El-Tonbary, A., 2020. A review of long-term carbon dioxide storage in shale reservoirs (p. D023S028R003). SPE/AAPG/SEG Unconventional Resources Technology Conference. URTEC.
Fello, N., Lüning, S., Štorch, P., Redfern, J., 2006. Identification of early Llandovery (Silurian) anoxic palaeo-depressions at the western margin of the Murzuq Basin (southwest Libya), based on gamma-ray spectrometry in surface exposures. GeoArabia 11, 101–118.
Feng, C., Deng, X., Yin, W., Wang, Z., Mao, Z., 2018. Brittleness Index Prediction via Well Logs and Reservoir Classification Based on Brittleness. SPE Asia Pac. Oil Gas. Conf. Exhib. https://doi.org/10.2118/191934-ms.
Feng, Q., Xu, S., Xing, X., Zhang, W., Wang, S., 2020. Advances and challenges in shale oil development: A critical review. Advances in Geo-Energy. Research 4, 406–418.
Feng, Z., Jia, C., Xie, X., Zhang, S., Feng, Z., Cross, T.A., 2010. Tectonostratigraphic units and stratigraphic sequences of the nonmarine Songliao basin, northeast China. Basin Res. 22, 79–95.
Figari, E.G., Strelkov, E., Laffitte, G., Cid de la Paz, M.S., Courtade, S.F., Celaya, J., Vottero, A., Lafourcade, P., Martínez, R., Villar, H., 1999. Los Sistemas Petroleros de la Cuenca del Golfo San Jorge: Sintesis Estructural, Estratigrafía y Geoquímica. Actas IV Congreso de Exploración y Desarollode Hidrocarburos. Mar. Del. Plata, I 197–237.
Fitzgerald, M.G., Mitchum Jr., R.M., Uliana, M.A., Biddle, K.T., 1990. Evolution of the San JorgeBasin. Argent. Am. Assoc. Pet. Geol. Bull. 74, 879–920.
Friedman, G.M., 2003. Classification of Sediments and Sedimentary Rocks. In: Middleton, G.V., et al. (Eds.), Encyclopedia of Sediments and Sedimentary Rocks. Kluwer Academic Publishers, Dordrecht, pp. 132–135. ISBN 1-4020-0872-4.
Froidl, F., Littke, R., Baniasad, A., Zheng, T., Röth, J., Böcker, J., Hartkopf-Fröder, C., Strauss, H., 2021. Peculiar Berriasian "Wealden" Shales of northwest Germany: Organic facies, depositional environment, thermal maturity and kinetics of petroleum generation. Mar. Pet. Geol. 124, 104819.
Fulfaro, V.J., Saad, A.R., Perinotto, J.A.J., Etoherehere, M.L.C., Verolavsky, G., 1997. Paraná Basin: Mineral Resource Potentials in Brazil, Uruguay, and Paraguay. Int. Geol. Rev. 39, 703–722.
Gale, R.S., Baskerville, R.C., 1967. Capillary suction method for determinationof the filtration properties of a solid/liquid suspension. Chem. Ind. 9, 355–356.
Gao, Y., Wang, C., Liu, Z., Du, X., Ibarra, D.E., 2015. Diagenetic and paleoenvironmental controls on late cretaceous clay minerals in the songliao basin, northeast china. Clays Clay Miner. 63, 469–484.
Gao, Y., Huang, H., Tao, H., Carroll, A.R., Qin, J., Chen, J., Yuan, X., Wang, C., 2019. Paleoenvironmental setting, mechanism and consequence of massive organic carbon burial in Permian Junggar Basin, NW China. J. Asian Earth Sci. 194, 104222.
Gao, Z., et al., 2024. Shale oil migration across multiple scales: A review of characterization methods and different patterns. Earth-Sci. Rev. 254, 104819.
Geel, C., Schulz, H.-M., Booth, P., DeWit, M., Horsfield, B., 2013. Shale Gas Characteristics of Permian Black Shales in South Africa: Results from Recent Drilling in the Ecca Group (Eastern Cape). Energy Procedia 40, 256–265.
Geel, C., Wit, M.De, Booth, P., Schulz, H.-M., Horsfield, B., 2015. Palaeo-environment, diagenesis and characteristics of permian black shales in the lower karoo supergroup flanking the cape fold belt near jansenville, eastern cape, south africa: implications for the shale gas potential of the karoo basin. South Afr. J. Geol. 118, 249–274.
Ghanizadeh, A., Gasparik, M., Amann-Hildenbrand, A., Gensterblum, Y., Krooss, B.M., 2014. Experimental study of fluid transport processes in the matrix system of the European organic-rich shales: I. Scandinavian Alum Shale. Mar. Pet. Geol. 51, 79–99.
Ghulam, M.S., Christopher, D.H., Qamar, Y., 2020. An integrated petrophysical and geomechanical characterization of Sembar Shale in the Lower Indus Basin, Pakistan, using well logs and seismic data. J. Nat. Gas. Sci. Eng. 78, 103–327.

Gluyas, J., Swarbick, R., 2004. Petroleum Geoscience. Blackwell Science Ltd. ISBN 978-0-632-03767.
Godec, M., Koperna, G., Petrusak, R., Oudinot, A., 2013. Potential for enhanced gas recovery and CO2 storage in the Marcellus Shale in the Eastern United States. Int. J. Coal Geol. 118, 95–104.
Goergen, E.T., Curtis, M.E., Jernigen, J., Sondergeld, C., Rai, C., 2014. Integrated petrophysical properties and multi-scaled SEM. Unconv. Resour. Technol. Conf. Pap. 1922739.
Goncharov, I.V., Samoilenko, V.V., Oblasov, N.V., 2014. Prospects of Shale Oil Bazhenov Formation in the South-East of Western Siberia. SPE Russ. Oil Gas. Explor. Prod. Tech. Conf. Exhib. https://doi.org/10.2118/171170-ms.
Gornitz, V., 2009. Encyclopedia of Paleoclimatology and Ancient Environments. Springer, pp. 876–877. ISBN 978-1-4020-4551-6.
Greenhalgh, E., 2016. The Jurassic shales of the Wessex area: geology and shale oil and shale gas resource estimation. Lond., UK, Br. Geol. Surv. Oil Gas. Auth. 82.
Gross, D., Sachsenhofer, R.F., Bechtel, A., Pytlak, L., Rupprecht, B., Wegerer, E., 2014. Organic geochemistry of Mississippian shales (Bowland Shale Formation) in central Britain: implications for depositional environment, source rock and gas shale potential. Mar. Pet. Geol. 59, 1–21.
Gumati, Y., 1992. Lithostratigraphy Of Oil-Bearing Tertiary Bioherms In the Sirte Basin, Libya. J. Pet. Geol. 15, 305–318.
Gumati, Y.D., Schamel, S., 1988. Thermal Maturation History of The Sirte Basin, Libya. J. Pet. Geol. 11, 205–218.
Gumati, Y.D., Kanes, W.H., Schamel, S., 1996. An Evaluation of The Hydrocarbon Potential of The Sedimentary Basins of Libya. J. Pet. Geol. 19, 95–112.
Gupta, S.K., 2006. Basin Archit. Pet. Syst. Krishna Godavari Basin, East Coast India Lead. Edge 25, 830–837.
Guzman-Vega, M.A., Castro Ortiz, L., Roman-Ramos, J.R., Medrano-Morales, L., Valdez, L.C., Vazquez-Covarrrubias, E., Ziga-Rodriguez, G., 2001. Classification and Origin of Petroleum in the Mexican Gulf Coast Basin: An Overview. In: Bartolini, C., Buffler, R.T., Cantú-Chapa, A. (Eds.), The Western Gulf of Mexico Basin: Tectonics, Sedimentary Basins and PetroleumSystems, 75. American Association of Petroleum Geologists, Memoir, pp. 127–142.
Hackley, P., Cardott, B., 2016. Application of organic petrography in North American shale petroleum systems: A review. Int. J. Coal Geol. 163, 8–51.
Hadded, A., Layeb, M., Mannai-Tayech, B., Milad, B., Saïdi, M., Soussi, M., 2021. Subsurface geochemical and mineralogical evaluation for unconventional "shale" oil play of the Bahloul Formation (Cenomanian-Turonian) in the Sahel Basin, Eastern Tunisia. Arab. J. Geosci. 14, 1701.
Hafiz, M., Hakhoo, N., Bhat, G.M., Kanungo, S., Thusu, B., Craig, J., Ahmed, W., 2020. Source potential and reservoir characterization of the Cambay Shale, Cambay Basin, India: Implications for tight gas and tight oil resource development. AAPG Bull. 104, 1707–1749.
Haider, B.A., Aizad, T., Ayaz, S.A., Shoukry, A., 2012. A Comprehensive Shale Gas Exploitation Sequence for Pakistan and Other Emerging Shale Plays. SPE/PAPG Annu. Tech. Conf. – Islamabad.
Hampson, D.P., Schuelke, J.S., Quirein, J.A., 2001. Use of multiattribute transforms to predict log properties from seismic data. Geophysics 66, 220–236.
Han, H., Guo, C., Zhong, N., Pang, P., Chen, S., Lu, J., Gao, Y., 2019. Pore structure evolution of lacustrine shales containing Type I organic matter from the Upper Cretaceous Qingshankou Formation, Songliao Basin, China: A study of artificial samples from hydrous pyrolysis experiments. Mar. Pet. Geol. 104, 375–388.
Han, H., Guo, C., Zhong, N., Pang, P., Ding, Z., Chen, J., Huang, Z., Gao, Y., Luo, J., Li, Q., Zhang, Z., 2020. Pore Characteristics and Controlling Factors of Lacustrine Shales From the Upper Cretaceous Qingshankou Formation of the Songliao Basin, Northeast China: A Study Combining SEM, Low Temperature Gas Adsorption and MICP Experiments. Acta Geol. Sin. 95, 585–601.
Han, L., Shi, X., Ni, H., Zhang, W., Gao, Q., 2024. Review of CO2 Fracturing and Carbon Storage in Shale Reservoirs. Energy Fuels 38, 15913–15934.
Han, S., Xiang, C., Du, X., Xie, L., Bai, S., Wang, C., 2022. Logging evaluation of deep multi-type unconventional gas reservoirs in the Songliao basin, northeast China: Implications from continental scientific drilling. Geosci. Front. 13, 101451.
Hansen, D.L., Blundell, D.J., Nielsen, S.B., 2002. A Model for the Evolution of the Weald Basin; Bulletin of the Geological Society of Denmark: Copenhagen. Denmark 49 (Part 2), 109–118.
Harahap, B.H., 2012. Tectonostratigraphy of the southern part of Papua and Arafura Sea, Eastern Indonesia. Indones. J. Geosci. 7, 167–187.
Haris, A., Seno, B., Riyanto, A., Bachtiar, A., 2017. Integrated approach for characterizing unconventional reservoir shale hydrocarbon: case study of north sumatra basin. Paper Presented at the IOP Conference Series: Earth and Environmental Science. Bali, Indonesia.
Harper, J., 2008. The marcellus shale: An old "new" gas reservoir in pennsylvania. Pa. Geol. 38, 2–13.
Hasany, S.T., Khan, F., 2012. Paleozoic Sequences as Potential Source Rocks for Petroleum in Northwestern Pakistan, with Particular Reference to the Silurian System, a Major Petroleum Source in the Middle East and North Africa. AAPG Annual Technical Conference.
Hashimoto, T., Bailey, A., Chirinos, A., Carr, L., 2018. Onshore Basin Inventory Volume 2. Cann., Perth Off. Basins 2, 1–126. ISBN: 978-1-925297-88-1.
Hazra, B., Varma, A.K., Bandopadhyay, A.K., Chakravarty, S., Buragohain, J., Samad, S. K., Prasad, A.K., 2016. FTIR, XRF, XRD and SEM characteristics of Permian shales, India. J. Nat. Gas. Sci. Eng. 32, 239–255.
Hazra, B., Wood, D.A., Mani, D., Singh, P.K., Singh, A.K., 2019. Evaluation of Shale Source Rocks & Reservoirs. Springer. ISBN 978-3-030-13042-8.
Hazra, B., Singh, D.P., Crosdale, P.J., Singh, V., Singh, P.K., Gangopadhyay, M., Chakraborty, P., 2021a. Critical insights from Rock-Eval analysis of vitrains. Int. J. Coal Geol. 238, 103717.
Hazra, B., Singh, D.P., Chakraborty, P., Singh, P.K., Sahu, S.G., Adak, A.K., 2021b. Using rock-eval S4Tpeak as thermal maturity proxy for shales. Mar. Pet. Geol. 127, 104977.
Hazra, B., Vishal, V., Sethi, C., Chandra, D., 2022. Impact of supercritical CO2 on shale reservoirs and its implication for CO2 sequestration. Energy Fuels 36, 9882–9903.
Hazra, B., Chandra, D., Vishal, V., 2024. Unconventional Hydrocarbon Reservoirs: Coal and Shale. Springer, pp. 1–169.
He, W., Sun, Y., Guo, W., Shan, X., Su, S., Zheng, S., Deng, S., Kang, S., Zhang, X., 2019. Organic Geochemical Characteristics of the Upper Cretaceous Qingshankou Formation Oil Shales in the Fuyu Oilfield, Songliao Basin, China: Implications for Oil-Generation Potential and Depositional Environment. Energies 12, 4778.
Heath, J.E., Dewers, T.A., McPherson, B.J.O.L., Petrusak, R., Chidsey Jr., T.C., Rinehart, A.J., Mozley, P.S., 2011. Pore networks in continental and marine mudstones: characteristics and controls on sealing behavior. Geosphere 7, 429–454.
Heege, J.T., Zijp, M., Nelskamp, S., Douma, L., Verreussel, R., Ten Veen, J., Peters, R., 2015. Sweet spot identification in underexplored shales using multidisciplinary reservoir characterization and key performance indicators: Example of the Posidonia Shale Formation in the Netherlands. J. Nat. Gas. Sci. Eng. 27, 558–577.
Henk, A., Davaa, B., Geerdts, P., Vogler, M., Wemmer, K., 2007. Structure and Evolution of the Tamtsag Basin / NEMongolia. Geophys. Res. Abstr. 9, 2415.
Hennissen, J.A., Hough, E., Vane, C.H., Leng, M.J., Kemp, S.J., Stephenson, M.H., 2017. The prospectivity of a potential shale gas play: An example from the southern Pennine Basin (central England, UK). Mar. Pet. Geol. 86, 1047–1066.
Henry, J.D., 1982. Stratigraphy of the Barnett Shale (Mississippian) and associated reefs in the northern Fort Worth Basin. In: Martin, C.A. (Ed.), Petroleum Geology of the Fort Worth Basin and Bend Arch Area. Dallas Geological Society, pp. 157–178.
Hepbasli, A., 2004. Oil Shale as an Alternative Energy Source. Energy Sources 26, 107–118.
Herber, R., Jager, J.De, 2010. Oil and Gas in the Netherlands-Is there a future? Neth. J. Geosci. 89-2, 91–107.
Heron, D.P.L., Craig, J., Etienne, J.L., 2009. Anc. Glaciat. Hydrocarb. Accumul. North Afr. Middle East 93, 47–76.
Hill, T., 2010. Unconventional Oil and Gas Opportunities in South Australia. DMITRE, Energy Resources Division. URL: 〈https://wds.squiz.cloud/_data/assets/pdf_file/0010/690832/Australia_House_Mar_5_2012_AJH.pdf〉 (Accessed on 10-Aug-2023).
Holland, C.H., 1990. The Yangtze Platform: a gateway to Chinese geology. Proc. Geol. ' Assoc. 101, 1–17.
Hollander, D.J., Bessereau, G., Belin, S., Huc, A.Y., Houzay, J.P., 1991. Organic Matter in the Early Toarcian Shales, Paris Basin, France: a Response to Environmental Changes, Oil & Gas Science and Technology - Rev. IFP 46, 543–562.
Hou, L., Luo, X., Han, W., Lin, S., Pang, Z., Liu, J., 2020. Geochemical Evaluation of the Hydrocarbon Potential of Shale Oil and Its Correlation with Different Mineralsâ "a Case Study of the TYP Shale in the Songliao Basin, China. Energy Fuels 34, 11998–12009.
Hou, Y., Wang, F., He, S., Dong, T., Wu, S., 2017. Properties and shale oil potential of saline lacustrine shales in the Qianjiang Depression, Jianghan Basin, China. Mar. Pet. Geol. 86, 1173–1190.
Howell, J.A., Schwarz, E., Spalletti, L.A., Veiga, G.D., 2005. The Neuquén Basin: An Overview. In: Viega, G.D., Spalletti, L.A., Howell, J.A., Schwarz, E. (Eds.), The Neuquén Basin, Argentina: A Case Study in Sequence Stratigraphy and Basin Dynamics. Geologic Society, 252. Special Publications, London, pp. 1–14.
Hu, F., Wang, J., Liu, Z., 2022. Sedimentary Characteristics of the Permian Zhesi Formation in Eastern Inner Mongolia, China: Implications for Sedimentary Background and Shale Gas Resource Potential. ACS Omega 7, 45287–45300.
Hu, K., Herdegen, V., Mischo, H., 2022. Carbon dioxide adsorption to 40 MPa on extracted shale from Sichuan Basin, southwestern China. Fuel 318, 123666.
Hu, T., Pang, X., Wang, Q., Jiang, S., Wang, X., Huang, C., Xu, Y., Li, L., Li, H., Chen, Z.-Q., 2017. Geochemical and geological characteristics of Permian Lucaogou Formation shale of the well Ji174, Jimusar Sag, Junggar Basin, China: Implications for shale oil exploration. Geol. J. 53, 2371–2385.
Huang, J., Zou, C., Li, J., Dong, D., Wang, S., Wang, S., Cheng, K., 2012. Shale gas generation and potential of the Lower Cambrian Qiongzhusi Formation in the Southern Sichuan Basin, China. Pet. Explor. Dev. 39, 75–81.
Hughes, R.V., 1978. Oil Shale. In: Fairbridge, R.W., Bourgeois, J. (Eds.), The Encyclopedia of Sedimentology. Hutchinson & Ross, Inc, Dowden, pp. 507–508.
Huo, P., Zhang, D., Yang, Z., Li, W., Zhang, J., Jia, S., 2017. CO_2 geological sequestration: displacement behavior of shale gas methane by carbon dioxide injection. Int. J. Greenh. Gas. Control 66, 48–59.
Hupp, B.N., Donovan, J.J., 2018. Quantitative mineralogy for facies definition in the Marcellus Shale (Appalachian basin, USA) using XRD-XRF integration. Sediment. Geol. 371, 16–31.
Hupp, B.N., Donovan, J.J., 2018. Quantitative mineralogy for facies definition in the Marcellus Shale (Appalachian Basin, USA) using XRD-XRF integration. Sediment. Geol. 371, 16–31.
Hupp, B.N., Weislogel, A.L., 2018. Geochemical insights into provenance of the middle devonian Hamilton group of the central appalachian basin, USA. J. Sediment. Res. 88, 1153–1165.
Huvaz, O., Sarikaya, H., Işık, T., 2007. Petroleum systems and hydrocarbon potential analysis of the northwestern Uralsk basin, NW Kazakhstan, by utilizing 3D basin modeling methods. Mar. Pet. Geol. 24, 247–275.
ICF International, 2014. Recent Australian Natural Gas Pricing Dynamics and Inmplications for the U. S. LNG Export Debate. The American Petroleum Institute. API, Washington, D.C.

Indrajaya, H., Susanti, D.N., Usman, T.K., Wicaksono, A.F., Sijabat, H., Wahyudin, M., 2016. Integrated Interpretation of Borehole and Geophysical Data for Fault Configuration and Its Implication to Hydrocarbon Distribution in Bunyu Area, Tarakan Basin. URL: ⟨https://archives.datapages.com/data/ipa_pdf/2016-east-indonesia-tech-symposium/9-TS-16.htm⟩.
Jaber, J., Probert, S., 1999. Pyrolysis and gasification kinetics of Jordanian oil-shales. Appl. Energy 63, 269–286.
Jaber, J.O., Probert, S.D., 1997. Exploitation of Jordanian oil-shales. Appl. Energy 58, 161–175.
Jabour, H., Nakayama, K., 1988. Basin Modeling of Tadla Basin, Morocco, for Hydrocarbon Potential. Am. Pet. Geol. 72, 1059–1073.
Jackson, J.-, Sweet, I.P., Powell, T.G., 1988. Studies On Petroleum Geology And Geochemistry, Middle Proterozoic, Mcarthur Basin Northern Australia I: Petroleum Potential. APPEA J. 28, 283.
Jaffe, A.M., 2016. Shale gas will rock the world. In: Lehr, J.H., Keeley, J. (Eds.), Alternative Energy and Shale Gas Encyclopedia, First Edition. John Wiley & Sons, pp. 689–691. ISBN: 978-0-470-89441-5.
Jain, T., Sharma, A., Agarwal, A., 2012. Current Scenario and Future Prospects of Shale Gas in India. Search Discov. Article #80276.
Jaju, M.M., Nader, F.H., Roure, F., Matenco, L., 2016. Optimal aquifers and reservoirs for CCS and EOR in the Kingdom of Saudi Arabia: an overview. Arab J. Geosci. 9, 604.
Jarrett, A.J.M., Cox, G.M., Brocks, J.J., Grosjean, E., Boreham, C.J., Edwards, D.S., 2019. Microbial assemblage and palaeoenvironmental reconstruction of the 1.38 Ga Velkerri Formation, McArthur Basin, northern Australia. Geobiology 17, 360–380.
Jarvie, D.M., 2012. Components and processes affecting producibility and commerciality of shale resource systems. International Symposium on Shale Oil Technologies. Worlwide Geochemistry. LLC, Wuxi, China.
Jarvie, D.M., Hill, R.J., Pollastro, R.M., Cardott, B.J., 2005. Assessment of the gas potential and yields from shales: The Barnett Shale model. Okla. Geol. Surv. Circ. 110, 37–50.
Jarvie, D.M., Hill, R.J., Ruble, T.E., Pollastro, R.M., 2007. Unconventional shale-gas systems: The Mississippian Barnett Shale of north-central Texas as one model for thermogenic shale-gas assessment. AAPG Bull. 91, 475–499.
Javed, T., Siyar, S.M., Sajjad, S.M.W., Ali, F., Raziq, F., Ullah, S., Khan, N., Ali, I., 2023. Hydrocarbon Source Rock Potential of the Late Paleocene Patala Formation, Kohat Basin, Pakistan: Organic geochemical and palynofacies approach. J. Earth Syst. Sci. 127, 98.
Ji, W., Hao, F., Schulz, H.M., Song, Y., Tian, J., 2019. The architecture of organic matter and its pores in highly mature gas shales of the lower Silurian Longmaxi Formation in the upper Yangtze platform, south China. AAPG Bull. 103, 2909–2942.
Jia, B., Tsau, J.S., Barati, R., 2019. A review of the current progress of CO2 injection EOR and carbon storage in shale oil reservoirs. Fuel 236, 404–427.
Jia, C., Wei, G., 2002. Structural characteristics and petroliferous features of Tarim Basin. Chin. Sci. Bull. 47, 1–11.
Jia, J., Liu, Z., Miao, C., Fang, S., Zhou, R., Meng, Q., Yang, D., 2014. Depositional model and evolution for a deep-water sublacustrine fan system from the syn-rift Lower Cretaceous Nantun Formation of the Tanan Depression (Tamtsag Basin, Mongolia). Mar. Pet. Geol. 57, 264–282.
Jiang, F., Hu, T., Liu, L., Wang, Q., Gao, X., Zhang, P., Li, H., Ning, K., Liu, Y., Zhu, C., Chen, Z.-Q., 2018. Geochemical and geological characteristics of the Jurassic continental black shale in the Southwestern Depression of Tarim Basin. Geol. J. 54, 1115–1131.
Jiang, F., Huo, L., Chen, D., Cao, L., Zhao, R., Li, Y., Guo, T., 2023. The controlling factors and prediction model of pore structure in global shale sediments based on random forest machine learning. Earth-Sci. Rev. 241, 104442.
Jiang, S., et al., 2017. Reservoir quality, gas accumulation and completion quality assessment of Silurian Longmaxi marine shale gas play in the Sichuan Basin. China J. Nat. Gas. Sci. Eng. 39, 203–215.
Jiao, K., Yao, S., Liu, C., Gao, Y., Wu, H., Li, M., Tang, Z., 2014. The characterization and quantitative analysis of nanopores in unconventional gas reservoirs utilizing FESEM–FIB and image processing: an example from the lower Silurian Longmaxi Shale, upper Yangtze region, China. Int. J. Coal Geol. 128-129, 1–11.
Jin, H., Sonnenberg, S., Sarg, R., 2015. Source Rock Potential and Sequence Stratigraphy of Bakken Shales in the Williston Basin. Proc. 3rd Unconv. Resour. Technol. Conf. https://doi.org/10.15530/urtec-2015-2169797.
Jin, L., et al., 2017. Advancing CO2 enhanced oil recovery and storage in unconventional oil play—Experimental studies on Bakken shales. Appl. Energy 208, 171–183.
Johnson, C.L., 2004. Polyphase evolution of the East Gobi basin: sedimentary and structural records of Mesozoic–Cenozoic intraplate deformation in Mongolia. Basin Res. 16, 79–99.
Johnson, M.R., Van Vuuren, C.J., Visser, J.N.J., Cole, D.I., Wickens, H., de, V., Christie, A.D.M., Roberts, D.L., Brandl, G., 2006. Sedimentary rocks of the Karoo Supergroup. In: Johnson, M.R., Anhaeusser, C.R., Thomas, R.J. (Eds.), The Geology of South Africa. Geological Society of South Africa, Johannesburg/Council for Geoscience, pp. 461–499.
Josh, M., Esteban, L., Delle Piane, C., Sarout, J., Dewhurst, D.N., Clennell, M.B., 2012. Laboratory characterization of shale properties. J. Pet. Sci. Eng. 88–89, 107–124.
Kala, S., Devaraju, J., Tiwari, D.M., Rasheed, M.A., Lakhan, N., 2021. Organic petrology and geochemistry of Early Permian shales from the Krishna-Godavari Basin, India: Implications for Gondwana palaeoenvironment and climate. Geol. J. 56, 5621–5641.
Kang, Z., Zhao, Y., Yang, D., 2020. Review of oil shale in-situ conversion technology. Appl. Energy 269, 115121.
Kar, N.R., Mani, D., Mukherjee, S., Dasgupta, S., Puniya, M.K., Kaushik, A.K., Biswas, M., Babu, E.V.S.S.K., 2022. Source rock properties and kerogen decomposition kinetics of Eocene shales from petroliferous Barmer basin, western Rajasthan, India. J. Nat. Gas. Sci. Eng. 100, 104497.
Keary, P., 1994. The Encyclopedia of Solid Earth Sciences. Blackwell Scientific Publications, London, p. 61.
Kern, M., Machado, G., Franco, N., Mexias, A., Vargas, T., Costa, J., Kalkreuth, W., 2004. Source Rock Characterization of Paraná Basin, Brazil: Sem and XRD Study of Irati and Ponta Grossa Formations Samples. 3° Congr. Bras. De. PD em Petróleo e GáS., 2 a 5 De. outubro De. 2005.
Khamidullin, R.A., Kalmykov, G.A., Korost, D.V., et al., 2012. Reservoir properties of the Bazhenov Formation. Soc. Petrol. Engin. Russian Oil and Gas Explor. and Pro duction Techn. Conf, Exhib.
Khosrokhavar, R., Griffiths, S., Wolf, K.H., 2014. Shale gas formations and their potential for carbon storage: opportunities and outlook. Environ. Process. 1, 595–611.
Klaver, J., Desbois, G., Urai, J.L., Littke, R., 2012. BIB-SEM study of the pore space morphology in early mature Posidonia Shale from the Hils area, Germany. Int. J. Coal Geol. 103, 12–25.
Klaver, J., Desbois, G., Littke, R., Urai, J.L., 2015. BIB-SEM characterization of pore space morphology and distribution in postmature to overmature samples from the Haynesville and Bossier shales. Mar. Pet. Geol. 59, 451–466.
Klett, T.R., 2000. Total Petroleum Systems of the Grand Erg/Ahnet Province, Algeria and Morocco—The Tanezzuft-Timimoun, Tanezzuft-Ahnet, Tanezzuft-Sbaa, Tanezzuft-Mouydir, Tanezzuft-Benoud, and Tanezzuft-Béchar/Abadla. U. S. Geol. Bull. 2202-B.
Klett, T.R., 2001. Total Pet. Syst. Pelagian Prov., Tunis., Libya, Italy, Malta– Bou Dabbous-Tert. Jurass. -Cretac. Compos. 1–27.
Kocherla, M., Teichert, B., Pillai, S., Satyanarayanan, M., Ramamurthy, P.B., Patil, D., Narsing Rao, A., 2015. Formation of methane-related authigenic carbonates in a highly dynamic biogeochemical system in the Krishna-Godavari Basin, Bay of Bengal. Mar. Pet. Geol. 64, 324–333.
Kockel, F., Hermann, W., Peter, G., 1994. Petroleum Systsms of the Lower Saxony Basin, Germany. In The Petroleum System-from Source to Trap, 573-586. AAPG Mem. 60, 573–586.
Kok, M.V., Merey, S., 2014. Shale Gas: Current Perspectives and Future Prospects in Turkey and the World. In: Energy Sources, Part A: Recovery, Utilization, and Environmental Effects, 36. Taylor & Francis, pp. 2492–2501.
Kontorovich, A.E., Nesterov, I.I., Salmanov, F.K., Surkov, V.S., Trofimuk, A.A., Ervie, Yu. G., 1975. Petroleum Geology of West Siberia [in Russian]. Nauka, Moscow.
Kosakowski, P., Kotarba, M.J., Piestrzyński, A., Shogenova, A., Więcław, D., 2016. Petroleum source rock evaluation of the Alum and Dictyonema Shales (Upper Cambrian–Lower Ordovician) in the Baltic Basin and Podlasie Depression (eastern Poland). Int. J. Earth Sci. 106, 743–761.
Kralik, M., 1982. Rb -Sr age determinations on carbon ate rocks of the Carpentarian McArthur Basin, North ern Territory, Australia. Precambrian Res. 18 (157), 170.
Krzywiec, P., 2006. Triassic-Jurassic Evolution of the Pomeranian Segment of the Mid-Polish Trough—Basement Tectonicsand Subsidence Patterns. Geol. Q. 50, 139–150.
Kukla, P.A. et al., 2012. Pressure Generation and Deflation Mechanisms in Deeply Buried Intra-Salt Reservoirs of the Late Neoproterozoic to Early Cambrian South Oman Salt Basin, Search and Discovery Article #41112 (2012).
Kumar, A., Hakimi, M.H., Singh, A.K., Abdullah, W.H., Zainal Abidin, N.S., Rahim, A., Mustapha, K.A., Yelwa, N.A., 2022. Geochemical and Petrological Characterization of the Early Eocene Carbonaceous Shales: Implications for Oil and Gas Exploration in the Barmer Basin, Northwest India. ACS Omega 7, 42960–42974.
Kumar, D., Sharma, R., Maurya, A.S., Pandey, R., 2024. Petroleum source-rock characterization and the depositional environment of Kimmeridgian–Tithonian sequences, Jaisalmer Basin, western Rajasthan, India. Pet. Geosci. 30.
Kumar, S., Ojha, K., Bastia, R., Garg, K., Das, S., Mohanty, D., 2017. Evaluation of Eocene source rock for potential shale oil and gas generation in north Cambay Basin, India. Mar. Pet. Geol. 88, 141–154.
Kumar, S., Das, S., Bastia, R., Ojha, K., 2018. Mineralogical and morphological characterization of Older Cambay Shale from North Cambay Basin, India: Implication for shale oil/gas development. Mar. Pet. Geol. 97, 339–354.
Kuske, T., Hall, L., Hill, A., Troup, A., Edwards, D., Boreham, C., Buckler, T., 2015. Source Rocks of the Cooper Basin. AAPG Search Discov. 549-549.
Kuuskraa, V., Stevens, S., Leeuwen, T.V., Moodhe, K., 2011. World Shale Gas Resources: An Initial Assessment of 14 Regions Outside the United States. U. S Dep. Energy, Wash., DC 20585.
Laer, P.V., Leyrer, K., Povstyanova, M., Baig, M.Z., Makarychev, G., Marzooqi, H.Al, 2019. Cenomanian Shilaif Unconventional Shale Oil Potential in Onshore Abu Dhabi, UAE. Unconventional Resources Technology Conference. Denver, Colorado.
Lai, X., Chen, X., Wang, Y., Dai, D., Dong, J., Liu, W., 2022. Feasibility Analyses and Prospects of CO2 Geological Storage by Using Abandoned Shale Gas Wells in the Sichuan Basin. China Atmosphere 13, 1698.
Laksono, F.A.T., Kusdiantoro, F., Kovács, J., Purnomo, W.H., 2021. Analisis Kematangan Batuan Induk Hidrokarbon di Formasi Naintupo, Sub-Cekungan Tarakan, Provinsi Kalimantan Utara. TEKNIK 42, 260–272.
Lan, X.D., Zhu, Y.M., Ran, Q.G., Cheng, H.G., Zhu, C.J., 2009. Study on Hydrocarbon-Generation Evolution and Prediction of Favorable Exploration Areas in Gucheng Area of Tarim Basin. In: The 6th International Conference on Mining Science & Technology, 1. Procedia Earth and Planetary Science Letters, pp. 989–994.
Langford, F.F., Blanc-Valleron, M.-M., 1990. Interpreting Rock-Eval Pyrolysis Data Using Graphs of Pyrolizable Hydrocarbons vs. Total Organic Carbon. AAPG Bull. 74, 799–804.
Laughrey, C.D., 2022. Produced gas and condensate geochemistry of the Marcellus Formation in the Appalachian Basin: Insights into petroleum maturity, migration, and alteration in an unconventional shale reservoir. Minerals 12, 1222.
Lazreq, N., Kumar, R., Al Shamisi, E., Al Marzouqi, H., Al Dahmani, F., Al Hashmi, A.A., Luo, Y., Povstyanova, M., Bukovac, T., Muhannad, A.K., 2020. Tight Oil from Shale Rock in UAE: A Success Story of Unconventional Fracturing. Pap. Presente Abu Dhabi Int. Pet. Exhib. Conf.

Lee, D.S., Herman, J.D., Elsworth, D., Kim, H.T., Lee, H.S., 2011. A critical evaluation of unconventional gas recovery from the marcellus shale, northeastern United States. KSCE J. Civ. Eng. 15, 679.
Legarreta, L., Villar, H.J., 2011. Geological and Geochemical Keys of the Potential Shale Resources, Argentina Basins. Am. Assoc. Pet. Geol., Search Discov. Artic.
Lei, J., Pan, B., Guo, Y., Fan, Y., Xue, L., Deng, S., Zhang, L., Ruhan, A., 2021. A comprehensive analysis of the pyrolysis effects on oil shale pore structures at multiscale using different measurement methods. Energy 227, 120359.
Leventhal, J.S., 1991. Comparison of organic geochemistry and metal enrichment in two black shales: Cambrian Alum Shale of Sweden and Devonian Chattanooga Shale of United States. Mineral. Depos. 26, 104–112. https://doi.org/10.1007/BF00195256.
Li, G., Li, Zong, Li, D., Liu, H., Yan, S., Su, G., Tian, X., 2023. Continuous extensional uplift controls the Silurian structural evolution of the Sichuan Basin, southwest China. Mar. Pet. Geol. 155, 106383.
Li, M., Ma, X., Li, Z., Jiang, Q., Wu, S., 2018. Emerging Shale Oil Plays in Hypersaline Lacustrine Qianjiang Formation, Jianghan Basin. Cent. China Unconv. Resour. Technol. Conf.
Li, P., Jiang, Z., Zheng, M., Bi, He, Chen, L., 2016. Estimation of shale gas adsorption capacity of the Longmaxi Formation in the Upper Yangtze Platform, China. J. Nat. Gas. Sci. Eng. 34, 1034–1043.
Li, Qiqi, Xu, Shang, Zhang, Liang, Chen, Fengling, Wu, Shiqiang, Bai, Nan, 2022. Shale Oil Enrichment Mechanism of the Paleogene Xingouzui Formation, Jianghan Basin, China. Energies 15, 4038.
Li, X., Chen, S., Wang, X., Zhu, Y., Chang, M., Uwamahoro, C., 2019. Pore Structure Heterogeneity of the Xiamaling Formation Shale Gas Reservoir in the Yanshan Area of China: Evaluation of Geological Controlling Factors. Acta Geol. Sin. 93, 588–603.
Li, Z., Zhang, J., Gong, D., Tan, J., Liu, Y., Wang, D., Li, P., Tong, Z., Niu, J., 2020. Gas-bearing property of the Lower Cambrian Niutitang Formation shale and its influencing factors: A case study from the Cengong block, northern Guizhou Province, South China. Mar. Pet. Geol. 120, 104556.
Liang, C., Wang, J., Cao, Y., Xiong, Z., Liu, K., Hao, F., Han, W., 2024. Authigenic calcite in shales: Implications for tracing burial processes and diagenetic fluid evolution in sedimentary basins. Earth-Sci. Rev. 258, 104935.
Liang, Z., Jiang, Z., Li, Z., Song, Y., Gao, F., Liu, X., Xiang, S., 2021. Nanopores Structure and Multifractal Characterization of Bulk Shale and Isolated Kerogen—An Application in Songliao Basin, China. Energy Fuels 35, 5818–5842.
Lin, R., Saller, A., Dunham, J., Teas, P., Kacewicz, M., Curiale, J., & Decker, J., 2005. Source, generation, migration and critical controls on oil versus gas in the deepwater Kutei petroleum system.
Lindquist, S.J., 1999. The Timan-Pechora Basin Province of northwest Arctic Russia Domanik - Paleozoic total petroleum system. Denver, Colo: U.S. Dept. of the Interior, U.S. Geological Survey,
Lindsay, J., 2000. South Australia Source Rock Potential and Algal-Matter Abundance, Cooper Basin, South Australia. South Aust. Dep. Prim. Ind. Resour., Rep. Book 2000/00032 172.
Lipski, P., 2001. Geology and Hydrocarbon Potential of the Jurassic-Cretaceous Maryborough Basin. Petroleum Exploration Society of Australia (PESA) Eastern Australasian Basins Symposium. Melborne 25–28.
Liu, B., Shi, J., Fu, X., Lyu, Y., Sun, X., Gong, L., Bai, Y., 2018. Petrological characteristics and shale oil enrichment of lacustrine fine-grained sedimentary system: A case study of organic-rich shale in first member of Cretaceous Qingshankou Formation in Gulong Sag, Songliao Basin, NE China. Pet. Explor. Dev. 45, 884–894.
Liu, B., Gao, Y., Liu, K., Liu, J., Ostadhassan, M., Wu, T., Li, X., 2021. Pore structure and adsorption hysteresis of the middle Jurassic Xishanyao shale formation in the Southern Junggar Basin, northwest China. Energy Explor. Exploit. 39, 761–778.
Liu, D., Li, Z., Jiang, Z., Zhang, C., Zhang, Z., Wang, J., Yang, D., Song, Y., Luo, Q., 2019. Impact of laminae on pore structures of lacustrine shales in the southern Songliao Basin, NE China. J. Asian Earth Sci. 182, 103935.
Liu, Q., Jin, Z., Zhou, B., Zhu, D., Meng, Q., 2017. Main factors for large accumulations of natural gas in the marine carbonate strata of the Eastern Sichuan Basin, China. J. Nat. Gas. Geosci. 2, 81–97.
Liu, S., Zhao, S., Yang, X., Zhang, J., Yin, M., Meng, Q.A., et al., 2023. Tri-in-One" Accumulation Model of Lithologic Reservoirs in Continental Downfaulted Basins: A Case Study of the Lithologic Reservoir of Nantun Formation in Tanan Sag. Mong. Process. 11, 2352.
Liu, X., Zhang, J., Bai, Y., Zhang, Y., Zhao, Y., Cheng, X., Lv, J., Yang, H., Liu, J., 2020. Pore Structure Petrophysical Characterization of the Upper Cretaceous Oil Shale from the Songliao Basin (NE China) Using Low-Field NMR. Journal of Spectroscopy 1–11. Artic. ID 9067684.
Logan, P., Duddy, I., 1998. An Investigation of the Thermal History of the Ahnet and Reggane Basins, Central Algeria, andthe Consequences for Hydrocarbon Generation and Accumulation. In: Macgregor, D.S., Moody, R.T.J., Clark-Lowes, D.D. (Eds.), Petroleum, Geology of North Africa, 132. Special Publication, Geological Society, London, pp. 131–155.
Lopatin, N.V., Zubairaev, S.L., Kos, I.M., Emets, T.P., Romanov, E.A., Malchikhina, O.V., 2003. Unconventional oil accumulations in the Upper Jurassic Bazhenov black shale formation, West Siberian Basin: A self-sourced Reservoir System. J. Pet. Geol. 26, 225–244.
Loucks, R.G., Ruppel, S.C., 2007. Mississippian Barnett Shale: lithofacies and depositional setting of a deep-water shale-gas succession in the Fort Worth Basin, Texas. Am. Assoc. Pet. Geol. Bull. 91, 579–601.
Loucks, R.G., Reed, R.M., Ruppel, S.C., Hammes, U., 2010. Preliminary classification of matrix pores in mudrocks. Gulf Coast Assoc. Geol. Soc. Trans. 60, 435–441.
Loucks, R.G., Reed, R.M., Ruppel, S.C., Hammes, U., 2012. Spectrum of pore types and networks in mudrocks and a descriptive classification for matrix-related mudrock pores. Am. Assoc. Pet. Geol. Bull. 96, 1071–1098.
Lüning, S., J, Craig, D.K., Loydell, P., Storch, W.R., Fitches, B., 2000. Lowermost Silurian 'hot' shales in North Africa and Arabia: regional distribution and depositional model. Earth-Sci. Rev. 49, 121–200.
Lüning, S., Loydell, D.K., Storch, P., Shahin, Y., Craig, J., 2006. Origin sequence stratigraphy and depositional environment of an upper Ordovician (Hirnantian) deglacial black shale, Jordan. Discussion. Palaeogeogr., Palaeoclimatol., Palaeoecol. 230, 352–355.
Luo, Q., Gong, L., Qu, Y., Zhang, K., Zhang, G., Wang, S., 2018. The tight oil potential of the Lucaogou Formation from the southern Junggar Basin, China. Fuel 234, 858–871.
Lyu, Q., Tan, J., Li, L., Ju, Y., Busch, A., Wood, D.A., Ranjith, P.G., Middleton, R., Shu, B., Hu, R., 2021. The role of supercritical carbon dioxide for recovery of shale gas and sequestration in gas shale reservoirs. Energy Environ. Sci. 14, 4203–4227.
Ma, L., Taylor, K.G., Dowey, P.J., Courtois, L., Gholinia, A., Lee, P.D., 2017. Multi-scale 3D characterisation of porosity and organic matter in shales with variable TOC content and thermal maturity: Examples from the Lublin and Baltic Basins, Poland and Lithuania. Int. J. Coal Geol. 180, 100–112.
Ma, X., Li, M., Pang, X., Wei, X., Qian, M., Tao, G., Liu, P., Jiang, Q., Li, Z., Zhao, Y., Wu, S., 2019. Paradox in bulk and molecular geochemical data and implications for hydrocarbon migration in the inter-salt lacustrine shale oil reservoir, Qianjiang Formation, Jianghan Basin, central China. Int. J. Coal Geol. 209, 72–88.
Ma, X., Wen, D.G., Li, X.F., Diao, Y.J., Dong, H.H., Cao, W., Yin, S.G., Zhang, Y.M., 2021. Potential assessment of CO_2 geological storage based on injection scenario simulation: A case study in eastern Junggar Basin. J. Groundw. Sci. Eng. 9, 279–291.
Macgregor, D.S., 1996. The hydrocarbon systems of North Africa: Marine and Petroleum Geology 13, 329–340.
Madisheva, R.K., Portnov, V.S., Amangeldiyeva, G.B., Demeuova, A.B., Seitkhaziyev, Y. S., Azhgaliev, D.K., 2024. Geochemical prerequisites for the formation of oil and gas accumulation zones in the South Turgay basin, Kazakhstan. Acta Geochim. 43, 520–534.
Mahesar, A.A., Shar, A.M., Ali, M., Tunio, A.H., Uqailli, M.A., Mohanty, U.S., Akhondzadeh, H., Iglauer, S., Keshavarz, A., 2020. Morphological and petro physical estimation of Eocene tight carbonate formation cracking by cryogenic liquid nitrogen; a case study of Lower Indus basin, Pakistan. J. Pet. Sci. Eng. 192, 107318.
Mahmood, M.F., Ahmad, Z., Ehsan, M., 2018. Total organic carbon content and total porosity estimation in unconventional resource play using integrated approach through seismic inversion and well logs analysis within the Talhar Shale. Pak. J. Nat. Gas. Sci. Eng. 52, 13–24.
Mani, D., Patil, D.J., Dayal, A.M., Prasad, B.N., 2015. Thermal maturity, source rock potential and kinetics of hydrocarbon generation in Permian shales from the Damodar Valley basin, Eastern India. Mar. Pet. Geol. 66, 1056–1072.
Mani, D., Kalpana, M.S., Patil, D.J., Dayal, A.M., 2017. Organic Matter in Gas Shales: Origin, Evolution, and Characterization. In: Mohan, A., Mani, D.D. (Eds.), Shale Gas Exploration and Environmental and Economic Impacts. Elsevier, Amsterdam, pp. 25–54. ISBN: 978-0-12-809573-7.
Mani, D., Ratnam, B., Kalpana, M.S., Patil, D.J., Dayal, A.M., 2016. Elemental and organic geochemistry of Gondwana sediments from the Krishna–Godavari Basin, India. Geochemistry 76, 117–131.
Marshall, S.K., Fontaine, K., Kilgour, P.L., Lewis, S.J., 2015. Regional Hydrogeological Characterisation of the Maryborough Basin, Queensland. Tech. Rep. Natl. Collab. Framew. Reg. Hydrogeol. Proj., Geosci. Aust. ISBN 978-1-925124-73-6.
Martinez, M.A., Prámparo, M.B., Quattrocchio, M.E., Zavala, C.A., 2008. Depositional Environments and Hydrocarbon Potential of the Middle Jurassic Los Molles Formation. NeuquéN. Basin Argent.: Palynofacies Org. Geochem. Data. Rev. Geol. ógica De. Chile 35, 279–305.
Martinsen, O.J., Collinson, J.D., Holdsworth, B.K., 1995. Millstone Grit Cyclicity Revisited. II: Sequence Stratigraphy and Sedimentary Responses to Changes of Relative Sea-level. Sedimentary Facies Analysis Blackwell Publishing Ltd, pp. 305–327. ⟨https://doi.org/10.1002/9781444304091.ch13⟩.
Maynard, J.R., Leeder, M.R., 1992. On the periodicity and magnitude of Late Carboniferous glacio-eustatic sea-level changes. J. Geol. Soc. 149, 303–311.
Mayol, J.C., Moridis, N., McVay, D.A., Lee, W.J., 2020. Assessment of Oil and Gas Resources in the Vaca Muerta Shale, Neuquén Basin. Argent. Pap. Presente SPE Lat. Am. Caribb. Pet. Eng. Conf., Virtual July 2020.
Mazumdar, A., Dewangan, P., J, M., Peketi, A., Khosla, V.R., Kocherla, M., Badesab, F., Joshi, R.K., Roxanne, P., Ramamurty, P.B., SM, K., Patil, D., Dayal, A., Ramprasad, T., Hawkesworth, C., Avanzinelli, R., 2009. Evidence of paleo-cold seep activity from the Bay of Bengal, offshore India. Geochem., Geophys., Geosystems 10, Q06005.
Mcmahon, T.P., Larson, T.E., Zhang, T., Shuster, M., 2024. Geologic characteristics, exploration and production progress of shale oil and gas in the United States: An overview. Pet. Explor. Dev. 51, 925–948.
Meinhold, G., Howard, J.P., Strogen, D., Kaye, M.D., Abutarruma, Y., Elgadry, M., Thusu, B., Whitham, A.G., 2013. Hydrocarbon source rock potential and elemental composition of lower Silurian subsurface shales of the eastern Murzuq Basin, southern Libya. Mar. Pet. Geol. 48, 224–246.
Meinhold, G., Howard, J., Abutarruma, Y., Thusu, B., Whitham, A.G., 2021. Mineralogical and geochemical changes in subsurface shales straddling the Ordovician–Silurian boundary in the eastern Kufra Basin, Libya. J. Afr. Earth Sci. 184, 104378.
Mendez, J., Lobo, C., Movil, R., Alcantara, C., Yegres, L. and Brown, J., 2023, June. Exploring La Luna Formation Unconventional Plays in the Maracaibo Lake Basin, Through 3D Modeling Based on Acoustic Seismic Inversion. In SPE/AAPG/SEG Unconventional Resources Technology Conference (p. D031S070R001). URTEC.

Mengjun, Yu, Weinthal, E., Dalia, P.E., Deshusses, M.A., Zou, C., Yunyan, N., Vengosh, A., 2016. Water Availability for Shale Gas Development in Sichuan Basin. China Environ. Sci. Technol., Am. Chem. Soc. A-I.
Mezzar, A., et al., 2024. Sweet Spots Identification: Geological and Engineering Integrated Shale Gas: A Case Study of Shale Gas Ahnet Basin Algeria. The Iraqi. Geol. J. 57, 162–190.
Michel, G., Coughlan, M., Arosio, R., Emery, A.R., Wheeler, A.J., 2023. Stratigraphic and palaeo-geomorphological evidence for the glacial-deglacial history of the last British-Irish Ice Sheet in the north-western Irish Sea. Quat. Sci. Rev. 300, 107909.
Mir, A., Khan, M.R., Wahid, A., Iqbal, M.A., Rezaee, R., Ali, S.H., Erdal, Y.D., 2023. Petroleum System Modeling of a Fold and Thrust Belt: A Case Study from the Bannu Basin, Pakistan. Energies 16, 4710.
Mishra, H.K., Cook, A.C., 1992. Petrology and Thermal Maturity of Coals in the Jharia Basin: Implications for Oil andGas Origins. Int. J. Coal Geol. 20, 277–313.
Mogali, P., Singh, A., Desai, B.G., 2024. Unlocking the hidden potential: Petrophysical analysis of adjoining basement reservoirs in the Cauvery Basin's Madanam Palaeo-High. J. Earth Syst. Sci. 133, 133.
Monti, L.J., Suarez, M., Thompson, A.R., Vega Velasquez, L., 2013. Modeling Vertical Multifractured Wells in Vaca Muerta Shale Oil Play. Argent. SPE Unconv. Resour. Conf. -USA.
Morabet, A.M., Bouchta, R., Jabour, H., 1998. An overview of the petroleum systems of Morocco. In: Macgregor, D.S., Moody, R.T.J., Clark-Lowes, D.D. (Eds.), Petroleum Geology of North Africa, 132. Geological Society, London, Special Publication, pp. 283–296.
Moretti, I., 2010. South Alamein Petroleum System (Western Desert, Egypt). Pet. Geosci. 16, 121–132.
Morozov, V.P., Jin, Z., Liang, X., Korolev, E.A., Liu, Q., Kolchugin, A.N., Eskin, A.A., Nizamova, A.V., Assumption, B.V., Liu, G., 2021. Comparison of source rocks from the Lower Silurian Longmaxi Formation in the Yangzi Platform and the Upper Devonian Semiluksk Formation in East European Platform. Energy Geosci. 2, 63–72.
Morse, J.W., Mackenzie, F.T., 1990. Geochemistry of Sedimentary Carbonates, 1st Edition, 48. Elsevier. ISBN: 9780444887818.
Mukherjee, S., 2015. Petroleum Geosciences: Indian Contexts. Springe Geol. ISBN 978-3-319-03119-4.
Mukherjee, S., Ansari, K., Raha, A., Biswas, M., Mazumder, S., 2025. Tectonics of Cauvery basin in onshore and offshore portions. Mar. Pet. Geol. 171, 107142.
Mukhopadhyay, G., Mukhopadhyay, S.K., Roychowdhury, M., Parui, P.K., 2010. Stratigr. Correl. Differ. Gondwana Basins India J. Geol. Soc. India 76, 251–266.
Mukhopadhyay, P., Prusty, B.K., Turlapati, V.Y., 2021. Source rock characterization and its influence on pore volumes in Lower Gondwana shale samples of Damodar Valley, India. J. Nat. Gas. Sci. Eng. 90, 103886.
Muntendam-Bos, A.G., et al., 2009. Inventory Non-Conventional Gas. TNO Rep. TNO-034-UT-2009-00774/B, 03 September.
Musu, J.T., Widarsono, B., Ruswandi, A., Sutanto, H., Purba, H., 2015. Determination of Shale Gas Potential of North Sumatra Basin: An Integration of Geology, Geochemistry, Petrophysics and Geophysics Analysis. Sci. Contrib. Oil Gas. 38 (3), 193–212.
Nagendra, R., Nallapa Reddy, A., 2017. Major geologic events of the Cauvery Basin. India their Correl. Glob. Signat. – A Rev. J. Palaeogeogr. 6, 69–83.
Nanda, J., Shukla, K.M., Lall, M.V., Yadav, U.S., Kumar, P., 2019. Lithofacies characterization of gas hydrate prospects discovered during the National Gas Hydrate Program expedition 02, offshore Krishna-Godavari Basin, India. Mar. Pet. Geol. 108, 226–238.
Narasimha Chari, M.V., Sahu, J.N., Banerjee, B., Zutshi, P.L., Chandra, K., 1995. Evolution of the Cauvery basin, India from subsidence modelling. Mar. Pet. Geol. 12, 667–675.
Narkiewicz, K., Narkiewicz, M., 2008. The Mid-Frasnian Subsidence Pulse in the Lublin Basin (SE Poland): SedimentaryRecord, Conodont Biostratigraphy and Regional Significance. Acta Geol. Pol. 58, 287–301.
Nie, H., Li, P., Ding, J., 2024. Enrichment characteristics and exploration potential of the Permian marine shale gas in the Wujiaping Formation, Sichuan Basin, SW China. Geol. J. 59, 965–979.
Nolte, S., Geel, C., Amann-Hildenbrand, A., Krooss, B.M., Littke, R., 2019. Petrophysical and geochemical characterization of potential unconventional gas shale reservoirs in the southern Karoo Basin, South Africa. Int. J. Coal Geol. 212, 103–249.
Noon, S., Harrington, J., Darman, H., 2003. The Tarakan basin, East Kalimantan: proven Neogene fluvio-deltaic, prospective deep-water and Paleogene plays in a regional stratigraphic context. URL: ⟨https://archives.datapages.com/data/ipa/data/029/029001/1_ipa029aipa03-g-136.htm⟩.
Nurbekova, R., Smirnova, N., Goncharev, I., Sachsenhofer, R.F., Hazlett, R., Smirnov, G., Yensepbayev, T., Mametov, S., Fustic, M., 2023. High-quality source rocks in an underexplored basin: The upper Carboniferous–Permian succession in the Zaysan Basin (Kazakhstan). Int. J. Coal Geol. 272, 104254.
Nutall, B.C., Drahovzal, J.A., Eble, C.F., Bustin, R.M., 2009. Regional assessment of suitability of organic-rich gas shales for carbon sequestration: An example from the Devonian shales of the Illinois and Appalachian Basins, Kentucky. In: Grobe, M., Pashin, J.C., Dodge, R.L. (Eds.), Carbon dioxide sequestration in geological media—State of the science, 59. AAPG Studies in Geology, pp. 173–190.
O'Brien N.R., Slatt R.G. 1990. Argillaceous Rocks Atlas. Springer Science + Business Media. New York. ISBN: 978-1-4612-3422-7.
Ostadhassan M., Liu K., Li C., Khatibi S. 2018. Fine Scale Charzcterization of Shale Reservoirs: Methods and Challenges. ISBN: 978-3-319-76086-5.
Ouadfeul, S., Aliouane, L., 2016b. Total organic carbon estimation in shale-gas reservoirs using seismic genetic inversion with an example from the Barnett Shale. Lead. Edge 35, 790–794.
Ouadfeul, S., Aliouane, L., 2016a. Shale gas lithofacies classification and gas contentprediction using artificial neural network. In: ECMOR XV-15th European Conferenceon the Mathematics of Oil Recovery, August.
Ozdemir, A., Karataş, A., Palabiyik, Y., Yaşar, E., Sahinoglu, A., 2020. Oil and gas exploration in Seferihisar Uplift (Western Turkey) containing an operable-size gold deposit: Geochemical evidence for the presence of a working petroleum system. Geomech. Geophys. Geo-Energy Geo-Resour. 6, 30.
Padhy, P.K., Das, S.K., Kumar, A., 2013. Krishna-Godavari Continental Rift Basin: Shale Gas and Oil Play Systems. 10th Biennial International Conference & Exposition. Kochi.
Page, A.A., Zalasiewicz, J.A., Williams, M., Popov, L.E., 2007. Were transgressive black shales a negative feedback modulating glacioeustacy in the Early Palaeozoic icehouse? In: Williams, M., Haywood, A., Gregory, F.J., Schnmidt, D.N. (Eds.), Deep-Time perspectives on Climate Change: Marrying the Signal from Computer Models and Biological Proxies. Special Publication of the Geological Society of London, The Micropalaeontological Society, pp. 123–156.
Palci, F., Fraser, A.J., Neumaier, M., Goode, T., Parkin, K., Wilson, T., 2020. Shale oil and gas resource evaluation through 3D basin and petroleum systems modelling. Acase Study East Midl., Onshore Uk. Pet. Geosci. 26, 525–543.
Pang, H., Pang, X., Dong, L., Zhao, X., 2018. Factors impacting on oil retention in lacustrine shale: Permian Lucaogou Formation in Jimusaer Depression, Junggar Basin. J. Pet. Sci. Eng. 163, 79–90.
Paredes, J.M., Foix, N., Piñol, F.C., Nillni, A., Allard, J.O., Marquillas, R.A., 2008. Volcanic and Climatic Controls on Fluvial Style in a High-Energy System: The Lower Cretaceous MatasieteFormation, Golfo San Jorge Basin, Argentina. Sediment. Geol. 202, 96–123.
Parkhomchik, L., Syrlybayeva, B., 2016. Evaluation of the Shale Gas Potential in Kazakhstan. Shale Gas: Ecology, Politics, Economy by Zhiltsov, S. S. Springer., pp. 193–204
Parsons, M.G., Zagaar, A.M., Curry, J.J., 1980. Hydrocarbon Occurrences in the Sirte Basin. Libiya. Worldw. Pet. Prov. Facts Princ. World Pet. Occur. — Mem. 6, 723–732.
Passey, Q.R., Bohacs, K.M., Esch, W.L., Klimentidis, R., Sinha, S., 2010. From oil-prone source rock to gas-producing shale reservoir: geologic and petrophysical characterization of unconventional shale-gas reservoirs. Chinese Petroleum Society/ Society of Petroleum Engineers International Oil and Gas Conference and Exhibition, Beijing. SPE Paper 131350.
Paterson, D.W., Bachtiar, A., Bates, J.A., Moon, J.A., & Surdam, R.C. (1997). Petroleum system of the Kutei basin, Kalimantan, Indonesia.
Patricia, V., 1996. Palynology of Pozo D-129 Formation in the San Jorge Gulf Basin, Lower Cretaceous, Patagonia, Argentina. Congr. Bras. De. Geol. 7, 423–426.
Pearce, J.M., Ren, M., Li, W., Chen, S.G., Li, Vincent, C.J., Kirk, K.L., 2011. CO2 storage capacity estimates for selected regions of China - results from the China-UK Near Zero Emissions. Coal (NZEC) Initiative. Energy Procedia 4, 6037–6044.
Peng, J., Li, L., Du, C., Liu, Xu, Zhu, J., Liang, S., Qiu, Q., Wang, D., 2023. Hydrocarbon generation and expulsion modeling of different lithological combination source rocks from the Funing Formation in the Subei Basin. Front. Earth Sci. 10, 1071466.
Peng, S., Shan, H., Li, Y., Yang, Z., Zhong, Z., 2013. Feasibility of CO2 Geological Storage in the Xingou Oil Field, Jianghan Basin, China. Procedia Earth Planet. Sci. 7, 669–672.
Peng, Y., Pan, J., An, X., 2022. A preliminary study on the geological conditions and indexes for the accumulation of shale gas in the marine-continental transitional facies sediments in the South North China Basin. Front. Earth Sci. 10, 985302.
Peters, J., Das, K.C., 2008. In: Kapoor, P.N. (Ed.), Exploration of Kerala-Konkan Basin: The Way Ahead, 2. Association of Petroleum Geologists Bulletin, pp. 11–24.
Peters, K., Cassa, M., 1994. Applied Source Rock Geochemistry. In: Magoon, L.B., Dow, W.G. (Eds.), The PetroleumSystem from Source to Trap, 60. AAPG Memoir, pp. 93–117.
Petersen, H.I., Sanei, H., Gelin, F., Loustaunau, E., Despujols, V., 2020. Kerogen composition and maturity assessment of a solid bitumen-rich and vitrinite-lean shale: Insights from the Upper Jurassic Vaca Muerta shale, Argentina. Int. J. Coal Geol. 229, 103575.
Petrusak, R., Riestenberg, D., Goad, P., Schepers, K., Pashin, J., Esposito, R., Trautz, R., 2009. World class CO2 sequestration potential in saline formations, oil and gas fields, coal, and shale: the US southeast regional carbon sequestration partnership has it all. SPE International Conference on CO2 Capture. Storage, and Utilization. SPE-126619.
Pettijohn, F.J., 2004. Sedimentary Rocks. CBS Publishers, New Delhi. ISBN: 81-239-0875-X.
Pittion, J.L., Arbe, H.A., 1999. Sistemes Petroleros de la Cuenca Austral.IV CongresoExploracion y Desarrollo de Hidrocarburos, Mar del Plata, Argentina. Actas I 239–262.
Playford, P.E., Cockbain, A.E., Low, G.H., 1976. Geology of the Perth Basin, Western Australia. Bull. 124. Geol. Surv. West. Aust., Perth.
Pommer, M., Milliken, K., 2015. Pore types and pore-size distributions across thermal maturity. Eagle Ford. Form., South. Tex. Am. Assoc. Pet. Geol. Bull. 99, 1713–1744.
Poprawa, P., 2010. Shale gas potential of the lower palaeozoic complex in the baltic and Lublin-Podlasie basins (Poland). Prz. Geol. 58, 226–249.
Poprawa, P., 2015. Lower Paleozoic Oil and Gas Shales in the Baltic-Podlasie-Lublin Basin (Poland). Eur. Reg. Conf. Exhib., Lisbon, Port.
Potter, P.E., Maynard, B.J., Pryor, W.A., 1980. Sedimentology of Shale. Springer-Verlag New York Inc. Print. USA. ISBN 0-387-90430-1.
Pozo, M., Pino, D., Bessieres, D., 2017. Effect of thermal events on maturation and methane adsorption of Silurian black shales (Checa, Spain). Appl. Clay Sci. 136, 208–218.

Prischepa, O.M., Bazhenova, T.K., Bogatskii, V.I., 2011. Petroleum systems of the Timan–Pechora sedimentary basin (including the offshore Pechora Sea). Russ. Geol. Geophys. 52, 888–905.
Prost, G., 2004. Tectonics and hydrocarbon systems of the East Gobi basin, Mongolia. AAPG Bull. 88, 483–513.
Putun, E., Akar, A., Ekinci, E., Bartle, K., 1988. Chemistry and geochemistry of Turkish oil shale kerogens. Fuel 67, 1106–1110.
Putzer, H., 1984. The geological evolution of the Amazon basin and its mineral resources. In: Sioli, H. (Ed.), The Amazon. Monographiae Biologicae, 56. Springer, Dordrecht. ISBN: 978-94-009-6542-3.
Qi, Z., 2002. Conodont Color Alteration Index (CAI) Maps of Cambrian Through Triassic fromthe Lower Yangtze Region in Jiangsu East China and their Implications. Acta Micropaleontol. Sin. 19, 63–75.
Qian, J., Yin, L., Wang, J., Li, S., Han, F., He, Y., 2011. Oil shale-supplementary energy of petroleum. Beijing. China Petrochem. Press.
Qiao, J., Liu, L., Shen, B., Shang, X., 2019. Geologic and geochemical characteristics of the Cambrian marine shale in the Tarim Basin of China and their implication for the prediction of shale-gas resources. Interpretation 7, T657–T669.
Qiu, N.S., Zhang, Z.H., Xu, E.S., 2008. Geothermal Regime and Jurassic Source Rock Maturity ofthe Junggar Basin, Northwest China. J. Asian Earth Sci. 31, 464–478.
Qu, Y., Sun, W., Guo, S., Shao, S., Lv, X., 2019. A Gas Content Calculation Model for Terrestrial Shales in the Kuqa Depression, the Tarim Basin, Western China. Interpretation 7, 1–50.
Quadri, Viqar-Un-Nisa, Shuaib, S., 1968. Hydrocarbon Prospects of Southern Indus Basin, Pakistan. AAPG Bull. 70, 730–747.
Quesada, S., Dorronsoro, C., Robles, S., Chaler, R., Grimalt, J.O., 1997. Geochemical correlation of oil from the Ayoluengo field to Liassic black shale units in the southwestern Basque-Cantabrian Basin (northern Spain). Org. Geochem. 27, 25–40.
Rahmani, A., Kaced, M., Arab, M., 2012. The Potential of Shale Gas Plays in Algeria. Sonatrach Amont/InternationalGas Union Shale Gas Workshop, Oran, Algeria, February.
Raju, D.S.N., 2018. Paleogene stratigraphy of India: an overview. In: Bajpai, S., et al. (Eds.), The Indian Paleogene. Springer, pp. 1–89.
Ramana, M.V., Ramprasad, T., Paropkari, A.L., Borole, D.V., Ramalingeswara Rao, B., Karisiddaiah, S.M., Desa, M., Kocherla, M., Joao, H.M., Lokabharati, P., Gonsalves, Maria-Judith, Pattan, J.N., Khadge, N.H., Prakash Babu, C., Sathe, A.V., Kumar, P., Sethi, A.K., 2009. Multidisciplinary investigations exploring indicators of gas hydrate occurrence in the Krishna-Godavari basin offshore, east coast of India. Geo-Mar. Lett. 2, 25–38.
Ramirez-Corredores, M.M., 2017. Chapter 1 - Unconventional Oils. Editor(s): Maria Magdalena Ramirez-Corredores. The Science and Technology of Unconventional Oils. Academic Press, pp. 1–40. ISBN 9780128012253.
Ramsbottom, W.H.C., 1979. Rates of transgression and regression in the Carboniferous of NW Europe. J. Geol. Soc. 136, 147–153. https://doi.org/10.1144/gsjgs.136.2.0147.
Ramseyer, K., Amthor, J.E., Matter, A., Pettke, T., Wille, M., Fallick, A.E., 2013. Primary silica precipitate at the Precambrian/Cambrian boundary in the South Oman Salt Basin, Sultanate of Oman. Mar. Pet. Geol. 39, 187–197.
Rani, S., Prusty, B.K., Pal, S.K., 2020. Characterization of shales from Damodar valley coalfields for CH4 recovery and CO2 sequestration. Environ. Technol. Innov. 18, 100739.
Rao, G.N., 2001. Sedimentation, stratigraphy, and petroleum potential of Krishna-Godavari basin, East Coast of India. AAPG Bull. 85, 1623–1643.
Raseroka, A.L., 2009. Natural Gas and Conventional Oil Potential in South Africa's Karoo Basin.AAPG International Conference and Exhibition, Rio de Janeiro.
Reynolds, S.D., Mildren, S.D., Hillis, R.R., Meyer, J.J., 2006. Constraining Stress Magnitudes Using Petroleum Exploration Data in the Cooper-Eromanga Basins, Australia. Tectonophysics 415, 123–140.
Rezouga, N., Belhaj Mohamed, A., Saidi, M., Bouazizi, I., 2012. Assessment of Unconventional shale Reservoir, The Fegaguira Fm, Chotts Basin. Tunis. North Afr. Tech. Conf. Exhib. https://doi.org/10.2118/150830-ms.
Rio, J.C.D., Garcia-Molla, J., Gonzalez-Vila, F.J., Martin, F., 1994. Composition and origin of the aliphatic extr actable hydrocarbons in the Puertollano (Spain) oil shale. Org. Geochem. 21, 897–909.
Rippen, D., Littke, R., Bruns, B., Mahlstedt, N., 2013. Organic geochemistry and petrography of Lower Cretaceous Wealden black shales of the Lower Saxony Basin: The transition from lacustrine oil shales to gas shales. Org. Geochem. 63, 18–36.
Rivard, C., Bordeleau, G., Lavoie, D., Lefebvre, R., Ladevèze, P., Duchesne, M.J., Séjourné, S., Crow, H., Pinet, N., Brake, V., Bouchedda, A., Gloaguen, E., Ahad, J.M. E., Malet, X., Aznar, J.C., Malo, M., 2018. Assessing potential impacts of shale gas development on shallow aquifers through upward fluid migration: A multi-disciplinary approach applied to the Utica Shale in eastern Canada. Mar. Pet. Geol. 100, 466–483.
Rocha, G.O., Da, A., Jeancarlo, P., Dos, A., Jailson, B., 2015. De Energy trends and the water-energy binomium for Brazil. An. da Acad. Bras. De. Ciências 87, 569–594.
Rodriguez, J.F.R., Littke, R., 2001. Petroleum Generation and Accumulation in the Golfo SanJorge Basin. Argent.: A Basin Model. Study Mar. Pet. Geol. 995–1028.
Romero-Sarmiento, M.F., et al., 2013. Quantitative evaluation of TOC, organic porosity and gas retention distribution in a gas shale play using petroleum system modeling: Application to the Mississippian Barnett Shale. Mar. Pet. Geol. 45, 315–330.
Romero-Sarmiento, M.-F., Pillot, D., Letort, G., Lamoureux-Var, V., Beaumont, V., Huc, A.-Y., Garcia, B., 2015. New Rock-Eval Method for Characterization of Unconventional Shale Resource Systems. Oil Gas. Sci. Technol. – Rev. D. `IFP Energ. Nouv. 71, 37.
Roussel, A., Cui, X., Summons, R.E., 2020. Biomarker stratigraphy in the Athel Trough of the South Oman Salt Basin at the Ediacaran Cambrian Boundary. Geobiology 18, 663–681.
Ryacudu, R., Sjahbuddin, 1994. Tampur Formation, the Forgotten Objective in the North Sumatra Basin? Proc. Pet. Assoc., 23rd Annu. Conv.
Sahai, R., 2022. Field Development and asset management. Chapter 1. In: Moghanloo, R. G. (Ed.), Unconventional Shale Oil Development. Gulf Professional Publishing, Cambridge, pp. 1–31. ISBN: 978-323-90185-7.
Sahoo, M., Gogoi, K.D., 2010. In: Kapoor, P.N. (Ed.), Geologic controls on Sequence Stacking and Architecture of Eocene SiliciclasticDeposits in Upper Assam Foreland Basin, India, 6. Association of Petroleum Geologists Bulletin, pp. 19–32.
Sain, K., Rai, M., Sen, M.K., 2014. A review on shale gas prospect in Indian sedimentary basin. J. Ind. Geophys. Union 18, 183–194.
Salvador, A., 1991. Plate 6: Cross Sections of the Gulf of Mexico Basin. The Geology of North America. Vol. J, The Gulf of Mexico Basin. The Geological Society of America.
Salygin, V., Guliev, I., Chernysheva, N., Sokolova, E., Toropova, N., Egorova, L., 2019. Global Shale Revolution: Successes, Challenges, and Prospects. Sustainability 11, 1627.
Samuelsson, J., Middleton, M.F., 1998. The Caledonian foreland basin in Scandinavia: Constrained by the thermal maturation of the Alum Shale. GFF 120, 307–314.
San Leon Energy, Quarterly Corporate Presentation, Q3 2012, 64 p.
Sari, A., Aliyev, S.A., 2005. Source Rock Evaluation of the Lacustrine Oil Shale Bearing Deposits: Göynük/Bolu, Turkey. Energy Sources 27, 279–298.
Satyana, A.H., 2022. The Neogene in Indonesia: The Most Important Period of Geologic Evolution and Formation of Petroleum Resources.
Scheeder, G., Ostertag-Henning, C. and Blumenberg, M., 2023, September. N-Alkyl and Phytanyl Toluenes as Markers for Maturity and Source of Petroleum in the Lower Saxony Basin (N Germany). pp. 1-2. European Association of Geoscientists & Engineers.
Schieber, J., Lazar, R., Bohacs, K., Klimentidis, B., Dumitrescu, M., Ottmann, J., 2016. An SEM study of porosity in the Eagle Ford Shale of Texas— Pore types and porosity distribution in a depositional and sequence stratigraphic context. In: Breyer, J.A. (Ed.), The Eagle Ford Shale: A renaissance in U.S, 110. oil production: AAPG Memoir, pp. 167–186.
Schlanger, S.O., Jenkyns, H.C., 1976. Cretaceous anoxic events: causes and consequences. Geol. Mijnb. 55, 179–184.
Schon, J.H., 2011. Physical properties of rocks: A workbook. Elsevier, Amsterdam.
Schulz, H.-M., Biermann, S., van Berk, W., Krüger, M., Straaten, N., Bechtel, A., Crabtree, S., 2015. From shale oil to biogenic shale gas: retracing organic-inorganic interactions in the Alum Shale (Furongian-Lower Ordovician) in southern Sweden. AAPG Bull. 99 (05), 927–956.
Scotese, C., 2016. A new global temperature curve for the Phanerozoic. Geological Society of America, Abstracts with Programs 48, Paper No. 74-31.
Searle, M., 2019. Geology of the Oman mountains, eastern Arabia. Springer. ISBN: 978-3-030-18452-0.
Seghedi, A., 2012. Palaeozoic Formations from Dobrogea and Pre-Dobrogea – An Overview. Turk. J. Earth Sci. 21, 669–721.
Selley, R.C., 1968. Near-shore marine and continental sediments of the Sirte basin, Libya. Q. J. Geol. Soc. 124, 419–460.
Selley, R.C., 1987. British Shale Gas Potential Scrutinized. Oil Gas. J. 85, 62–64.
Selley, R.C., 2005. UK shale-gas resources. In: Geological Society, 6. Geology Conference Series, London, Petroleum, pp. 707–714.
Selley, R.C., 2012. UK shale gas: The story so far. Mar. Pet. Geol. 31, 100–109.
Shalaby, M.R., Hakimi, M.H., Abdullah, W.H., 2012. Organic geochemical characteristics and interpreted depositional environment of the Khatatba Formation, northern Western Desert, Egypt. AAPG Bull. 96, 2019–2036.
Shalaby, M.R., Hakimi, M.H., Abdullah, W.H., 2014. Petroleum system analysis of the Khatatba Formation in the Shoushan Basin, north Western Desert. Egypt. Arab J. Geosci. 7, 4303–4320.
Shaldybin, M.V., Lopushnyak, Y.M., Goncharov, I.V., Wilson, M.J., Wilson, L., Mendis, B. G., 2017. The mineralogy of the clayey-silty siliceous rocks in the Bazhenov Shale Formation (Upper Jurassic) in the west Siberian Basin, Russia: The role of diagenesis and possible implications for their exploitation as an unconventional hydrocarbon reservoir. Appl. Clay Sci. 136, 75–89.
Sharma, K.P., 2002. A Study of Sediment Fluxes to the Coastal Zone in South Asia and Their Relationships to Human Activities, Project Report on APN Project on a Study of Nutrient. Sediment Carbon Fluxes Coast. Zone South Asia Their Relatsh. Hum. Act. 20.
Sharma, S., Agrawal, V., McGrath, S., Hakala, J.A., Lopano, C., Goodman, A., 2021. Geochemical controls on CO2 interactions with deep subsurface shales: implications for geologic carbon sequestration. Environ. Sci.: Process. Impacts 23, 1278–1300.
Sharma, V., Sircar, A., 2020. Petroleum geochemical characterization of the shales from tertiary formation of Western Cambay Basin, India. Int. J. Earth Sci. 109, 1529–1546.
Shaw, R., Mukherjee, S., 2022. The development of carbon capture and storage (CCS) in India: A critical review. Carbon Capture Sci. Technol. 2, 100036.
Siebels, A., Bults, A., Nolten, M., Wierenga, J., Doust, H., Verbeek, J., 2022. Potential for CO2 sequestration in saline formations in the western offshore Netherlands: A preliminary study—Expanding carbon capture and storage beyond depleted fields. AAPG Bull. 106 (9), 1855–1876.
Silva, M., Webster, M., Werlem, H., Darlly, R., Jefferson, F., 2015. Analysis Of The Hydrocarbon Maturation Windows Of The Amazon Basin. In: Brazilian Geophysical Society 14th International Congress of the Brazilian Geophysical Society & EXPOGEF, Rio de Janeiro.
Silva, P.N.K.De, Simons, S.J.R., Stevens, P., Philip, L.M., 2015. A comparison of North American shale plays with emerging non-marine shale plays in Australia. Mar. Pet. Geol. 67, 16–29.

Silverman, M., Ahlbrandt, T., 2011. Mesoproterozoic Unconv. Plays Beetaloo Basin, Aust.: World'S. Oldest Pet. Syst. Am. Assoc. Pet. Geol. (AAPG), Search Discov. Artic. # 10295.

Singh, A., Das, S.K., Sinha, A.D., Singh, P., 2018. Global shale gas and oil distribution with geological age vis-à-vis Indian Synrift Shale Sequences. ONGC Bull. 53, 149–162.

Singh, R.P., Rawat, S., Chandra, K., 1999. Hydrocarbon potential in Indian deep waters. Explor. Geophys. 30, 83–95.

Sliaupa, S., Sliaupiene, R., Zaludiene, G., Vaskaboinikava, T., Bibikava, A., Evstratenko, L., Kovkhuto, A., 2016. Prospects of Lithuanian Silurian shale gas. Balt. Sediment. Basin Oil Shale 33, 357–372.

Sliwa, T., Sapińska-Śliwa, A., Korzec, M., Gonet, A., Jaszczur, M., Ciepielowska, M., Gajdosz, A., 2021. Investigation of Old Exploration Boreholes in the Lublin Basin with Regard to Potential Rotary-Percussion Drilling of Shale Gas Wells. Energies 14, 1–21.

Smith, M.G., Bustin, R.M., 1995. Sedimentology of the Late Devonian and Early Mississippian Bakken Formation. Williston Basin Williston Basin Symp.

Smith, N., Turner, P., Williams, G., 2010. UK data and analysis for shale gas prospectivity. In: Geological Society, 7. Petroleum Geology Conference Series, London, pp. 1087–1098.

Smith, T., Kelman, A., Laurie, J., Nicoll, R., Carr, L., Hall, L., Edwards, D., 2013. An updated stratigraphic framework for the Georgina Basin. North. Territ. Qld. APPEA Conf., Brisb.

Soeder, D.J., 2010. The Marcellus Shale: Resources and Reservations. Eos, Trans. Am. Geophys. Union 91, 277–278.

Sohail, G.M., Hawkes, Christopher, D., Yasin, Q., 2020. An integrated petrophysical and geomechanical characterization of Sembar Shale in the Lower Indus Basin, Pakistan, using well logs and seismic data. J. Nat. Gas. Sci. Eng. 78, 103327.

Soldo, J., 2015. Shale Oil Play Exploration Delineation Using Rock Mechanics Template and Seismic Inversion Data, Vaca Muerta Formation, Neuquén Basin, Argentina. Proceedings of the 3rd Unconventional Resources Technology Conference. doi:10.15530/urtec-2015-2190705.

Solomon, E., Spivack, A., Kastner, M., Torres, M., Robertson, G., 2014. Gas hydrate distribution and carbon sequestration through coupled microbial methanogenesis and silicate weathering in the Krishna–Godavari Basin, offshore India. Mar. Pet. Geol. 58, 233–253.

Song, J., Littke, R., Weniger, P., Ostertag-Henning, C., Nelskamp, S., 2015. Shale oil potential and thermal maturity of the Lower Toarcian Posidonia Shale in NW. Eur., Int. J. Coal Geol. 150–151, 127–153.

Song, L., Martin, K., Carr, T.R., Ghahfarokhi, P.K., 2019. Porosity and storage capacity of Middle Devonian shale: A function of thermal maturity, total organic carbon, and clay content. Fuel 241, 1036–1044.

Sorkhabi, R., 2009. Source rocks in space and through time: EGI ArcGIS Database, distribution analysis and Palaeogeography, phase 1: Gondwana continents & margins. GeoExpro.

Soua, M., 2015. Cretaceous oceanic anoxic events (OAEs) recorded in the northern margin of Africa as possible oil and gas shale potential in Tunisia: An overview. Int. Geol. Rev. 58, 277–320.

Sounders-Smith, A., 2001. Neuquen Province Offers Areas with Exploration Potential. Oil Gas. J. 99, 50.

Southby, C., Carr, L.K., Henson, P., Haines, P.W., Zhan, A., Anderson, J.R., MacFarlane, S., Fomin, T.R., 2020. Exploring for the Future: Kidson Sub-basin seismic interpretation. Explor. Future Ext. Abstr. Geosci. Aust. https://doi.org/10.11636/132743.

Souza, J.M.S., Cerqueira, J.R., Garcia, K.S., Ribeiro, H.J.P.P.S., Oliveira, O.M.C., Queiroz, A.F.S., Teixeira, L.S.G., 2021. Geochemical characterization and origin of kerogens from source-rock of Devonian in the Amazonas Basin, Brazil. J. South Am. Earth Sci. 111, 103437.

Srivastava, M.K., Kishor, K., Singh, A.K., Mukherjee, S., Bharti, S., 2025. Tectonically Deformed Coal: Focus on Microstructures & Implications for Basin Evolution. Mar. Pet. Geol. 172, 107223.

Stephenson, R.A., et al., 1993. Continental Rift Development in Precambrian and Phanerozoic Europe: EUROPROBE and the Dnieper-Donets Rift and Polish Trough Basins. Sediment. Geol. 86, 159–175.

Sterling Resources, 2012. Onshore Romania – Craiova: UCG Silurian Shale Gas. Poster.

Stevens, S.H., Moodhe, K., 2016. New Bid Round Accelerates Mexico's Shale Potential. Oil Gas. J. 39–42.

Stevens, S.H., Moodhe, K.D., 2015. Evaluation of Mexico & Shale Oil and Gas Potential. Society of Petroleum Engineers SPE Latin American and Caribbean Petroleum Engineering Conference. doi:10.2118/177139-MS.

Stuart, W.J., 1976. Genes. Permian Low. Triassic Reserv. sandstones phases South. Cooper Basin Dev.: Aust. Pet. Explor. Assoc. J. 16, 37–42.

Su, A., Chen, H., Feng, Y., Zhao, J., Nguyen, A.D., 2022. Multistage fracturing history in the Paleocene lacustrine shale oil reservoirs of the Subei Basin, Eastern China. Mar. Pet. Geol. 144, 105835.

Subroto, E.A., Muritno, B.P., Noeradi, D., 2005. Petroleum Geochemistry Study in a Sequence Stratigraphic Framework in the Simenggaris Block, Tarakan Basin, East Kalimantan, Indonesia. Proceedings, Indonesian Petroleum Association. Thirtieth Annual Convention & Exhibition. IPA 05-G-159.

Sun, X., Alcalde, J., Gomez-Rivas, E., Struth, L., Johnson, G., Travé, A., 2020. Appraisal of CO2 storage potential in compressional hydrocarbon-bearing basins: Global assessment and case study in the Sichuan Basin (China). Geosci. Front. 11, 2309–2321.

Sun, Y., Joachimski, M.M., Wignall, P.B., Yan, C., Chen, Y., Jiang, H., Wang, L., Lai, X., 2012. Lethallyhot temperatures during the early Triassic greenhouse. Science 338, 366–370.

Surabhi, K., Biswas, M., Mukherjee, S., 2024. Remote Sensing-based Morphometry on the Petroliferous Cambay Rift Basin (Gujarat, Western India). J. Geol. Soc. India 100, 473–485.

Suriamin, F., Ko, L.T., 2022. Geological characterization of unconventional shale-gas reservoirs. Chapter 1. In: Moghanloo, R.G. (Ed.), Unconventional Shale Oil Development. Gulf Professional Publishing. Cambridge, pp. 1–31. ISBN: 978-323-90185-7.

Svendsen, N.B., 2004. The Sahmah Formation of Oman: exploration implications for the Rub' Al-Khali Basin. GeoArabia 9, 119–136.

Swanson, V.E., 1960. Oil yield and uranium content of black shales. Geological Survey Professional paper 356-A. United States Government Printing office, Washington, pp. 1–28.

Swanson, V.E., 1961. Geology and Geochemistry of uranium in marine black shales- a review. U. S. Geol. Surv. Prof. Pap. 356-C. 67–112.

Sweeney, J.J., Burnham, A.K., 1990. Evaluation of a simple model of vitrinite reflectance based on chemical kinetics. AAPG Bull. 74, 1559–1570.

Taghavinejad, A., Mstadhassan, M., Daneshfar, R., 2022. Unconventional reservoirs: rate and pressure transient analysis techniques: A reservoir engineering approach. Springer, pp. 2509–3134. ISSN: 2509-3134.

Talbi, R., Lakhdar, R., Smati, A., Spiller, R., Levey, R., 2018. Aptian–Albian oil shale unconventional system as registration of Cretaceous oceanic anoxic sub-events in the southern Tethys (Bir M'Cherga basin, Tunisia). J. Pet. Explor. Prod. Technol. 9, 1007–1022.

Tan, J., Horsfield, B., Fink, R., Krooss, B., Schulz, H.-M., Rybacki, E., Zhang, J., Boreham, C.J., van Graas, G., Tocher, B.A., 2014. Shale Gas Potential of the Major Marine Shale Formations in the Upper Yangtze Platform, South China, Part III: Mineralogical, Lithofacial, Petrophysical, and Rock Mechanical Properties. Energy Fuels 28, 2322–2342.

Tan, M., Zhu, X., Geng, M., Zhu, S., Liu, W., 2017. The occurrence and transformation of lacustrine sediment gravity flow related to depositional variation and paleoclimate in the Lower Cretaceous Prosopis Formation of the Bongor Basin, Chad. J. Afr. Earth Sci. 134, 134–148.

Tao, Z., Clarens, A., 2013. Estimating the carbon sequestration capacity of shale formations using methane production rates. Environ. Sci. Technol. 47, 11318–11325.

Teichert, B.M.A., Johnson, J.E., Solomon, E.A., Giosan, L., Rose, K., Kocherla, M., Connolly, E.C., Torres, M.E., 2014. Composition and origin of authigenic carbonates in the Krishna- Godavari and Mahanadi Basins, eastern continental margin of India. Mar. Petrol. Geol. 58, 438–460.

Teichmüller, M., Durand, B., 1983. Fluorescence microscopical rank studies on liptinites and vitrinites in peat and coals, and comparison with results of the rock-eval pyrolysis. Int. J. Coal Geol. 2 (3), 197–230. https://doi.org/10.1016/0166-5162(83)90001-0.

Terken, J.M.J., 1999. The Natih Petroleum System of North Oman. GeoArabia 4, 157–180.

Terken, J.M.J., Frewin, N.L., Indrelid, S.L., 2001. Petroleum Systems of Oman: Charge Timing and Risks. AAPG Bull. 85, 1817–1845.

Thickpenny, A., 1984. The sedimentology of the Swedish Alum Shales. Geol. Soc. Lond. Spec. Publ. 15 (1), 511–525. https://doi.org/10.1144/GSL.SP.1984.015.01.33.

Thornton, R.C.N., 1979. Regional stratigraphic analysis of the Gidgealpa Group, southern Cooper basin, Australia. Geol. Surv. South Aust., Bull. 49, 140.

Tian, X.H., 1983. The outline of plate tectonics in Xinjiang, Eastern Xinjiang. Geology 1, 35–49.

Tong, J., Han, X., Wang, S., Jiang, X., 2011. Evaluation of Structural Characteristics of Huadian Oil Shale Kerogen Using Direct Techniques (Solid-State^{13}C NMR, XPS, FT-IR, and XRD). Energy Fuels 25, 4006–4013.

Törő, B., Pratt, B., 2015. Characteristics and Implications of Sedimentary Deformation Features in the Green River Formation (Eocene) in Utah and Colorado. Utah Geol. Assoc. Guideb. 44, 371–422.

Torres, E., Slatt, R.M., O'Brien, N., Phip, R.P., Rodrigues, H.L., 2012. Characterization of the Cretaceous La Luna Formation as a Shale Gas System, Middle Magdalena Basin, Colombia. Houston Geological Society Conference onUnconventional Resource Shales, poster.

Tourtelot, H.A., 1979. Black Shale—Its Deposition and Diagenesis. Clays Clay Miner. 27, 313–321.

Tucker, M.E., Jones, S.J., 2023. Sedimentary Petrology, Fourth Edition. Wiley, LCCN. 2023001483.

Turlapati, V.Y., Prusty, B.K., Bakshi, T., 2020. Detailed Pore Structure Study of Damodar Valley and Upper Assam Basin Shales Using Fractal Analysis. Energy Fuels 34, 14001–14011.

U.S. Energy Information Administration (E.I.A), 2013. Technically Recoverable Shale Oil and Shale Gas Resources: Canada. World Shale Resource Assessments, U.S. Department of Energy, Washington, DC 20585. Pp. I-1 –57.

Uliasz-Misiak, B., Przybycin, A., Winid, B., 2014. Shale and tight gas in Poland—legal and environmental issues. Energy Policy 65, 68–77.

Ulmishek, G.F., 1990. Uzen Field–USSR Middle Caspian Basin, South Mangyshlak Region.

Ulmishek, G.F., 2003. West Siberia structural map. Petroleum Geology and Resources of the West Siberian Basin, Russia. USGS Bulletin 2201-G. ⟨https://pubs.usgs.gov/bul/2201/G/⟩.

Underdown, R., Redfern, J., 2008. Petroleum generation and migration in the Ghadames Basin, north Africa: A two-dimensional basin-modeling study. AAPG Bull. 92, 53–76.

Underhill, J.R., Monaghan, A.A., Browne, M.A.E., 2008. Controls on Structural Styles. Basin Dev. andPetroleum Prospect. Midl. Val. Scotl. Mar. Pet. Geol. 25, 1000–1022.

USGS, National and Global Petroleum Assessment, 2014. Assessment of unconventional oil and gas resources in Northeast Mexico. 〈https://pubs.usgs.gov/fs/2014/3047/pdf/fs2014-3047.pdf〉.
Veevers, J.J., Tewari, R.C., 1995. Gondwana Master Basin Penins. India Tethys Inter. theGondwanaland Prov. Pangea. Geol. Soc. Am. Mem. 187, 1–73.
Vesely, F.F., Rostirolla, S.P., Appi, C.J., Kraft, E.P., 2007. Late Paleozoic Glacially Related Sandstone Reservoirs in the Parana Basin, Brazil. Am. Assoc. Pet. Geol., Bull. 91, 151–160.
Wan, L., Liu, J., Mao, F., Lv, M., Liu, B., 2014. The petroleum geochemistry of the Termit Basin, Eastern Niger. Mar. Pet. Geol. 51, 167–183.
Wandrey, C.J., 2004. Sylhet-Kopili/Barail-Tipam composite petroleum systems, Assam Geologic Province, India: US GeologicalSurvey Bulletin 2208-D.
Wang, B., Liu, B., Yang, J., Bai, L., Li, S., 2022. Compatibility characteristics of fracturing fluid and shale oil reservoir: A case study of the first member of Qingshankou Formation, northern Songliao Basin, Northeast China. J. Pet. Sci. Eng. 211, 110161.
Wang, G., Carr, T.R., 2012. Methodology of organic-rich shale lithofacies identification and prediction: a case study from Marcellus Shale in the Appalachian basin. Comput. Geosci. 49, 151e163.
Wang, J., Cao, Y., Liu, K., Gao, Y., Qin, Z., 2019. Fractal characteristics of the pore structures of fine-grained, mixed sedimentary rocks from the Jimsar Sag, Junggar Basin: Implications for lacustrine tight oil accumulations. J. Pet. Sci. Eng. 182, 106363.
Wang, J., Wang, K., Shan, X., Taylor, K.G., Ma, L., 2024. Potential for CO2 storage in shale basins in China. Int. J. Greenh. Gas. Control 132, 104060.
Wang, L., et al., 2023. A systematic review of CO2 injection for enhanced oil recovery and carbon storage in shale reservoirs. Int. J. Hydrog. Energy 48, 37134–37165.
Wang, L., Tian, Y., Yu, X., Wang, C., Yao, B., Wang, S., Wu, Y.S., 2017. Advances in improved/enhanced oil recovery technologies for tight and shale reservoirs. Fuel 210, 425–445.
Wang, M., Xue, H., Tian, S., Wilkins, R.W.T., Wang, Z., 2015. Fractal characteristics of Upper Cretaceous lacustrine shale from the Songliao Basin, NE China. Mar. Pet. Geol. 67, 144–153.
Wang, M., Lu, S., Wang, Z., Liu, Y., Huang, W., Chen, F., Xu, X., Li, X., Li, J., 2016. Reservoir Characteristics of Lacustrine Shale and Marine Shale: Examples from the Songliao Basin. Bohai Bay Basin Qiannan Depress Acta Geol. Sin. 90, 1024–1038.
Wang, P., Chen, X., Pang, X., Li, J., Yang, H., Jiang, F., Guo, J., Guo, F., Peng, W., Xu, J., Wang, Y., 2014. Gas generation and expulsion characteristics of Middle–Upper Triassic source rocks, eastern Kuqa Depression, Tarim Basin, China: implications for shale gas resource potential. Aust. J. Earth Sci. 61, 1001–1013.
Wang, P.J., Liu, H.B., Ren, Y.G., Wan, X.Q., Wang, S.X., Qu, X.J., Meng, Q.A., Huang, Y.J., Huang, Q.H., Gao, Y.F., Wang, C.S., 2022. How to choose a right drilling site for the ICDP Cretaceous Continental Scientific Drilling in the Songliao Basin (SK2), Northeast China. Earth Sci. Front 24, 216–228.
Wang, Q.M., Nishidai, T., Coward, M.P., 1992. The Tarim Basin. NW China.: Form. Asp. Pet. Geol. J. Pet. Geol. 15, 5–34.
Warner, N., Darrah, T., Jackson, R., Millot, R., Kloppmann, W., Vengosh, A., 2014. New Tracers Identify Hydraulic Fracturing Fluids and Accidental Releases from Oil and Gas Operations. Environ. Sci. Technol. 48, 12552–12560.
Warren, et al., 1998. Proterozoic Source Rocks: Sedimentology and Organic Characteristics of the Velkerri Formation, Northern Territory, Australia. AAPG Bull. 82, 442–463.
Watkinson, M.P., Hart, M.B., Joshi, A., 2007. Cretac. tectonostratigraphy Dev. Cauvery Basin, Southeast India Pet. Geosci. 13, 181–191.
Wei, N., Li, X., Fang, Z., Bai, B., Li, Q., Liu, S., Jia, Y., 2015. Regional resource distribution of onshore carbon geological utilization in China. J. CO2 Util. 11, 20–30.
Wei, W., Littke, R., Swennen, R., 2023. Geochemical study of Mississippian to Pennsylvanian Namurian Shale in the Namur Synclinorium and Campine Basin (Belgium and S-Netherlands): Implication for paleo-redox reconstruction and organic matter characteristics. Int. J. Coal Geol. 265, 104150.
Wei, Y., Sheng, H., Ao, S., Gangyi, Z., Zhi, Z., Tian, D., Ze, T., 2021. Methane Adsorption Capacities Investigation of the Ediacaran Organic-Rich Doushantuo Shale in the Middle Yangtze Platform, South China. Energy Fuels 20, 16452–16464.
Weller, J.M., 1960. Stratigraphic Principles and Practice. Harper & Brothers Publisher. N. Y. 55.
Wilcox, R.D., Fisk, J., 1983. Tests show behaviours aid well planning. Oil Gas. J. 12, 106–125.
Wisesa, K.D., Mangala, A., Arbi, H., Adlan, Q. and Gani, R.M.G., 2017. Distribution of Permian Source Rocks Maturation Related to Lengguru Fold-Thrust Belt Position in Bintuni Basin. AAPG Database. URL: 〈https://archives.datapages.com/data/ipa_pdf/2017/IPA17-405-SG.htm〉.
Wood D.A., Cai J. 2022. Sustainable geocience for natural gas subsurface systems. Gulf Professional Publishing. ISBN: 978-0-323-85465-8.
Wu, K., Zhang, T., Yang, Y., Sun, Y., Yuan, D., 2016. Contribution of oxygenic photosynthesis to palaeo-oceanic organic carbon sink fluxes in Early Cambrian Upper Yangtze shallow sea: Evidence from black shale record. J. Earth Sci. 27, 211–224.
Wu, L., Guan, S.W., Ren, R., Zhang, C.Y., Feng, X.Q., 2021a. Neoproterozoic glaciations and rift evolution in the northwest Tarim Craton, China: new constraints from geochronological, geochemical, and geophysical data. Int. Geol. Rev. 63, 1–20.
Wu, L., Zhu, G.Y., Yan, L., Feng, X.Q., Zhang, Z.Y., 2021b. Late ediacaran to early cambrian tectonic–sedimentary controls on lower cambrian black shales in the Tarim Basin, northwest China. Glob. Planet. Change 205, 103612.
Wu, L., Zhu, M., Feng, X.Q., Ji, D.S., Zhou, L., Liu, S.X., Zhang, L.Y., Tan, Y.L., Qian, Z.L., Yang, Z., 2022b. Interpretaion on tectonic stress and deformation of Sikeshu sag in Junggar Basin. Acta Pet. Sin. 43, 494–506.
Wu, L., Feng, X.Q., Guan, S.W., Zhu, G.Y., Yang, H.J., 2022a. Proterozoic basin–orogen framework in the northern Tarim Craton, China. Precambrian Res 373, 106627.
Wu, L., Wang, P., Zhang, C., Feng, X., Qian, Z., Zhou, L., 2023. Long-lived paleo-uplift controls on Neoproterozoic–Cambrian black shales in the Tarim basin. Mar. Pet. Geol. 155, 106343.
Wu, S., Zhai, X., Yang, Z., Bale, H., Hong, Y., Cui, J., Pan, S., Lin, S., 2019. Characterization of fracture formation in organic-rich shales - An experimental and real time study of the Permian Lucaogou Formation, Junggar Basin, northwestern China. Mar. Pet. Geol. 107, 397–406.
Wu, W., Liao, Z., Chen, H., Li, S., Su, A., Hussain, I., Zhao, N., 2021. Jurassic terrestrial shale gas potential of the northern Kashi Sag in the Tarim Basin, Northwestern Chin. Geofluid 1, 5542447.
Wust, R.A.J., Nassichuk, B.R., Brezovski, R., Hackley, P.C., Willment, N., 2013. Vitrinite reflectance versus pyrolysis Tmax data: Assessing thermal maturity in shale plays with special reference to the Duvernay shale play of the Western Canadian Sedimentary Basin, Alberta. Can. Soc. Pet. Eng. SPE Unconv. Resour. Conf. Exhib. -Asia Pac. - Brisb., Aust. (2013-11-11)].
Xiao, H., Li, M., Cheng, D., 2023. Late Cretaceous marine incursion into Central African continent. Res. Sq. (Prepr.). https://doi.org/10.21203/rs.3.rs-2656821/v1.
Xiaofeng, W., Erdtmann, B.D., Xiaohong, C., Xiaodong, M., 1998. Integrated sequence-, bio- and chemo-stratigraphy of the terminal Proterozoic to Lowermost Cambrian "black rock series" from central South China. Episodes 21, 178–189.
Xiaoqi, W., Liang, S., Rukai, Z., Xu, J., Jianming, L., Songtao, W., Lina, B., Xiaodan, L., 2015. Application of charging effects in evaluating storage space of tight reservoirs: A case study from Permian Lucaogou Formation in Jimusar sag, Junggar Basin, NW China. Pet. Explor. Dev. 42, 516–524.
Xiong, F., Wang, Y., Puckette, J., Grammer, M., Awejori, G., Radonjic, M., 2024. Geochemical and Microstructural Characterization of Shale Rock: A Workflow for Site Evaluation for Energy–Fluids Storage. Energy Fuels 38, 20875–20891.
Xu, T., Apps, J.A., Pruess, K., 2005. Mineral sequestration of carbon dioxide in a sandstone–shale system. Chem. Geol. 217, 295–318.
Xu, W., Ruhl, M., Jenkyns, H., Hesselbo, S.P., Riding, J.B., Selby, D., Naafs, D., Weijers, J.W.H., Pancost, R.D., Tegelaar, E., Idiz, E.F., 2017. Carbon sequestration in an expanded lake system during the Toarcian oceanic anoxic event. Nat. Geosci. 10, 129–134.
Yaalon, D.H., 1978. Shale. In: Fairbridge, R.W., Bourgeois, J. (Eds.), The Encyclopedia of Sedimentology. Dowden. Hutchinson & Ross, Inc, pp. 736–739.
Yahi, N., Schaefe, R.G., Littke, R., 2001. Petroleum generation and accumulation in the Berkine basin, eastern Algeria. AAPG Bull. 85, 1439–1467.
Yang, R., He, S., Wang, X., Hu, Q., Hu, D., Yi, J., 2016. Paleo-ocean redox environments of the upper Ordovician Wufeng and the first member in lower Silurian Longmaxi Formations in Jiaoshiba area, Sichuan Basin. Can. J. Earth Sci. 53, 426–440.
Yang, W., Pan, J., 2023. The role of vegetation carbon sequestration in offsetting energy carbon emissions in the Yangtze River Basin. China Environ. Dev. Sustain.
Yang, Z., Li, M., Cheng, D. and Xiao, H., 2018. Geochemical characteristics of source rocks in the Bongor Basin, Chad. URL: 〈https://archives.datapages.com/data/tsop/tsop-v35-2018/abstracts/yang3.htm〉.
Yasin, Q., Baklouti, S., Khalid, P., Haroon Ali, S., Boateng, C.D., Du, Q., 2021. Evaluation of shale gas reservoirs in complex structural enclosures: A case study from Patala Formation in the Kohat-Potwar Plateau, Pakistan. J. Pet. Sci. Eng. 198, 108–225.
Ye, J., Afifi, A., Rowaihy, F., Baby, G., De Santiago, A., Tasianas, A., Hamieh, A., Khodayeva, A., Juaied, M.A., Meckel, T.A., Hoteit, H., 2023. Evaluation of geological CO2 storage potential in Saudi Arabian sedimentary basins. Earth-Sci. Rev. 244, 104539.
Yensepbayev, T., Izart, A., Joltaev, G., Hautevelle, Y., Elie, M., Suarze-Ruiz, I., 2010. Geochemical Characterization of Source Rocks and Oils from the Eastern Part of the Precaspian and Pre-Uralian Basins (Kazakhstan): Palaeoenvironmental and Palaeothermal Interpretation. Org. Geochem. 41, 242–262.
Yin, P.F., Yang, S.Q., Ranjith, P.G., 2024. Anisotropic Mechanical Behaviors of Shale Rock and Their Relation to Hydraulic Fracturing in a Shale Reservoir: A Review. Energies 17, 1761.
Yong, T.S., 1983. Carboniferous lithofacies palaeogeography and its oil-bearing properties of Tarim platform. Xinjiang Pet. Geol. 3, 13–24.
Yongsheng, Ma., 2020. Marine Oil and Gas Exploration in China. Springer Science and Business Media LLC.
Younes, M.A., 2012. In: Younes, M. (Ed.), Hydrocarbon Potentials in the Northern Western Desert of Egypt. InTech. ISBN: 978-953-51-0379-0.
Younes, M.A.A., 2002. Alamein basin hydrocarbon potential of the Jurassic-Cretaceous source rocks, north western desert, Egypt. Oil Gas. Eur. Mag. 28, 22–28.
Yuan, W., Chen, Z., Kong, B., Zhao, G., 2023. Hybrid geothermal energy and hydrocarbon resources production by repurposing horizontal wells in shale gas reservoirs in Horn River Basin, British Columbia, Canada. Geoenergy Sci. Eng. 227, 211913.
Yue, P., Zhang, R., Sheng, J.J., Yu, G., Liu, F., 2022. Study on the Influential Factors of CO2 Storage in Low Permeability Reservoir. Energies 15, 344.
Yurewicz, D.A., Advocate, D.M., Lo, H.B., Hernandez, E.A., 1998. Source Rocks and Oil Families, SouthwestMaracaibo Basin (Catatumbo Subbasin), Colombia. Am. Assoc. Pet. Geol., Bull. 82, 1329–1352.
Zendehboudi, S., Bahadori, A., 2017. Shale Oil and Gas Handbook: Theory, technologies, and Challenges. Elsevier, Amsterdam. ISBN: 978-0-12-802100-2.
Zhang, J., Xu, X., Bai, J., Liu, W., Chen, S., Liu, C., Li, Y., 2020. Enrichment and exploration of deep lacustrine shale oil in the first member of Cretaceous Qingshankou Formation, southern Songliao Basin, NE China. Pet. Explor. Dev. 47, 683–698.
Zhang, J., Lin, L., Tang, X., Jiang, S., Li, Y., 2022. The distribution patterns of organic-rich shale and exploration prospect of shale gas in China. Adv. Resour. Res. 2, 16–30.

Zhang, Q., Littke, R., Zieger, L., Shabani, M., Tang, X., Zhang, J., 2019. Ediacaran, Cambrian, Ordovician, Silurian and Permian shales of the Upper Yangtze Platform, South China: Deposition, thermal maturity and shale gas potential. Int. J. Coal Geol. 216, 103281.

[802] Zhang, W., Li, Y., Xu, T., Cheng, H., Zheng, Y., Xiong, P., 2009. Long-term variations of CO2 trapped in different mechanisms in deep saline formations: A case study of the Songliao Basin, China. Int. J. Greenh. Gas. Control 3, 161–180.

Zhang, X., Bi, Z., Chang, X., Wang, L., Yang, H., 2021. Experimental Investigation on Hydraulic Fracture Morphology of Inter-Salt Shale Formation. Front. Energy Res. 9, 800521.

Zhang, X., Zhu, L., Wang, T., Shi, X., Han, B., Shen, J., Gao, H., 2023. Fluid property identification of the Lower Cretaceous reservoirs with complex oil-water contacts in Deseo Basin, Chad. Energy Geosci. 5, 100219.

Zhang, Y., He, J., Li, F., Fan, X., Li, X., 2019. Characteristics of Fracture Propagation Induced by Supercritical CO_2 in Inter-Salt-Shale Reservoir. Geofluids 2019. Article ID 7132843.

Zhao, J., Ji, G., Tian, Y., Chen, Y., Wang, Z., 2018. Environmental vulnerability assessment for mainland China based on entropy method. Ecol. Indic. 91, 410–422.

Zhao, S., Wang, Y., Li, Y., Li, H., Xu, Z., Gong, X., 2021. Geochemistry and Mineralogy of Lower Paleozoic Heituao Shale from Tadong Low Uplift of Tarim Basin, China: Implication for Shale Gas Development. Minerals 11, 635.

Zhao, T., Xu, S., Hao, F., 2023. Differential adsorption of clay minerals: Implications for organic matter enrichment. Earth-Sci. Rev. 246, 104598.

Zhao, Y., Xu, Q., Li, Y., Bai, X., Ding, R., Wang, J., Hou, T., 2022. Main Factors of Mesozoic Tectonic Deformation in the Erlian Basin. Inner Mongolia. Insights from Physical Modelling, China. Geofluids 2022. Article ID 8130349.

Zhao, Z., et al., 2017. Depositional environment and geochemical characteristics of the Lower Carboniferous source rocks in the Marsel area, Chu-Sarysu Basin, Southern Kazakhstan. Mar. Pet. Geol. 81, 134–148.

Zholtaev, G.Zh, Mussina, E.S., Fazylov, E.M., Aliakbar, M., 2019. Prospects for discovering new unconventional hydrocarbon deposits in the Caspian sedimentary basin (shale oil and gas). Int. Multidiscip. Sci. GeoConference: SGEM; Sofia 19 (Iss. 1.1).

Zhou, J., Xie, S., Jiang, Y., Xian, X., Liu, Q., Lu, Z., Lyu, Q., 2018. Influence of supercritical CO2 Exposure on CH4 and CO2 Adsorption behaviors of shale: Implications for CO2 Sequestration. Energy Fuels 32, 6073–6089.

Zhou, J., Tian, S., Xian, X., Zheng, Y., Yang, K., Liu, J., 2022. Comprehensive review of property alterations induced by CO2–shale interaction: implications for CO2 sequestration in shale. Energy Fuels 36, 8066–8080.

Zimmerele, W., 1995. Petroleum Sedimentology. Academic Publishers, Dordrecht. ISBN: 0-7923-3418-3.

Zoback, M.D., Kohli, A.H., 2019. Unconventional Reservoir Geomechanics: Shale Gas. Tight Gas, and Induced Seismicity. Cambridge University Press. ISBN 978-1-107-08707-1.

Zou, C., 2017. Unconventional Petroleum Geology, Second Ed. Elsevier, Amsterdam. ISBN: 978-0-12-812234-1.

Zou, C., Yang, Z., Dai, J., Dong, D., Zhang, B., Wang, Y., Deng, S., Huang, J., Liu, K., Yang, C., Wei, G., Pan, S., 2015. The characteristics and significance of conventional and unconventional Sinian–Silurian gas systems in the Sichuan Basin, central China. Mar. Pet. Geol. 64, 386–402.

Zou, Z., Yun, Y., Sun, J., 2006. Entropy method for determination of weight of evaluating indicators in fuzzy synthetic evaluation for water quality assessment. J. Environ. Sci. 18, 1020–1023.

Zumberge, J.E., Curtis, J.B., Brown, S.W., 2014. Petroleum Geochemistry of Upper Jurassic Bazhenov Shale Source Rocks and Corresponding Crude Oils, West Siberian Basin, Russia. In: American Association of Petroleum Geologists Unconventional Resources Technology Conference - Denver. doi:10.15530/URTEC-2014-1922785.